



FEDERAL UNIVERSITY OF RIO GRANDE - FURG
CENTER FOR COMPUTATIONAL SCIENCES
POST GRADUATE PROGRAM IN COMPUTATIONAL MODELING
DOCTORATE COURSE IN COMPUTATIONAL MODELING

Doctoral Thesis

A Family of Edge Detection Approaches Based on Generalizations of the Choquet Integral

Miquéias Amorim Santos Silva

Doctoral Dissertation submitted to the Post Graduate Program in Computational Modeling at Federal University of Rio Grande - FURG, as partial fulfillment of the requirements for the degree of Doctor in Computational Modeling

Advisor: Prof[a]. Dr.[a] Graçaliz Pereira Dimuro
Co-advisors: Prof. Dr. Giancarlo Lucca
Prof. Dr. Cedric Marco-Detchart

Rio Grande, 2026

S586f

Silva, Miquéias Amorim Santos
A family of edge detection approaches based on generalizations of the choquet integral / Miquéias Amorim Santos Silva -- 2026.
200f.

Tese (Doutorado) – Universidade Federal do Rio Grande – Programa de Pós-Graduação em Modelagem Computacional, 2026.

Orientadora: Dra.Graçaliz Pereira Dimuro
Co-orientadores: Dr.Giancarlo Lucca
Dr. Cedric Marco-Detchart

1. Modelagem Computacional. 2. Funções de agregação. 3. Funções de pré-agregação. 4. Medidas Fuzzy. 5. Detecção de bordas. 6. Visão computacional. I. Dimuro, Graçaliz Pereira. II. Lucca, Giancarlo. III. Marco-Detchart, Cedric. IV. Título.

CDU 004.414.23

Catalogação na fonte: Bibliotecária Brenda Sequeira CRB10/1979





Doctoral Thesis

A Family of Edge Detection Approaches Based on Generalizations of the Choquet Integral

Miquéias Amorim Santos Silva

Examination Committee:

Prof[a]. Dr.[a] Viviane Leite Dias de Matos

Prof. Dr. Benjamin Rene Callejas Bedregal

Prof. Dr. Pedro Melo Pinto

Prof. Dr. Rui Eduardo Brasileiro Paiva

In memory of the victims of the floods in Rio Grande do Sul in 2024

ACKNOWLEDGMENTS

First and foremost, I would like to express my deepest gratitude to God, whose grace, strength, and providence sustained me throughout this journey. In moments of uncertainty, difficulty, and perseverance, I found in Him the wisdom, courage, and hope necessary to continue. This thesis is, above all, a testimony of His faithfulness and care throughout my academic and personal path.

I would like to express my sincere gratitude to my advisor, Prof. Dr. Graçaliz Pereira Dimuro, whose expertise, understanding, and patience have greatly contributed to my personal and academic growth. Her guidance has been invaluable throughout the research and writing of this thesis.

I would also like to thank Prof. Dr. Giancarlo Lucca and Prof. Dr. Cedric Marco-Detchart for their valuable insights and fundamental contributions to the review of this work. Their knowledge and attention to detail have been a major source of inspiration and improvement for my research.

I cannot fail to mention Prof. Dr. Eduardo Borges, who has supported and guided me since the very beginning of my admission to the program, providing crucial assistance to overcome the challenges faced during this work and academic experience.

Finally, I would like to express my sincere gratitude to the Postgraduate Program in Computational Modeling at the Federal University of Rio Grande — FURG, as well as to all professors, coordinators, and members of the program who contributed to my academic formation during this doctoral journey. I am also deeply grateful to the secretarial staff and to all university employees who, with attention, professionalism, and generosity, offered their time and support whenever needed throughout my period as a doctoral student. I also acknowledge the financial support provided by the funding agencies CAPES and FAURG, which contributed to the development of part of this research.

For the perception of sensible forms arises from sensible impression, but not so with the aforementioned intentional species. [...] Whereas, to apprehend the intentional species, which are not received through the senses, is destined for the estimative power

— SAINT THOMAS AQUINAS, SUMMA THEOLOGICA, 1265-1274

ABSTRACT

SILVA, Miquéias Amorim Santos. **A Family of Edge Detection Approaches Based on Generalizations of the Choquet Integral**. 2026. 200 f. Doctoral Thesis – Post Graduate Program in Computational Modeling. Federal University of Rio Grande - FURG, Rio Grande.

One of the fundamental problems in image processing and computer vision is the identification of relevant discontinuities in a scene. In this context, edge detection aims to locate significant transitions between regions with distinct properties, such as intensity, color, texture, or structure. This task is essential in several applications, including image segmentation, object detection, pattern recognition, tracking, facial recognition, autonomous vehicles, and medical image processing. Over the last decades, different methods have been proposed for edge detection, ranging from classical approaches based on derivatives and differential operators, such as Sobel, LoG, and Canny, to recent methods based on convolutional neural networks. Although relevant, traditional methods often present limitations related to noise sensitivity, parameter dependence, and the occurrence of false positives. On the other hand, supervised methods depend on large annotated datasets and may be influenced by the subjectivity of annotations. In this scenario, approaches based on fuzzy logic, aggregation functions, pre-aggregation functions, and fuzzy measures have shown promise for modeling uncertainties, imprecisions, and different local evidence present in digital images. This thesis investigates the use of these tools in the development of edge detection methods, starting from conceptual and mathematical foundations involving the notion of edge, aggregation functions, pre-aggregation functions, fuzzy measures, and generalizations of the Choquet integral. Then, systematic reviews and experimental investigations are presented on fuzzy edge detection methods, the impact of smoothing filters on classical detectors, and the use of aggregation operators in computational models. Based on these foundations, an edge detection model based on a sliding window and fuzzy measures is proposed, as well as a family of non-trained, multiscale methods based on pointwise aggregation. The results indicate that the proposed approaches are adaptive, accurate, and competitive on benchmark datasets, even when compared with classical methods, trained models, and other aggregation-based techniques.

Keywords: Aggregation Functions, Pre-aggregation Functions, Fuzzy Measures, Edge Detection, Computer Vision.

RESUMO

SILVA, Miquéias Amorim Santos. **Uma Família de Abordagens para Detecção de Bordas Baseada em Generalizações da Integral de Choquet**. 2026. 200 f. Doctoral Thesis – Post Graduate Program in Computational Modeling. Federal University of Rio Grande - FURG, Rio Grande.

Um dos problemas fundamentais do processamento de imagens e da visão computacional é a identificação de descontinuidades relevantes em uma cena. Nesse contexto, a detecção de bordas busca localizar transições significativas entre regiões com propriedades distintas, como intensidade, cor, textura ou estrutura. Essa tarefa é essencial em diversas aplicações, incluindo segmentação de imagens, detecção de objetos, reconhecimento de padrões, rastreamento, reconhecimento facial, veículos autônomos e processamento de imagens médicas. Ao longo das últimas décadas, diferentes métodos foram propostos para a detecção de bordas, desde abordagens clássicas baseadas em derivadas e operadores diferenciais, como Sobel, LoG e Canny, até métodos recentes baseados em redes neurais convolucionais. Embora relevantes, métodos tradicionais frequentemente apresentam limitações relacionadas à sensibilidade ao ruído, à dependência de parâmetros e à ocorrência de falsos positivos. Por outro lado, métodos supervisionados dependem de grandes conjuntos de dados anotados e podem ser influenciados pela subjetividade das anotações. Diante desse cenário, abordagens baseadas em lógica fuzzy, funções de agregação, pré-agregação e medidas fuzzy têm se mostrado promissoras para modelar incertezas, imprecisões e diferentes evidências locais presentes em imagens digitais. Esta tese investiga o uso dessas ferramentas no desenvolvimento de métodos de detecção de bordas, partindo de fundamentos conceituais e matemáticos que envolvem a noção de borda, funções de agregação, pré-agregação, medidas fuzzy e generalizações da integral de Choquet. Em seguida, são apresentadas revisões sistemáticas e investigações experimentais sobre métodos fuzzy de detecção de bordas, impacto de filtros de suavização em detectores clássicos e uso de operadores de agregação em modelos computacionais. A partir dessas bases, propõe-se um modelo de detecção de bordas baseado em janela deslizante e medidas fuzzy, bem como uma família de métodos não treinados, multiescala e baseados em agregação pontual. Os resultados indicam que as abordagens propostas são adaptáveis, precisas e competitivas em conjuntos de dados de referência, mesmo quando comparadas a métodos clássicos, modelos treinados e outras técnicas baseadas em agregação.

Palavras-chave: Funções de Agregação, Funções de Pré-agregação,Medidas Fuzzy, Detecção de Bordas, Visão Computacional.

FIGURE LIST

1 Overview of the thesis methodology. 28

2 Illustration of the Kanizsa Triangle, demonstrating the phenomenon of visual perception of illusory contours and shapes. Adapted from (SAKIYAMA; SASAKI; GUNJI, 2014). 33

3 "The Seine at Le Grande Jatte," a work by Georges Seurat from 1888, is an oil on canvas painting. This artwork exemplifies the technique of pointillism, an innovative approach to painting where small points of pure color are applied in a way that forms a coherent image when viewed from a distance. This technique was fundamental to the development of the post-impressionist movement in modern art. Retrieved from (GALLERY, 2024) 34

4 Explanation of edge, boundary, and contour. The first row consists of three natural images, the second row shows their corresponding manually annotated ground truth, and the third row contains three synthetic images. The first two columns of images in the first two rows are sourced from BSDS500, while the last column of images are from BIPEDv2. Retrieved from (HUANG; HUANG, 2025) 37

5 Illustration of how the choice of scale and visual feature affects the computational accessibility of edges. Adapted from Mnttzri (2021). . 42

6 Schematic overview of standard and expanded Choquet-type constructions. 65

7 Original image without intensity representation on z axis. Source: author 71

8 Smoothing effect: Gaussian and box filter. Source: author 72

9 Smoothing effect: Gaussian and mean shift. Source: author 72

10 Schematic overview of gradient-based methods. Source: author . . . 73

11 Chronology of detection methods without using aggregation functions or fuzzy methods (ROBERTS, 1980; SOBEL; FELDMAN, 1973; PREWITT, 1970; MARR; HILDRETH, 1980; CANNY, 1986; ARBELAEZ et al., 2011; MCILHAGGA, 2010; YANG et al., 2013; XIE; TU, 2017; YANG et al., 2016; LIU et al., 2019; ZHANG et al., 2017; DENG et al., 2018; WIBISONO; HANG, 2021; SU et al., 2021; PU et al., 2022; HE et al., 2022) 74

12 Schema of Fuzzy-Based Methods. Source: author 76

13 Chronology of fuzzy methods presented above (RUSSO, 1998; GHOSH et al., 2020; VERSACI; MORABITO, 2021; MELIN et al., 2014) 76
14 Image 236017 from BSDS500 with three of its hand-labeled ground-truth boundary maps. 77

15 Most cited papers in absolute numbers. 84
16 Word clouds of key terms of RQG edge detection methods. Retrieved from (SILVA et al., 2023) 85
17 Chronology of non-fuzzy methods RQG. Retrieved from (SILVA et al., 2023) 86
18 Chronology of fuzzy methods RQF. Retrieved from (SILVA et al., 2023) 88
19 Most cited for fuzzy methods. Source: author. 90
20 Word cloud of key terms of fuzzy methods. Retrieved from (SILVA et al., 2023) 92
21 Clustering of abstracts from leading works. Source: author. 94

22 Terms of inclusion, exclusion, and number of selected papers. Source: author. 101

23 Percentiles for canny 2.25 with Gaussian sigma interval = **[0.1-5.0]** . 117
24 Percentiles for canny 2.25 with mshift iterations interval = **[1-50]** . . 117
25 Percentiles for canny 2.25 with gravitational iterations interval = **[1-50]** 117
26 Relationship between edge parameter and blur parameter with Blob Style Density: **Precision** 119
27 Relationship between edge parameter and blur parameter with Blob Style Density: **Recall** 120
28 Relationship between edge parameter and blur parameter with Blob Style Density: **F** 121

29 Feature extraction process with the central pixel a_{22} and its 8-neighbourhood, along with the intensity variation computation and the representation of the rolling window used. 125
30 Diagram illustrating the BBS approach used in this study and the process for evaluating performance. In the depiction of the sliding window, a_{22} is identified as the central pixel. 127
31 Visual comparison of features and edges extracted from the original image 106005 in the BSDS test set using the most effective methods in comparison to the conventional Canny edge detector. 129

32 Methodology pipeline proposed for our work 133
33 Illustrative single-window computation on a 3×3 neighbourhood and the computation example for this window. 136
34 Four operator pairs on the house image. Each block shows feature (left) and edge (right). Top row: gravitational smoothing with C_F and F_{BPC} using $\delta_0 = |x - y|$. Bottom row: Gaussian smoothing with T_M using $\delta_4 = |x^2 - y^2|$ (left) and $\delta_5 = (\sqrt{x} - \sqrt{y})^2$ (right). All cases use the power measure $\mathfrak{m}_{PM}(q = 0.1)$. 142

35 Multiscale channel mixed edge detection approach based on generalizations of choquet integral 149
36 Comparative Visualization of Edge Detection Algorithms: This figure presents the evaluation results of various edge detection algorithms against a predefined ground truth. The images are color-coded to reflect the detection accuracy: Green for True Positives (correct edge detection), Red for False Positives (incorrectly identified edges), Yellow for False Negatives (missed true edges), and White for True Negatives (correct non-edge identification). 153
37 Overview of the full experimental pipeline, from Gaussian–Sobel gradient extraction to multiscale Choquet-based fusion 157
38 Step signal $f(x)$ with a discontinuity at $x{=}0$ and its responses after Gaussian smoothing, $G_\sigma * f(x)$ for $\sigma \in \{0.5, 1, 2\}$. Increasing σ progressively blurs the step, reducing gradient sharpness and making gradients across scales not directly comparable. As discussed by (LOPEZ-MOLINA et al., 2011), this motivates the use of a scale-compensation factor so that multiscale gradients can be fairly fused/compared—an idea aligned with our pixelwise multiscale aggregation strategy. (Figure adapted from (LOPEZ-MOLINA et al., 2011).) 158
39 Multiscale edge behavior and fusion. *Top row:* Gaussian smoothing at $\sigma \in \{0, 1, 2, 4, 8\}$ progressively blurs tonal transitions. *Middle row:* per-scale edge maps (e.g., Canny/Sobel-based) show that small σ preserves sharp details but is noise-prone (higher FP), while large σ suppresses noise (lower FP) yet broadens contours and may miss fine structures (lower TP). *Bottom:* pixelwise multiscale fusion (example: $D\text{-}XCE$ with F_{NA} and F_{SqSum} color aggregation) combines both regimes, improving the precision–recall balance. See (LOPEZ-MOLINA et al., 2011) for the rationale behind inter-scale compensation. 159
40 Visual comparison of edge continuity between our two best methods. Top: original image and one ground–truth map. Middle: response of $\mathfrak{C}_{\mathfrak{m}}^{O_{RS},O_{RS}}$. Bottom: response of $\mathfrak{C}_{\mathfrak{m}}^{F_{NA},F_{NA}}$. The red ROI highlights regions where $\mathfrak{C}_{\mathfrak{m}}^{F_{NA},F_{NA}}$ exhibits longer, more connected contours with fewer breaks. 164
41 PR curve for the $\mathfrak{C}_{\mathfrak{m}}^{O_{RS},O_{RS}}$ 165
42 Comparison of our best method with other methods from the literature. 167

TABLE LIST

1 Aspectual model of an edge according to the Clouser–Dooyeweerd ontology. 41

2 Functions used to expand the Choquet Integral 56

3 $\mathfrak{C}_{\mathfrak{m}}^{T}$ and $\mathfrak{C}_{\mathfrak{m}}^{F}$-integrals used in Chapter 10, as generalisations of the Choquet integral for a fuzzy measure $\mathfrak{m}$ 59

4 Examples of Restricted Dissimilarity Functions (RDFs). 63

5 The gradient magnitude and orientation calculation for a scalar image I where I_θ represents the derivative of the image using the first-order filter in orientation θ in radians (MAGNIER; ABDULRAHMAN; MONTESINOS, 2018). 74

6 Terms of Inclusion and Exclusion and Number of Selected Papers. Retrieved from (SILVA et al., 2023). 82

7 Papers in edge detection (RQG). Retrieved from (SILVA et al., 2023). 83

8 Works in edge detection based on fuzzy logic (RQF). Retrieved from (SILVA et al., 2023) 91

9 Found and included papers 102

10 Summary of papers by method 103

11 Queries Used in Research on the Effects of Blurring on Edge Detection 107

12 Correlations between Sigma, Precision (Prec), and Recall (Rec) for different types of blurring 116

13 Statistics for Gravitational, mshift, and Gaussian methods 116

14 Optimal values of metrics for each method with Canny fixed at 2.25 . 118

15 Median and Standard Deviation of blur parameter for Different Percentiles of the Metrics Prec, Rec, and F 119

16 Quantitative analysis results 120

17 Comparison of various setups for the power measure using the Choquet integral and its generalisations, alongside the Canny method, in terms of PREC, REC, and $\mathrm{F}_{0.5}$. The tests were conducted after applying Gaussian smoothing with sigma (σ) values of 1 (S_1) and 2 (S_2) and using adaptive q from intensity variations. 128

18 Comparison of various setups for the power measure using the Choquet integral and its generalisations, alongside the Canny method, in terms of PREC, REC, and $F_{0.5}$. The tests were conducted after applying Gaussian smoothing with sigma (σ) values of 1 (S_1) and 2 (S_2) and using adaptive q from pixel intensity values. 131

19 Channel-fusion formulas organized for reference. 137
20 Best operators per scenario and criterion (mean/median of F over $n = 200$ images), using the notation adopted in the chapters for functions, measures, and dissimilarities. 141
21 External context. Reported best-F values on BSDS500 from prior work (LIU et al., 2019; LIU et al., 2021; LIU et al., 2018; CHENG et al., 2016). Numbers are not directly comparable to our single-scale, fixed-threshold evaluation; no inferential claims are made against these methods. 144
22 External aggregation-based context on BSDS500 (S_2, reporting $F_{0.5}$ only). Left: representative top entries from Marco-Detchart et al. (2025); centre: representative top entries from Marco-Detchart et al. (2021); right: ours (fixed q=0.1, single–scale, fixed threshold). Descriptive only: values reproduced from prior work; not directly comparable to our single–scale evaluation; no hypothesis testing is performed against these methods. 145
23 Mean $F_{0.5}$ of the three best results for methods in UDED database and Optimal Dataset Scale (ODS) of the benchmark reported in (SORIA et al., 2023). 146

24 Standard extensions results with individual Canny channel results . . 151
25 Descriptive summary of $\bar{F}$ (F-measure) for the reference method and the F_{GL} and AVG operators. 154
26 Inferential summary of the comparison between the reference method and the F_{GL} and AVG operators. 154
27 Expanded extensions results 155

28 Top 10 results of our method with different aggregation and color fusion strategies. 162
29 Top configurations and their performance metrics 162
30 Top configurations and their performance metrics 162
31 Approximate ($F_{0.5}$) ranges of h_i 163
32 ODS/OIS/AP on BSDS500 for a range of trained and untrained methods reported in prior work, compared to our two best configurations. 166
33 Top 10 results of our method for UDED database using the functions applied to the BSDS500 dataset 169
34 Top 18 results of our method for UDED database with all combinations.170

SYMBOLS LIST

N	Set of indices, defined by $N = \{1, \ldots, n\}$
n	Number of elements or dimension of the input vector
2^N	Power set of N
$[0, 1]$	Unit interval
$[a, b]$	Arbitrary closed interval
$\vec{x}$	Input vector, typically $\vec{x} = (x_1, \ldots, x_n)$
$\boldsymbol{x}$	Input vector in bold notation
x_i	i-th component of the input vector
$x_{(i)}$	i-th component of $\boldsymbol{x}$ after increasing rearrangement
$x_{(0)}$	Convention used in the integrals, with $x_{(0)} = 0$
$A_{(i)}$	Subset of indices corresponding to the $n - i + 1$ largest components of $\boldsymbol{x}$
$\vec{r}$	Direction vector used in directional monotonicity
$\vec{0}$	Null vector
$\vec{1}$	Unit direction vector
c	Positive scalar used in directional shifts
k	Positive scalar used in $\vec{k}$-increasing and $\vec{k}$-pre-aggregation contexts
X, Y	Subsets of N
$\lvert X \rvert$	Cardinality of the set X
$\emptyset$	Empty set
$\mathfrak{m}$	Fuzzy measure
$\mathfrak{m}_{PM}$	Power measure
q	Exponent parameter of the power measure
$m_{(i)}$	Shorthand notation for $m(A_{(i)})$
F	Generic fusion function used in the experiments
A	Aggregation function
PA	Pre-aggregation function

F_1, F_2	Pair of fusion functions used in the $C_{F_1F_2}$-integral
$\mathfrak{C}_{\mathfrak{m}}$	Discrete Choquet integral with respect to the fuzzy measure $\mathfrak{m}$
CI	Abbreviation for Choquet integral
$\mathfrak{C}_{\mathfrak{m}}^{F}$	CF-integral with respect to the fuzzy measure $\mathfrak{m}$ and fusion function F
CF	Choquet-type integral obtained by replacing the product with a fusion function
$\mathfrak{C}_{\mathfrak{m}}^{C}$	CC-integral with respect to the fuzzy measure $\mathfrak{m}$ and copula C
CC	Choquet-type integral obtained from the expanded form using a copula
$\mathfrak{C}_{\mathfrak{m}}^{F_1,F_2}$	$C_{F_1F_2}$-integral with respect to the fuzzy measure $\mathfrak{m}$
$\mathfrak{C}_{\mathfrak{m}}^{(F_1,F_2)}$	Alternative notation for the $C_{F_1F_2}$-integral
$C_{F_1F_2}$	Generalized Choquet-type integral based on the pair (F_1, F_2)
T	t-norm
S	t-conorm or, when explicitly defined as $S(x, y)$, a specific bivariate function
C	Bivariate copula
O	Overlap function
AVG	Arithmetic mean aggregation function
T_M	Minimum t-norm
T_P	Algebraic product t-norm
$T_{\text{Ł}}$	Łukasiewicz t-norm
T_{DP}	Drastic product t-norm
T_{NM}	Nilpotent minimum t-norm
T_{HP}	Hamacher product t-norm
O_B	Overlap function defined by $O_B(x, y) = \min\{x\sqrt{y},\ y\sqrt{x}\}$
O_{mM}	Overlap function defined by $O_{mM}(x, y) = \min\{x, y\}\max\{x^2, y^2\}$
O_{Div}	Overlap function defined by $O_{Div}(x, y) = \dfrac{xy + \min\{x, y\}}{2}$
O_{RS}	Overlap function defined by $O_{RS}(x, y) = \min\left\{\dfrac{(x+1)\sqrt{y}}{2},\ y\sqrt{x}\right\}$
O_α	Family of copulas or overlap functions
α	Parameter of the family O_α, with $\alpha \in [-1, 1]$
GM	Geometric mean
HM	Harmonic mean
S_M	Maximum t-conorm
C_F	Copula defined by $C_F(x, y) = xy + x^2y(1-x)(1-y)$
C_L	Copula defined by $C_L(x, y) = \max\{\min\{x, \frac{y}{2}\},\ x + y - 1\}$

F_{GL}	Fusion function defined by $F_{GL}(x,y) = \sqrt{\frac{x(y+1)}{2}}$
F_{BPC}	Function defined by $F_{BPC}(x,y) = xy^2$
F_{NA}	Pre-aggregation function
F_{NA2}	Pre-aggregation function
x, y	Input values in the unit interval
$\min$	Minimum operator
$\max$	Maximum operator

CONTENTS

1 Introduction **20**
1.1 Justification . . . 23
1.2 Research Problem . . . 24
1.3 Objectives . . . 24
1.4 Thesis Organization . . . 25

2 Thesis Methodology **27**

3 Philosophical Concepts and Reflections **30**
3.1 Initial Provocations on Perception for Philosophy and Neuroscience . . . 31
3.2 Attempts to Establish a Definition of Edges . . . 32
3.3 The Issue of the Fuzzy Nature of Edges . . . 35
3.4 Proposed Definition and Reflection on Edge Detection Models . . . 36
3.5 Chapter Conclusion . . . 43

4 Mathematical Foundations **45**
4.1 Aggregation and Pre-aggregation functions . . . 45
4.1.1 Introduction to Aggregation-like Functions . . . 46
4.1.2 Fuzzy measure-based fuzzy integrals . . . 53
4.1.3 Generalizations of the standard form of the Choquet integral . . . 56
4.1.4 Generalizations of the expanded form of the Choquet integral . . . 60
4.1.5 Generalizations of the Choquet Integral by Restricted Dissimilarity Functions (RDF) . . . 62
4.2 Chapter Conclusion . . . 65

5 Image Processing Topics **68**
5.1 Filtering . . . 68
5.1.1 Filtering methods in digital images . . . 69
5.1.2 Conditioning filters . . . 69
5.1.3 Derivation filters . . . 71
5.2 Edge Detection Methods . . . 72
5.2.1 Gradient-based methods . . . 72
5.2.2 Region-based segmentation methods . . . 75
5.2.3 Methods based on machine learning . . . 75
5.2.4 Fuzzy Logic-based methods . . . 75
5.3 Dataset and quantification of the results . . . 77
5.4 Chapter Conclusion . . . 78

6 Systematic Review of Edge Detection Methods Based on Fuzzy Logic 80
6.1 Methodology . . . 80
6.1.1 Systematic literature review . . . 80
6.1.2 Definition of criteria, search in the indexing bases and obtaining primary research . . . 81
6.1.3 Bibliometric analysis . . . 82
6.2 Results and discussion . . . 82
6.2.1 State of the Art in Edge Detection (RQG) . . . 83
6.2.2 Fuzzy logic-based edge detection methods (RQF) . . . 89
6.3 Chapter Conclusion . . . 95
6.3.1 Publication . . . 97

7 Systematic Review of Aggregation Functions Applied to Edge Detection in Digital Images 98
7.1 Materials and Methods . . . 99
7.1.1 Systematic literature review scope . . . 99
7.1.2 Definition of criteria, search in indexing databases and obtaining primary research . . . 99
7.2 Results and Discussion . . . 100
7.2.1 Summary of methods . . . 101
7.3 Chapter Conclusion . . . 104
7.3.1 Publication . . . 105

8 Systematic Review of the Impact of Smoothing on the Performance of Edge Detection 106
8.1 Materials and Methods . . . 106
8.2 Results and discussion . . . 107
8.3 Chapter Conclusion . . . 110
8.3.1 Publication . . . 111

9 Experimental Investigation of the Impact of Smoothing on the Performance of Edge Detection 112
9.1 Related works . . . 112
9.2 Objectives . . . 113
9.3 Materials and Methods . . . 114
9.3.1 Dataset and quantification of the results . . . 115
9.4 Results and discussion . . . 115
9.5 Chapter Conclusion . . . 120
9.5.1 Publication . . . 122

10 Sliding-window-based adaptive fuzzy measure for edge detection 123
10.1 Sliding-window based adaptative fuzzy measure framework . . . 124
10.2 Experimental setup . . . 126
10.3 Results . . . 127
10.4 Chapter Conclusion . . . 132
10.4.1 Publication . . . 132

11 Edge Detection Approach Based on Generalizations of Choquet-like Integrals by Restricted Dissimilarity Functions **133**
11.1 Edge Detection Framework Proposed . . . 133
11.2 Quantitative Evaluation . . . 137
11.2.1 Quantitative evaluation . . . 137
11.2.2 External comparative evaluation . . . 139
11.3 Results And Discussion . . . 140
11.3.1 Significance testing (paired design) . . . 141
11.3.2 External context . . . 142
11.3.3 Testing in the Unified Dataset for Edge Detection . . . 144
11.4 Chapter Conclusion . . . 146
11.4.1 Publication . . . 147

12 Multiscale Channel-Mixed Edge Detection Approach Based on Generalizations of the Choquet Integral **148**
12.1 Methodology . . . 148
12.2 Results . . . 151
12.3 Chapter Conclusion . . . 154

13 Multiscale Choquet-based Aggregation Approach for Edge Detection **156**
13.1 Introducing the New Choquet Multiscale – Edge Detection (GMC-ED) . 156
13.1.1 Processing Step . . . 157
13.2 Experimental Framework . . . 160
13.3 Results and Discussion . . . 161
13.3.1 Evaluation on the Unified Dataset for Edge Detection . . . 168
13.4 Chapter Conclusion . . . 169

14 Conclusion **172**
14.1 Scientific Contributions Developed During the Thesis Period . . . 176

References **180**

1 INTRODUCTION

Edge detection represents an important task in several steps of computer vision and image processing (ZHANG et al., 2016; WEI et al., 2017; ARBELAEZ et al., 2014; WANG; HUANG; XU, 2010), such as object detection, pattern recognition, photo-sketching, image retrieval, face recognition, corner detection, road detection, and target tracking, multi-agent system applications, and more.(YANG; KRIEGMAN; AHUJA, 2002; ZHAO; HUANG; SUN, 2004; CHEN et al., 2005; DOLLAR; TU; BELONGIE, 2006; MAHDJOUB et al., 2006; SHOTTON; BLAKE; CIPOLLA, 2008; LI; ZHENG; HUANG, 2008; VU; CAPLIER, 2012; ZHANG et al., 2014; LIN et al., 2015; OJHA; SAKHARE, 2015; ZHANG; SHUI, 2015; GORDO et al., 2016; LEAL-TAIXé; CANTON-FERRER; SCHINDLER, 2016; DROLIA et al., 2017; CHI et al., 2017; PAVITHRA; SHARMILA, 2018; RADENOVIC et al., 2018; XU; BROWNJOHN; KONG, 2018; LI et al., 2019; ZHANG et al., 2019; MOHAN et al., 2021). Broadly speaking, we can say that edge detection consists of algorithms capable of locating, or segmenting, the contours of an object in an image.

In recent years, the study of edge detection has gained momentum due to its importance in various applications such as autonomous cars (MUTHALAGU; BOLIMERA; KALAICHELVI, 2020; DAOU et al., 2020); augmented reality (ORHEI; VERT; VASIU, 2020; KüHNE; RICHTER; BEIER, 2001); image colorization (HUANG et al., 2005; SUN et al., 2019; WHARTON; PANETTA; AGAIAN, 2007), medical image processing (ORUJOV et al., 2020; JAMAL; ISHAK; ABDEL-KHALEK, 2021; QIU et al., 2021a) and more (HUANG; HUANG, 2025; MAHADEV et al., 2026; SHAHADE; DESHMUKH, 2026; HUANG et al., 2026).

In the history of computation, the development of edge detection methods sought to operationalize analogous definitions within the paradigm of properties such as variations or differences in tone and texture. The method proposed by Roberts (ROBERTS, 1980) is the earliest found in the literature, having emerged in 1963 as a result of his doctoral thesis. Roberts calculates the derivative by taking the square root of the difference between diagonally adjacent pixels, focusing on the invariant properties exhibited by edges.

Subsequently, the Sobel (SOBEL; FELDMAN, 1973) and Prewitt (PREWITT, 1970)

operators emerged, emphasizing the importance of gradients in identifying edges. The Sobel detector computes the gradient value at each pixel using a fixed operator, whereas the Prewitt method uses a similar technique but without adjustment coefficients, varying only by a constant value, and calculates the gradient magnitude based on image orientations.

Later, the Canny method (CANNY, 1986) significantly enhanced the edge detection process by incorporating Gaussian smoothing followed by a gradient operation and thresholding, becoming one of the most widely used methods to this day and strongly influencing subsequent research. The use of pyramidal methods (ADELSON et al., 1983) enabled multiscale image analysis, while the introduction of fuzzy concepts by Kosko (KOSKO, 1996) and Russo (RUSSO, 1998) represented a substantial advancement in edge detection under noisy conditions (ABE, 1997).

As edge detectors became more complex, a need arose to understand the process clearly and to establish a standardized approach, enabling consistent comparisons between different methods. One of the most influential proposals in this regard is that of Bezdek, Chandrasekhar e Attikouzel (1998a), which decomposes edge detection into four stages, including the conditioning stage and the blending, or fusion stage.

Initially, edges were seen as just the basic building blocks for more complex visuals in pictures. It was believed that edges were crucial for how the whole system worked. This idea was supported by neurophysiological experiments by Hubel and Wiesel (HUBEL; WIESEL, 1961; HUBEL; WIESEL, 1962b), proving that contour detection was based on early receptive fields in the human visual system, and inspired works like the brain-inspired approach proposed by Marr and Hildreth (MARR; HILDRETH, 1980; MARR, 1982), Marr thought edges were so crucial that he made them an essential part of his *Primal Sketch* idea (MARR, 1976).

The beginning of the 21st century marked notable progress in the fusion of local and global features, highlighting the fuzzy K-nearest neighbor algorithm, Celenk's approach, and Lowe's SIFT technique (KELLER; GRAY; GIVENS, 1985; LOWE, 2004), all of which are fundamental to image recognition.

Recent research has emphasized the fusion stage and edge detection with deep learning, including multiscale methods and deep convolutional networks such as AlexNet, alongside the refinement of classical techniques like modified Sobel methods (LOPEZ-MOLINA et al., 2011; KRIZHEVSKY; SUTSKEVER; HINTON, 2017), while also using models based on fuzzy theory (ZADEH, 2008) and aggregation functions (GRABISCH et al., 2009). This includes fuzzy integrals, such as those proposed by Marco-Detchart et al. (2023a), Marco-Detchart et al. (2023b), Marco-Detchart et al. (2021), which apply generalizations of the Choquet integral (CHOQUET, 1953–1954) to consider interrelationships between inputs (SILVA et al., 2023; TICALA; PINTEA; MATEI, 2021; AMORIM et al., 2023; AMORIM et al., 2025).

This integral have been applied to simulate the behavior of the information flow in the visual cortex in the task of edge detection and image segmentation, as well as to assist in the decision making of other algorithms with the same objective (see, e.g: (MARCO-DETCHART et al., 2021; QIU et al., 2021b; PAP; NEDOVIć; RALEVIć, 2021; MARCO-DETCHART et al., 2018a; RALEVIć; DELIć; NEDOVIć, 2022; AGGARWAL et al., 2019; DIMURO et al., 2017; DELIć; NEDOVIć; PAP, 2019; NEDOVIC; RALEVIC; PAVKOV, 2018)).

Despite the efforts devoted to the development of edge detection methods within an unsupervised paradigm, as highlighted by Huang e Huang (2025), the current state of the art in edge detection is still largely dominated by approaches based on deep neural networks:

> In recent years, deep learning has achieved groundbreaking advancements in the field of image recognition, sparking a wave of research interest in neural network-driven approaches. As a result, a wide array of deep learning-based methods for edge and contour detection have emerged, consistently surpassing the performance of traditional algorithms. These methods not only offer *superior accuracy* [...], these neural network-based methods can autonomously learn complex feature hierarchies, enabling more nuanced and robust edge and contour detection. (HUANG; HUANG, 2025).

According to the authors, although deep learning models achieve remarkable performance, they rely heavily on carefully annotated datasets, which entail high computational costs and substantial human effort (SHORTEN; KHOSHGOFTAAR, 2019; HUANG; HUANG, 2025). In line with this critique, Zhou et al. (2023) further emphasizes that the impressive advances in deep edge detection are fundamentally constrained by their dependence on large-scale, high-quality manual annotations. As discussed by the authors, edge labeling is particularly expensive and subjective, often requiring several minutes per image and leading to inconsistencies among annotators, which, in turn, complicates training and limits scalability. For this reason, according with Huang e Huang (2025) "[...]some studies are beginning to explore self-supervised, weakly supervised, and unsupervised learning to mitigate reliance on labeled datasets.".

Moreover, supervised deep models tend to conflate edges arising from object boundaries with those induced by texture or noise, especially when trained on datasets with ambiguous or heterogeneous annotations. This reliance on human-labeled data not only introduces epistemic uncertainty into the learning process but also conflicts with the theoretical characterization of edge detection as a low-level visual task, traditionally addressed through unsupervised or weakly supervised mechanisms inspired by early human vision. Consequently, as argued by Zhou et al. (2023), the dominance of fully supervised deep learning approaches reveals structural limitations that motivate the investigation of unsu-

pervised frameworks capable of leveraging multiscale information while reducing dependence on costly and inconsistent ground-truth annotations.

Additionally, their *black-box* nature limits interpretability and does not fully align with human visual processes, making it difficult to overcome conceptual and cognitive bottlenecks (ELDER, 2018). In contrast, biologically inspired approaches show potential to mitigate these limitations by seeking closer alignment with principles of the biological visual system (HUANG; HUANG, 2025).

Nevertheless, as also emphasized by Huang e Huang (2025), biologically inspired methods still face relevant challenges. With a few recent exceptions (LIN et al., 2024; DING et al., 2024; ZENG et al., 2011; LUO et al., 2023; PANG et al., 2024), most of these approaches are unsupervised, yet they often achieve performance comparable to classical methods.

The main bottlenecks lie in the fact that many biologically inspired models still lack explicit learning mechanisms and therefore rely on manual parameter tuning, which reduces adaptability, hinders systematic optimization, and may introduce biases. In addition, several approaches place excessive emphasis on local information while neglecting global contextual cues, thereby compromising robust edge and contour detection in complex scenes. Finally, despite recent advances, these models reproduce only a limited fraction of the capabilities of the biological visual system.

1.1 Justification

The growing demand for computer vision solutions, both in cloud-based environments and in edge computing, has reinforced the need for methods that are efficient, lightweight, and reliable. Even in cloud architectures, especially in large-scale projects involving massive data processing, reducing computational costs can be a decisive factor in making a solution viable. At the same time, in embedded and edge-based scenarios, local processing remains highly relevant, particularly when privacy, data security, and data sovereignty are key concerns. Within this context, edge detection plays a fundamental role, as it serves as a basic step for many downstream computer vision tasks, including segmentation, pattern recognition, tracking, and scene analysis. For this reason, investigating methods that combine low computational cost with strong generalization ability remains both timely and strategically important, especially for deployment on devices with limited resources.

On the other hand, trained approaches, such as those based on neural networks, usually depend on large labeled or manually annotated datasets, which involve substantial costs in time, human effort, and quality control. Even when annotations are assisted by other artificial intelligence systems, manual validation is still required to ensure consistency and reliability. In addition, these methods demand considerable computational power, particularly during the training of new models, which limits their adoption in scenarios

with hardware and energy constraints.

In this scenario, it becomes particularly relevant to investigate alternatives that do not rely on intensive supervised training or large volumes of human annotations, yet are still capable of consistently exploiting relationships among visual attributes across different scales and channels. This perspective is especially promising in edge detection, since this task involves the integration of heterogeneous information, such as contrast, local intensity variations, and spatial structure, whose combination can be modeled by mathematical aggregation functions with different properties.

1.2 Research Problem

Considering the inherent challenges of the edge detection task and the importance of this topic for advancing the state-of-the-art in the areas of computer vision and image processing, with diverse applications in various fields and growing notoriety, as already mentioned, it is noteworthy that "black box"edge detection methods, such the need for large datasets for training. This can generate significant financial implications in the future, as data is becoming an increasingly valuable resource. In this context, "white box"methods, based on rules and functions that do not require training, are assuming increasing importance. In view of this, the feasibility of integrating and resolving the different approaches and problems mentioned is questioned. This questioning instigates the following research problem:

Is it possible to integrate generalizations of the Choquet integral, taking into account the fuzzy aspects inherently associated with edges, into a edge detection method capable of approaching the performance of supervised, learning-based edge detection models reducing dependence on annotated data?

1.3 Objectives

Therefore, the general objective of this thesis is:

To propose a family of new edge detection methods based on generalizations of the Choquet Integral, aiming to improve the metrics in computer vision and image processing applications.

In order to achieve the general objective of this research, some specific objectives have been outlined:

1. Evaluate the state of the art of edge detection methods using fuzzy methods, considering modeling that takes into account the diffuse nature of edges through fuzzy theory, aiming to identify the strengths and limitations of these methods (See Chapter 6).

2. Assess the state of the art of edge detection methods using aggregation and pre-aggregation functions, analyzing how these techniques can contribute to more precise and robust edge detection in images (See Chapter 7).

3. Understand the effects of smoothing, the main stage of conditioning an image for edge detection, by exploring different smoothing methods and their impact on edge detection (See Chapters 8 and 9).

4. Develop a family of edge detection method based on Generalizations of Choquet Integral, and a fuzzy measure, aiming to integrate contextual and spatial information for more precise and adaptive edge detection in different types of images (See Chapter 10 and 11).

5. Develop a family of edge detection methods based on generalizations of the Choquet integral and a fuzzy measure, using a pointwise and multiscale approach (see Chapters 12 and 13).

1.4 Thesis Organization

Beyond this introduction, this thesis is organized as follows: Chapter 2 presents the general methodology of the thesis and explains the relationship among the chapters. Chapter 3 discusses philosophical concepts and initial reflections on the notion of edges. Chapter 4 presents the mathematical foundations of the thesis, including the definitions of aggregation functions, pre-aggregation functions, and fuzzy measures, as well as the family of functions adopted in this work, particularly in Section 4.1. In addition, the chapter devoted to topics in image processing (Chapter 5) addresses concepts related to filtering, edge detection methods, and the main segmentation dataset used throughout the thesis, as presented in Sections 5.1, 5.2, and 5.3, respectively.

Chapter 6 will present a systematic review of fuzzy edge detection methods. Chapter 7 will conduct an extensive systematic review of aggregation and pre-aggregation methods applied to edge detection. Chapter 8 will undertake a systematic review of the impact of smoothing filters. Chapter 9 will present an experimental investigation into the impacts of smoothing filters. Chapter 10 will introduce a sliding window-based edge detection model using fuzzy measures. Chapter 11 proposes an edge detection method based on the aggregation of local visual cues and employs different operators derived from variants of the Choquet integral with restricted dissimilarity functions (RDFs). Chapter 12 will propose a multiscale channel mixed edge detection based on aggregation functions, with partial results presented. Lastly, in Chapter 13, we propose a new multiscale edge detection approach based on generalizations of the Choquet integral. This method consists of performing multiple edge detections at different scales using Gaussian filtering with

Sobel operators, followed by a pointwise aggregation of the extracted features or visual cues.

In addition, the thesis includes a final chapter devoted to the main conclusions, contributions, limitations, and possible directions for future research.

2 THESIS METHODOLOGY

In order to address the specific questions outlined and, consequently, the proposed research problem, a general methodology was designed consisting of a comprehensive set of theoretical foundations, three systematic literature reviews, an experimental investigation on the impact of smoothing filters, and a series of methodological chapters aimed at exploring, from different perspectives, the use of generalizations of the Choquet integral in edge detection problems

Figure 1 summarizes the overall methodological structure of the thesis, highlighting the relationship between the review stages, the experimental analysis of smoothing filters, and the four proposed edge detection methods.

Initially, this work establishes the essential theoretical foundations, encompassing the philosophical, mathematical, and image processing concepts that underpin the research. Proceeding from the broadest scope to the most specific one in this thesis, the systematic reviews sought to identify the state of the art, first, in fuzzy-based edge detection methods, presented in Chapter 6, and, subsequently, in aggregation and pre-aggregation functions applied to edge detection, discussed in Chapter 7. In addition, a third systematic review, developed in Chapter 8, investigated the impact of smoothing filters on the performance of edge detection methods, since the conditioning stage constitutes an important part of the preprocessing of images submitted to segmentation.

Complementing this review stage, Chapter 9 presents an experimental investigation devoted to analyzing, in empirical terms, the effects of smoothing filters on edge detection performance. Thus, the thesis is not limited to a theoretical survey of the literature, but also incorporates a specific experimental stage to verify how these preprocessing strategies influence the obtained results.

After these investigations, groups of methods sharing common characteristics were identified, which made it possible to position the contribution of the family of methods proposed in this thesis and to justify some specific methodological choices adopted in each proposal. The literature review stages developed throughout the thesis were not conceived as identical methodological steps, but as complementary components serving distinct purposes within the overall research structure.

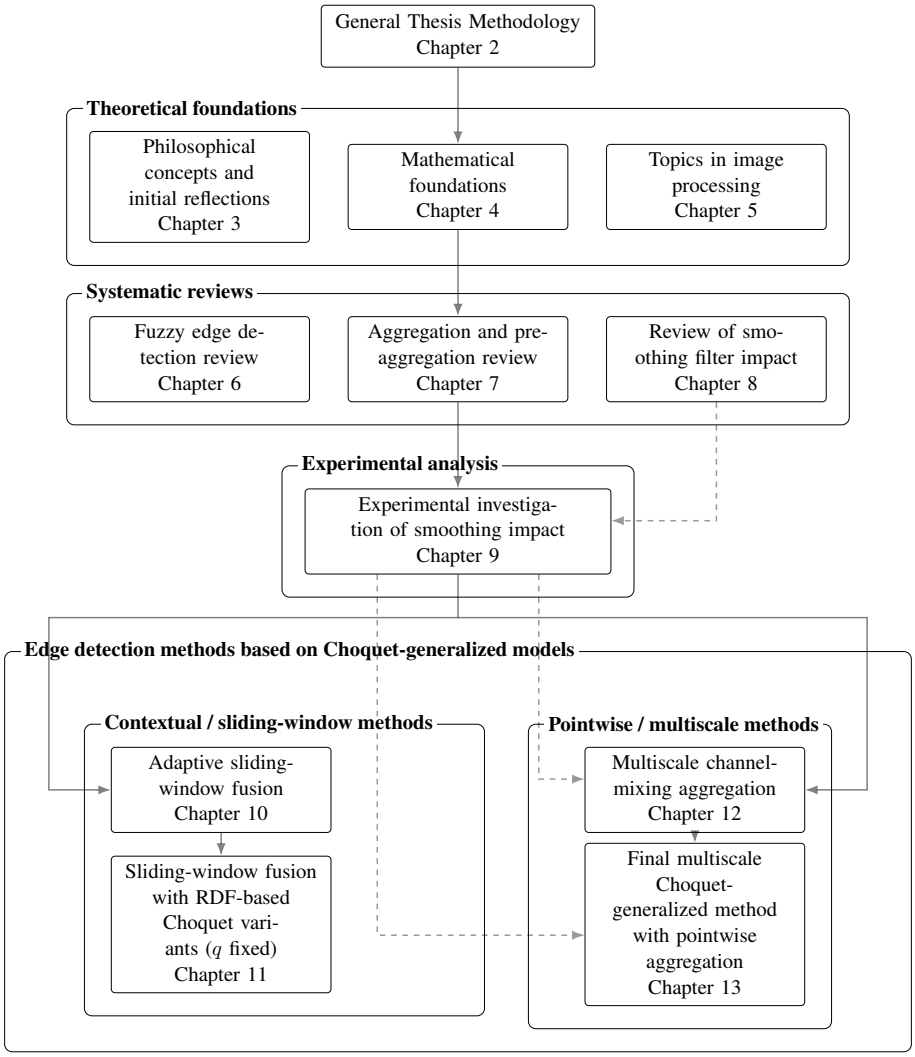


Figure 1: Overview of the thesis methodology.

In particular, bibliometric analysis was employed when the objective was to obtain a broader quantitative view of the field, including publication trends, thematic evolution, and the general structure of the scientific production related to the topic. In contrast, in the review stages devoted to the technical, mathematical, and experimental analysis of edge detection methods, bibliometric tools were not adopted, since the main goal was not to characterize the field statistically, but rather to critically examine methodological choices, operator properties, evaluation strategies, and performance behavior. In this way, the use or non-use of bibliometrics was defined according to the specific role that each review played in supporting the theoretical and methodological development of the thesis.

The first method in the family of edge detectors based on generalizations of the Choquet integral is presented in Chapter 10 and consists of an adaptive sliding-window-based approach that takes into account the immediate neighborhood of each processed pixel. In this case, the integrals are employed within an adaptive and contextual paradigm, in line with some trends observed in the literature.

Next, Chapter 11 continues the study of an edge detection method based on sliding-

window fusion, following the approach introduced in the previous chapter. In this case, however, the investigation incorporates operators derived from variants of the Choquet integral based on restricted dissimilarity functions (RDFs). In addition, the parameter q of the *power measure* is kept fixed, since the main goal at this stage is not to analyze the effect of the fuzzy measure itself, but rather to understand, in a more isolated way, the effects of the RDFs on edge detection performance, especially on the harmonic mean between precision and recall.

Chapter 12, in turn, presents a multiscale channel-mixing approach based on aggregation functions, in which partial results obtained from the combination of information extracted from different channels and scales are discussed. This stage contributes to broadening the investigation of fusion strategies in the context of edge detection.

Based on the partial results of this approach, the last method was developed and refined from the previous experiments. Chapter 13 then proposes a new multiscale edge detection method based on generalizations of the Choquet integral. This approach consists of performing multiple edge detections at different scales by means of Gaussian smoothing combined with Sobel operators, followed by a pointwise aggregation stage of the extracted features or visual cues. Compared with the previous chapters, this experiment is more comprehensive, allowing results in terms of precision, recall, and harmonic mean to be compared with several methods from the literature, including neural-network-based approaches.

Finally, it is worth noting that while this chapter outlines the general framework of the thesis, each subsequent chapter includes its own specific methodology section. These sections detail the particular procedures, experimental setups, and evaluation metrics adopted for the development of each specific study or proposed method.

3 PHILOSOPHICAL CONCEPTS AND REFLECTIONS

In order to provide a better understanding of the techniques that will be presented in this thesis, initially, in Section 3, we will address the issue of defining our object of study through a review of the philosophical concepts that involve this delimitation. Some initial provocations and an exposition of the philosophical and neuroscientific views regarding perception in a more comprehensive manner will be detailed in Subsection 3.1. Following this, attempts to establish a definition for edges, drawing from classical philosophy and modern psychology, will be addressed in Subsection 3.2. Subsequently, in Subsection 3.3, there will be some reflections on the diffuse nature of edges. Finally, in Subsection 3.4, a proposed definition of edges, developed by the author, will be presented, followed by a brief reflection on the impact of a clear and objective definition of this object on performance analysis through ground truths.

In his book "Urban Poverty", Milton Santos (SANTOS, 1978) discusses the application of statistical models in his field of research, asserting that these depend on a systematic understanding of the mechanisms of the phenomena under study. He continues by quoting Ch. Bettelheim (BETTELHEIM, 1951), who argues: "every measurement implies the development of a concept of what is measured [...] A measure results from a process of abstraction that, from the beginning, completely eliminates certain qualities.". In this context, it would be necessary to reexamine and renew concepts even before collecting statistics (SANTOS, 1978) (cited by McGee (MCGEE, 1971), 1971, p. 68).

Similarly, a computational or mathematical model advocates for the selection of a set of variables or qualities that are processed in a specific manner, which presupposes a prior understanding of what is being modeled and, consequently, excludes all other qualities and processes. Paraphrasing Bachelard (BACHELARD, 1993), it is more important to understand the phenomenon than to develop a model for it.

Therefore, establishing a precise definition through a deep understanding of the phenomenon to be modeled becomes essential within the mathematical-computational context. Defining what constitutes an edge is more crucial than simply measuring or creating a model to detect it.

To achieve an adequate definition of the concept of an edge in computer vision, it is

imperative to consider the concept of perception in the history of philosophy and neuroscience. These fields have influenced and continue to influence the assumptions of existing mathematical-computational models.

3.1 Initial Provocations on Perception for Philosophy and Neuroscience

Perception has been extensively debated in philosophy since antiquity, with discussions by Aristotle, Thomas Aquinas, Descartes, and Locke, thus permeating the tensions between rationalism and empiricism. These definitions of perception even impact epistemic questions; for example, in Descartes' rationalism, it is emphasized that true understanding of reality comes exclusively from reason, independent of sensory experiences. In this context, the transition from sensation to perception occurs through an action of the intellect of the individual who knows, which assigns organization and meaning to sensations (DESCARTES, 1999; MARÍAS; BERLINER, 2004; COSTA, 2005).

Empiricism, defended by Locke and Hume, argues that knowledge originates solely from sensory experiences. Sensation and perception would depend on external things that act upon the nervous system and receive a response from the brain (HESSEN, 1968). There is also a differentiation between primary and secondary qualities of objects, suggesting that some qualities are inherent to the objects while others depend on the observer (LOCKE, 1823; SCHULTZ; SCHULTZ, 1996). Hume further posits that ideas are derived from the simplest perceptions and emanate directly from sensory experience (HUME, 2013).

The theory of perception has significantly evolved with contributions from Kant, who was influenced by Hume's empiricism and the rationalism of Newton and Leibniz. Kant proposed a synthetic approach that considers knowledge to be initiated by experience but not entirely derived from it (KANT, 2020). In the 20th century, phenomenology and Gestalt psychology advanced the understanding of perception by highlighting that perception and sensation are interconnected, forming a process in which the mind perceives holistic structures rather than just isolated elements (FUSTER, 2002; LUIJPEN, 1973). These approaches reinforce the dynamic interaction between subject and object in perception, demonstrating the complexity of human perceptual experience and the inseparability of mind and body in the constitution of perceptual knowledge.

In the field of neuroscience, perception is understood as the ability of human beings to associate sensory information with memory and cognition, forming concepts about the world and guiding behaviors (LENT, 2004). This capacity transcends mere sensory reception, involving complex processes that integrate memory, cognition, and actions, highlighted by perceptual constancy. Perception preserves the identity of objects despite variations in the images projected onto the retina, enabling the recognition of an object un-

der different lighting conditions or perspectives (PURVES et al., 2007; BRODAL, 1981).

Moreover, visual perception, like other sensory modalities such as auditory and somesthetic, begins with sensory analysis that fragments perceptions into their fundamental characteristics, such as color, movement, among others. However, the final perceptual experience does not merely consist of the sum of these parts but rather in a holistic and unified perception of the world. This suggests that, in addition to analytical mechanisms, there are synthetic processes in the brain that integrate this information into a coherent and meaningful whole (KELSO, 1995).

This advanced perspective on perception highlights the complexity and dynamics of brain interactions that shape how we perceive reality. Therefore, models of perception must incorporate mechanisms capable of integrating various sources of sensory information to produce a unified and coherent representation of the world. Consequently, such models do not treat each sensory element in isolation, but consider how these elements interact and combine to form the complete perceptual experience.

3.2 Attempts to Establish a Definition of Edges

The contents of visual perception are typically structured, in a simplified manner, according to the figure-ground relationship, where the organization of the visual field is mediated by objects that stand out from their backgrounds (RUBIN, 1915). This configuration creates a tension between articulations of bona fide, or natural, edges and fiduciary, or artificial, edges.

On one hand, the objects we track easily are those distinguished by the natural borders they appear to possess. On the other hand, it is also true that the analysis of a visual scene incorporates the creative contribution of the perceptual apparatus. The classic study by Schumann on illusory contours demonstrates the tendency to represent reality in terms of continuous edges, even though these may not actually exist (SCHUMANN, 1900).

The Kanizsa Triangle (KANIZSA, 1955) remarkably exemplifies this phenomenon (Figure 2). Other examples where boundaries emerge from figure-ground organization can be elucidated by the basic factors studied in Gestalt psychology, such as proximity, continuity, closure, similarity of color and texture, Prägnanz, good form, unity, segregation, and unification (WERTHEIMER, 1923; KOFFKA, 1935). Any work by the artist Seurat (Figure 3)[1] illustrates this dynamic well; he does not directly delineate lines or borders between objects, yet we perceive each object as if it has a defined contour.

Edge detection techniques for object recognition in image processing and computer vision (DAVIES, 2012) consider these bona fide aspects. Under certain circumstances, it can be said that edges correspond to significant discontinuities in the depth and luminosity of the scene. “Natural” discontinuities in visual scene segmentation stem from the

[1] Available at: www.artchive.com/artwork/the-seine-at-le-grande-jatte-georges-seurat-1888

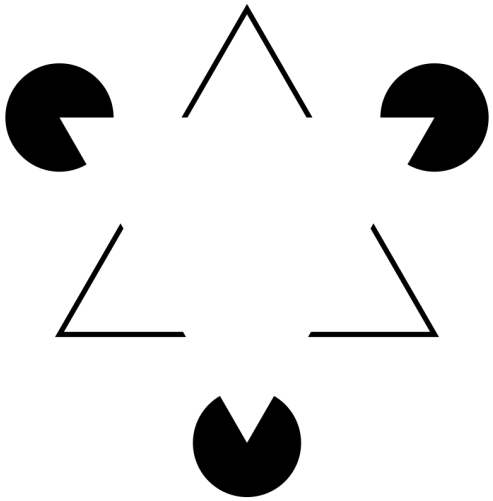


Figure 2: Illustration of the Kanizsa Triangle, demonstrating the phenomenon of visual perception of illusory contours and shapes. Adapted from (SAKIYAMA; SASAKI; GUNJI, 2014).

existence of a genuine boundary or edge, which constitutes an indicator of objectivity. It is observed that humans, from childhood, identify non-material entities, or ontologically negative ones, such as holes and shadows, as readily as they discern ontologically positive objects, such as material objects (GIRALT; BLOOM, 2000; NELSON; PALMER, 2001). However, this does not exhaust the possible definitions for this issue.

When reflecting on the concept of an edge or boundary, one generally conceives of an entity delimited by its surroundings, a limit that defines and contains it. This definition often encompasses any physical discontinuity or qualitative differentiation. At times, its exact location can be ambiguous or subject to controversy; however, whether sharp or diffuse, natural or artificial, it seems that each object has a boundary that distinguishes and separates it from the rest of the world.

There is a multitude of debates on whether the notion of an edge or boundary is coherent and reflects the structure of the world, or if it is merely the result of our mind's organizing activity or collective practices and conventions. These are controversial issues in the field of philosophy. However, it seems necessary to adopt a realistic stance within a computational scientific perspective, given that the purpose of scientific inquiry is the pursuit of objective truth rather than merely perceptual insights regarding the object of study. As aptly defined by St. Thomas Aquinas in his Summa Theologica, in question 78, article 4(AQUINO, 1947):

> "For the perception of sensible forms comes from sensible mutation, but not that of the intended intentional species. [...] Whereas, to apprehend the intentional species, which are not received by the sense, is the function of the estimative power." (Summa Theologica, 1265-

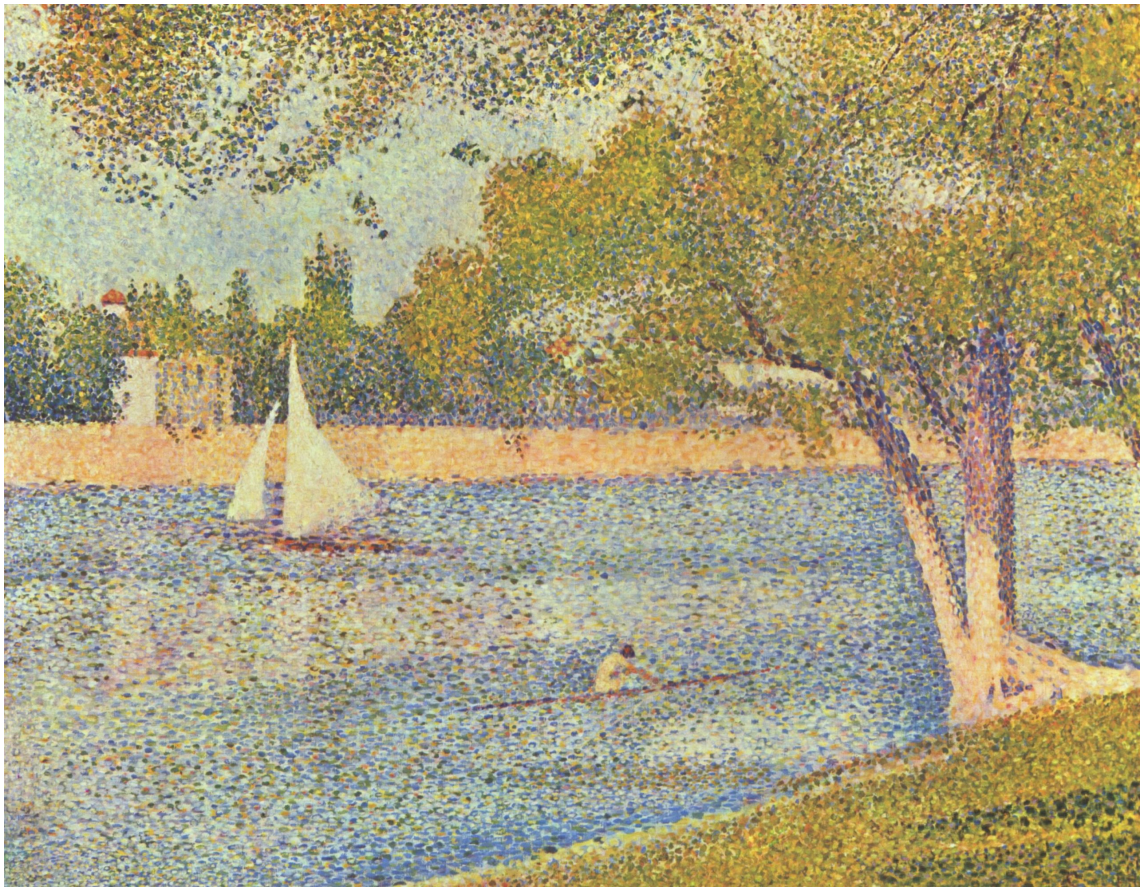


Figure 3: “The Seine at Le Grande Jatte,” a work by Georges Seurat from 1888, is an oil on canvas painting. This artwork exemplifies the technique of pointillism, an innovative approach to painting where small points of pure color are applied in a way that forms a coherent image when viewed from a distance. This technique was fundamental to the development of the post-impressionist movement in modern art. Retrieved from (GALLERY, 2024)

1274)(AQUINO, 1947)

Euclides defined an edge or boundary as “that which is the extremity of anything” (EUCLID, 1926) (Elements, I, def. 13). Aristotle, in Metaphysics, described it as “the first thing beyond which it is not possible to find any part [of the given thing], and the first within which every part is” (ARISTOTLE, 1984). These classical accounts are intuitive and comprehensive, providing a natural starting point for any further investigation into the concept of a boundary. In topology, as defined by Hausdorff in 1914 (HAUSDORFF, 1914) (in its Section 7.2), essentially reflects the same intuition: the boundary of a set A is the set of points whose neighbors intersect both A and its complement, forming a set of points that “surround” it. According to Merleau-Ponty in Phenomenology of Perception (MERLEAU-PONTY, 1962):

> “A contour is merely a sum of local views, and consciousness of a contour is a collective being. The sensory elements from which it is made cannot lose the opacity that defines them as sensory in order to open

> themselves to an intrinsic connection, to a common constitution law. Let A, B, and C be three points taken on the contour of a figure; their order in space is both their way of coexisting before our eyes and that very coexistence; no matter how close I choose them, it is the sum of their separate existences, the juxtaposition of A, plus the juxtaposition of B, plus the position of C. [...] But a contour is not just the set of present data; these evoke others that come to complete them. When I say that I have a red spot in front of me, the meaning of the word spot is provided by previous experiences during which I learned to use it. The spatial distribution of the three points A, B, and C evokes other analogous distributions, and I say that I see a circle" (MERLEAU-PONTY, 1962) (p. 36).

Throughout history, puzzles regarding the concept of a boundary or edge have arisen in the minds of great thinkers. Leonardo Da Vinci, in his Notebooks (VINCI, 1938), questioned: "What divides the atmosphere from the water? Is it the air or the water?" Francisco Suárez, in his Disputations (SUAREZ, 2023), inquired about the color of the demarcation line between a black spot and its white background, based on the principle that the boundary is always a property of the figure, while the background is topologically "open" (JACKENDOFF, 1987) (in its appendix B). These reflections naturally lead to the thought that all entities of the same type behave similarly.

Plato, in Parmenides, addressed the issue of boundaries concerning the problem of motion (PLATO, 1997): when an object begins to move or an object in motion stops, is it in motion or at rest? This is the famous problem of transition: to whom does the moment of transition belong, to the interval of motion or to the rest of the interval? (MEDLIN, 1963). Middle academics, in texts such as Noctes Atticae (GELLIUS, 1565) (VI, xiii, 5-6), were concerned with the situation of the dying person: does she die when already within the reach of death or while still alive? In summary, these dilemmas illustrate the paradoxical nature of instantaneous change.

3.3 The Issue of the Fuzzy Nature of Edges

There are conceptual distinctions between natural boundaries, which are objective insofar as they are based on some physical discontinuity or qualitative heterogeneity between an entity and its surroundings, and artificial boundaries, which, is supposed, are not as grounded in the autonomous and independent world apart from the mind (SMITH, 1995).

This is precisely one of the major concerns regarding boundaries: imprecision. Aristotle's definition, as well as standard topology, suggests a kind of delineation between the interior and exterior of a thing. However, it is observable that objects and events, as well as the extents of a range of concepts, may have boundaries that are uncertain, diffuse,

or indeterminate. Predicates like “bald” or “pile” seemingly do not have clearly defined boundaries. A radical approach would be to completely dismiss the question, after all, “an undefined boundary is not really a boundary” (WITTGENSTEIN, 1953).

However, perhaps the fuzzyness is purely epistemic, meaning that it arises from ignorance regarding the exact location of these relevant boundaries or edges, which in themselves would be perfectly clear. More adequately, fuzziness can be ontological in a non-reductionist sense, i.e., grounded in reality’s multiaspectual structure rather than exhausted by epistemic ignorance. Some predicates are vague precisely because their set does indeed have a diffuse boundary, as proposed by Zadeh (ZADEH, 1965). Therefore, there would be a linguistic or stipulative difficulty in precisely defining the set of objects corresponding to the extension of the predicate, an uncertainty or imprecision, indecision regarding the belonging of a certain object or entity to a certain group.

Another important issue relates to scale. It is observed, for example, that the boundaries of an object change depending on the scale of observation. This variation in perspective can reveal details that are imperceptible at a broader scale, while other aspects may become less evident or even disappear at smaller scales, as well as becoming more diffuse.

This phenomenon is particularly relevant in geographical and biological sciences, where understanding the boundaries of an ecosystem or a cell can vary significantly depending on the resolution of the observation instrument used. In cartography, for example, the level of detail in a map can influence the perception of political or natural boundaries, altering the way they are represented and understood. This has even motivated studies on fractal dimension in the literature, as seen in the works of Mandelbrot (MANDELBROT, 1983).

3.4 Proposed Definition and Reflection on Edge Detection Models

According to Huang e Huang (2025), the hierarchical model of object recognition suggests that perception involves, at a minimum, two stages: a low-level stage, which extracts visual features such as edges, contours, and boundaries; and a high-level stage, which relates visual stimuli to stored features for identification. This highlights the importance of edge and contour detection in object recognition. Here, it becomes clear how the authors present a distinction already established in the literature between edges, contours, and boundaries.

The difference among these three entities has been the subject of debate and discussion for decades. According to Huang e Huang (2025), edges are “the most fundamental local features, representing areas in an image where significant changes in intensity (brightness, color, etc.) occur, typically indicating transitions between different materials, lighting, or textures on an object’s surface,” whereas contours are higher-level features

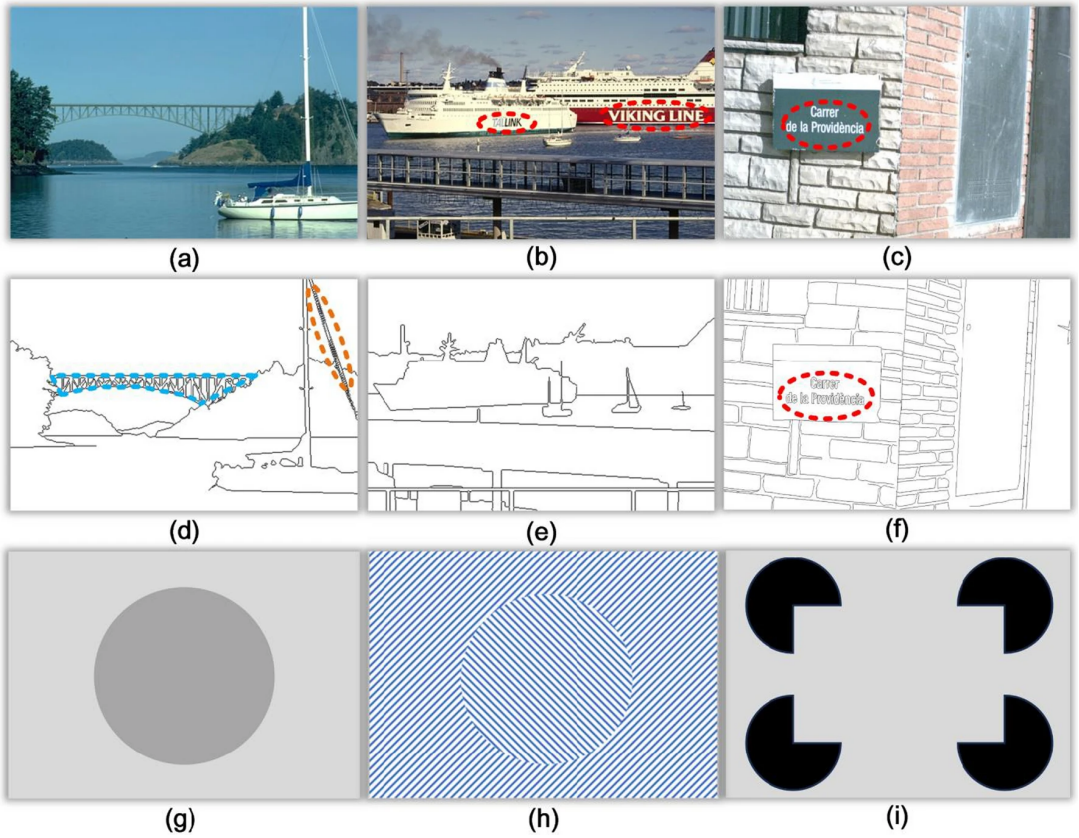


Figure 4: Explanation of edge, boundary, and contour. The first row consists of three natural images, the second row shows their corresponding manually annotated ground truth, and the third row contains three synthetic images. The first two columns of images in the first two rows are sourced from BSDS500, while the last column of images are from BIPEDv2. Retrieved from (HUANG; HUANG, 2025)

that "outline the shape or boundary of an object, typically formed by connecting a series of edge points, meaning they may be part of the edges." In this sense, contours emphasize the overall shape and the "contour" of an object, capturing both physical changes and structural information; boundaries, in turn, refer to the dividing line between different regions or objects. As the authors state, "In other words, boundaries can serve as either global or local features. Boundaries and contours often imply continuity and closure, and in most cases, region boundaries coincide with object contours, but not always, whereas edges are usually discontinuous" (HUANG; HUANG, 2025).

According to the authors, the main difference between edges and contours lies in texture. In their words, referring to Figure 4:

> "Fig. 4b, c shows two natural images, with Fig. 4e being the hand-labeled contour map corresponding to Fig. 4b, and Fig. 4f showing the edge map corresponding to Fig. 4c. The characters marked by red dashed lines in Fig. 4b, c are not regarded as contours in Fig. 4e, but are clearly considered part of the edges in Fig. 4f. This indicates that contours are object-level features representing the overall shape and ge-

> ometry of an object, while edges are local features. Figure 4d presents a hand-labeled contour map, where the approximate contour of a bridge is marked with blue dashed lines. Notably, the complex internal textures of the bridge are also marked as contours, though these are actually texture edges."(HUANG; HUANG, 2025).

In order to further differentiate boundaries and contours, the authors show that:

> "In Fig. 4d, most of the contours align with region boundaries, but the rope marked by the orange dashed line is not a region boundary. For further clarification, observe Fig. 4g, h, where the circular contours arise from changes in brightness and texture, respectively. In both cases, the region boundaries and contours overlap perfectly. However, the rectangular contour in Fig. 4i is generated by global perception, which is not a region boundary."(HUANG; HUANG, 2025).

For the authors, edge, contour, and boundary are distinct concepts, yet closely interconnected. While contours are used as object-level features and edges as local features, edge detection encompasses both. Moreover, in computer vision, these terms are often used interchangeably.

In the preceding paragraphs, this interchangeable usage has been adopted by referring to all three entities as "edges," while introducing a distinction between two broader categories that subsume the others: *bona fide* edges, corresponding to what the authors describe as real edges or contours proper, and *fiduciary* edges, which are more closely related to boundaries and involve sensory processes to a greater extent.

As discussed, the definitions of edge, contour, and boundary are frequently used interchangeably and often overlap conceptually. The distinction between bona fide and fiduciary edges, adopted thus far, is intended precisely to encompass these different meanings, indicating that there is, in some sense, a differentiation in the perceptual experience associated with each type of edge. Nevertheless, a fundamental question arises: are these genuinely distinct entities, or do they represent different manifestations of the same perceptual phenomenon?

When the authors define edges and contours in an attempt to discriminate perceptual experiences related to boundaries, they predominantly invoke physical aspects—such as texture, illumination, and local intensity variations—as well as spatial and structural aspects, insofar as these elements delimit objects, regions, or semantically interpretable entities. In doing so, these categories tend to be reduced to their physical-geometric characteristics. By contrast, when defining boundaries, particularly through examples associated with so-called illusory contours, the authors emphasize sensory and perceptual aspects, bringing these phenomena closer to an explanation centered almost exclusively on sensory experience.

However, the authors themselves acknowledge that it is not possible, ultimately, to

establish a rigid separation between bona fide and fiduciary edges. It becomes evident that edges of the fiduciary type do not depend solely on isolated sensory properties. If there were not a specific configuration of color, geometry, texture, and spatial arrangement of elements, such structures would not be perceived as contours or boundaries in pre-theoretical experience. Thus, even when they do not manifest through explicit local discontinuities, these edges fundamentally depend on physical aspects and properties, albeit of a more global and contextual nature—that is, on a coherent organization of elements and physical properties in space. Huang e Huang (2025) shows that defining an edge is not merely a terminological or operational issue, but involves deeper ontological assumptions concerning the structure of perceptual reality. It is precisely at this level that the philosophical framework developed by Clouser (2022), grounded in the modal ontology of Dooyeweerd (1984a), provides an appropriate conceptual foundation.

As systematized by Costa (2023), Dooyeweerdian ontology understands empirical reality as structured by irreducible modal aspects, such as the quantitative, spatial, physical, biotic, sensory, logical, historical, linguistic, social, aesthetic, ethical, and fiduciary aspects, each governed by its own laws, and rejects any absolutization of a single aspect. Within this framework, every concrete entity is subject to the laws of all aspects, but may function actively, when it is the direct subject of the functioning regulated by that aspect or passively, when it is merely subject to the laws of an aspect (for example, by being perceptible or measurable), within them (DOOYEWEERD, 1984b; COSTA, 2023). Entities may further be characterized by a founding function and a guiding function, which respectively determine their ontological grounding and normative orientation (DOOYEWEERD, 1984a; CLOUSER, 2022).

Applied to the concept of an edge, this framework allows for the construction of a non-reductionist definition of edge. Both the edges previously referred to as bona fide and those termed fiduciary have the quantitative, spatial, kinematic, and physical aspects as their active functions. This can be understood by recognizing that every edge exhibits defining physical characteristics—such as color, illumination, texture, and materiality—and also possesses a kinematic dimension, insofar as it may undergo variations over time. Furthermore, an edge is spatially defined, has a geometry, and can be quantified. The remaining aspects—such as the biotic, the sensory, and even the fiduciary (pistic) aspect—operate passively in the entity, since, although an edge does not itself sense, believe, or perform linguistic functions, it nevertheless remains subject to the functioning of these aspects. Thus, an edge may be perceived by sentient beings, such as animals, and in certain cases depends on perceptual functioning in order to be recognized—as occurs in phenomena of Gestalt closure or illusory contours—and it may also become an object of belief, interpretation, and linguistic designation by human beings. In this way, the edge has the physical aspect as its founding function, being most fundamentally represented by variations in luminance, texture, or material, while being logically guided

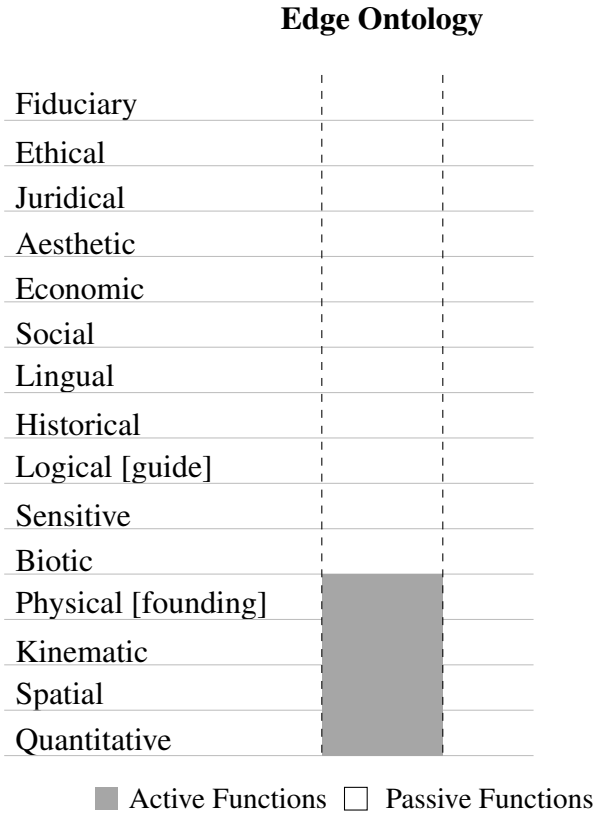
by the normative distinction between figure and ground (guiding function: logical). This characterization is fully consistent with the principle of irreducibility formulated by Dooyeweerd, according to which no aspect can be ontologically reduced to another, even though all aspects remain mutually coherent in concrete experience (DOOYEWEERD, 1984a; COSTA, 2023).

From a computational point of view, this definition is decisive. Mathematical–computational models operate on measurable and quantifiable local features, implicitly presupposing a a physically grounded notion of edge when computing gradients and intensity discontinuities, as already noted by Huang e Huang (2025), while also addressing higher-level information when global and contextual structures are taken into account. However, one of the central outcomes of this ontology, in recognizing the different fundamental aspects of reality, is the explicit acknowledgment of the limitations of computational processes as logical–formal entities in emulating active processes proper to fiduciary functioning. This is because what emerges from the sensory, aesthetic, and fiduciary aspects cannot be reduced to the logical or mathematical domains. As emphasized by Clouser (2022), such ontological presuppositions often remain unthematized in scientific practice. The Clouser–Dooyeweerdian framework does not deny the effectiveness of these models, but clarifies both their scope and their limitations.

Table 1 provides a visual representation of this modal structure. The filled gray block indicates that the Edge functions actively for quantitative to physical aspect, which serves as its founding function. This illustrates its ontological independence, as its material existence is governed by physical laws regardless of the presence of a perceiving subject. Conversely, the empty rows represent the edge's passive functions in all other modal spheres; for instance, the edge is perceived in the sensitive aspect or designated in the lingual aspect only when it becomes an object for an active subject. The model further specifies the logical aspect as the guiding function, providing the analytical distinctness necessary for the edge to be identified as a discrete entity.

While Merleau-Ponty conceives the edge primarily as a phenomenon emerging from perceptual synthesis (that is, as a whole that cannot be reduced to the sum of local sensory data, but is constituted through the evocation of past experiences and implicit laws of conscious organization), and Plato addresses the notion of boundary through the paradox of transition, emphasizing the ontological indeterminacy of liminal instants between states such as motion and rest, our ontological approach departs from both positions by situating the concept of edge neither exclusively in the perceptual subject nor merely as a logical problem of temporal liminality. Instead, we adopt a non-reductionist ontology, inspired by the Clouser–Dooyeweerdian tradition, according to which an edge is understood as a concrete entity or property that manifests itself multiaspectually within reality, being simultaneously subject to different, irreducible orders of law. This framework allows us to recognize edges as grounded in real physical discontinuities and logically guided

Table 1: Aspectual model of an edge according to the Clouser–Dooyeweerd ontology.



by the normative distinction between figure and ground; thus, our proposal preserves the ontological objectivity of the phenomenon while accounting for its epistemic variability, offering a conceptual framework better suited to both philosophical analysis and computational modeling of edges.

From a Clouser–Dooyeweerdian perspective, the issue of the fuzzy nature of edges can be coherently situated within the fiduciary aspect of reality, understood as the modal domain governing trust, commitment, and certitudinal orientation. While physical discontinuities may ground edges in an objective sense, fuzziness emerges when the identification and delimitation of a boundary require a tacit act of assent regarding where an edge ought to be taken as decisive. In such cases, the indeterminacy is not exhausted by epistemic ignorance nor fully reducible to ontological vagueness in the physical substrate; rather, it reflects the fact that boundary attribution often involves a fiduciary commitment to a classificatory stance, scale of relevance, or level of abstraction. This is particularly evident in predicates with vague extensions, scale-dependent boundaries, and cartographic or biological demarcations, where no purely physical criterion suffices to settle the question without appealing to normative decisions about significance and applicability. Consequently, fuzziness manifests not as a failure of objectivity, but as an expression of the fiduciary dimension of boundary formation, wherein the observer or model must implicitly "trust" a chosen resolution, threshold, or conceptual framing. In



(a) Original image

(b) Coarse-scale edge emphasizing the silhouette.

(c) Finer-scale chromatic boundaries in the checkered pattern.

Figure 5: Illustration of how the choice of scale and visual feature affects the computational accessibility of edges. Adapted from Mnttzri (2021).

this sense, fuzzy boundaries are best understood as fiduciarily qualified phenomena: they presuppose physical, spatial, and logical aspects, but attain their determinacy only through a certitudinal act that stabilizes meaning in the face of irreducible ambiguity.

After all the foregoing discussion, an edge can be defined as follows:

Concept 3.1 (Philosophical notion of edge)**.** *An edge is defined as a physically grounded boundary corresponding to a maximal transition between two regions exhibiting distinct properties—such as color, luminance, texture, material composition, or structured combinations thereof—at a given scale. It represents the frontier between objects, surfaces, or regions in an image, emerging from measurable local discontinuities while potentially being reinforced or stabilized by contextual and global configurations of properties. From a computational standpoint, an edge is characterized by quantifiable variations in image features, whose detection relies on local measurements but may incorporate contextual information across scales, reflecting its physical foundation and logical distinctness within the scene.*

Taking as an example the image of a man wearing a checkered shirt (Image 5), we can clarify how scale and the choice of properties affect the *computational access* to an edge without altering the edge's ontological status. The shirt is made of a single material and thus presents a broadly homogeneous physical substrate, yet it exhibits a checkered arrangement of colors. If, at a coarse scale, the task is to separate foreground and background and the selected cues emphasize global organization (e.g., figure–ground segregation), the relevant edge will typically coincide with the silhouette of the shirt and the body (Figure 5b). If, instead, the task privileges chromatic contrast at a finer scale, the computationally salient edges will include the boundaries between adjacent checkered patches. At an even finer scale, where microscopic variations become relevant, the same physical object may yield detectable transitions corresponding to fibers or weave-level

structure (Figure 5c). According to Zhou et al. (2023) “real-world objects exhibit structures of different hierarchies at different scales”. In all such cases, what changes is not “the existence” of an edge as a concrete phenomenon, but the *scale of analysis* and the *feature space* by which a model operationalizes the edge for a given objective.

This observation has direct implications for the evaluation of edge detection methods. Different datasets and annotation protocols implicitly encode different assumptions about which properties and scales qualify as “relevant” edges. Consequently, a method may be penalized not because it fails to detect edges *as such*, but because it targets a different aspectual emphasis than the ground-truth annotations. If the reference annotation prioritizes chromatic or textural transitions (e.g., internal checkered boundaries), while the method is tuned to recover figure–ground separation (e.g., the global silhouette), evaluation metrics will understandably yield poor scores. Such mismatches therefore reveal not merely algorithmic shortcomings, but unthematized ontological and methodological commitments embedded in the validation procedure.

3.5 Chapter Conclusion

Within the Clouser–Dooyeweerdian framework developed above, this is best understood by noting that an edge is a single multiaspectual phenomenon with a physical founding function and a logical guiding function, while the sensory and fiduciary (pistic) aspects operate passively in the edge yet decisively condition its *recognition* and *stabilization* in practice. In particular, there are cases in which the locally measurable physical discontinuities are weak, fragmented, or insufficient to determine a boundary unambiguously. Even then, an edge may be recognized because the *contextual arrangement* of physical cues (geometry, alignment, closure, regularity, or global contrast relations) supports the guiding logical function of separating regions in the image. In such situations, the sensory and pistic dimensions do not introduce a different kind of edge, but rather enable the same physically grounded phenomenon to be taken as an edge under conditions of incompleteness or ambiguity of local evidence.

Hence, to delimit an edge detection task with methodological rigor, it is necessary to make explicit (i) the intended scale(s) of operation and (ii) the properties or structured combinations of properties that the model is expected to treat as decisive for region separation. Without such specification, performance becomes vulnerable to annotation arbitrariness—not in the sense that edges become subjective entities, but in the sense that the fiduciary commitments of the dataset (what counts as decisive, at what scale, and for which purpose) remain implicit and may conflict with the commitments encoded in the model. In highly constrained domains (e.g., medical imaging, cell segmentation, or concrete microtomography), this ambiguity is often reduced because the task affords clearer criteria of relevance; however, in general-purpose vision benchmarks the lack of explicit

ontological–methodological alignment can compromise reproducibility and interpretability of comparative results.

Finally, the tradition of phenomenology and Gestalt, together with contemporary neuroscience, reinforces the practical necessity of incorporating contextual information. If perceptual organization arises from the integration of multiple cues into coherent wholes, then computational models should be able to fuse local and contextual evidence across scales. This provides a natural motivation for aggregation and pre-aggregation functions (Section 4.1), which can combine heterogeneous features to infer edge location. Importantly, such fusion does not replace the physical grounding of edges; rather, it operationalizes how globally structured physical configurations can support edge recognition when local measurements alone are insufficient, thereby making explicit the role of passive sensory and fiduciary aspects in the computational stabilization of boundaries.

4 MATHEMATICAL FOUNDATIONS

In this Chapter we show a rigorous presentation regarding aggregation and pre-aggregation functions and some extensions and generalizations of this concept that emerged recently on scientific literature.

4.1 Aggregation and Pre-aggregation functions

Aggregation functions, also known as aggregation operators, are a type of function characterized by special properties aimed at combining or fusing inputs typically interpreted as membership degrees (in fuzzy sets), preference degrees, evidence strength, hypothesis support, among other interpretations (BELIAKOV; PRADERA; CALVO, 2007). Initially, the discussion will focus solely on aggregation functions that take real values from closed intervals $[0, 1]$ as arguments and produce real values within the interval $[0, 1]$. This interval may be replaced by any other closed interval $[a, b]$ through a certain transformation, to be discussed later. To elucidate the breadth of different applications for an aggregation function, the following examples are provided (BELIAKOV; PRADERA; CALVO, 2007).

Example 1 (Multi-criteria decision-making problem)**.** *Consider two or more alternatives, with n evaluation criteria per alternative, or perhaps a preference for each alternative. Denote the scores or preferences as $x_1, x_2, ..., x_n$ for alternative x and $y_1, y_2, ..., y_n$ for alternative y, respectively. The goal is to combine these scores using some aggregation function f, and compare the values $f(x_1, x_2, ..., x_n)$ and $f(y_1, y_2, ..., y_n)$ to determine the winning alternative.*

Example 2 (Connectives in fuzzy logic)**.** *An object x may have different membership degrees in n fuzzy sets, denoted by $\mu_1, \mu_2, ..., \mu_n$. One may ascertain the overall membership value in the combined fuzzy set, $\mu = f(\mu_1, \mu_2, ..., \mu_n)$, where f is an aggregation operator; the combination of such fuzzy sets may involve operations such as union, intersection, or more complex operations.*

Example 3 (Group decision-making problem)**.** *There are two or more alternatives, and n experts or individuals express their evaluations on each alternative as $x_1, x_2, ..., x_n$. The objective is to combine these evaluations using an aggregation function $f(x_1, x_2, ..., x_n)$, to derive the global score f for each alternative.*

Example 4 (Rule-based system)**.** *Consider a rule-based system formulated as: IF t_1 is A_1, AND t_2 is A_2, AND ... t_n is A_n, THEN...; $x_1, x_2, ..., x_n$ denotes the degree of satisfaction of the predicate rules t_1 is A_1, t_2 is A_2, etc. The goal is to compute the overall satisfaction degree of the combined antecedent rules' predicates, as $f(x_1, x_2, ..., x_n)$, where f is an aggregation function.*

Certain boundary criteria are typically considered in aggregation or fusion functions. Firstly, an input value of "0" is interpreted as no membership, preference, evidence, satisfaction, etc., and naturally, an aggregation of n zeros should result in "0". Similarly, the value "1" is interpreted as absolute membership, strongest preference, evidence, etc., so an aggregation of 1's should naturally lead to "1", embodying a fundamental property of aggregation functions, which is the preservation of their boundary.

The second fundamental property is monotonicity. Consider an aggregation of two inputs X and Y, such that $x_1 < y_1$ and $x_j = y_j$ for all $j = 2, ..., n$. Imagine the j-th argument of f as the degree of preference regarding the j-th criterion, and x and y as vectors representing two alternatives, A and B. Thus, B is preferred over A with respect to the first criterion and is equally preferred with respect to the other criteria. Hence, it would not be reasonable to prefer A over B. It should be noted that the numbering of the criterion is irrelevant; thus, monotonicity is crucial not only for the first but for all arguments x_i (Definition 4.1.1). It is important to note that an aggregation function is a type of fusion function (Definition 4.1.1), a specific case that demands adherence to these properties presented above.

Following, all formal definitions for a fusion function (Section 4.1.1, Definition 4.1.1), aggregation (Definition 4.1.1), pre-aggregation (Definition 4.1.6), as well as the Choquet-standard integrals (Definition 4.1.11) and Expanded (Definition 4.1.3); and fuzzy measures (Definition 4.1.10) will be presented.

4.1.1 Introduction to Aggregation-like Functions

Any n-ary function $F : [0, 1]^n \to [0, 1]$ is called by a fusion function. In what follows, consider $N = \{1, \ldots, n\}$, for $n > 0$.

A fusion function $F : [0, 1]^2 \to [0, 1]$ is said to be a semi-uninorm if it is monotonic and possesses a neutral element $e \in [0, 1]$.

A bivariate fusion function $F : [0, 1]^2 \to [0, 1]$ with 0 as left annihilator element, that is, satisfying:

(LAE) $\forall y \in [0,1] : F(0,y) = 0$,

is said to be left 0-absorbent. Moreover, the following two basic properties of a fusion function F are also important in this paper:

(RNE-1) Right Neutral Element 1: $\forall x \in [0,1] : F(x,1) = x$;

(LC) Left Conjunctive Property: $\forall x, y \in [0,1] : F(x,y) \leq x$;

Any bivariate fusion function $F : [0,1]^2 \to [0,1]$ satisfying both **(LAE)** and **(RNE-1)** is called left 0-absorbent **(RNE-1)**-function.

Consider a pair of fusion functions (F_1, F_2). Then, we define:

(DM) F_1-Dominance (or, equivalently, F_2-Subordination): $F_1 \geq F_2$, that is: $\forall$ x,y $\in$ [0,1]: F_1 (x,y) $\geq F_2$(x,y).

In the forthcoming subsections, we will introduce the conventional notion of aggregation functions. Subsequently, we will discuss some of the extensions and generalizations of this concept that have recently emerged in the scientific literature, including pre-aggregation functions and monotonically ordered directionality (OD) functions, which meet the established boundary conditions.

4.1.1.1 Aggregation Functions

Definition 4.1.1. *(BELIAKOV; PRADERA; CALVO, 2007) A function $A : [0,1]^n \to [0,1]$ is an aggregation function whenever the following conditions hold:*

(A1) *A is increasing[1] in each argument: for each $i \in \{1, \ldots, n\}$, if $x_i \leq y$, then*

$$A(x_1, \ldots, x_n) \leq A(x_1, \ldots, x_{i-1}, y, x_{i+1}, \ldots, x_n);$$

(A2) *A satisfies the boundary conditions: **(i)** $A(0, \ldots, 0) = 0$ and **(ii)** $A(1, \ldots, 1) = 1$.*

A fusion function $F : [0,1]^n \to [0,1]$ is said to be idempotent if and only if:

(ID) $\forall x \in [0,1] : F(x, \ldots, x) = x$, and

it is said to be averaging if and only if:

(AV) $\forall (x_1, \ldots, x_n) \in [0,1]^n : \min\{x_1, \ldots, x_n\} \leq F(x_1, \ldots, x_n) \leq \max\{x_1, \ldots, x_n\}$.

It is observed that, since aggregation functions are increasing, the idempotent and average behaviors are shown to be equivalent in the context of these functions (BELIAKOV; PRADERA; CALVO, 2007; MAYOR; TRILLAS, 1986).

[1] For an increasing (decreasing) function we do not mean a strictly increasing (decreasing) function.

Notable examples of aggregation functions include t-norms and t-conorms (KLEMENT; MESIAR; PAP, 2000; ALSINA; FRANK; SCHWEIZER, 2006), overlap and grouping functions (BUSTINCE et al., 2010; BEDREGAL et al., 2013; DIMURO et al., 2016b; DIMURO et al., 2017a; QIAO; HU, 2018b), copulas and semicopulas (ALSINA; FRANK; SCHWEIZER, 2006; MESIAR; SEMPI, 2010; DURANTE; FERNANDEZ-SANCHEZ; QUESADA-MOLINA, 2012), weighted (quasi-)arithmetic means (BELIAKOV; PRADERA; CALVO, 2007), and OWA operators (YAGER, 1988; BEDREGAL et al., 2017).

Definition 4.1.2. *(KLEMENT; MESIAR; PAP, 2000) An aggregation function* $T : [0,1]^2 \to [0,1]$ *is a t-norm if the following conditions hold, for all* $x, y, z \in [0,1]$*:*

(T1) *Commutativity:* $T(x,y) = T(y,x)$*;*

(T2) *Associativity:* $T(x, T(y,z)) = T(T(x,y), z)$*;*

(T3) *Boundary condition:* $T(x,1) = x$*.*

If an aggregation function T adheres solely to the property ***(T3)*** and fulfills the condition $T(1,x) = x$, it is designated as a semicopula; specifically, a semicopula represents a semiuninorm with 1 as its neutral element.

For an element $x \in]0,1]$, it is recognized as a non-trivial zero divisor of T if there exists $y \in]0,1]$ for which $T(x,y) = 0$. A t-norm is deemed positive if it lacks any non-trivial zero divisors, meaning if $T(x,y) = 0$, then necessarily $x = 0$ or $y = 0$.

Example 5. *Illustrative instances of t-norms include the Minimum, the Product, the Łukasiewicz t-norm, the Hamacher Product, and the Drastic t-norm, denoted as* $T_M, T_P, T_L, T_{HP}, T_D : [0,1]^2 \to [0,1]$*. Each of these t-norms is defined for any* $x, y \in [0,1]$ *as per (KLEMENT; MESIAR; PAP, 2000):*

$$
\begin{aligned}
T_M(x,y) &= \min\{x,y\};\\
T_P(x,y) &= xy;\\
T_L(x,y) &= \max\{0, x+y-1\};\\
T_{HP}(x,y) &= \begin{cases} 0 & \text{if } x = y = 0\\ \frac{xy}{x+y-xy} & \text{otherwise;} \end{cases}\\
T_D(x,y) &= \begin{cases} y & \text{if } x = 1\\ x & \text{if } y = 1\\ 0 & \text{otherwise.} \end{cases}
\end{aligned}
$$

Observe that the T_M*,* T_P *and* T_{HP} *are positive t-norms.*

Overlap functions, which may not be associative, were first introduced by Bustince

et al. (BUSTINCE et al., 2010) primarily for use in image processing. Currently, they are extensively employed in various domains where associativity is not a necessary condition, as elaborated in references (BEDREGAL et al., 2013; DIMURO; BEDREGAL, 2015; DIMURO; BEDREGAL, 2014; QIAO; HU, 2017; QIAO; HU, 2018c; QIAO; HU, 2018a).

Definition 4.1.3. *(BUSTINCE et al., 2010) A fusion function $O : [0,1]^2 \to [0,1]$ is said to be an overlap function if the following conditions hold, for all $x, y, z \in [0,1]$:*

(O1) *O is commutative;*

(O2) *$O(x,y) = 0$ if and only if $xy = 0$;*

(O3) *$O(x,y) = 1$ if and only if $xy = 1$;*

(O4) *O is increasing;*

(O5) *O is continuous.*

Observe that any positive continuous t-norm, like T_M and T_P, is an overlap function (BUSTINCE et al., 2010).

Example 6. *Examples of overlap functions are the Cuadras-Augé family of copulas $O_{B,\alpha} : [0,1]^2 \to [0,1]$, for $\alpha \in [0,1]$, used in (BUSTINCE et al., 2010, Theorem 8) and (NELSEN, 1999), $O_{mM} : [0,1]^2 \to [0,1]$, presented in (DIMURO; BEDREGAL, 2014, Ex. 3.1.(i)), (DIMURO; BEDREGAL, 2013, Ex. 4) and (DIMURO et al., 2016b, Ex. 3.1), the Eyraud-Farlie-Gumbel-Morgenstern (EFGM) 2-copulas $O_\alpha : [0,1]^2 \to [0,1]$, with $\alpha \in [-1,1]$, found in (NELSEN, 1999), (ALSINA; FRANK; SCHWEIZER, 2006, Appendix A (A.2.1)) and (LUCCA et al., 2015), and the Geometric Mean $GM : [0,1]^2 \to [0,1]$, used in (ELKANO et al., 2015, Ex. 1), defined, respectively, for all $x, y \in [0,1]$ by:*

$$\begin{aligned} O_{B,\alpha}(x,y) &= (T_M(x,y))^\alpha \cdot (T_P(x,y))^{(1-\alpha)}, \text{ for } \alpha \in [0,1];; \\ O_{mM}(x,y) &= \min\{x,y\} \max\{x^2, y^2\}; \\ O_\alpha(x,y) &= xy(1 + \alpha(1-x)(1-y)), \text{ for } \alpha \in [-1,1]; \\ GM(x,y) &= \sqrt{xy}. \end{aligned} \tag{1}$$

Copulas are functions that connect (two-dimensional) probability distribution functions to their one-dimensional margins, serving a crucial function in the domains of probabilistic metric spaces and statistics (ALSINA; FRANK; SCHWEIZER, 2006).

Definition 4.1.4. *(ALSINA; FRANK; SCHWEIZER, 2006) A bivariate function $C : [0,1]^2 \to [0,1]$ is a copula if it satisfies the following conditions, for all $x, x', y, y' \in [0,1]$ with $x \leq x'$ and $y \leq y'$:*

(C1) $C(x, y) + C(x', y') \geq C(x, y') + C(x', y)$;

(C2) $C(x, 0) = C(0, x) = 0$;

(C3) $C(x, 1) = C(1, x) = x$.

Given that all copulas fulfill the 1-Lipschitz condition and are increasing, it follows from (KLEMENT; MESIAR; PAP, 2000, Proposition 9.8) and (SCHWEIZER; SKLAR, 1983, Lemma 6.1.8, Lemma 6.3.1) that every copula exhibits continuity. Moreover, each associative copula qualifies as a continuous t-norm (KLEMENT; MESIAR; PAP, 2000, Corollary 9.9).

Example 7. *Examples of copulas that also function as t-norms include the Minimum T_M, the Product T_P, the Łukasiewicz, and the Hamacher T_{HP} t-norms (referenced in Example 5). Additionally, some copulas double as overlap functions, such as $O_{B,0.5}$ and O_α (mentioned in Example 6). Conversely, examples of copulas that are neither t-norms nor overlap functions include $C_F : [0,1]^2 \to [0,1]$, discussed in (KLEMENT; MESIAR; PAP, 2000, Ex. 9.5 (v)),(LUCCA et al., 2017, Table 1), and $C_L : [0,1]^2 \to [0,1]$, presented in (ALSINA; FRANK; SCHWEIZER, 2006, Ap. A (A.5.3a)), (LUCCA et al., 2017, Table 1). These are defined, respectively, for all $x, y \in [0,1]$ as follows:*

$$\begin{aligned} C_F(x,y) &= xy + x^2y(1-x)(1-y); \\ C_L(x,y) &= \max\left\{\min\left\{x, \frac{y}{2}\right\}, x+y-1\right\}. \end{aligned}$$

Finally, examples of aggregation functions that are neither t-norms, overlap functions, nor copulas (BELIAKOV; PRADERA; CALVO, 2007, Ex. 1.80), which were used in (LUCCA et al., 2019; DIMURO et al., 2019), are $F_{BPC}, F_{GL} : [0,1]^2 \to [0,1]$, defined, respectively, for all $x, y \in [0,1]$, by

$$\begin{aligned} F_{BPC}(x,y) &= xy^2 \\ F_{GL}(x,y) &= \sqrt{\frac{x(y+1)}{2}}. \end{aligned}$$

4.1.1.2 Pre-aggregation functions

It is noted that the requirement for monotonic increase along every direction defined by vectors in the first quadrant, essential for aggregation functions, is not met by certain statistical tools, such as the mode. To address this, Wilkin and Beliakov (WILKIN; BELIAKOV, 2015) introduced the concept of weak monotonicity to expand the traditional notion of monotonicity by only necessitating it along the diagonal of the first quadrant.

Subsequently, Bustince et al. (BUSTINCE et al., 2015) further developed this idea by proposing the concept of directional monotonicity, which permits monotonicity along

certain fixed directions. Specifically, weakly monotone functions, including the mode and any aggregation function, qualify as directionally monotonic.

Definition 4.1.5. *(BUSTINCE et al., 2015) Let $\vec{r} = (r_1, \ldots, r_n)$ be a real n-dimensional vector, $\vec{r} \neq \vec{0} = (0, \ldots, 0)$. A function $F : [0,1]^n \to [0,1]$ is said to be $\vec{r}$-increasing if for all $\vec{x} = (x_1, \ldots, x_n) \in [0,1]^n$ and for all $c > 0$ such that $\vec{x} + c\vec{r} = (x_1 + cr_1, \ldots, x_n + cr_n) \in [0,1]^n$ it holds*

$$F(\vec{x} + c\vec{r}) \geq F(\vec{x}).$$

Similarly, one defines an $\vec{r}$-decreasing function.

In Definition 4.1.5, when $\vec{r} = (1, \ldots, 1) = \vec{1}$, a function F that is increasing in the direction of $\vec{r}$ is termed weakly increasing (WILKIN; BELIAKOV, 2015). Building on the idea of directional monotonicity, Lucca et al. (LUCCA et al., 2016) introduced the concept of a pre-aggregation function:

Definition 4.1.6. *(LUCCA et al., 2016) A function $PA : [0,1]^n \to [0,1]$ is said to be an n-ary pre-aggregation function if the following conditions hold:*

(PA1) *Directional Increasingness: there exists $\vec{r} = (r_1, \ldots, r_n) \in [0,1]^n$, $\vec{r} \neq \vec{0}$, such that PA is $\vec{r}$-increasing;*

(PA2) *Boundary conditions: (i) $PA(0, \ldots, 0) = 0$ and (ii) $PA(1, \ldots, 1) = 1$.*

If F is a pre-aggregation function with respect to a vector $\vec{r}$ we just say that F is an $\vec{r}$-pre-aggregation function.

Example 8. *Examples of $(0,1)$-pre-aggregation functions are $F_{NA}, F_{NA2} : [0,1]^2 \to [0,1]$, and of $(1,0)$-pre-aggregation functions are $F_\alpha, F_{PA} : [0,1]^2 \to [0,1]$, defined by: (LUCCA et al., 2018a; LUCCA et al., 2019; DIMURO et al., 2019).*

$$F_{NA}(x,y) = \begin{cases} x & \text{if } x \leq y \\ \min\{\frac{x}{2}, y\} & \text{otherwise;} \end{cases}$$

$$F_{NA2}(x,y) = \begin{cases} 0 & \text{if } x = 0 \\ \frac{x+y}{2} & \text{if } 0 < x \leq y \\ \min\{\frac{x}{2}, y\} & \text{otherwise;} \end{cases}$$

$$F_\alpha(x,y) = \begin{cases} \alpha x & \text{if } x < y \\ \max\{\alpha x, y\} & \text{otherwise;} \end{cases} \quad \text{for } 0 < \alpha < 1$$

$$F_{PA}(x,y) = \begin{cases} 0 & \text{if } x = 0 \vee y = 0 \\ \frac{x+y}{2} & \text{if } 0 < x \leq y \\ x & \text{otherwise.} \end{cases}$$

Observe that the fusion function $F_{IP} : [0,1]^2 \to [0,1]$, defined by $F_{IP}(x,y) = 1 - y + xy$

(DIMURO et al., 2019), although $(1,0)$*-increasing, is not a pre-aggregation function, since* $F_{IP}(0,0) = 1$.

For properties and related concepts of pre-aggregation functions see also (DIMURO et al., 2016a; DIMURO et al., 2018b; DIMURO et al., 2017b; DIMURO et al., 2017).

4.1.1.3 Pseudo pre-aggregation function pair

In this Section, we explore the concept of a pseudo pre-aggregation function pair, as introduced in (DIMURO et al., 2019), which is pivotal in examining the generalizations of the Choquet Integral.

Definition 4.1.7. *(DIMURO et al., 2019, Definition 3.1) Consider two fusion functions* $F_1, F_2 : [0,1]^2 \to [0,1]$*. The pair* (F_1, F_2) *is said to be a pseudo pre-aggregation function pair whenever the following conditions hold:*

(DI) *Directional Increasingness:* F_1 *is* $(1,0)$*-increasing, that is, it is increasing in the first coordinate;*

(BC0) *Boundary Conditions for 0:*

(i) $\forall y \in [0,1] : F_1(0,y) = F_2(0,y)$ *and*

(ii) $F_1(0,1) = 0$*;*

(BC1) *Boundary Condition for 1:* $F_1(1,1) = 1$*;*

(DM) F_1*-Dominance (or, equivalently,* F_2*-Subordination):* $F_1 \geq F_2$.

Example 9. *Examples of pseudo pre-aggregation function pairs are:* (T_P, T_L)*,* (T_M, O_α)*,* (T_M, F_{NA})*,* (T_P, F_{BPC})*,* (F_{BPC}, F_{BPC})*,* (T_M, T_M)*,* (F_{PA}, F_{PA})*,* (F_{IP}, F_{IP})*,* (F_{GL}, T_M)*,* (T_P, kT_P) *for* $k \in]0,1]$*, where* T_P, T_L *and* T_M *are t-norms given in Example 5,* O_α *is an overlap function given in Example 6 ,* F_{NA} *and* F_{PA} *are pre-aggregation functions given in Example 8,* F_{BPC} *and* F_{GL} *are aggregation functions that are neither t-norms, overlap function, nor copulae, as given in Example 7, and* F_{IP} *is not even a pre-aggregation function, as discussed in Example 8.*

Definition 4.1.8. *(DIMURO et al., 2019, Definition 3.2) A pseudo pre-aggregation function pair* (F_1, F_2) *is pairwise increasing if, for all* $x, y_1, y_2 \in [0,1]$ *and* $h > 0$ *such that* $x + h \in [0,1]$*, the following condition holds:*

(PI) *If* $y_2 \leq y_1$ *then* $F_1(x, y_1) - F_2(x, y_2) \leq F_1(x + h, y_1) - F_2(x + h, y_2)$.

By (DIMURO et al., 2019, Corollary 3.1), for any copula C, (C, C) is a pseudo pre-aggregation function pair satisfying **(PI)**.

4.1.1.4 Ordered directionally (OD) monotone functions

When considering directional monotonicity, it is assumed that the direction along which monotonicity is required remains constant for all vectors $\vec{x} \in [0,1]^n$. Differing from standard directional monotonicity, Bustince et al., in (BUSTINCE et al., 2017), introduced the concept of ordered directional (OD) monotonicity. This approach permits monotonicity along varying directions depending on the ordinal size of the coordinates of each input $\vec{x} \in [0,1]^n$.

To facilitate this, a permutation $\sigma : \{1,\ldots,n\} \to \{1,\ldots,n\}$ is first employed to arrange the elements of $\vec{x} \in [0,1]^n$ in decreasing order, resulting in $\vec{x}_\sigma \in [0,1]^n$. Subsequently, a fusion function $F : [0,1]^n \to [0,1]$ is deemed OD $\vec{r}$-increasing, for a real vector $\vec{r} = (r_1,\ldots,r_n)$, with $\vec{r} \neq \vec{0}$, if $F(\vec{x})$ is less than or equal to the values of F when applied to

$$(\vec{x}_\sigma + c\vec{r})_{\sigma^{-1}} = \vec{x} + c\vec{r}_{\sigma^{-1}},$$

under the condition that $\vec{x}_\sigma$ and $\vec{x}_\sigma + c\vec{r}$ are comonotone (i.e., they increase or decrease simultaneously).

Definition 4.1.9. *(BUSTINCE et al., 2017) Consider a function $F : [0,1]^n \to [0;1]$ and let $\vec{r} = (r_1,\ldots,r_n)$ be a real n-dimensional vector, $\vec{r} \neq \vec{0}$. F is said to be ordered directionally (OD) $\vec{r}$-increasing if, for each $\vec{x} \in [0,1]^n$, any permutation $\sigma : \{1,\ldots,n\} \to \{1,\ldots,n\}$ with $x_{\sigma(1)} \geq \ldots \geq x_{\sigma(n)}$, and $c > 0$ such that $1 \geq x_{\sigma(1)} + cr_1 \geq \ldots \geq x_{\sigma(n)} + cr_n$, it holds that*

$$F(\vec{x} + c\vec{r}_{\sigma^{-1}}) \geq F(\vec{x}),$$

where $\vec{r}_{\sigma^{-1}} = (r_{\sigma^{-1}(1)},\ldots,r_{\sigma^{-1}(n)})$. Similarly, one defines an ordered directionally (OD) $\vec{r}$-decreasing function.

It follows directly that for any $k > 0$, a fusion function $F : [0,1]^n \to [0,1]$ qualifies as OD $(k,\ldots,k)$-increasing and meets the boundary conditions if and only if F acts as a $(k,\ldots,k)$-pre-aggregation function.

4.1.2 Fuzzy measure-based fuzzy integrals

In this section, we introduce the concept of a fuzzy measure, also referred to as a capacity, a notion independently proposed by Sugeno and Choquet (GRABISCH, 2005; GRABISCH, 2015). We then proceed to review the standard definitions of the discrete Choquet and Sugeno integrals, focusing on the space $N = \{1,\ldots,n\}$.

Definition 4.1.10. *(CHOQUET, 1953–1954; MUROFUSHI; SUGENO; MACHIDA, 1994) A function $\mathfrak{m} : 2^N \to [0,1]$ is said to be a fuzzy measure if, for all $X, Y \subseteq N$, the following conditions hold:*

($\mathfrak{m}$1) *Increasingness: if* $X \subseteq Y$*, then* $\mathfrak{m}(X) \leq \mathfrak{m}(Y)$*;*

($\mathfrak{m}$2) *Boundary conditions:* $\mathfrak{m}(\emptyset) = 0$ *and* $\mathfrak{m}(N) = 1$.

A fuzzy measure $\mathfrak{m}$ is defined as symmetric (**SYM**) if, for any subsets $X, Y \subseteq N$, the following condition is satisfied:

(SYM) $\mid X \mid = \mid Y \mid \Rightarrow \mathfrak{m}(X) = \mathfrak{m}(Y)$.

Fuzzy measures are utilized to analyze the relationships among elements that are intended to be aggregated, highlighting the significance of a coalition. An example of a fuzzy measure is the power measure, denoted as $\mathfrak{m}_{PM} : 2^N \to [0, 1]$, which is defined for all subsets $X \subseteq N$ by:

$$\mathfrak{m}_{PM}(X) = \left(\frac{|X|}{n}\right)^q, \text{ with } q > 0. \tag{2}$$

The power measure is **SYM**. In some studies, the exponent q can be optimized using genetic algorithms to better tailor the fuzzy measure to specific datasets. This approach is discussed in more detail in (BARRENECHEA et al., 2013; LUCCA et al., 2017).

To manage the complexity associated with identifying fuzzy measures, some researchers have proposed different representations, such as expressing them in terms of Möbius values. This representation also offers an efficient alternative for depicting the Choquet integral and calculating probabilistic simultaneous interaction indices, including the Shapley and Banzhaf indices, as elaborated by Wu and Beliakov (WU; BELIAKOV, 2018; WU; BELIAKOV, 2019).

The Choquet integral extends the concept of the Lebesgue integral, which is based on additive measures. In contrast, the Choquet integral allows for the incorporation of fuzzy measures more broadly. The discrete Choquet integral (CHOQUET, 1953–1954) is specifically defined for finite spaces:

Definition 4.1.11. *(CHOQUET, 1953–1954) The discrete Choquet integral with respect to a fuzzy measure* $\mathfrak{m}$ *is the function* $\mathfrak{C}_{\mathfrak{m}} : [0, 1]^n \to [0, 1]$*, defined, for all of* $\vec{x} = (x_1, \ldots, x_n) \in [0, 1]^n$*, by:*

$$\mathfrak{C}_{\mathfrak{m}}(\vec{x}) = \sum_{i=1}^{n} \left(x_{(i)} - x_{(i-1)}\right) \cdot \mathfrak{m}\left(A_{(i)}\right), \tag{3}$$

where:

(i) $\left(x_{(1)}, \ldots, x_{(n)}\right)$ *is an increasing permutation on the input* $\vec{x}$*, that is,* $x_{(1)} \leq \ldots \leq x_{(n)}$*;*

(ii) $x_{(0)} = 0$*; and*

(iii) $A_{(i)} = \{(i), \ldots, (n)\}$ *is the subset of indices corresponding to the* $n - i + 1$ *largest components of* $\vec{x}$.

Whenever one distributes the product operation in Equation (3), we obtain the Choquet integral in its expanded form:

$$\mathfrak{C}_{\mathfrak{m}}(\vec{x}) = \sum_{i=1}^{n} \left(x_{(i)} \cdot \mathfrak{m}\left(A_{(i)}\right) - x_{(i-1)} \cdot \mathfrak{m}\left(A_{(i)}\right) \right). \tag{4}$$

It is important to mention that the expanded form of the Choquet integral follows the same properties as the original one. Another integral that is related to fuzzy measure is the Sugeno integral (SUGENO, 1974):

Definition 4.1.12. *(SUGENO, 1974) The discrete Sugeno integral with respect to a fuzzy measure* $\mathfrak{m}$ *is the function* $S_{\mathfrak{m}} : [0,1]^n \to [0,1]$*, defined, for all of* $\vec{x} = (x_1, \ldots, x_n) \in [0,1]^n$*, by:*

$$S_{\mathfrak{m}}(\vec{x}) = \max_{i=1}^{n} \left\{ \min \left\{ x_{(i)}, \mathfrak{m}\left(A_{(i)}\right) \right\} \right\}, \tag{5}$$

considering the conditions ***(i)*** *to* ***(iii)*** *stated in Definition 4.1.11.*

Considering that the power measure has achieved the highest accuracy in classification problems (LUCCA et al., 2017; LUCCA et al., 2016; LUCCA et al., 2018a; WIECZYNSKI et al., 2023; LUCCA et al., 2019; LUCCA et al., 2018b), image processing(MARCO-DETCHART et al., 2021; MARCO-DETCHART et al., 2023b; SILVA et al., 2023; AMORIM et al., 2023), neuro-brain computer interface(WIECZYNSKI et al., 2022), and decision making(WIECZYNSKI et al., 2022; WIECZYNSKI et al., 2020), it appears promising to adopt it in edge detection applications.

In previous works(MARCO-DETCHART et al., 2021; MARCO-DETCHART et al., 2023b) regarding edge detection, authors analyzed a collection of fixed values of the exponent q in the definition of the power measure. As will be seen in Chapter 10, in one of the models proposed in this work, we considered the performance of power measures in an adaptive framework, where we determine the value of q by considering the elements (pixel information) to be aggregated in each sliding window along the image, as detailed in Section 10.1.

In this process, we used different fusion functions to aggregate the information carried by pixels in a specific window. These functions are referred to as *aggregation functions* (GRABISCH et al., 2009; BELIAKOV; Bustince Sola; CALVO, 2016), represented by functions $A : [0,1]^n \to [0,1]$ that are increasing in each argument and satisfy the boundary conditions $A(0, \ldots, 0) = 0$ and $A(1, \ldots, 1) = 1$. Examples of such functions include the arithmetic mean AVG and the functions F_{GL}, both presented in Table 2.

Table 2: Functions used to expand the Choquet Integral

Definition	Family	Reference
$T_M(x,y) = \min\{x,y\}$	t-norm, copula	Klement, Mesiar e Pap (2000)
$T_P(x,y) = xy$	t-norm, copula	Klement, Mesiar e Pap (2000)
$T_{\text{Ł}}(x,y) = \max\{0, x+y-1\}$	t-norm, copula	Klement, Mesiar e Pap (2000)
$T_{DP}(x,y) = \begin{cases} x, & y = 1 \\ y, & x = 1 \\ 0, & \text{otherwise} \end{cases}$	t-norm	Alsina, Frank e Schweizer (2006)
$T_{HP}(x,y) = \begin{cases} 0, & \text{if } x = y = 0, \\ \dfrac{xy}{x+y-xy}, & \text{otherwise} \end{cases}$	t-norm, copula	Klement, Mesiar e Pap (2000)
$O_B(x,y) = \min\{x\sqrt{y},\, y\sqrt{x}\}$	overlap function, copula	Bustince et al. (2010); Nelsen (1999)
$O_{mM}(x,y) = \min\{x,y\}\max\{x^2,y^2\}$	overlap function, copula	Dimuro e Bedregal (2014); Dimuro e Bedregal (2013); Dimuro et al. (2016b); Dimuro e Bedregal (2015)
$O_{Div}(x,y) = \dfrac{xy + \min\{x,y\}}{2}$	overlap function, copula	Alsina, Frank e Schweizer (2006)
$GM(x,y) = \sqrt{xy}$	overlap function	Elkano et al. (2015)
$HM(x,y) = \begin{cases} 0, & \text{if } x = 0 \text{ or } y = 0, \\ \dfrac{2}{\frac{1}{x}+\frac{1}{y}}, & \text{otherwise} \end{cases}$	overlap function	Elkano et al. (2015)
$S(x,y) = \sin\left(\dfrac{\pi}{2}(xy)^{1/4}\right)$	overlap function	Elkano et al. (2015)
$C_F(x,y) = xy + x^2y(1-x)(1-y)$	copula	Klement, Mesiar e Pap (2000); Lucca et al. (2017)
$C_L(x,y) = \max\left\{\min\left\{x, \dfrac{y}{2}\right\}, x+y-1\right\}$	copula	Alsina, Frank e Schweizer (2006); Lucca et al. (2017)
$AVG(x,y) = \dfrac{x+y}{2}$	overlap function	–
$O_{RS}(x,y) = \min\left\{\dfrac{(x+1)\sqrt{y}}{2},\, y\sqrt{x}\right\}$	aggregation function	Lucca et al. (2018a)
$F_{GL}(x,y) = \sqrt{\dfrac{x(y+1)}{2}}$	aggregation function	Lucca et al. (2018a)
$F_{BPC}(x,y) = xy^2$	overlap function	Lucca et al. (2019)
$F_{NA}(x,y) = \begin{cases} x, & \text{if } x \leq y, \\ \min\left\{\dfrac{x}{2}, y\right\}, & \text{otherwise} \end{cases}$	pre-aggregation function	Lucca et al. (2018a)
$F_{NA2}(x,y) = \begin{cases} 0, & \text{if } x = 0, \\ \dfrac{x+y}{2}, & \text{if } 0 < x \leq y, \\ \min\left\{\dfrac{x}{2}, y\right\}, & \text{otherwise} \end{cases}$	pre-aggregation function	Lucca et al. (2018a)
$F_{IM}(x,y) = \max\{1-y, x\}$	non pre-aggregation function	Lucca et al. (2019)
$F_{IP}(x,y) = 1 - y + xy$	non pre-aggregation function	Lucca et al. (2019)

4.1.3 Generalizations of the standard form of the Choquet integral

In this Section, we explore the state-of-the-art generalizations of the standard form of the Choquet integral. The methodology employed in these generalizations involves

replacing the product operation in Equation (3)—commonly interpreted as the product t-norm—with various other fusion functions possessing suitable properties. This substitution aims to derive a function that exhibits characteristics akin to aggregation.

Specifically, the generalizations of the Choquet integral achieved through this methodology qualify as pre-aggregation functions. For the subsequent discussions, let us define $N = \{1, \ldots, n\}$.

4.1.3.1 C_T-integrals

The initial generalization of the standard form of the Choquet integral using this approach is identified as the family of C_T-integrals. This generalization is achieved by substituting the product t-norm, in wich the Choquet integral is based (Equation 3) with various other t-norms. This adaptation was proposed by Lucca et al. in (LUCCA et al., 2016) as a construction way of pre-aggregation functions, which where used to address classification problems using Fuzzy Rule-Based Systems (FRBSs) (ISHIBUCHI; NOJIMA, 2008):

Definition 4.1.13. *Let $\mathfrak{m} : 2^N \to [0,1]$ be a fuzzy measure and $T : [0,1]^2 \to [0,1]$ be a t-norm. Taking as basis the Choquet integral, a C_T-integral is defined as the function $C_{\mathfrak{m}}^T : [0,1]^n \to [0,1]$, given, for all $\vec{x} = (x_1, \ldots, x_n) \in [0,1]^n$, by*

$$\mathfrak{C}_{\mathfrak{m}}^T(\vec{x}) = \sum_{i=1}^{n} T\left(x_{(i)} - x_{(i-1)}, \mathfrak{m}\left(A_{(i)}\right)\right), \tag{6}$$

*considering the conditions **(i)** to **(iii)** stated in Definition 4.1.11.*

Example 10. *The most relevant example of a C_T-integral is the one obtained using the Hamacher product t-norm T_{HP} , denoted here by $C_{T_{HP}}$, which is defined as:*

$$\mathfrak{C}_{\mathfrak{m}}^{HP}(\vec{x}) = \sum_{i=1}^{n} \begin{cases} 0 & \text{if } x_{(i)} = x_{(i-1)} \text{ and } \mathfrak{m}\left(A_{(i)}\right) = 0 \\ \frac{\left(x_{(i)} - x_{(i-1)}\right) \cdot \mathfrak{m}\left(A_{(i)}\right)}{x_{(i)} - x_{(i-1)} + \mathfrak{m}\left(A_{(i)}\right) - \left(x_{(i)} - x_{(i-1)}\right) \cdot \mathfrak{m}\left(A_{(i)}\right)} & \text{otherwise.} \end{cases} \tag{7}$$

The C_T-integral $C_{T_{HP}}$ has demonstrated notable efficacy when utilized as the aggregation operator in the Fuzzy Rule Model (FRM) of Fuzzy Rule-Based Systems (FRBSs). It enhances the performance over the classical Choquet integral, which employs the product t-norm. Moreover, when paired with the power measure, which is genetically learned as described in Equation (2), it further improves the results obtained by the traditional FRM of the WR (Weighted Rule), which uses the maximum as its aggregation function (LUCCA et al., 2016). The $C_{T_{HP}}$ integral has also been applied to augment brain-computer interface systems that incorporate fuzzy integrals, particularly in the fusion processes for classifying brain-computer interface commands (Ko et al., 2019).

In (LUCCA et al., 2016, Theorem 4.1), Lucca et al. present a general result, from which it is concluded that C_T-integrals are both idempotent and averaging pre-aggregation functions:

Theorem 4.1.1. *(LUCCA et al., 2016, Theorem 4.1) Let $M : [0,1]^2 \to [0,1]$ be a function such that for all $x, y \in [0,1]$ it satisfies $M(x,y) \leq x$, $M(x,1) = x$ and M is $(0,1)$-increasing. Define the integral $C^M_{\mathfrak{m}} : [0,1]^n \to [0,1]$, given, for all $\vec{x} = (x_1, \ldots, x_n) \in [0,1]^n$, by*

$$\mathfrak{C}^M_{\mathfrak{m}}(\vec{x}) = \sum_{i=1}^{n} M\left(x_{(i)} - x_{(i-1)}, \mathfrak{m}\left(A_{(i)}\right)\right), \tag{8}$$

where any $x_{(i)}$ and $A_{(i)}$ are defined as stated in Definition 4.1.13. Then, for any fuzzy measure $\mathfrak{m}$, $\mathfrak{C}^M_{\mathfrak{m}}$ is a pre-aggregation function that is idempotent and averaging.

4.1.3.2 C_F-integrals

Seeking to develop more comprehensive definitions of Choquet-based integrals, Lucca et al. introduced the concept of C_F-integrals in (LUCCA et al., 2018a). These integrals are pre-aggregation functions that generalize the Choquet integral by incorporating a bivariate function F that is left 0-absorbent **(LAE)**.

Definition 4.1.14. *(LUCCA et al., 2018a, Definition 11) Let $F : [0,1]^2 \to [0,1]$ be a bivariate fusion function and $\mathfrak{m} : 2^N \to [0,1]$ be a fuzzy measure. The Choquet-like integral based on F with respect to $\mathfrak{m}$, called C_F-integral, is the function $\mathfrak{C}^F_{\mathfrak{m}} : [0,1]^n \to [0,1]$, defined, for all $\vec{x} \in [0,1]^n$, by*

$$\mathfrak{C}^F_{\mathfrak{m}}(\vec{x}) = \min\left\{1, \sum_{i=1}^{n} F\left(x_{(i)} - x_{(i-1)}, \mathfrak{m}\left(A_{(i)}\right)\right)\right\}, \tag{9}$$

*considering the conditions **(i)** to **(iii)** stated in Definition 4.1.11.*

An intriguing aspect of the C_F-integral is that a pre-aggregation function can be derived using two different sets of constraints on the fusion function F. Initially, F must fulfill the **(LAE)** condition, which denotes left 0-absorbency. Subsequently, F must also meet one of the following criteria: either (i) **(RNE-1)**, or (ii) **(A2)** combined with $(1,0)$-increasingness. These requirements were detailed in (LUCCA et al., 2018a) through the presentation of specific theorems:

Theorem 4.1.2. *(LUCCA et al., 2018a, Theorem 1) For any fuzzy measure $\mathfrak{m} : 2^N \to [0,1]$ and left 0-absorbent **(RNE-1)**-function $F : [0,1]^2 \to [0,1]$, $\mathfrak{C}^F_{\mathfrak{m}}$ is a $\vec{1}$-pre-aggregation function.*

Theorem 4.1.3. *(LUCCA et al., 2018a, Theorem 2) For any fuzzy measure $\mathfrak{m} : 2^N \to$*

$[0,1]$ *and left 0-absorbent* $(1,0)$*-pre-aggregation function* $F : [0,1]^2 \to [0,1]$, $\mathfrak{C}_{\mathfrak{m}}^{F}$ *is a* $\vec{1}$*-pre-aggregation function.*

Additionally, whenever F satisfy **(LC)** then $\mathfrak{C}_{\mathfrak{m}}^{F}$ is idempotent and averaging (LUCCA et al., 2018a, Corollary 1).

Example 11. *In (LUCCA et al., 2018a), two distinct left 0-absorbent fusion functions were employed in classification problems, namely,* F_{NA} *and* F_{NA2}*, defined in Example 8. Observe that* F_{NA} *satisfies both* ***(RNE-1)*** *and* ***(LC)****, thereby rendering* $\mathfrak{C}_{\mathfrak{m}}^{F_{NA}}$ *as an idempotent and averaging* $\vec{1}$*-pre-aggregation function for any fuzzy measure* $\mathfrak{m}$*. On the contrary,* F_{NA2} *does not meet the criteria of* ***(RNE-1)****,* ***(LC)****, nor* $(0,1)$*-increasingness, yet* $\mathfrak{C}_{\mathfrak{m}}^{F_{NA2}}$ *still qualifies as a* $\vec{1}$*-pre-aggregation function. Moreover, it is shown in (LUCCA et al., 2018a) that* $\mathfrak{C}_{\mathfrak{m}}^{F_{NA2}}$ *is not averaging.*

Remark 1. *It should be noted that the family of* C_T*-integrals constitutes a sub-category within the* C_F*-integrals, where* F *is a t-norm. When deploying the averaging and non-averaging* C_F*-integrals as the aggregation operator in fuzzy rule-based classification systems, as discussed in Example 10, an intriguing outcome emerges. Among the averaging* C_F*-integrals, the one showing the highest accuracy rate is the* C_T*-integral utilizing the Hamacher t-norm (*$C_{T_{HP}}$*) presented in Example 10. However, the best performance among non-averaging* C_F*-integrals is achieved using* F_{NA2}*. Indeed, the non-averaging* C_F*-integrals demonstrate a superior accuracy rate compared to their averaging counterparts. Furthermore, the top-performing* C_F*-integral, specifically that of* F_{NA2}*, delivers results that are statistically superior to all traditional fuzzy reasoning methods (FRM) and are highly competitive with classical non-averaging FRMs such as the additive combination or the probabilistic sum (LUCCA et al., 2018a).*

Table 3 presents the $\mathfrak{C}_{\mathfrak{m}}^{F}$-integrals used in Chapter 10 , which are all $\mathbf{1}$-pre-aggregation functions.

Table 3: $\mathfrak{C}_{\mathfrak{m}}^{T}$ and $\mathfrak{C}_{\mathfrak{m}}^{F}$-integrals used in Chapter 10, as generalisations of the Choquet integral for a fuzzy measure $\mathfrak{m}$

Choquet-like integral	Base Function
$\mathfrak{C}_{\mathfrak{m}}^{C_F}$	$C_F(x,y) = xy + x^2y(1-x)(1-y)$
$\mathfrak{C}_{\mathfrak{m}}^{O_B}$	$O_B(x,y) = \min\{x\sqrt{y}, y\sqrt{x}\}$ (overlap function
$\mathfrak{C}_{\mathfrak{m}}^{F_{BPC}}$	$F_{BPC}(x,y) = xy^2$ (overlap function)
$\mathfrak{C}_{\mathfrak{m}}^{\text{Hamacher}}$	$T_{HP}(x,y) = \begin{cases} 0 & \text{if } x = y = 0 \\ \frac{xy}{x+y-xy} & \text{otherwise} \end{cases}$ (t-norm)

4.1.4 Generalizations of the expanded form of the Choquet integral

In this section, we discuss the state-of-the-art regarding the generalizations of the expanded form of the Choquet integral. The primary methodology in these generalizations involves replacing the two instances of the product operation in Equation (4) with two distinct fusion functions, F_1 and F_2, each possessing specific attributes that contribute to forming an aggregation-like function.

The nature of the functions F_1 and F_2, depending on the properties they satisfy, determines the classification of the resulting function. This classification can range from an aggregation function to a pre-aggregation function, or to an OD monotonic function that meets the specified boundary conditions.

4.1.4.1 CC-integrals

The first generalization of the Choquet integral in its expanded form was introduced by Lucca et al. (LUCCA et al., 2017) by utilizing F_1 and F_2 as copulas. This adaptation led to the creation of the so-called CC-integrals, which invariably function as aggregation functions.

Definition 4.1.15. *(LUCCA et al., 2017, Definition 7) Let $\mathfrak{m} : 2^N \to [0,1]$ be a fuzzy measure and $C : [0,1]^2 \to [0,1]$ be a bivariate copula. The CC-integral with respect to $\mathfrak{m}$ is defined as a function $\mathfrak{C}_{\mathfrak{m}}^{C} : [0,1]^n \to [0,1]$, given, for all $x \in [0,1]^n$, by*

$$\mathfrak{C}_{\mathfrak{m}}^{C}(\vec{x}) = \sum_{i=1}^{n} C\left(x_{(i)}, \mathfrak{m}\left(A_{(i)}\right)\right) - C\left(x_{(i-1)}, \mathfrak{m}\left(A_{(i)}\right)\right), \tag{10}$$

*considering the conditions **(i)** to **(iii)** stated in Definition 4.1.11.*

Theorem 4.1.4. *(LUCCA et al., 2017, Theorem 4) For any bivariate copula $C : [0,1]^2 \to [0,1]$ and fuzzy measure $\mathfrak{m} : 2^N \to [0,1]$, $\mathfrak{C}_{\mathfrak{m}}^{C}$ is an averaging aggregation function.*

Remark 2. *In (MESIAR; STUPŇANOVÁ, 2019, Theorem 1), Mesiar and Stupňanová demonstrated that the CC-Integral is a C-based universal integral I_m^C (KLEMENT et al., 2014), applicable to a fuzzy measure $\mathfrak{m}$ and a copula C. This equivalence is also highlighted in (DIMURO et al., 2019, Remark 5.1).*

Example 12. *Here, we discuss some CC-integrals utilized in the literature: The $CMin$-integral, when employing the copula T_M, is the most commonly used CC-integral in fields such as classification, motor-imagery-based brain computer interfaces, and image resizing (referenced in (LUCCA et al., 2018b; DIMURO et al., 2018a; LUCCA et al., 2018a),*

(Ko et al., 2019) and (DIAS et al., 2018) respectively). It is defined for all $\vec{x} \in [0,1]^n$ *as:*

$$\mathfrak{C}_{\mathfrak{m}}^{C_{T_M}}(\vec{x}) = \sum_{i=1}^{n} (\min\{x_{(i)}, \mathfrak{m}(A_{(i)})\} - \min\{x_{(i-1)}, \mathfrak{m}(A_{(i)})\}).$$

This integral notably achieved the highest accuracy rate among CC-integrals in classification as shown in (LUCCA et al., 2017). According to (MESIAR; STUPŇANOVÁ, 2019, Corollary 1), the $CMin$*-integral is equivalent to the Sugeno integral, a fact also discussed in (DIMURO et al., 2019, Example 5.5).*

4.1.4.2 $C_{F_1F_2}$*-integrals*

To enhance the performance of fuzzy rule-based classification systems, Lucca et al. (LUCCA et al., 2019) expanded upon the concept of CC-integrals by substituting the conventional pair of identical copulas with a pair of more general fusion functions (F_1, F_2) that meet specific criteria, thereby introducing the $C_{F_1F_2}$-integrals. This modification, while broadening the applicability of the integrals, resulted in the loss of certain desirable properties that CC-integrals inherited from copulas, such as invariance when processing repeated elements in an input. Consequently, to ensure a robust definition of this generalization, only symmetric measures were considered in the context of $C_{F_1F_2}$-integrals.

Definition 4.1.16. *(LUCCA et al., 2019, Definition) Let* $\mathfrak{m} : 2^N \to [0,1]$ *be a symmetric fuzzy measure and* $F_1, F_2 : [0,1]^2 \to [0,1]$ *be two fusion functions fulfilling:*

(i) F_1*-dominates* F_2*,*

(ii) F_1 *is* $(1,0)$*-increasing,*

A $C_{F_1F_2}$*-integral is defined as a function* $\mathfrak{C}_{\mathfrak{m}}^{(F_1,F_2)} : [0,1]^n \to [0,1]$*, given, for all* $\vec{x} \in [0,1]^n$*, by*

$$\mathfrak{C}_{\mathfrak{m}}^{(F_1,F_2)}(\vec{x}) = \min\left\{1, x_{(1)} + \sum_{i=2}^{n} F_1\left(x_{(i)}, \mathfrak{m}\left(A_{(i)}\right)\right) - F_2\left(x_{(i-1)}, \mathfrak{m}\left(A_{(i)}\right)\right)\right\}, \quad (11)$$

considering the conditions ***(i)*** *to* ***(iii)*** *stated in Definition 4.1.11.*

In this example, we construct a $C_{F_1F_2}$-integral, which has been applied in fuzzy rule-based classification systems. For the function F_1, we select the geometric mean GM, discussed in Example 6. Given that GM is an overlap function, it satisfies condition **(ii)** from Definition 4.1.16. For the function F_2, we choose the aggregation function F_{BPC} outlined in Example 7. Notably, F_{BPC} is neither a t-norm, an overlap function, nor a copula. It is clear that GM dominates F_{BPC}, fulfilling condition **(i)** from Definition 4.1.16.

Utilizing GM, F_{BPC}, and any symmetric fuzzy measure $\mathfrak{m}$, we can define the $C_{F_1F_2}$-integral $\mathfrak{C}_{\mathfrak{m}}^{(GM,F_{BPC})}$ for all $\vec{x} \in [0,1]^n$ as:

$$\mathfrak{C}_{\mathfrak{m}}^{(GM,F_{BPC})}(\vec{x}) = \min\left\{1, x_{(1)} + \sum_{i=2}^{n}\left(\sqrt{x_{(i)} \cdot \mathfrak{m}\left(A_{(i)}\right)} - x_{(i-1)} \cdot \left(\mathfrak{m}\left(A_{(i)}\right)\right)^2\right)\right\}.$$

As an additional illustration, consider $F_1 = F_{GL}$, the aggregation function from Example 7, and $F_2 = T_M$ (the minimum t-norm from Example 5). The conditions of Definition 4.1.16 are readily met, allowing for the use of any symmetric fuzzy measure $\mathfrak{m}$ to define the $C_{F_1F_2}$-integral $\mathfrak{C}_{\mathfrak{m}}^{(F_{GL},T_M)}$.

While $C_{F_1F_2}$-integrals might not always qualify as aggregation functions or even pre-aggregation functions, there are instances where such integrals, besides satisfying the boundary condition **(A2)**, also meet certain increasingness conditions. These properties make them suitable candidates to function as "aggregation operators".

Theorem 4.1.5. *(LUCCA et al., 2019, Theorem 1, Theorem 2, Proposition 1) For any symmetric fuzzy measure* $\mathfrak{m} : 2^N \to [0,1]$ *and* $k > 0$, $\mathfrak{C}_{\mathfrak{m}}^{(GM,F_{BPC})}$ *is a non-averaging (OD)* $(k, 0, \ldots, 0)$*-increasing function satisfying the boundary conditions (A2).*

Similarly, one can validate the findings of Theorem 4.1.5 for a series of $C_{F_1F_2}$-integrals that have demonstrated remarkable performance in fuzzy rule-based classification systems. Specifically, the highest accuracy rate was achieved by $\mathfrak{C}_{\mathfrak{m}}^{(F_{GL},T_M)}$. This underscores the effectiveness of this integral configuration in enhancing classification outcomes.

4.1.5 Generalizations of the Choquet Integral by Restricted Dissimilarity Functions (RDF)

To make operators sensitive to local contrasts between ordered components, *restricted dissimilarity functions* (RDFs) on $[0,1]$ can be applied, acting as calibrated substitutes for absolute differences. The notion of RDF adopted in (BUSTINCE et al., 2021) is as follows.

Definition 1 (Restricted Dissimilarity function)**.** *A* Restricted Dissimilarity Function (RDF) *is a function* $\delta : [0,1]^2 \to [0,1]$ *that satisfies, for all* $x, y, z \in [0,1]$*, the following conditions:*

(d1) $\delta(x,y) = \delta(y,x)$*;*

(d2) $\delta(x,y) = 1$ *if and only if* $\{x,y\} = \{0,1\}$*;*

(d3) $\delta(x,y) = 0$ *if and only if* $x = y$*;*

(d4) if $x \leq y \leq z$*, then* $\delta(x,y) \leq \delta(x,z)$ *and* $\delta(y,z) \leq \delta(x,z)$.

Table 4: Examples of Restricted Dissimilarity Functions (RDFs).

δ	RDF	δ	RDF
δ_0	$\lvert x-y\rvert$	δ_3	$\lvert\sqrt{x}-\sqrt{y}\rvert$
δ_1	$(x-y)^2$	δ_4	$\lvert x^2-y^2\rvert$
δ_2	$\sqrt{\lvert x-y\rvert}$	δ_5	$\left(\sqrt{x}-\sqrt{y}\right)^{\frac{1}{2}}$

Starting from the standard (non-expanded) form, replacing the adjacent difference by an RDF produces the *d-Choquet* integral, a contrast-aware variant that preserves the $0,1$-conditions and returns values in $[0,n]$.

4.1.5.1 d-Choquet integral

Definition 2 (d-Choquet integral)**.** *(BUSTINCE et al., 2021) A discrete* d-Choquet integral *with respect to a fuzzy measure $m : 2^N \to [0,1]$ and a restricted dissimilarity function $\delta : [0,1]^2 \to [0,1]$ is a mapping $\mathfrak{C}_{m,\delta} : [0,1]^n \to [0,n]$, defined, for all $\boldsymbol{x} \in [0,1]^n$, by:*

$$\mathfrak{C}_{m,\delta}(\boldsymbol{x}) = \sum_{i=1}^{n} \delta\left(x_{(i)}, x_{(i-1)}\right) \cdot m\left(A_{(i)}\right) \tag{12}$$

where $x_{(i)}$ and $A_{(i)}$ were previously defined.

Some examples of RDFs are presented in Table 4. Observe that if δ_0 is considered, the standard Choquet integral is obtained.

Generalizing CF-integrals (Definition 4.1.14) by RDFs, dCF-integrals are obtained:

4.1.5.2 dCF-integral

Definition 3 (dCF-integral)**.** *(WIECZYNSKI et al., 2023) Let $F : [0,1]^2 \to [0,1]$ be a function having zero as left annihilator, $\delta : [0,1]^2 \to [0,1]$ be a restricted dissimilarity function, and $\mathfrak{m} : 2^N \to [0,1]$ be a fuzzy measure. For any $\boldsymbol{x} \in [0,1]^n$, with $(x_{(1)}, \ldots, x_{(n)})$ the increasing permutation of $\boldsymbol{x}$ and $A_{(i)} = \{(i), \ldots, (n)\}$ the subset of indices of the $n-i+1$ largest components of $\boldsymbol{x}$, the generalization of the CI by F and δ, with respect to and $\mathfrak{m}$, called* dCF-integral*, is the function $\mathfrak{C}^F_{\mathfrak{m},\delta} : [0,1]^n \to [0,1]$ defined by*

$$\mathfrak{C}^F_{\mathfrak{m}\delta}(\boldsymbol{x}) \;=\; x_{(1)} \;+\; \sum_{i=2}^{n} F\big(\delta(x_{(i)}, x_{(i-1)}),\, \mathfrak{m}(A_{(i)})\big). \tag{13}$$

4.1.5.3 d-XChoquet

Considering the expanded form of the Choquet integral (Equation (4), and replacing the difference by RDFs, leads to the *d-XChoquet* integrals. These operators are ordered-directional increasing (see (WIECZYNSKI et al., 2022, Theorem 6)), retaining a meaningful monotone behavior even when full coordinatewise increase does not hold.

Definition 4 (d-XChoquet integral)**.** *(WIECZYNSKI et al., 2022) Let $\delta : [0,1]^2 \to [0,1]$ be a restricted dissimilarity function and $\mathfrak{m} : 2^N \to [0,1]$ a fuzzy measure. For any $\boldsymbol{x} \in [0,1]^n$, with $(x_{(1)}, \ldots, x_{(n)})$ the increasing permutation of $\boldsymbol{x}$ and $A_{(i)} = \{(i), \ldots, (n)\}$ the subset of indices of the $n - i + 1$ largest components of $\boldsymbol{x}$, the generalization of the expanded form of the CI by δ, with respect to $\mathfrak{m}$, called the d-XChoquet integral (d-XC), is the function $\mathrm{X}\mathfrak{C}_{\delta,\mathfrak{m}} : [0,1]^n \to [0,n]$ defined by*

$$\mathrm{X}\mathfrak{C}_{\delta,\mathfrak{m}}(\boldsymbol{x}) = x_{(1)} + \sum_{i=2}^{n} \delta\Big(x_{(i)}\, \mathfrak{m}(A_{(i)}),\; x_{(i-1)}\, \mathfrak{m}(A_{(i)})\Big). \tag{14}$$

4.1.5.4 d-CC-integral

The generalization of CC-integrals with RDFs leads to the *d-CC*-integral (LUCCA et al., 2025). When the RDF $\delta(x,y) = |x - y|$ is chosen, full increasingness is maintained, thereby recovering the standard CC-integral. In the general case, the d-CC-integral ensures directional monotonicity (under certain constraints) and ordered directional monotonicity (LUCCA et al., 2025, Theorem 2, Theorem 3), providing an appropriate framework in situations where full monotonicity cannot be achieved.

Definition 5 (d-CC-integral)**.** *(LUCCA et al., 2025) Let $C : [0,1]^2 \to [0,1]$ be a copula, $\delta : [0,1]^2 \to [0,1]$ a restricted dissimilarity function, and $\mathfrak{m} : 2^N \to [0,1]$ a fuzzy measure. For any $\boldsymbol{x} \in [0,1]^n$, with $(x_{(1)}, \ldots, x_{(n)})$ the increasing permutation of $\boldsymbol{x}$ and $A_{(i)} = \{(i), \ldots, (n)\}$ the subset of indices of the $n - i + 1$ largest components of $\boldsymbol{x}$, the generalization of the CC-integral by δ, with respect to $\mathfrak{m}$, called the d-CC-integral (d-CC), is the function $\mathfrak{C}^{C}_{\delta,\mathfrak{m}} : [0,1]^n \to [0,n]$ defined by*

$$\mathfrak{C}^{C}_{\delta,\mathfrak{m}}(\boldsymbol{x}) = x_{(1)} + \sum_{i=2}^{n} \delta\Big(C\big(x_{(i)},\, \mathfrak{m}(A_{(i)})\big),\; C\big(x_{(i-1)},\, \mathfrak{m}(A_{(i)})\big)\Big). \tag{15}$$

4.1.5.5 $d - CF_1F_2 - integral$

Similarly, we can extend this framework to define the *d-CF_1F_2-integral*:

Definition 6 (d-CF_1F_2-integral)**.** *Let $F_1, F_2 : [0,1]^2 \to [0,1]$ be two bivariate fusion functions such that:*

(i) *F_1 dominates F_2, i.e., $F_1(x,y) \geq F_2(x,y)$ for all $x, y \in [0,1]$;*

(ii) *F_1 is $(1,0)$-increasing.*

Let $\delta : [0,1]^2 \to [0,1]$ be a restricted dissimilarity function and $\mathfrak{m} : 2^N \to [0,1]$ a (symmetric) fuzzy measure. For any $\boldsymbol{x} \in [0,1]^n$, with $(x_{(1)}, \ldots, x_{(n)})$ the increasing per-

mutation of $\boldsymbol{x}$ *and* $A_{(i)} = \{(i), \ldots, (n)\}$ *the subset of indices of the* $n - i + 1$ *largest components of* $\boldsymbol{x}$*, the* d-$\mathrm{CF_1F_2}$-integral *of* $\boldsymbol{x}$ *w.r.t.* $\mathfrak{m}$*,* F_1*,* F_2 *and* δ *is defined by*

$$\mathfrak{C}_{\mathfrak{m},\delta}^{F_1,F_2}(\boldsymbol{x}) = \min\Bigg\{1,\ x_{(1)} + \sum_{i=2}^{n} \delta\Big(F_1\big(x_{(i)},\ \mathfrak{m}(A_{(i)})\big),\ F_2\big(x_{(i-1)},\ \mathfrak{m}(A_{(i)})\big)\Big)\Bigg\}. \tag{16}$$

Notation. We henceforth write $m(A_{(i)})$ simply as $m_{(i)}$.

4.2 Chapter Conclusion

Throughout the development of the fuzzy literature, several extensions and generalizations of the Choquet integral have been proposed with the aim of broadening its ability to model interactions among criteria, making the aggregation stage more flexible, and producing new operators with properties suitable for different application contexts. In this chapter, the main of these constructions were presented, starting from the classical Choquet integral, introduced by Choquet (1953–1954), understood as an extension of the concept of the Lebesgue integral through the use of fuzzy measures.

Next, the expanded form of the Choquet integral was considered, obtained by the algebraic distribution of the product appearing in its original formulation. This rewriting opens the way to new families of generalizations, since it allows the product operation to be explicitly replaced by other bivariate functions with specific properties. Figure 6 resume all the Choquet generalizations seen in this chapter and how it can be obtained.

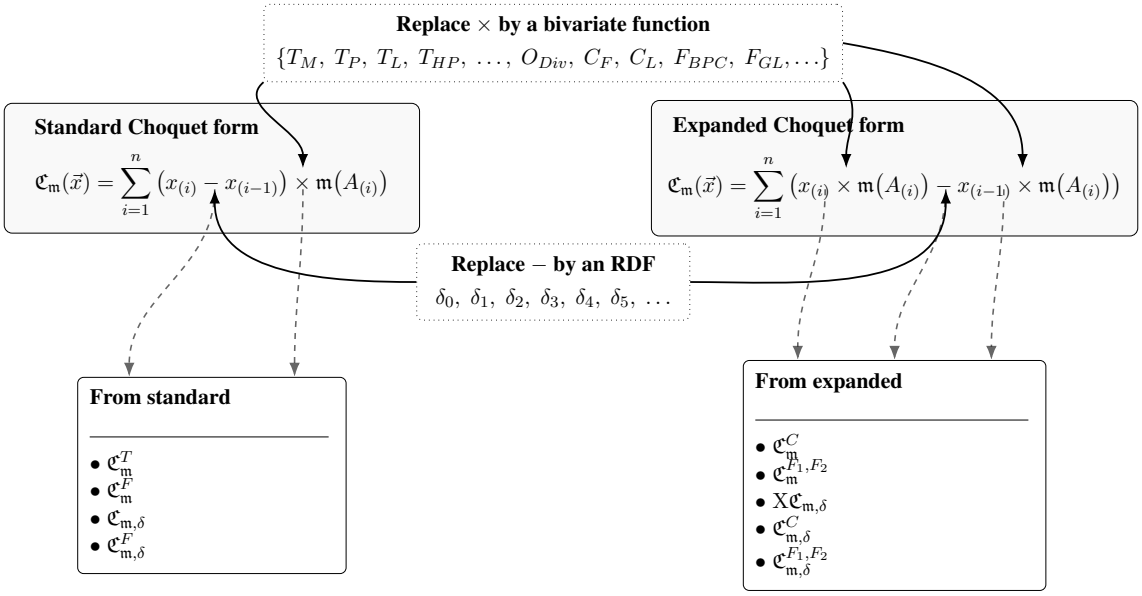


Figure 6: Schematic overview of standard and expanded Choquet-type constructions.

Starting from the standard form of the integral, Lucca et al. (2016) proposed the family

of integrals of the type $\mathfrak{C}_{\mathrm{m}}^{T}$, obtained by replacing the product operation with t-norms. From this perspective, the classical Choquet integral can be interpreted as a particular case of a broader class of operators, built from the combination of fuzzy measures and bivariate functions with well-established aggregative properties.

Still within the scope of the standard form, Lucca et al. (2018a) introduced the integrals $\mathfrak{C}_{\mathrm{m}}^{F}$, in which the generalization is achieved by means of more general fusion functions. This approach significantly broadens the scope of the previous construction, since it allows the use not only of t-norms, but also copulas, overlap functions, aggregation functions, pre-aggregation functions, and even functions that do not belong to these classes, provided that they satisfy suitable conditions to preserve desirable properties of the resulting operator.

On the other hand, in the context of the expanded form, Lucca et al. (2017) proposed the copula-based integrals $\mathfrak{C}_{\mathrm{m}}^{C}$, in which the products arising from the algebraic expansion of the classical integral are replaced by a copula. This construction shows that the expanded form is not merely an algebraic rewriting of the Choquet integral, but also a starting point for new generalizations whose properties may differ from those obtained from the standard formulation.

The expanded form also allows for more general constructions based on pairs of bivariate functions. In this context, one considers integrals of the type $\mathfrak{C}_{\mathrm{m}}^{F_1,F_2}$, in which distinct functions may act on different algebraic roles inherited from the expansion of the classical integral. This approach further increases the flexibility of the model, since it makes it possible to decouple the combination mechanisms involved in the structure of the integral, producing operators potentially different from those obtained when a single function is used throughout the whole formulation.

Finally, extensions based on RDFs were presented, which explicitly introduce the notion of contrast or difference between consecutive ordered values of the input vector. In this context, replacing the classical adjacent difference by an RDF leads to the so-called d-Choquet integral, $\mathfrak{C}_{\mathrm{m},\delta}$, proposed in Bustince et al. (2021). Analogously, combining the approach of the integrals $\mathfrak{C}_{\mathrm{m}}^{F}$ with RDFs gives rise to the integrals $\mathfrak{C}_{\mathrm{m},\delta}^{F}$, formalized by Wieczynski et al. (2023). These constructions further increase the flexibility of the Choquet-like framework, since they allow different forms of sensitivity to variations among the components of the input vector to be modeled.

Still in the context of RDF-based extensions, applying this same idea to the classical expanded form of the Choquet integral leads to the integral of type $\mathrm{X}\mathfrak{C}_{\mathrm{m},\delta}$, also called the dXC integral, formalized by Wieczynski et al. (2022).

In an analogous way, incorporating RDFs into the family of copula-based integrals $\mathfrak{C}_{\mathrm{m}}^{C}$ gives rise to the integrals $\mathfrak{C}_{\mathrm{m},\delta}^{C}$, that is, the dCC integrals, studied by Lucca et al. (2025). In this family, the copula-based structure is preserved, while at the same time an explicit measure of dissimilarity between consecutive ordered values is introduced.

Finally, when the RDF-based approach is combined with integrals of the form $\mathfrak{C}_{\mathfrak{m}}^{F_1,F_2}$, one obtains extensions of the type $\mathfrak{C}_{\mathfrak{m},\delta}^{F_1,F_2}$. These constructions represent a further step in the generalization process, since they allow the simultaneous combination of: i) the flexibility resulting from the use of two potentially distinct bivariate functions in the expanded form; and ii) the ability to model local differences through RDFs. In this way, this type of operator broadens the scope of the Choquet-like framework and reinforces its potential for applications in scenarios in which both the nature of fuzzy interaction and the sensitivity to variations among inputs play a relevant role.

5 IMAGE PROCESSING TOPICS

In this chapter, we review some important topics in image processing that are essential for understanding this thesis. In Section 5.1.1, the initial topics specifically related to image processing and computer vision will be presented, starting with the concept of filtering. This section will cover the issue of smoothing filters and introduce the idea of edge detection using derivative-based filters. Then in Section 5.2, a summary of the classical and most widespread edge detection techniques in recent years is presented. This rationale is based on four major review articles published in the last years (AGGARWAL et al., 2019; JING et al., 2022; MUBASHAR et al., 2022; GHOSH et al., 2020). The following is a summary grouped by approach: Gradient-based methods (Section 5.2.1), Region segmentation-based methods (Section 5.2.2), Methods based on machine learning (Section 5.2.3) and Fuzzy Logic based methods (Section 5.2.4). Finally, but no less importantly, Section 5.3 introduces the main dataset employed in the experimental investigations and validations of the proposed models.

5.1 Filtering

The concept of filtering in image processing, as presented by Gonzalez and Woods (GONZALEZ; WOODS, 2002), encompasses techniques aimed at modifying or enhancing the visual characteristics of images. These techniques are crucial for improving visual interpretation and optimizing the performance of algorithms in pattern recognition tasks and image analysis. Filters are categorized into linear, non-linear, and transform-based methods.

Linear filters, also known as convolution filters, use a kernel or matrix that is applied to the image to produce a desired effect. Non-linear filters, such as the median filter, are typically used when preserving edges is desired during noise reduction. Finally, transform-based filters such as the Fourier Transform and the Wavelet Transform operate in the frequency domain, allowing for the application of low-pass and high-pass filters to meet specific image processing needs.

This section provides a synthesis of the main filtering techniques that are essential for

understanding this work. Initially, an introduction to filtering methods in digital image processing is presented (Section 5.1.1). Subsequently, smoothing methods are discussed (Section 5.1.2), and finally, derivation methods are addressed (Section 5.1.3).

5.1.1 Filtering methods in digital images

Image filtering involves applying an operator, or kernel, to an image to produce a modified version. This process can be conducted in both the spatial and frequency domains. In the spatial domain, conditioning operations are directly applied to the image pixels. In the frequency domain, images are transformed into the frequency space (typically using the Fourier Transform) before the conditioning is applied, and then converted back to the spatial domain.

Spatial domain conditioning involves manipulating the image's pixels directly. These operations can be described by the function, defined for all pixels' positions (x, y), by :

$$g(x, y) = T\{f(x, y)\},$$

where $f(x, y)$ represents the original image, $g(x, y)$ signifies the processed result, and T serves as an operator that interacts with f, defined around a specific point (x, y). This operator can also be applied to several images simultaneously. A common approach to define a neighborhood around (x, y) includes using a square or rectangular subimage centered on this point. This subimage is moved across the original image, starting from the upper left corner, for example, and applying T at each location to generate g. Masks or kernels, often small matrices like 3×3, are employed in this context for tasks such as sharpening or smoothing (GONZALEZ; WOODS, 2002).

Frequency domain approaches rely on the principle of convolution. Considering $g(x, y)$ as the result of convolving the image $f(x, y)$ with a linear operator $h(x, y)$, the relationship in the frequency domain is expressed as

$$G(u, v) = H(u, v) \cdot F(u, v)$$

where G, H, and F are the Fourier transforms of g, h, and f, respectively. $H(u, v)$ acts as the system's transfer function. Frequency conditioning involves the multiplication of the Fourier transforms of f and h, yielding G. Subsequently, the processed image is reconstructed through the inverse Fourier transform of G (OPPENHEIM; SCHAFER, 1999).

5.1.2 Conditioning filters

Conditioning, or smoothing filters, play an important role in digital image processing. They are engineered to diminish details and noise, yielding a smoother image. These filters are extensively used for both enhancing the visual quality of images and preparing

them for analysis and pattern recognition processes. The filters can be either linear, such as the average filter, or nonlinear, like the median filter, and are effective in reducing image noise (JAIN, 1989). Among the various filters in the spatial domain, the most largely used in the literature are:

(a) Gaussian Blur: It is a usual technique that employs the Gaussian function for image smoothing. It is based on convolving the image with a Gaussian kernel, where each image point is weighted by its distance from the central point, following a normal distribution. The application of this filter results in a blurring effect that preserves edges and is particularly useful for noise reduction and detail minimization (JAIN, 1989).

(b) Mean Shift: This is an iterative procedure that involves shifting each pixel to the average of the pixels in its vicinity. Often used in cluster analysis and image segmentation, this technique adjusts pixel positions to converge to areas of maximum pixel density. Through this process, Mean Shift can smooth the image while maintaining consistency in color and texture regions, making it effective for image segmentation and noise reduction in homogeneous areas (COMANICIU; MEER, 2002).

(c) GF-Smoothing (Gravitational Force Smoothing): This method consists in an approach to image smoothing inspired by the Universal Law of Gravitation. In this method, image pixels are treated as particles influencing each other through gravitational forces, where the attraction force is proportional to the product of the 'masses' (color intensities) and inversely proportional to the distance between them. Each pixel is represented in a five-dimensional space, encompassing its spatial positions and the color intensity values in the RGB color space. The gravitational forces applied to the pixels cause them to alter their color intensities, while their spatial positions remain fixed. Smoothing is achieved through continuous variation in the color intensity of the pixels, controlled by an influence factor on the color variables and a gravitational constant adjusting the intensity of particle movement in the system, with the process applied iteratively to achieve the desired effect (MARCO-DETCHART et al., 2018b).

(d) Box Filter: This filter, also known as an average filter, is a simple and common image smoothing technique in digital image processing. The fundamental concept behind the box filter is to replace the value of each pixel in the image with the average of the pixel values in its immediate neighborhood (GONZALEZ; MELIN; CASTILLO, 2017).

Figures 7, 8 and 9 illustrate the differences between classic conditioning methods: Gaussian, box filter, and mean shift. Each first image in both figures represents the co-

lor intensities of the original image. The roughness of the edges, or supposed edges, is apparent. Following this, the effects of applying each corresponding filter are observed, starting with Gaussian, followed by the box filter in one figure and by mean shift in another. The preservation of edges varies with each method and can be discerned by the difference in the transitions from peaks to valleys in the surface image.

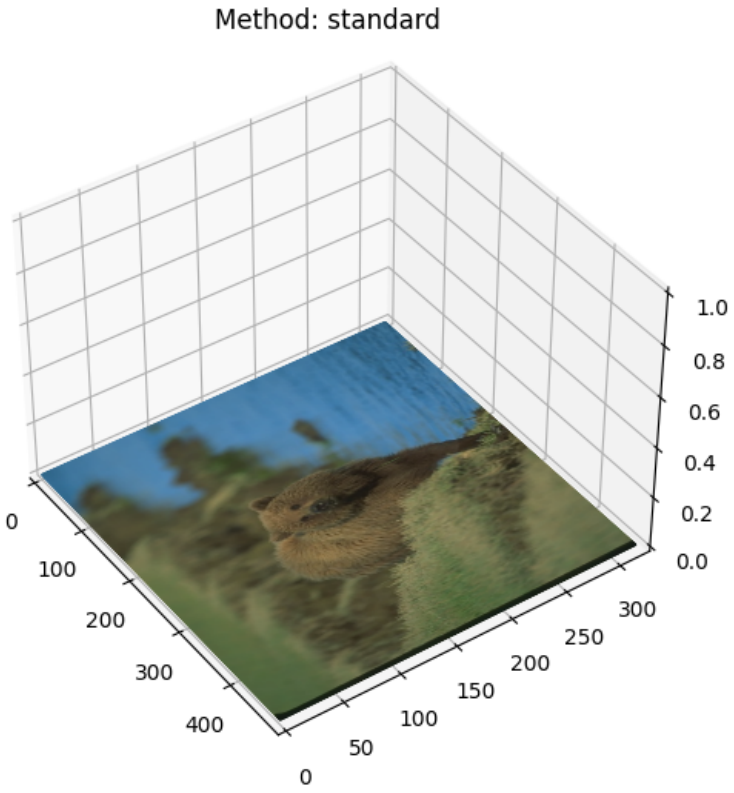


Figure 7: Original image without intensity representation on z axis. Source: author

In addition to spatial domain smoothing filters, frequency domain filters also exist. As discussed earlier, elements like edges and noise, which represent abrupt transitions in the image, contribute to the high frequency content in its Fourier transform. Therefore, smoothing in the frequency domain is achieved by attenuating the high-frequency components in the Fourier transform, commonly done through low-pass filters. This approach is particularly useful for identifying and manipulating specific image features, such as periodicities or orientations, and is often employed in applications requiring more sophisticated analyses (PRATT, 2007).

5.1.3 Derivation filters

The operation of averaging pixels in a region tends to smooth out details, analogous to mathematical integration. Conversely, differentiation operations, such as gradient computation, can enhance these details. The gradient of $f(x, y)$ is defined as $\nabla f = \left[\frac{\partial f}{\partial x}, \frac{\partial f}{\partial y}\right]$, with its magnitude $\|\nabla f\|$ employed in various image enhancement techniques. Alternati-

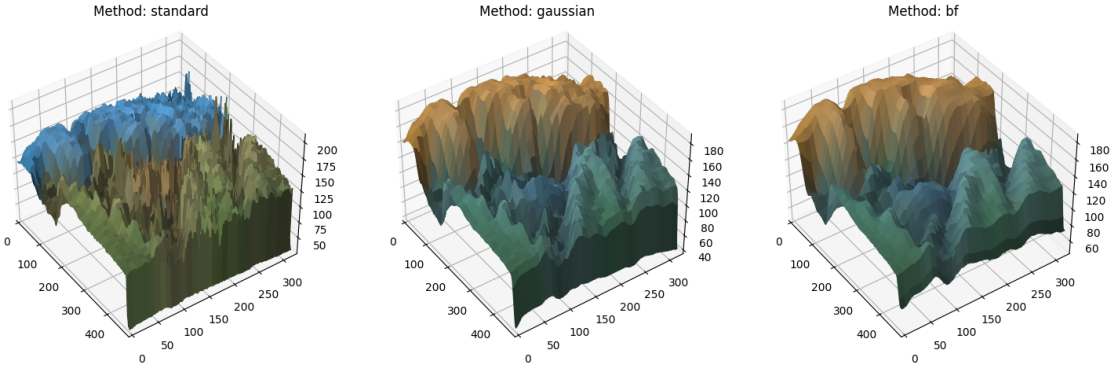


Figure 8: Smoothing effect: Gaussian and box filter. Source: author

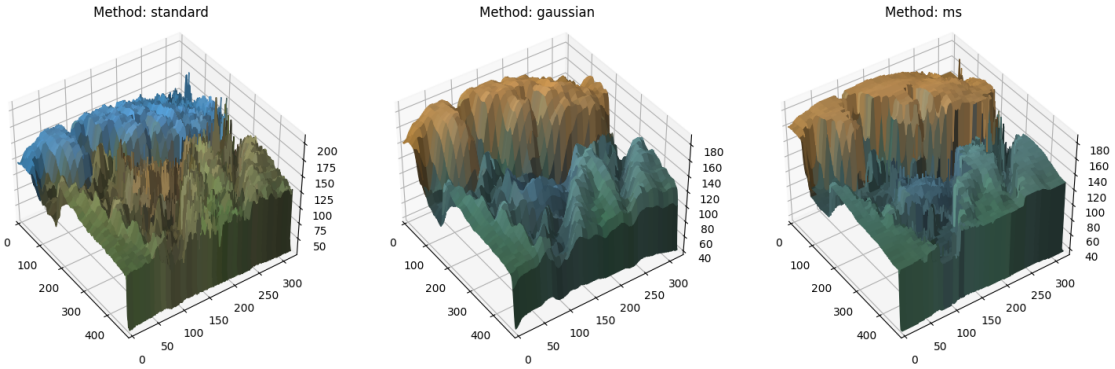


Figure 9: Smoothing effect: Gaussian and mean shift. Source: author

ves to complex calculations include using absolute values or cross differences (SONKA; HLAVAC; BOYLE, 2014). Edge detectors fall into this category of conditioning and will be discussed more extensively in the following Section 5.2.

5.2 Edge Detection Methods

There is a diversity of edge detection methods extensively discussed in the specialized literature. These methods are explored in more detail in Chapters 6 and 7, where systematic reviews addressing both theoretical aspects and practical applications are presented. In this section, however, we will provide a general overview of these techniques, highlighting their main characteristics and the role they play in enhancing image analysis.

5.2.1 Gradient-based methods

A digital image is a discrete representation of the variation of light in the real world. So each numerical value carried by the pixel represents the intensity of light or color at that point. The contours of objects in the image can be interpreted as a transition zone between these intensities. Much intense transitions have much higher chance of being an edge than too smooth transitions. It should be noted that the first edge detectors that appeared in the literature took this point into account, based on the gradient of the image

(AGRAWAL; BHOGAL, 2019).

There are two approaches to gradient-based detection: (i) based on first-order derivatives, or (ii) based on the second-order derivatives. The most well-known gradient-based detection methods are: (i) first-order fixed operations; (ii) first-order oriented operations that use the maximum energy of the orientation, or, (iii) two-direction operations. Table 5 summarizes the first-order methods, which consist of three fundamental steps:

(i) Computation of the magnitude of the gradient $|\nabla I|$ and its orientation η, using a kernel 3×3, (Table 5), with a first-order, vertical and horizontal derivative filter such as steerable Gaussian, oriented anisotropic Gaussian kernels or a combination of two half-Gaussian kernels;

(ii) Non-maximum suppression operation for thinner edges: selection of pixels with a local maximum gradient magnitude along the direction η of the gradient, which is perpendicular to the orientation edge;

(iii) Determination of the thresholds of the fine contours to get the contour map.

These steps are described visually in Figure 10.

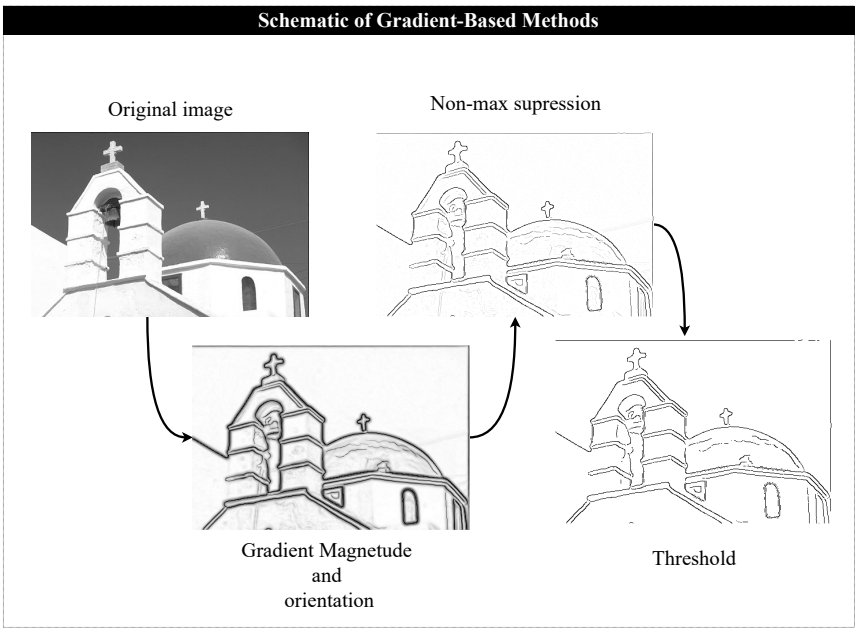


Figure 10: Schematic overview of gradient-based methods. Source: author

Considering the gradient-based methods (AGGARWAL et al., 2019), in Figure 11, we provide a timeline showing the main related works and their order of publication. Having this chronological order into account, in the following we discuss the main articles.

The Canny detector (CANNY, 1986), which is one of the most widely used method, was proposed considering a Gaussian smoothing followed by a gradient operation and finally thresholding. In (JING et al., 2022), the authors discussed other first-order

Table 5: The gradient magnitude and orientation calculation for a scalar image I where I_θ represents the derivative of the image using the first-order filter in orientation θ in radians (MAGNIER; ABDULRAHMAN; MONTESINOS, 2018).

Operator Type	**Fixed Operator**	**Filter Oriented**	**Half-Gaussian Kernels**
Magnitude of gradient	$\lvert\nabla I\rvert = \sqrt{I_0^2 + I_{\pi/2}^2}$	$\lvert\nabla I\rvert = \max_{\theta\in[0,\pi)} \lvert I_\theta\rvert$	$\lvert\nabla I\rvert = \max_{\theta\in[0,2\pi)} \lvert I_\theta\rvert - \min_{\theta\in[0,2\pi)} \lvert I_\theta\rvert$
Gradient direction	$\eta = \arctan \frac{I_{\pi/2}}{I_0}$	$\eta = \arg\max_{\theta\in[0,\pi)} \lvert I_\theta\rvert + \frac{\pi}{2}$	$\eta = \left(\arg\max_{\theta\in[0,2\pi)} I_\theta + \arg\min_{\theta\in[0,2\pi)} I_\theta\right)/2$

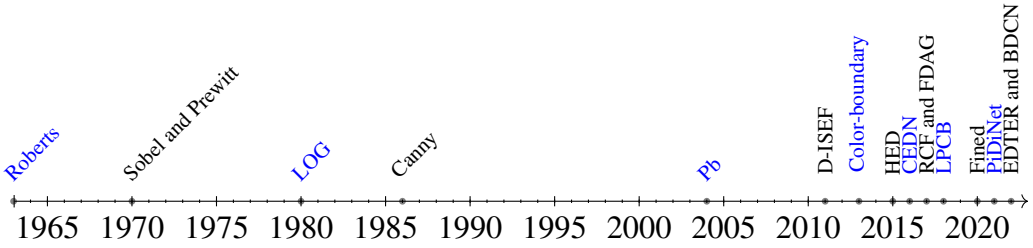


Figure 11: Chronology of detection methods without using aggregation functions or fuzzy methods (ROBERTS, 1980; SOBEL; FELDMAN, 1973; PREWITT, 1970; MARR; HILDRETH, 1980; CANNY, 1986; ARBELAEZ et al., 2011; MCILHAGGA, 2010; YANG et al., 2013; XIE; TU, 2017; YANG et al., 2016; LIU et al., 2019; ZHANG et al., 2017; DENG et al., 2018; WIBISONO; HANG, 2021; SU et al., 2021; PU et al., 2022; HE et al., 2022)

derivative-based methods inspired by Canny, such as D-ISEF (MCILHAGGA, 2010), color-boundary(YANG et al., 2013) and FDAG(ZHANG et al., 2017).

The detector proposed by Sobel et al. (SOBEL; FELDMAN, 1973) calculates the gradient value at each pixel position in the image using a fixed operator. In turn, Prewitt et al. (PREWITT, 1970) has a similar technique to Sobel, which, however, has no adjustment coefficients, varies by a constant value, and calculates the magnitude of the gradient with the image orientations. In Roberts (ROBERTS, 1980), the derivative is calculated using the root of the difference between diagonally adjacent pixels, as follows:

$$Z_{i,j} = \sqrt{(y_{i,j} - y_{i+1,j+1})^2 + (y_{i+1,j} - y_{i,j+1})^2} \tag{17}$$

where,

$$y_{i,j} = \sqrt{x_{i,j}}, \tag{18}$$

focusing on invariant properties that the edges exhibit.

Log filter (MARR; HILDRETH, 1980), or Gaussian Laplacian, is based on Gaussian filtering followed by a Laplacian operation, as follows:

$$\nabla^2 f(x,y) = \frac{\delta^2 f(x,y)}{\delta x^2} + \frac{\delta^2 f(x,y)}{\delta y^2}. \tag{19}$$

This approach considers a second-order operator, which seeks to identify the maximum and minimum points of the variation of intensities, so that, by finding these points that

cross to zero, the edge candidates in the image are found. The Gaussian filter step is important because it is a second-order method and therefore extremely sensitive to noise.

5.2.2 Region-based segmentation methods

In these methods, regions are segmented in various forms, such as clustering methods and automated thresholding. The edges are detected as the border of these regions. It is possible to leverage the regions formed by the textures in high-complexity images as an enabler for the process of detecting the edges between them (MUBASHAR et al., 2022).

In general, the region-based segmentation approach outperforms edge-based methods. Other methods such as those based on frequency domain filtering and statistical methods are used both in region-based segmentation methods and for direct edge detection. Through the emergence of texture descriptors and other local information such as brightness, texture, and color gradient, the probabilistic contour (Pb) method (ARBELAEZ et al., 2011; JING et al., 2022; MUBASHAR et al., 2022) has been one of the most representative approaches in this type of detectors.

5.2.3 Methods based on machine learning

By combining the Pb method with a logistic regression it was possible to develop another kind of edge detection model (JING et al., 2022). The method has been extended over the years in many ways, bringing, for example, the multiscale probabilistic contour method and the multiscale spectral clustering.

Currently, new techniques based on machine learning have emerged, in particular those based on Convolutional Neural Networks (CNN's). In (JING et al., 2022), the authors present other machine learning-based methods in their research, such as *holistically-nested edge detection*, better known as HED (XIE; TU, 2017), proposed to improve the performance of convolutional neural networks, which then inspired the methods: CEDN (YANG et al., 2016), RCF (LIU et al., 2019), LPCB (DENG et al., 2018), among others. Recently, the BDCN (HE et al., 2022) method emerged, proposing detection at different scales. Currently, techniques such as Fined (WIBISONO; HANG, 2021), EDTER (PU et al., 2022), and PiDiNet (SU et al., 2021) have been proposed, to deal with edge detection without the need for a voluminous database for model training.

5.2.4 Fuzzy Logic-based methods

A fuzzy inference system modeling to efficiently extract edges in noisy images, called the Russo method, was proposed in (RUSSO, 1998). From this point, the application of fuzzy set theory (ZADEH, 1965) in edge detection increased, justified by the fuzzy nature of object edges in a digital image, which makes fuzzy set theory suitable for solving such problems.

Detectors based on the junction of techniques such as divergence and fuzzy entropy

minimization (FED) (VERSACI; MORABITO, 2021), and detectors based on morphological gradient and type-2 fuzzy logic (Type-2 Color) (MELIN et al., 2014) have appeared in the literature. Hybrid techniques and fuzzy versions of neural networks have been created, improving the performance of other approaches and, in some cases, decreasing the computational complexity.

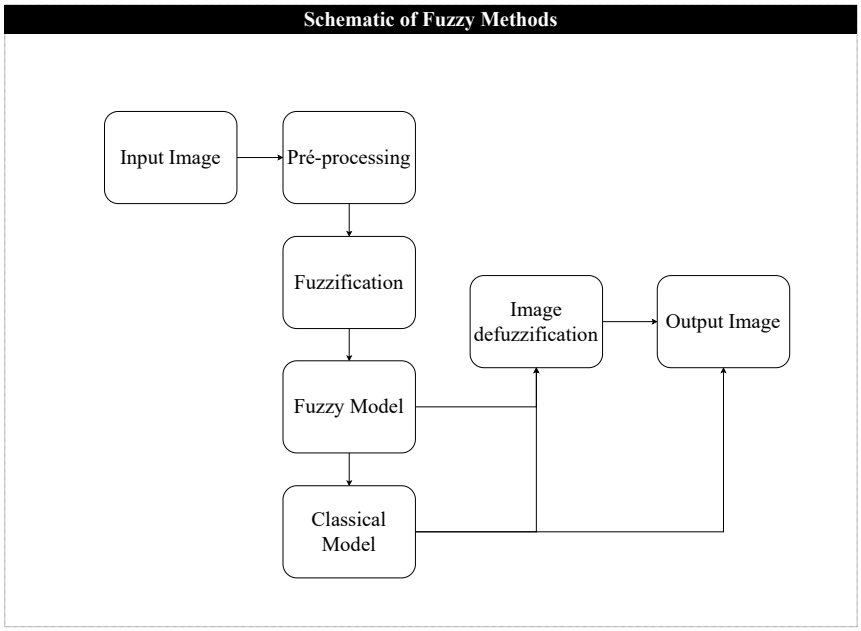


Figure 12: Schema of Fuzzy-Based Methods. Source: author

In the studies of hybrid methods (GHOSH et al., 2020) that use neural networks and fuzzy logic type-1, type-2, and type-3 (hybrid approach of neuro-fuzzy-1, neuro-fuzzy-2, and neuro-fuzzy-3, respectively), which are extensions of fuzzy logic with more degrees of associated uncertainty, can be also identified in the literature, as well as the use of fuzzy logic to improve classical methods, such as Canny (C&I-TYPE2), and a hybrid method that uses Sobel, type-1 fuzzy logic, and type-2 fuzzy interval system (T2FLS).

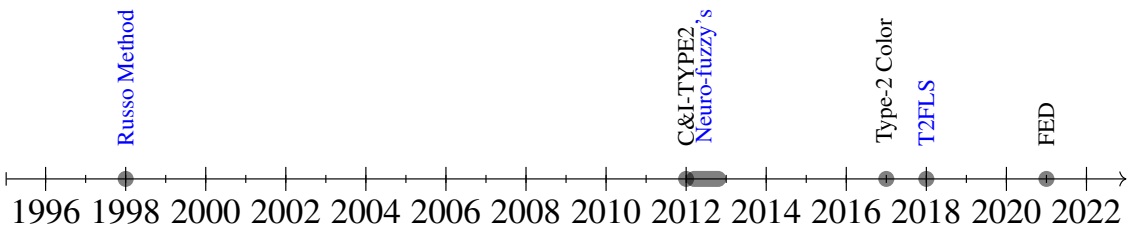


Figure 13: Chronology of fuzzy methods presented above (RUSSO, 1998; GHOSH et al., 2020; VERSACI; MORABITO, 2021; MELIN et al., 2014)

For a better understanding of fuzzy logic-based methods, Figure 13 shows a *timeline* presenting in chronological order the papers previously discussed. Figure 12 presents an attempt to broadly represent a schema for fuzzy logic-based methods.

5.3 Dataset and quantification of the results

In this thesis (in Chapters 9, 10,11, 13), we primarily used the Berkeley Segmentation Dataset (BSDS500) (ARBELAEZ et al., 2011), a canonical collection of natural images split into the official *train*, *val*, and *test* partitions. All images share a resolution of 481×321 pixels, differing only by orientation. Following standard practice, we report results exclusively on the *test* partition (200 images), ensuring direct comparability with the literature and a rigorous benchmark.

This dataset is particularly suitable for edge detection and segmentation research because it is both comprehensive and widely adopted in prior work (e.g., (MARCO-DETCHART et al., 2025; SORIA et al., 2023)). Each image is paired with multiple human-labeled boundary maps, typically four to nine per image, capturing variability in human perception (see Figure 14).

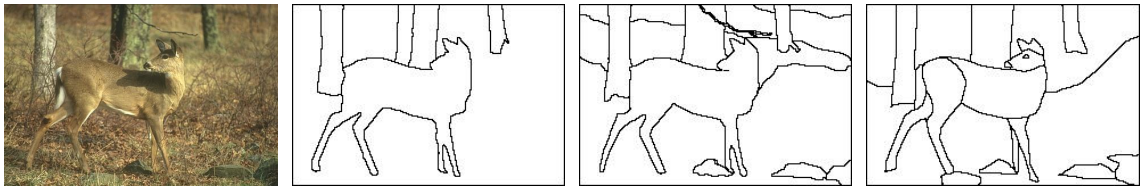


Figure 14: Image 236017 from BSDS500 with three of its hand-labeled ground-truth boundary maps.

As these outputs and annotations are represented as binary images, the comparison between them is treated as a binary classification problem. To construct a meaningful confusion matrix, it is crucial to employ a strategy that relates detected edges with reference annotations, even when slightly displaced.

We primally adopted the standard methodology by Estrada and Jepson (ESTRADA; JEPSON, 2009) (available via the KITT toolkit[1]), defining a spatial tolerance of 2.5% of the image diagonal. Following the framework outlined by Martin *et al.* (MARTIN; FOWLKES; MALIK, 2004), this process categorizes pixels into True Positives (TP), True Negatives (TN), False Positives (FP), and False Negatives (FN). These values are then used to calculate the: Precision (PREC), Recall (REC), and the F-measure (Fm_α):

$$\text{PREC} = \frac{\text{TP}}{\text{TP} + \text{FP}} \tag{20}$$

$$\text{REC} = \frac{\text{TP}}{\text{TP} + \text{FN}} \tag{21}$$

$$\text{F}_\alpha = \frac{\text{PREC} \cdot \text{REC}}{\alpha \cdot \text{PREC} + (1 - \alpha) \cdot \text{REC}} \tag{22}$$

[1] Available at: `https://github.com/giaracvi/KITT`. Accessed on: 28 Mar. 2026.

Consistent with previous studies in the field (MARTIN; FOWLKES; MALIK, 2004; LOPEZ-MOLINA; De Baets; BUSTINCE, 2013), we utilize the $\mathrm{F}_{0.5}$ measure as our primary performance metric.

5.4 Chapter Conclusion

In this chapter, we sought to summarize the main topics in image processing and computer vision that are important for understanding this thesis. First, we discussed the concept of filters, which consists of a transformation applied to an image, either in the frequency domain or in the spatial domain. Among the different types of filters, smoothing filters and derivative filters stand out.

Smoothing filters are mainly applied with the purpose of reducing noise in images. However, the concept of noise depends largely on the problem under analysis. There are textures in images that may be regarded as noise in one application, but in another they may represent an important characteristic to be analyzed. In this thesis, we address smoothing filters in accordance with Bezdek's framework (BEZDEK; CHANDRASEKHAR; ATTIKOUZEL, 1998b), which will be discussed in greater detail in the presentation of our first edge detection method, as a conditioning stage.

Next, derivative filters are presented. In this work, these filters are used in the feature extraction stage, where the extracted features are later aggregated by the functions discussed in the chapter on mathematical foundations. Such derivative filters are conditioned by the scale parameters defined in the conditioning stage.

We also addressed, in general terms, the main groups of edge detection methods: gradient-based methods, region segmentation-based methods, machine learning-based methods, and, finally, fuzzy logic-based methods. A general scheme of fuzzy logic-based methods was also presented. Among the stages of such a method are preprocessing, fuzzification, model application, and defuzzification, which ultimately leads to the output image.

In our models, preprocessing is given by the scale conditioning of the image, followed by feature extraction in the interval $[0, 1]$, which leads to the application of fuzzy functions (the mathematical model) responsible for aggregating fuzzy information. Then, an interpretation stage, or defuzzification, produces the final edge image. Specifically in our case, the stages of non-maximum suppression and hysteresis, or some other thresholding stage, are applied in our proposed methods in the following chapters, within the context of each experimental chapter.

Finally, the main dataset used in this thesis, as well as the main evaluation method adopted in accordance with the literature, are described. In the next chapter, as detailed in the thesis methodology, a systematic review of fuzzy logic-based edge detection methods is presented. In this way, also with the support of bibliometric analysis, we will identify

the methodological paths and trends in fuzzy logic-based methods that are relevant for contextualizing this thesis.

6 SYSTEMATIC REVIEW OF EDGE DETECTION METHODS BASED ON FUZZY LOGIC

In order to obtain a broader quantitative and qualitative view, encompassing publications, thematic evolution, and the overall structure of the scientific production related to fuzzy methods applied to edge detection, and considering the importance of research in edge detection already presented in Section 1, as well as the fact that, to the best of our knowledge, there is still a lack of reviews specifically devoted to fuzzy methods in this context, this chapter proposes a systematic literature review of fuzzy edge detection methods.

In this sense, the main research question that is intended to be answered is: **RQF - what is the state of the art of fuzzy edge detection methods?** To relate them to the rest of the literature in the area of edge detection, the following should also be answered: **RQG - what is the state of the art of edge detection methods?** For each research question, a bibliometric analysis was sought to provide a set of information that would appropriately position new research activities, this being another contribution of this work, besides summarizing and describing the found methods.

This chapter is organized as follows. In Section 6.1 (Methodology), the search terms, inclusion and exclusion criteria, as well as the number of papers found and admitted for review will be discussed. Next, in Section 6.2, the results and discussion are presented for each research question mentioned above, summarizing the reviewed methods with their respective bibliometric analyses. Finally, in Section 6.3, the conclusions are exposed.

6.1 Methodology

This section introduces the methodology used to address research problems via a systematic literature review.

6.1.1 Systematic literature review

According to (KITCHENHAM; CHARTERS, 2007) guidelines, a systematic literature review is a method of analysis with the objective of identifying, assessing, and com-

prehending all pertinent existing research concerning a particular research issue, subject, or area of interest. Among the numerous motives for conducting a systematic literature review, the most prevalent ones include:

i. Summarize the existing evidence regarding treatment or technology;

ii. Identify gaps in current research to suggest areas for future research;

iii. Provide a set of information that appropriately positions new research activities and;

iv. Reduce, or try to eliminate research bias.

In this context, this study aims to provide a concise overview of the current state of technology in the realm of fuzzy edge detection methods. To achieve this, the essential best practice inquiries for conducting a high-quality review, as outlined in (REVIEWS; DISSEMINATION, 2009), have been considered.

6.1.2 Definition of criteria, search in the indexing bases and obtaining primary research

In order to address the research problems, a search was conducted through two major bibliographic databases. Scopus (SC)[1] and Web of Science (WS)[2] A total of 34 papers were selected by combining the results from both databases (21 from SC and 16 from WS), which automatically excluded any duplicates.

The summary of all the included information and documents that underwent each exclusion step, to be discussed below, is presented in Table 6. The table displays, for each search question, the inclusion terms considered, with ABS() denoting terms found in the abstract and TITLE() referring to terms found in the title. The "number of occurrences"column represents the total number of papers retrieved by each database, where "inc"indicates the number of papers located in that search, and for each exclusion step ("exc"), it signifies the total number of selected papers.

One can see in Table (6) that four exclusion steps were considered:

i. Step one:

a) Exclusion of papers published before the year 2017.

ii. Step two:

a) Elimination of those that were not written in the English language;

b) Deletion those that have not been published in the computer science or related field and;

[1] www.scopus.com
[2] www.webofscience.com

Table 6: Terms of Inclusion and Exclusion and Number of Selected Papers. Retrieved from (SILVA et al., 2023).

Research Question	Terms of Inclusion	SCOPUS	WEB OF SCIENCE
RQG	*ABS(edge PRE/detection) OR ABS(image PRE/segmentation) AND TITLE(survey or review)*	inc: 768 1ª exc: 518 (i) 2ª exc: 244 (ii) 3ª exc: 15 (iii) 4ª exc: 15 (iv)	inc: 1,475 1ª exc: 1,038(i) 2ª exc: 248(ii) 3ª exc: 3(iii) 4ª exc: 3(iv)
RQF	*ABS(fuzzy AND (edge PRE/detection)) AND TITLE(fuzzy OR edge OR segmentation)*	inc: 870 1ª exc: 247 (i) 2ª exc: 7 (ii) 3ª exc: 6 (iii) 4ª exc: 6(iv)	inc: 717 1ª exc: 224 (i) 2ª exc: 21(ii) 3ª exc: 13(iii) 4ª exc: 13(iv)

c) Elimination papers that had a title that demonstrated the lack of relevance of that study to this review work.

iii. Step three:

a) Deletion of the works flagged as portrayed by the journal and;

b) Analysis of the abstract, eliminating articles that were outside the scope of this review.

iv. Step four:

a) Analysis of the methodology and exclusion of those with no validation of the proposed segmentation method.

6.1.3 Bibliometric analysis

Bibliometric analysis is defined as the quantitative exploration of the attributes of a collection of works, aimed at the management of knowledge and scientific information related to a particular theme or subject (ARIA; CUCCURULLO, 2017). Commonly examined observable parameters from the selected articles and papers include their references, authors, number of citations, and the most significant journals in the field.

For conducting the analysis of the papers in this study, the bibliometrix tool within the Rstudio software was employed (ARIA; CUCCURULLO, 2017). Each set of papers, chosen to address a specific research problem, underwent a comprehensive bibliometric analysis that included an assessment of keywords, authors, affiliations, abstracts, citations, and country of origin. Only the pertinent information related to the research problem was reported.

6.2 Results and discussion

This section presents the results, methods, and a summary of each bibliometric analysis for each group of papers, followed by a short discussion aimed at synthesizing the

Table 7: Papers in edge detection (RQG). Retrieved from (SILVA et al., 2023).

Reference	Paper title
(KAUR; KAUR, 2017)	An Edge detection technique with image segmentation using Ant Colony Optimization: A review
(CASTILLO et al., 2017)	Review of Recent Type-2 Fuzzy Image Processing Applications
(YOGESH et al., 2018)	A comparative review of various segmentation methods and its application
(MAGNIER; ABDULRAHMAN; MONTESINOS, 2018)	A review of supervised edge detection evaluation methods and an objective comparison of filtering gradient computations using hysteresis thresholds
(MAGNIER, 2018)	Edge detection: a review of dissimilarity evaluations and a proposed normalized measure
(AGRAWAL; BHOGAL, 2019)	A review—Edge detection techniques in dental images
(AGGARWAL et al., 2019)	Review of Segmentation Techniques on Multi-Dimensional Images
(ZHU; LI, 2019)	Survey on the image segmentation algorithms
(SURESH; SRINIVASA, 2019)	Various image segmentation algorithms: A survey
(GHOSH et al., 2020)	Different EDGE Detection Techniques: A Review
(BUDZYN; RZEPKA, 2020)	Review of edge detection algorithms for application in miniature dimension measurement modules
(CHAKRAPANI et al., 2021)	A Survey of Sobel Edge Detection VLSI Architectures
(ISA et al., 2021)	Review of Edge-based Image Segmentation on Electrical Tree Classification in Cross-linked Polyethylene (XLPE) Insulation
(MUBASHAR et al., 2022)	Have We Solved Edge Detection? A Review of State-of-the-art Datasets and DNN-based Techniques
(YADAV; PANDEY, 2022)	Image Segmentation Techniques: A Survey
(JING et al., 2022)	Recent advances on image edge detection: A comprehensive review

obtained information.

6.2.1 State of the Art in Edge Detection (RQG)

To identify state-of-the-art edge detection methods in the literature, the papers summarized in Table 7 were chosen. The bibliometric analysis was conducted to understand common terms, including those that have gained significance in the last six years.

First, the absolute numbers of citations received by each work were extracted from the metadata to identify those of greater relevance to the research topic. Furthermore, the most cited papers are those that potentially offer the best summary of the state of the art up to the year of publication and demonstrate a higher ratio between the number of

citations and the time elapsed since publication.

In this scenario, the articles (MAGNIER; ABDULRAHMAN; MONTESINOS, 2018; KAUR; KAUR, 2017; YOGESH et al., 2018) emerge as the most cited, occupying the first three positions. When assessing the number of citations per year, from the publication date to the present moment, it was found that the works (SURESH; SRINIVASA, 2019; MAGNIER; ABDULRAHMAN; MONTESINOS, 2018) attain the highest scores. Notably, (SURESH; SRINIVASA, 2019) stands out as the most recent work with the highest citation-to-year ratio. Figure 15 visually presents the relationships among the most frequently cited documents in terms of absolute numbers.

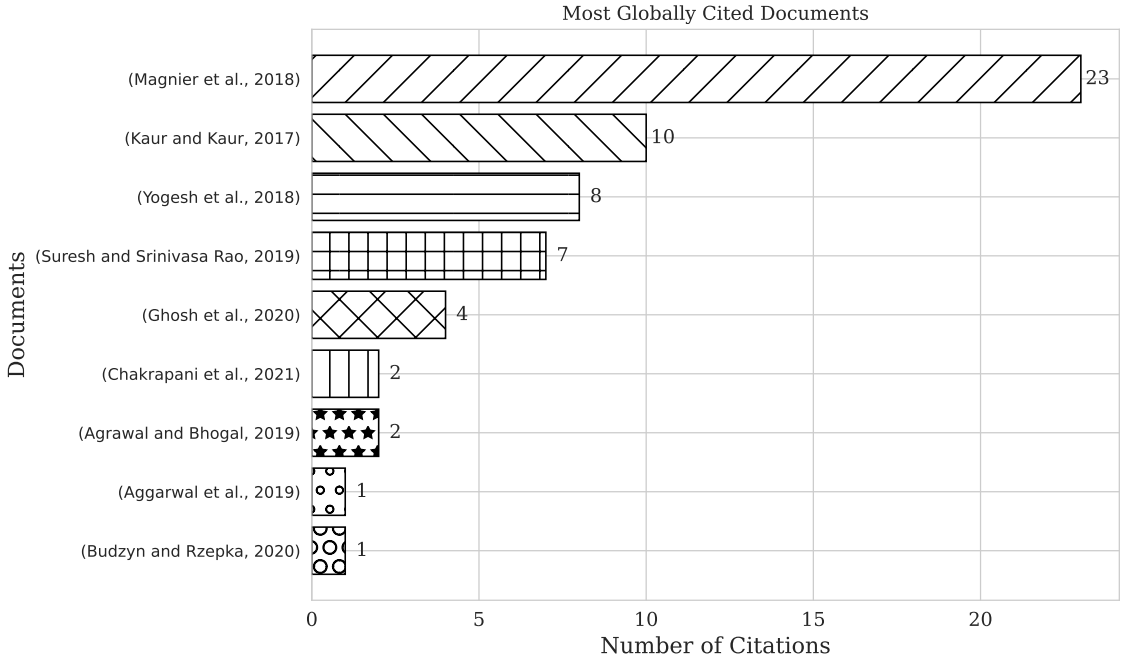


Figure 15: Most cited papers in absolute numbers.

Through the word cloud analysis of the keywords from all the papers, common terms like “edge detection”, “segmentation”, and “image processing”, along with their synonyms and homonyms, were omitted, as these are expected terms based on the search criteria. This process revealed recurring terms related to potential methods and applications that have evolved during the study period. Figure 16 presents a summary of the most frequently encountered terms, including those associated with fuzzy logic, machine learning, genetic algorithms, and various classical segmentation and edge detection techniques.

The appearance of terms related to classical segmentation and edge detection techniques such as Canny, Sobel, and Watershed in the keywords suggests a trend toward enhancing the performance of these extensively studied methods. To further investigate this, an analysis considering the occurrence of terms by year was conducted. Words with performance-related terms gaining prominence in 2022. From these papers, it is



Figure 16: Word clouds of key terms of RQG edge detection methods. Retrieved from (SILVA et al., 2023)

noteworthy to extract the methods reviewed by authors concerning the state of the art in edge detection. Consequently, the following section will provide a summary of these techniques, organized by approach.

Gradient-based methods: A digital image serves as a discrete representation of the variations in light present in the real world. Consequently, each numerical value assigned to a pixel corresponds to the intensity of light or color at that specific point. In the context of image analysis, object boundaries within the image can be perceived as transition zones between these intensities. In particular, sharper transitions in intensity are more likely to represent edges compared to smoother transitions. In essence, when examining a specific direction within the image, the rate of change or discrete difference between pixels helps identify potential object edges (MARCO-DETCHART et al., 2021).

It was through this rationale that the initial edge detection techniques were developed, as explained in (AGRAWAL; BHOGAL, 2019). These techniques can be categorized into two primary approaches: first-order derivative-based and second-order derivative-based methods.

The most well-known gradient-based edge detection methods fall into three main categories: first-order fixed operations, first-order oriented operations utilizing maximum energy of the orientation, and two-direction operations.

To enhance comprehension of the evolution of these techniques over time, a timeline has been compiled, showcasing the publication dates of the articles introducing the initial versions of each method, as depicted in Figure 17. In this section, an overview of classical gradient-based methods is presented, with a focus on their primary distinctions, as discussed in (AGGARWAL et al., 2019).

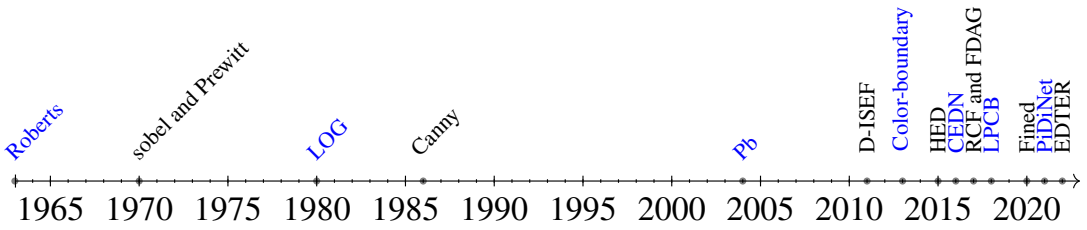


Figure 17: Chronology of non-fuzzy methods RQG. Retrieved from (SILVA et al., 2023)

The Canny Edge Detector, as proposed by Canny in 1986 (CANNY, 1986), remains one of the most extensively employed edge detection methods. It involves a sequence of steps, including Gaussian smoothing, followed by a gradient operation, and ultimately thresholding. In recent studies, like the ones outlined in (JING et al., 2022), other methods rooted in first-order derivatives and inspired by Canny's approach are encountered. These include techniques such as Infinite-size Symmetrical Exponential Filters (D-ISEF) and a color-boundary method combined with the first-order derivative of anisotropic Gaussian (FDAG).

Sobel's edge detector, introduced by Sobel in 1968 (SOBEL; FELDMAN, 1973), computes the gradient value at each pixel position in the image using a fixed operator.

On the other hand, the Prewitt edge detector, as described by Prewitt in 1970 (PREWITT, 1970), employs a technique similar to Sobel's. However, unlike Sobel, it does not involve adjustment coefficients; instead, it varies by a constant value and calculates the gradient's magnitude considering the image orientations.

The method introduced by Roberts (ROBERTS, 1980) made its initial appearance in the literature back in 1963 as a product of his doctoral thesis. This technique computes the derivative by evaluating the square root of the difference between diagonally adjacent pixels. It emphasizes the invariant properties exhibited by edges.

The LoG (Laplacian of Gaussian) edge detection method, as described in (MARR; HILDRETH, 1980), is founded on a two-step process. Initially, it applies a Gaussian filter to the image, followed by a Laplacian operation. This method utilizes a second-order operator, aiming to detect the maximum and minimum points in the intensity variation. By identifying the points where these variations cross zero, potential edges in the image are located. The Gaussian filtering step is crucial as it is a second-order method and, consequently, highly sensitive to noise.

Region segmentation-based methods: Another category of edge detection methods

is grounded in region segmentation. These techniques involve segmenting regions within an image, often utilizing approaches such as clustering and automated thresholding methods. The edges are then identified as the boundaries of these segmented regions. As noted in (MUBASHAR et al., 2022), regions formed by textures in high-complexity images can serve as facilitators in the edge detection process, aiding in the delineation of boundaries between these regions.

The region-based approach often exhibits superior performance compared to direct detection methods like gradient-based techniques. However, there are other methods, such as frequency domain filtering and statistical approaches, which can be classified as either region segmentation or direct edge detection methods based on how the detection modeling is approached. Further details about these methods can be found in (JING et al., 2022) and (MUBASHAR et al., 2022).

The emergence of texture descriptors and other local information, including brightness gradient, texture gradient, and color gradient, led to the development of the *probabilistic contour* (Pb) method, as outlined in (ARBELAEZ et al., 2011).

Methods based on machine learning and Neural Networks: By integrating the Pb method with logistic regression, a model for image edge detection was successfully developed, as discussed in (JING et al., 2022). Over time, this method has undergone extensions and improvements, including the incorporation of the multiscale probabilistic contouring technique and a multiscale spectral clustering approach.

In the current landscape, new machine learning-based techniques have emerged, with a particular focus on those built upon Convolutional Neural Networks (CNNs). (JING et al., 2022) presents a range of machine learning-based methods, including the well-known *Holistically-nested edge detection* (HED) approach. HED was introduced to enhance the performance of convolutional neural networks and has served as an inspiration for other methods like the *Convolutional Encoder-Decoder Network* (CEDN), *Richer Convolutional Features* (RCF), and *Learning to Predict Crisp Boundaries* (LPCB).

In 2019, the *bi-directional cascade network* (BDCN) method was introduced, which advocates for edge detection at various scales. More recently, techniques such as *Fined*, *Edge Detection TransformER* (EDTER), and *Pixel Difference Networks* (PiDiNet) have been proposed. These methods are designed to address edge detection without the necessity for extensive databases for model training, signifying advancements in the field (JING et al., 2022).

Fuzzy Logic based methods: The application of fuzzy theory in edge detection has been on the rise since Russo (RUSSO, 1998) initially introduced a fuzzy inference system modeling approach in 1998. This methodology was developed to effectively extract edges in high-noise images. The growing adoption of fuzzy theory in edge detection is rooted in the inherently fuzzy nature of object edges in digital images, rendering fuzzy theory a well-suited solution for addressing such challenges (RUSSO, 1998).

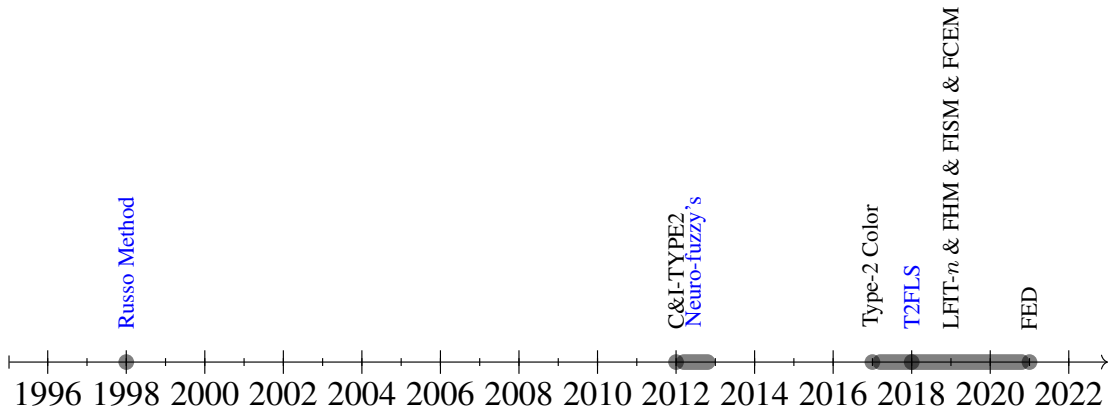


Figure 18: Chronology of fuzzy methods RQF. Retrieved from (SILVA et al., 2023)

According to the findings presented in (JING et al., 2022), edge detectors that combine techniques, such as *divergence and fuzzy entropy minimization* (FED), as well as detectors based on morphological gradient and type-2 fuzzy logic (Type-2 Color), have been introduced. Furthermore, hybrid techniques and fuzzy versions of neural networks have been developed, aiming to enhance the performance of existing approaches and, in certain instances, reduce computational complexity. These innovations represent valuable contributions to the field of edge detection.

In the research conducted by Ghosh et al. (2020), several hybrid methods have been identified that leverage neural networks in combination with various forms of fuzzy logic, including type-1, type-2, and type-3 fuzzy logic, which represent extensions of fuzzy logic with varying degrees of uncertainty. These hybrid approaches are referred to as *Hybrid approach neuro-fuzzy-1, neuro-fuzzy-2, and neuro-fuzzy-3* (Neuro-fuzzys). Additionally, fuzzy logic has been employed to enhance classical methods like Canny (C&I-TYPE2), and a hybrid method has been developed that combines Sobel, fuzzy logic type-1, and fuzzy interval system type-2 (T2FLS). These diverse approaches showcase the flexibility and adaptability of fuzzy logic and neural networks in the context of edge detection (GHOSH et al., 2020).

Figure 4 illustrates the chronological development of identified fuzzy methods in response to the two research questions posed. Notably, the figure highlights the prevalence of applications involving fuzzy logic of various types, including type-1, type-2, and type-3 fuzzy logic. Moreover, it showcases the growing trend of combining fuzzy logic with other techniques, signifying an evident direction in research and development within this field.

Over the years, there has been a pronounced emphasis on the rigorous evaluation and juxtaposition of diverse edge detection techniques, underscoring the ongoing quest for refinement and validation in this domain. This meticulous need for assessment suggests that, while significant strides have been made, there remains ample room for innovation

and enhancement.

In practical applications, particularly within the medical realm, the precision in edge detection is paramount. The ability to accurately pinpoint diseases and anomalies in imagery, such as dental X-rays, underscores the tangible relevance and direct impact of these techniques in real-world scenarios. This accentuates the notion that edge detection transcends mere academic discourse and bears significant practical implications.

With the advent of Deep Neural Network (DNN) based techniques, there has been a burgeoning promise of groundbreaking advancements in edge detection. These methodologies, often lauded for their prowess in surpassing human performance on specific datasets, have infused optimism into the field. However, challenges to generalization across diverse datasets and scenarios suggest that the definitive solution to edge detection remains an ongoing endeavor.

Moreover, the intricacies of real-time processing and the imperative to preserve salient edge information in multi-dimensional images spotlight the continuous challenges in optimizing edge detection for dynamic and real-time applications.

In conclusion, the state of the art in edge detection methods is advanced, with emerging techniques showcasing immense promise. Yet, the pursuit of more robust, generalizable, and efficient methods persists. Notably, the findings from the study indicate that, despite the advancements, the edge detection conundrum is far from conclusively resolved, especially when considering the generalizability across varying dataset distributions.

This challenge is further exemplified in textured images, as highlighted in the (MUBASHAR et al., 2022). In this context, the introduction of the Synthetic Textured Masks Dataset (STMD) and the Single-Scale Feed Forward Edge Detector (SFED) architecture emphasizes the complexities of detecting edges in textured visuals.

6.2.2 Fuzzy logic-based edge detection methods (RQF)

Given the current status of edge detection methods and the significant role of fuzzy logic-based approaches, as demonstrated in the preceding section, conducting a bibliometric analysis of these articles has provided valuable insights for comprehending the state of the art in fuzzy logic-based edge detection methods. This analysis can offer valuable information about trends, key contributors, and emerging directions within this field, assisting researchers and practitioners in staying updated with the latest developments and focusing their efforts on areas of relevance and innovation.

It's worth emphasizing that this review also included works that primarily focused on reviewing segmentation methods in general, utilizing fuzzy logic. This inclusion is justified by the recognition that the edge detection process essentially involves segmenting the boundary between two or more regions, essentially constituting a specific instance within the broader context of image segmentation. As a result, high-impact studies that were not explicitly centered on edge detection but emerged from the search and underwent the

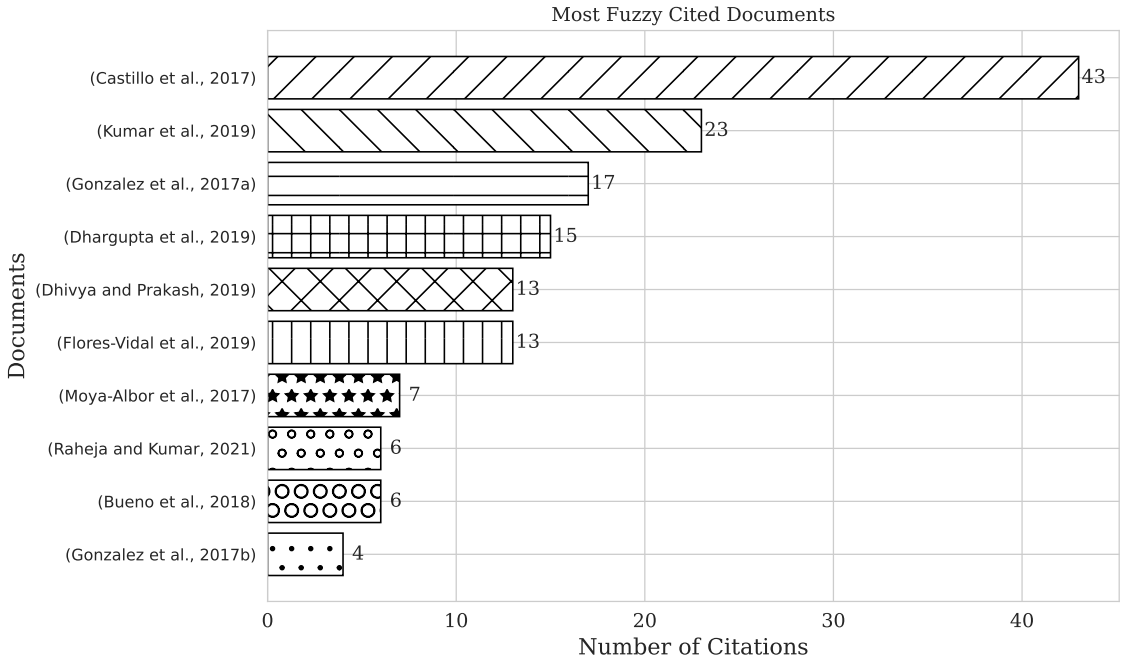


Figure 19: Most cited for fuzzy methods. Source: author.

exclusion processes were considered and incorporated into the review. This broader perspective adds depth and comprehensiveness to the analysis of fuzzy logic-based methods in the context of image analysis and segmentation.

Table 8 compiles the papers retrieved from the search, arranged chronologically by their publication dates. The first column presents the references, while the adjacent column displays the titles of the respective works.

Subsequently, the relevant results of the bibliometric analysis will be presented, with the intention of showcasing the most important papers and common terms found within the literature. This presentation is designed to enhance the understanding of research conducted in this field through method descriptions and to identify potential gaps in the literature on this topic.

By extracting paper metadata, as outlined in the previous chapter on general edge detection methods, it became possible to determine the most cited papers among the selected ones. The paper by (CASTILLO et al., 2017) garnered the highest number of absolute citations, while in the second and third positions, in terms of absolute citation numbers, the works authored by (KUMAR; SINGH; KUMAR, 2019) and (GONZALEZ; MELIN; CASTILLO, 2017), as shown in Figure 19.

When evaluating the ratio of citations per year, it's noteworthy that the top three most cited papers in absolute numbers also maintain their hierarchical order in terms of citations per year. Interestingly, two of these papers focus on edge detection utilizing type-2 interval fuzzy logic, and the second-ranked paper is relatively recent. This observation underscores the enduring relevance and impact of these contributions in the field of edge

Table 8: Works in edge detection based on fuzzy logic (RQF). Retrieved from (SILVA et al., 2023)

References	Paper title
(GONZALEZ et al., 2017)	Edge detection methods based on generalized type-2 fuzzy logic systems
(CASTILLO et al., 2017)	Review of Recent Type-2 Fuzzy Image Processing Applications
(MOYA-ALBOR; PONCE; BRIEVA, 2017)	An Edge Detection Method using a Fuzzy Ensemble Approach
(GONZALEZ; MELIN; CASTILLO, 2017)	Edge detection method based on general type-2 fuzzy logic applied to color images
(BALABANTARAY et al., 2017)	A Quantitative Performance Analysis of Edge Detectors with Hybrid Edge Detector
(FLORES-VIDAL et al., 2018)	A New Edge Detection Approach Based on Fuzzy Segments Clustering
(BUENO et al., 2018)	Two-phase flow bubble detection method applied to natural circulation system using fuzzy image processing
(BAGHBANI; JAMASB; KHODABAKHSHI, 2019)	A method for image edge detection based on interval-valued fuzzy sets
(FLORES-VIDAL et al., 2019)	A new edge detection method based on global evaluation using fuzzy clustering
(DHARGUPTA et al., 2019)	Fuzzy edge detection based steganography using modified Gaussian distribution
(KAUR; AAYUSHI, 2019)	Image Edge Detection Techniques Using Sobel, T1FLS, and IT2FLS
(KUMAR; SINGH; KUMAR, 2019)	Information hiding with adaptive steganography based on novel fuzzy edge identification
(DHIVYA; PRAKASH, 2019)	Edge detection of satellite image using fuzzy logic
(DORRANI; FARSI; MOHAMADZADEH, 2020)	Image Edge Detection with Fuzzy Ant Colony Optimization Algorithm
(KUMAWAT; PANDA, 2021)	A robust edge detection algorithm based on feature-based image registration (FBIR) using improved canny with fuzzy logic (ICWFL)
(RAHEJA; KUMAR, 2021)	Edge detection based on type-1 fuzzy logic and guided smoothening
(TRIPATHI et al., 2021)	Edge Detection on Medical Images Using Intuitionistic Fuzzy Logic

detection.

The word cloud analysis provides valuable insights into the terms that have garnered the attention of researchers in the realm of fuzzy treatment for addressing edge detection and image segmentation challenges. In Figure 20, one can discern terms such as “Medical

Imaging", "Computer Circuits", "General Type-2 fuzzy sets", "Classical Methods" and "Sobel Operator" This word cloud was generated based on the frequency of terms found within the keywords, which authors select to describe their work, utilizing R Studio software.

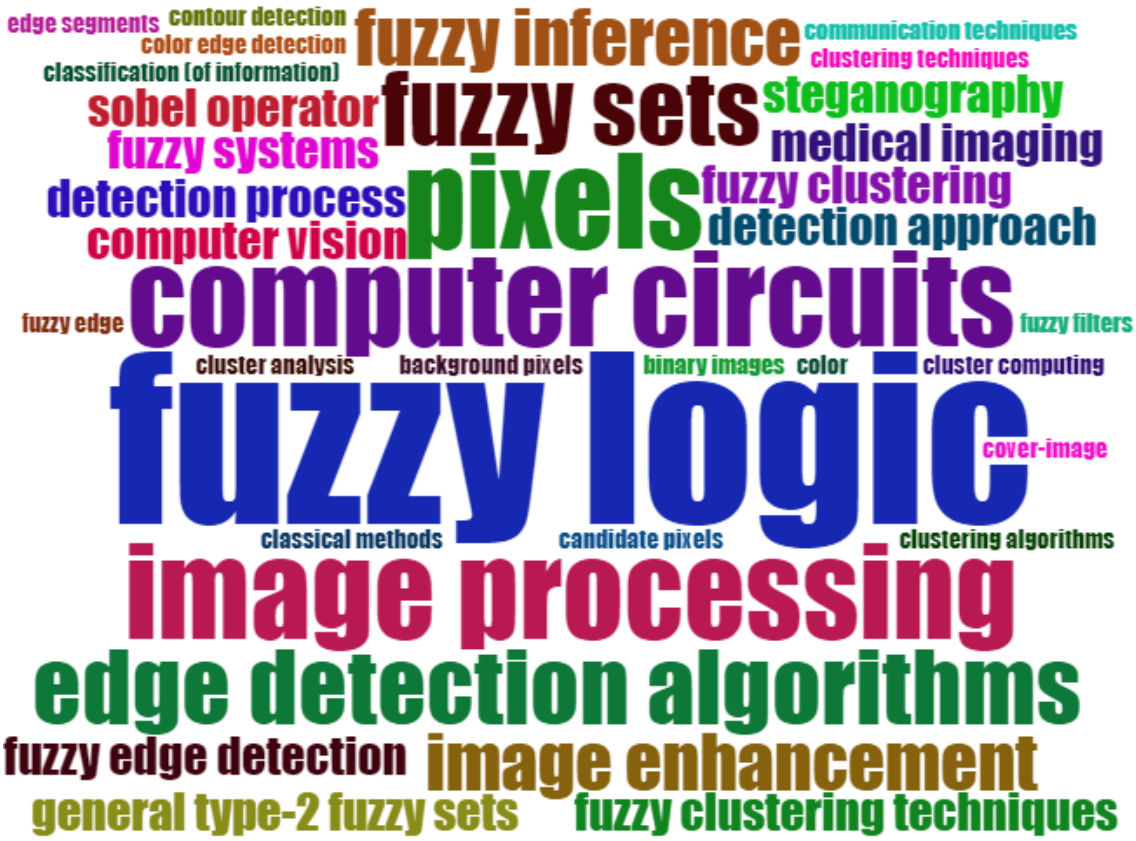


Figure 20: Word cloud of key terms of fuzzy methods. Retrieved from (SILVA et al., 2023)

The realm of edge detection, a fundamental step in image processing, has witnessed significant advancements over the years, with the incorporation of fuzzy logic being a notable development. As gleaned from the reviewed articles, fuzzy logic has emerged as a promising tool to enhance the accuracy and robustness of edge detection methods, addressing some of the limitations of traditional techniques.

Traditional edge detection methods, such as the Canny or Sobel operators, while effective, often struggle with noise and may not always provide clear edge demarcations in complex images. The introduction of fuzzy logic into this domain aims to harness its ability to handle uncertainty and vagueness, characteristics inherent in many real-world images. For instance, the article on (BAGHBANI; JAMASB; KHODABAKHSHI, 2019) introduced a technique where each pixel's interval membership is constructed from its original and neighboring intensities. This approach, which employs triangular norms and co-norms, showcased improved performance, especially when applied to medical images.

Another article, (FLORES-VIDAL et al., 2019) took inspiration from human vision.

Instead of evaluating edge candidate pixels as independent entities, this method connects pixels that form arcs or "segments."By employing fuzzy clustering techniques to select relevant segments, the approach demonstrated superior performance compared to standard edge detection algorithms.

The steganographic approach presented in (DHARGUPTA et al., 2019) leveraged fuzzy edge detection to conceal data within images effectively. Recognizing that human vision is less sensitive to changes near edges, this method embedded more data in edge regions, ensuring minimal visible distortion and higher payload.

Furthermore, the article (KUMAR; SINGH; KUMAR, 2019) emphasized the importance of precise edge detection in steganography. The proposed method used a fuzzy inference system to accurately identify edge areas, ensuring that the exact edge locations are maintained post-embedding, a crucial factor for accurate data extraction.

It's evident from these works that fuzzy logic, with its inherent ability to manage ambiguity, offers a refined approach to edge detection. By considering the uncertainty in pixel values and leveraging the strengths of fuzzy systems, these methods provide clearer, more accurate edge detection results, especially in images with complex textures or noise.

The state of the art in edge detection methods, as illuminated by the reviewed articles, is progressively leaning towards the integration of fuzzy logic. This trend is driven by the need for more accurate, robust, and adaptable edge detection techniques capable of handling the complexities and uncertainties of real-world images. The fusion of fuzzy logic with traditional edge detection paradigms promises a future where image processing is both more precise and more in tune with the intricacies of human vision.

To comprehend the similarity among the main works, they underwent a clustering process based on the abstracts of each of the documents. This procedure enables the identification of each group of works, highlighting their convergences and understanding the intrinsic relationships among them. Through the K-Means clustering algorithm, the abstracts were organized into distinct groups where the works exhibited similar characteristics and topics.

This approach allows for the identification of patterns and trends within the academic literature, aiding in the analysis of how different research areas interact and mutually influence each other. The chart separated fuzzy from non-fuzzy works with the aim of enhancing the understanding of the dynamics of distinct productions. The results can be observed in the Figure 21. It's worth noting that two of the three most cited works with the fuzzy approach are in the same group and significantly distinct from the others.

The methodology employed in this analysis utilized the K-Means clustering algorithm to group abstracts of academic works based on the similarity of their content. Firstly, the abstracts were pre-processed and vectorized using the TF-IDF (Term Frequency-Inverse Document Frequency) technique to represent them numerically. Subsequently, the data's dimensionality was reduced using Singular Value Decomposition (SVD), and normali-

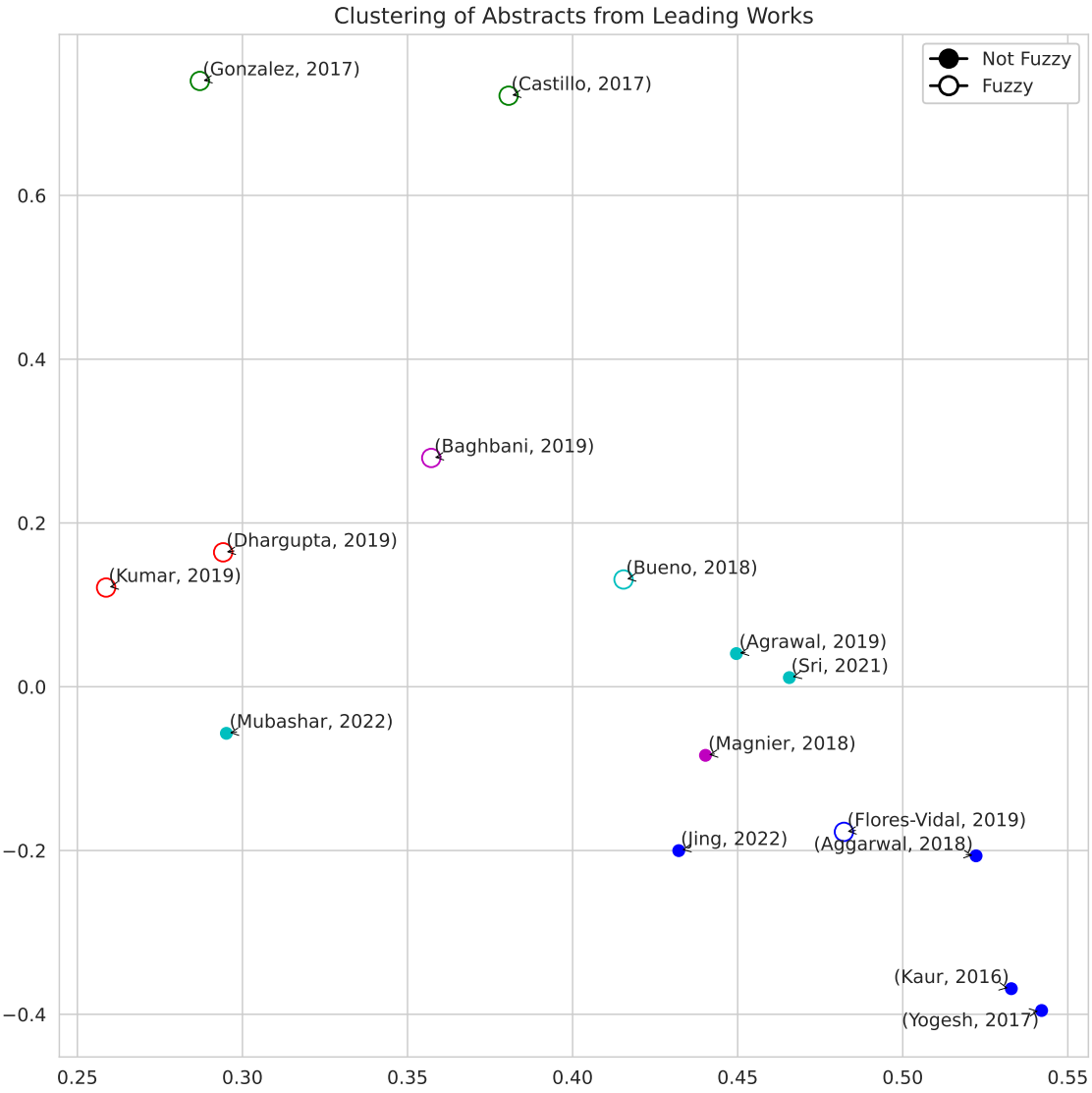


Figure 21: Clustering of abstracts from leading works. Source: author.

zation was applied to facilitate clustering. The K-Means algorithm was then applied to cluster the abstracts into a specified number of clusters.

Both the paper (CASTILLO et al., 2017) and (GONZALEZ; MELIN; CASTILLO, 2017) emphasize the significance and potential of type-2 fuzzy systems in the domain of image processing. While the former introduces a novel edge detection method specifically tailored for color images using general type-2 fuzzy logic, the latter provides a broader overview of the applications of type-2 fuzzy systems in various image processing tasks, including edge detection. A common thread between the two works is the recognition of the limitations of traditional edge detection methods, especially in the presence of noise and other uncertainties. Both papers advocate for the adoption of type-2 fuzzy systems, highlighting their ability to handle and represent complex uncertainties more effectively than their type-1 counterparts. Furthermore, the emphasis on the advantages of processing color images, as opposed to grayscale images, underscores the shared belief that

color images offer richer information, potentially enhancing the performance of image processing systems.

In general, the metrics presented in the results of these works in comparison with classical methods show that the approach plays a key role in improving the performance of classical and other existing methods.

The found methods can be divided into four classes:

i. Methods based on *interval fuzzy logic of the type-n* (LFIT-n) (BAGHBANI; JAMASB; KHODABAKHSHI, 2019; RAHEJA; KUMAR, 2021; GONZALEZ; MELIN; CASTILLO, 2017; KAUR; KAUR, 2017; CASTILLO et al., 2017; GONZALEZ et al., 2017);

ii. *Hybrid methods* (FHM), in combination with neural networks or improving the performance of classical edge detection techniques (BALABANTARAY et al., 2017; KUMAWAT; PANDA, 2021; MOYA-ALBOR; PONCE; BRIEVA, 2017; DHARGUPTA et al., 2019; KAUR; KAUR, 2017; DORRANI; FARSI; MOHAMADZADEH, 2020);

iii. Methods that are based on *fuzzy inference systems* (FISM) (DHIVYA; PRAKASH, 2019) e;

iv. Methods that are based on *fuzzy clustering methods* (FCEM) (FLORES-VIDAL et al., 2018).

6.3 Chapter Conclusion

Edge detection plays a crucial role in various stages of computer vision, as exemplified in (WEI et al., 2017), including tasks like object detection (YANG; KRIEGMAN; AHUJA, 2002), pattern recognition (MOHAN et al., 2021), and image retrieval (PAVITHRA; SHARMILA, 2018).

In recent times, research in the field of edge detection has been experiencing a surge in interest, driven by its critical role in numerous applications. These applications include augmented reality (ORHEI; VERT; VASIU, 2020), image colorization (SUN et al., 2019), and medical image processing (QIU et al., 2021a), among others. Given the inherently fuzzy nature of object edges in digital images, several methods have been developed over the years. More recently, the integration of fuzzy theory into these methods has shown promising advancements, leading to improved performance and application in diverse domains.

Given the progressing research in the domain of edge detection through fuzzy theory approaches and the absence of dedicated review papers for these methods, there is a clear justification for conducting a thorough investigation and review of these techniques. This

expert exploration sought to provide a comprehensive understanding of the contributions and advances achieved in the field of edge detection using fuzzy theory.

In this context, this study has presented a comprehensive review of edge detection methods to elucidate the current state of the art in fuzzy edge detection techniques. To accomplish this, extensive searches were conducted across two prominent databases, Scopus and Web of Science. In the process, specific criteria for inclusion and exclusion were established, resulting in the scrutiny of 3,830 papers returned by the searches, with only 34 papers ultimately passing through the exclusion steps. The methods identified were meticulously reviewed and categorized based on the approach proposed by each respective method.

Edge detection techniques can be broadly categorized into classical methods and fuzzy logic-based methods. Classical methods fall into four primary classes. The first class comprises methods based on gradient operations, which primarily utilize gradient information for edge detection. The second class encompasses methods that focus on segmenting regions within the image, with edges identified as the boundaries between these segmented regions. In the third class, methods based on machine learning and Neural Networks leverage advanced learning algorithms for edge detection. Lastly, the fourth class comprises methods rooted in Fuzzy Logic, which can be further subdivided into four subclasses. These subclasses encompass methods based on interval fuzzy logic type-n, hybrid approaches combining fuzzy logic with neural networks or enhancing classical techniques, methods employing fuzzy inference systems, and those utilizing clustering methods for edge detection.

The concept of fuzzy set theory, initially introduced by Zadeh (ZADEH, 1965), and the Roberts method of edge detection (ROBERTS, 1980) both emerged in the mid-1970s. However, despite the inherent suitability of edge detection for a fuzzy theory approach, the application of fuzzy logic to this task did not appear until the late 1990s. The utilization of fuzzy inference systems, as demonstrated by Russo (RUSSO, 1998), marked the first instance of fuzzy-based applications in edge detection during this period.

Following this initial effort, there was a relatively limited exploration of fuzzy-based edge detection methods over the years, with the first notable papers emerging around the year 2012. Additionally, a bibliometric analysis was undertaken, involving the examination of document metadata. This analysis was conducted to gain insights into potential gaps and trends in research concerning the topic under investigation.

The analysis has revealed that in recent years, beginning around 2012, fuzzy logic has found application in hybrid methods aimed at enhancing the performance of established techniques or streamlining computational complexity. Moreover, studies involving higher-order interval fuzzy logic have gained prominence due to their greater flexibility in addressing the inherent uncertainty associated with the task of edge detection.

It can be observed from this general review of fuzzy and edge detection methods

that, although many studies have addressed the application of aggregation functions to classification problems and to computer vision in general, no works of this kind were identified in our searches for the specific context investigated here. This finding highlights a gap in the literature regarding this type of investigation. In the next chapter, we therefore focus on methods based on aggregation functions and related concepts applied to edge detection. To this end, a review of the literature on aggregation, or fusion, functions related to the edge detection problem is presented.

6.3.1 Publication

This chapter was published as part of the proceedings of the 25th International Conference on Enterprise Information Systems (ICEIS 2023) (SILVA et al., 2023).

7 SYSTEMATIC REVIEW OF AGGREGATION FUNCTIONS APPLIED TO EDGE DETECTION IN DIGITAL IMAGES

Aggregation functions, as seen on Section 4.1.3, are a type of function with certain special properties, which aim to combine, or fuse, inputs into a value that is able to represent the set of inputs. Precisely, this function must respect two main properties, namely, (i) boundary conditions and (ii) monotonicity. The relaxation of the monotonicity condition has been the focus of recent investigations. The notion of weak monotonicity was introduced by Beliakov, Pradera e Calvo (2007) and extended to directional monotonicity by Bustince et al. (2020). After that, the concept of pre-aggregation function was introduced by Lucca et al. (2016), which are functions that respect the same boundary conditions as an aggregation function, however they are just directional increasing.

Given the advancement of research in image discontinuity detection, especially using clustering, aggregation, and pre-aggregation functions, and since, to the best of our knowledge, there are no systematic literature reviews specifically devoted to this topic, this chapter aims to gather and synthesize the current state of the art of this research field. In this sense, the question that is intended to be answered is:

What edge detection methods are based on aggregation and pre-aggregation functions?

Then, the main objectives of the study are:

1. Fill this gap in the literature of systematic reviews on the topic;

2. Summarize the existing technology regarding methods that make use of those functions in digital image processing, more specifically regarding edge detection;

3. Identify the gaps in the detection approach using aggregation or pre-aggregation functions, proposing themes for future work.

This chapter is organized, in addition to this introduction, The necessary theoretical foundations have been presented in Section 5 and can be consulted where the most widespread edge detection methods to date are presented chronologically. Section 7.1

(**Materials and Methods**) presents the search terms, where inclusion, delimitation and exclusion criteria are discussed, as well as the number of papers found and admitted for review. Then, in Section 7.2 (**Results and Discussion**), we present the aforementioned research question, summarizing the methods reviewed and performing a qualitative assessment, comparing the main techniques and approaches. Finally, Section 7.3 is the chapter **Conclusion**.

7.1 Materials and Methods

This section presents the methodology used in this research. Then, we first introduce the concept of a systematic literature review and the methodology used to answer the research problems.

7.1.1 Systematic literature review scope

A synthesized literature review is a form of secondary study that aims to identify, evaluate, and interpret all available relevant research on a specific research problem, topic, or phenomenon of interest (KITCHENHAM; CHARTERS, 2007). Among the many reasons to engage in a systematic literature review, the most common are: (i) to summarize the existing evidence regarding treatment or technology; (ii) to identify gaps in current research with the goal of suggesting areas of future investigation; (iii) to provide a body of information that appropriately positions new research activities; (iv) to reduce, or attempt to eliminate research bias.

In this context, this research seeks to summarize the existing technology regarding methods that make use of aggregation functions for digital image processing, more specifically, regarding edge detection. Another important contribution was the identification of gaps in the state of the art.

7.1.2 Definition of criteria, search in indexing databases and obtaining primary research

In order to answer the research problems, searches were conducted in two large databases widely used in the computer science field, Scopus (SC)[1] and Web Of Science (WS)[2]. The inclusion terms used to answer which edge detection methods use clustering and pre-aggregation functions were the terms:

(i) "preaggregation "OR "pre-aggregation"OR "aggregation "OR "fusion"OR "Sugeno"OR "Type-2"that appear in the abstract OR;

(ii) The terms of the item **(i)** joined to the terms "Fuzzy"and "Logic"concatenated with "Type-2"with the exception of "Sugeno"as terms that appear in the title; and

[1] Available at <www.scopus.com>
[2] Available at <www.webofscience.com>

(iii) The terms of the items **(i)** and **(ii)** in conjunction with the terms “image” AND “segmentation” OR “image” AND “processing” OR “edge” AND “detection” as terms that appear in the abstract.

To conduct the search, delimitation criteria were used, such as articles written in English, published from 2016 on, that have referenced the work of "Canny"or authors who have worked with "canny"and that were articles or reviews in the area of computing. This search returned 428 results, which were reduced by the exclusion criteria.

Initially, all the papers that had a title that demonstrated the lack of relevance of that study for this review work were eliminated; all the papers that were flagged as retracted by the journal were eliminated, and an analysis of the abstract was performed, observing, in particular, the objectives of that research, thus eliminating all the articles that were outside the scope of this review; finally, an analysis of the methodology of the papers was performed in order to check whether they present any serious technical problem that would justify discarding them even before their full reading.

At the end of the process, 17 articles remained. These remaining articles were used to find other relevant works. We analyzed the sections of related works, also searching using the keywords of such papers, whether from the same research groups or not, but that somehow composed the development of the concept or the history of what was developed in the papers, considering, thus, the presentation of what had already been completed and that somehow had missed in the initial search.

In total 7 works have been added and are marked in the second column of the Table 9. An overview of the systematic review performed is available in Figure 22. It is possible to observe that, given the search question, the inclusion terms are considered, where ABS() and TITLE() represent searches of the abstracts and titles of the papers, respectively.

In delimitation terms, PUBYEAR, REFAUTH, and REF are respectively the year of publication of the paper, papers that cite a specific author, and papers that present a specific term in their references. In a number of occurrences, one has in INC the number of papers found through the inclusion and delimitation terms. Then, filtering was performed By Title, Abstract, and the exclusion of articles Retrieved and Included After, where EXC represents the number of articles excluded and REM the remaining.

7.2 Results and Discussion

After filtering the papers, by the inclusion and exclusion criteria already discussed, 24 papers remained to be reviewed, listed in Table 9. Among them, 19 papers were found that are specifically dedicated to edge detection, either using multiple descriptors extraction and aggregation or based on fuzzy set theory: type-2 fuzzy and neutrosophic set (ZHANG et al., 2018; MARCO-DETCHART et al., 2021; MARCO-DETCHART et al., 2018a; GU et al., 2022; LIN; WANG; WAN, 2023; GE et al., 2021; FANG; ZHAO;

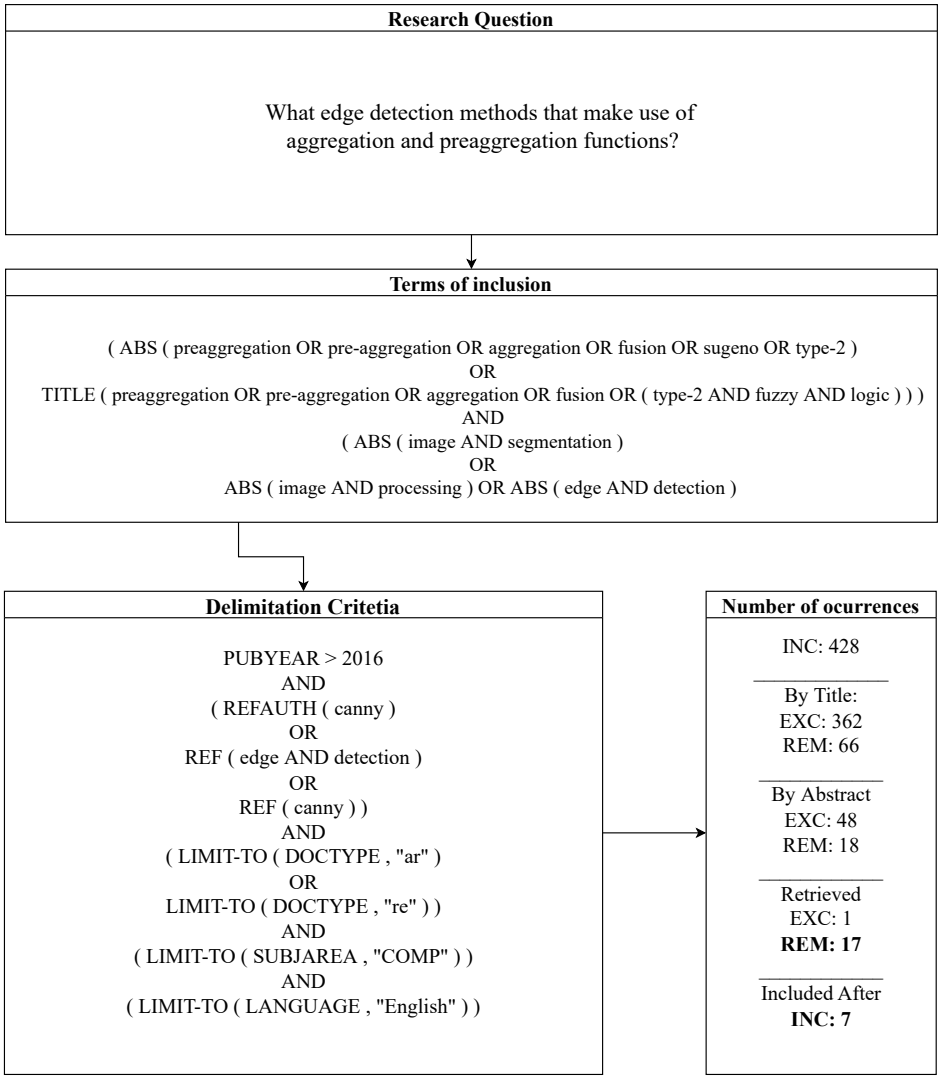


Figure 22: Terms of inclusion, exclusion, and number of selected papers. Source: author.

ZHANG, 2020; BENTKOWSKA et al., 2020; YANG et al., 2019; FLORES-VIDAL et al., 2022; NAGARAJAN et al., 2018a; NAGARAJAN et al., 2018b; MARTINEZ et al., 2019), or works that use clustering and pre-aggregation functions, which are dedicated to region segmentation, but considering their characteristics can be extended to the task of edge detection (LJUBO; MARIJA; M., 2018; NEDOVIC; RALEVIC; PAVKOV, 2018; DELIć; NEDOVIć; PAP, 2019; PAP; NEDOVIć; RALEVIć, 2021; RALEVIć; DELIć; NEDOVIć, 2022; RALEVIĆ et al., 2022).

7.2.1 Summary of methods

The found methods of segmentation or edge detection, based on aggregation and pre-aggregation functions, can be divided into 3 groups: (i) based on the aggregation of distance functions and FCM, (ii) multiple descriptors extraction and aggregation, and (iii) based on fuzzy set theory: type-2 fuzzy and neutrosophic set. Table 10 lists the papers included in each group.

Table 9: Found and included papers

Found papers	**Papers included**	**Total number of reviewed papers**
Li et al. (2020), Martinez et al. (2019), Zhang et al. (2018), Kaur e Garg (2022), Gu et al. (2022), Fang, Zhao e Zhang (2020), Lin, Wang e Wan (2023), Nagarajan et al. (2018b), Delić, Nedović e Pap (2019), Gudipalli et al. (2019), Yang et al. (2019), Marco-Detchart et al. (2021), Flores-Vidal et al. (2022), Lopez-Molina et al. (2018), Hait et al. (2022), Wang et al. (2018), Ge et al. (2021)	Pap, Nedović e Ralević (2021), Ralević, Delić e Nedović (2022), Ljubo, Marija e M. (2018), Qiu et al. (2021b), Bentkowska et al. (2020), Marco-Detchart et al. (2018a), Nagarajan et al. (2018a)	24

An extended version, providing a detailed discussion of the identified groups of methods, including their corresponding mathematical models and computational procedures, can be found in (AMORIM et al., 2023).

The first group considers methods inspired by the way the human visual system works. The idea is the integration of different global or local features, where each descriptor would have its own capacity to represent the visual clues or the primitive shapes that compose the edges of the composite shapes of the objects present in the image. In this sense, the aggregation functions model the behavior of the information processed in the cortex, and the descriptors play the role of the stimuli generated by the ganglion cells.

Each theorist proposes a different type of aggregation or pre-aggregation function to simulate the behavior of information fusion, and there is no consensus on this. Although there are no studies demonstrating which type or family of clustering or pre-clustering functions would be best suited for modeling feature fusion for edge detection purposes, some researchers directly argue that Choquet integrals would serve this purpose better, since they would better model the non-linear behavior of the problem. Another clue to the Choquet integral performance is possibly the use of a weighing vector that allows for the variation of the importance of the information to be fused, as well as some other functions presented here. It is noteworthy that only average functions were used in all papers, whether they are arithmetic weighted or geometric-weighted.

About the descriptors, taking into account that most of the works considered modeling the X and Y type cells, i.e., the visual information close to the image plane and the focal plane information, and the biological and performance justification that there is in the

Table 10: Summary of papers by method

Multiple descriptors extraction and aggregation	**Based on aggregation of distance functions and FCM**	**Based on fuzzy theory: type-2 fuzzy and neutrosophic set**
Li et al. (2020), Marco-Detchart et al. (2021), Lin, Wang e Wan (2023), Ge et al. (2021), Fang, Zhao e Zhang (2020), Qiu et al. (2021b), Bentkowska et al. (2020), Lopez-Molina et al. (2018), Zhang et al. (2018), Flores-Vidal et al. (2022), Hait et al. (2022), Gudipalli et al. (2019), Gu et al. (2022), Marco-Detchart et al. (2018a), Wang et al. (2018), Yang et al. (2019)	Ljubo, Marija e M. (2018), Nedovic, Ralevic e Pavkov (2018), Delić, Nedović e Pap (2019), Pap, Nedović e Ralević (2021), Ralević, Delić e Nedović (2022)	Nagarajan et al. (2018a), Nagarajan et al. (2018b), Martinez et al. (2019), Kaur e Garg (2022)

use of modeling for the visual information far from the plane, i.e., the modeling of W type cells, it could be concluded, that the use of depth data, such as disparity maps, laser sensor depth maps and the like, are fundamental, especially when working with images with complex backgrounds or low contrast. The importance of contrast as a descriptor for image edges becomes clear when one observes the features used by the researchers.

The edge detection approach in combination with aggregation methods, or information fusion techniques, is important because they enable the reduction of information uncertainty and minimize redundancy, improves reliability, and maximizes the information relevant to a task. This allows the approach of consensus detection, via aggregation, between different detectors or the same detector by varying parameters. Beyond this, features can also be used as information extractors, so that the image features themselves are identified using aggregation. Works that link extraction and detection with aggregation functions have not been found.

In summary, we can compile the results of this approach:

(i) These are methods that take direct inspiration from the way the human visual system works, seeking to simulate, through feature extraction, or determination of local or global descriptors, the visual stimuli and the processing of information for the recognition of some pattern through aggregation or pre-aggregation functions.

(ii) Functions that make use of weighing vectors and that enable better modeling of nonlinear behavior, such as the Choquet integral, would perform better.

(iii) Depth information is essential especially when working with images with complex backgrounds or low contrast, the latter being an important feature in the performance of the models.

(iv) Combining detection methods with aggregation methods, or information fusion, makes it possible to reduce information uncertainty and minimize redundancy, improve reliability, and maximize the information relevant to a task.

(v) Works that link extraction and detection via clustering functions have not been found.

The second set of techniques (based on the aggregation of distance functions and FCM) is based on the importance of distance functions as a criterion for decision-making about the belonging of an element to a certain group or segment in clustering algorithms. Through a set of distance functions or fuzzy measures, using a set of aggregation or pre-aggregation functions, it is possible to build new distance functions that can be used as a parameter of clustering algorithms such as FCM. After this segmentation, it is possible to apply a morphological operation or classical detection to obtain the contours of the main objects of the image. One of the main limitations of this work is that only experiments using FCM were performed since it theoretically allows the implementation in any clustering algorithm, or that in general uses a distance metric as a stopping or starting criterion.

In summary, this approach has the following characteristics:

(i) They are based on the importance of distance functions as decision criteria in data clustering algorithms;

(ii) Aggregation and pre-aggregation functions are used to construct new distance functions from others that represent some dimension relevant to the problem;

(iii) The papers are limited to application to a single clustering algorithm and do not make clear the performance of other methods.

The third group of techniques (based on fuzzy set theory: type-2 fuzzy and neutrosophic set) performs an interpretation of the image in terms of fuzzy logic. The gray levels of the image are treated as a variation on a fuzzy set. This allows the direct use of aggregation functions. Overall, this technique has proven to be quite robust and superior to those compared in their respective works, particularly with respect to noise sensitivity.

7.3 Chapter Conclusion

Edge detection represents an important task in several steps of computer vision and image processing, ranging from object detection to image retrieval. Studies in this area of

research have been gaining momentum in recent years, due to its importance in applications such as autonomous cars and augmented reality. The difficulties inherent to the task have required a continuous improvement of techniques and modeling.

Some approaches applied to solve this task consider using aggregation and pre-aggregation functions. Due to the lack of works that summarize and show the gaps in the area of edge detection by functions of this type, this paper developed a systematic review of the literature, which aimed to answer:

"Which edge detection methods use aggregation and pre-aggregation functions?"

Considering a review of 24 papers, filtered from 428 articles found in computer databases in the last seven years, it was possible to synthesize important information that was grouped into three approaches, which support the answering of the research question. Precisely, the groups are:

(i) Multiple descriptors extraction and aggregation;

(ii) Based on the aggregation of distance functions and FCM;

(iii) Based on fuzzy set theory: type-2 fuzzy and neutrosophic set.

In summary, through this systematic literature review research, it was possible:

(i) To fill an existing gap in the literature of systematic reviews on edge detection using clustering functions;

(ii) Summarize the existing technology regarding methods that make use of these functions in edge detection;

(iii) Identify the gaps in the detection approach using aggregation or pre-aggregation functions, proposing topics for future work, fulfilling the initial objectives of the research.

Considering the importance of the conditioning stage, as outlined in Chapter 5, we sought to investigate in the literature the impacts of the smoothing stage on edge detection. In the next chapter, a systematic review is presented with the aim of gaining a better understanding of this issue.

7.3.1 Publication

This chapter was published as a journal article in *Axioms* (AMORIM et al., 2023).

8 SYSTEMATIC REVIEW OF THE IMPACT OF SMOOTHING ON THE PERFORMANCE OF EDGE DETECTION

Given the relevance of smoothing filters and their significant impact on the results of edge detection, as seen on Section 1, questions arise about the quantitative effects of these techniques. To objectively address this issue, a comprehensive literature review is conducted. This review aimed to identify and analyze, in a quantitative manner, how smoothing techniques, especially Gaussian blur, influence the accuracy and effectiveness of edge detection algorithms in processed images.

This chapter includes results that have been published in the proceedings of the 22nd International Conference on Practical Applications of Agents and Multi-Agent Systems[1](SILVA et al., 2025b) and it's organized, beyond this introduction, into materials and methods, results and discussion, and finally the conclusion.

8.1 Materials and Methods

To investigate the quantitative impacts of blurring on images concerning quality evaluation metrics in edge detection, an extensive search was conducted across major academic databases, including Google Scholar, Scopus, ACM database and IEEE Xplore. The aim was to locate studies examining the connection between blurring, with an emphasis on Gaussian blur, and its effect on the accuracy of edge detection in images.

For this purpose, various combinations of keywords were used, structured into specific Queries, aiming to capture a broad range of research related to the topic. The Queries were carefully formulated to include terms such as "Gaussian Blur", "Edge Detection", "Accuracy", "Image Blurring", "Performance Metrics", "Edge Detection Precision", "Blur Conditions", "Canny", "Edge Detectors", and "Impact of Blurring". The research was delimited to the field of Computing (COMP) to ensure the relevance and specificity of the obtained results (The Queries can also be observed in Table 11).

The exclusion criteria adopted in the selection of articles included the removal of works that were not strictly from the field of computing, articles not written in English,

[1]https://www.paams.net

Table 11: Queries Used in Research on the Effects of Blurring on Edge Detection

Query	Query Details
1	TITLE-ABS-KEY("Gaussian Blur"AND "Edge Detection"AND "Accuracy")
2	TITLE-ABS-KEY("Image Blurring"AND "Edge Detection"AND "Performance Metrics")
3	TITLE-ABS-KEY("Edge Detection Precision"AND "Blur Conditions")
4	TITLE-ABS-KEY("Gaussian Blur"AND "Canny"AND "Edge Detectors"AND "Accuracy")
5	TITLE-ABS-KEY("Impact of Blurring"AND "Edge Detection"AND "Accuracy")
6	TITLE-ABS-KEY(blur AND effects AND on AND edge AND detection AND precision)

and those whose full texts were not available for access or purchase. Furthermore, articles that had been retracted were also excluded. These measures ensured a more precise focus on the topic of interest and secured the quality and relevance of the materials analyzed for the research.

8.2 Results and discussion

The initial search in the Scopus database returned 34 documents, of which 21 were from computer science but also related to other areas. After filtering only for articles and conference papers, 20 documents remained, consisting of 14 articles and 6 conference papers. Of these, only 18 were in English. Further filtering, excluding areas such as mathematics, engineering, physics, materials science, energy, decision sciences, chemistry, biochemistry, genetics, and molecular biology, ultimately left only 5 works. Two of these articles did not have the complete document available for acquisition, leaving 3 articles that were effectively read and analysed. The three studies examine advanced image processing and analysis technologies, applying them to fields such as medical diagnostics and image quality assessment. In particular, one study examines edge detection's role in image quality assessment, specifically through the Edge Error Measure, and presents a wavelet-based method that aligns closely with human visual perception.

During the exploration of the ACM database, we found an intriguing collection of 416 articles, which included 202 research papers and 52 journal entries. These publications cover a wide range of subjects, from the technical intricacies of image processing and computer vision to the cutting-edge applications of machine learning in diverse fields like healthcare, education, and digital security. There is a noticeable trend towards leveraging deep neural networks, highlighting their prowess in refining image analysis and enabling advanced, automated medical diagnostics accessible through mobile technology.

In a thorough investigation using IEEE Xplore, an initial search yielded 192,176 results, which was narrowed down to 81,975 entries after applying a filter based on the publication year. Among these, 21,695 were journal articles, and a more focused analysis on precision and recall within this group highlighted 2,639 publications dedicated to these metrics. A meticulous selection process further narrowed these down to 25 significant papers that represent the cutting edge in image processing, detection methods, and deep learning applications.

None of the studies identified through the aforementioned databases provided an analysis concerning the influence of image smoothing on the performance of edge detection, but, among the analyzed papers, the study by Garcia-Alvarez, Rodriguez e Führ (2013) delves into the significance of edge detection in image quality assessment, specifically employing the Edge Error Measure, and introduces a wavelet-based method that resonates well with human visual perception. Another paper explores a technique for segmenting defocused images by adeptly distinguishing between focused and defocused areas through sophisticated algorithms. Zhang et al. (2022) presents an innovative design of a Convolutional Neural Networks (CNNs) architecture that enhances parameter efficiency and accelerates inference. These insights sparked an interest in exploring articles related to parameter determination in edge detection, Gaussian blur, and ultimately led to the investigation of multiscale edge detection methods.

In Lopez-Molina et al. (2011), they explore refining the Sobel technique for identifying edges across various scales, intending to address the conventional method's vulnerability to noise. The proposed method was called Modified Sobel (M-Sobel). The authors employ Gaussian smoothing to process the image on different scales, cleverly integrating the finer scales' spatial accuracy with the broader scales' resilience to counteract erroneous signals. The approach involves using Gaussian filters with assorted standard deviations to create progressively smoother images, subsequently analyzed through the Sobel technique to detect edges. This strategy is further refined by implementing a fine-to-coarse edge tracking method, which ensures uniformity across different scales.

Through quantitative evaluation (LOPEZ-MOLINA et al., 2011), it was seen that True Positives (TP) generally outnumber False Positives (FP), particularly at lower σ (gaussian parameter) values where incorrect responses are more common. As σ increases, the method's ability to precisely locate edges gets better, although it also brings about a heightened risk of losing edges due to either displacement or too much smoothing. This observation underscores the need for a well-balanced processing scale to efficiently detect edges. Notably, the M-Sobel method's effectiveness over the traditional Sobel approach becomes more apparent with the increase in σ, demonstrating a steady decline in both TP and FP, which corroborates the notion that genuine edges persist while false detections are effectively eliminated.

The work by Lopez-Molina et al. (2013) serves as a continuation and expansion of

the study in Lopez-Molina et al. (2011). In this follow-up work, the authors develop an advanced methodology that utilizes Gaussian smoothing and coarse-to-fine edge tracking. The research underscores the method's ability to blend the spatial accuracy of fine scales with the robustness of larger scales, effectively mitigating spurious responses. This approach, which employs the Sobel operator on progressively smoothed images and then tracks the edges across scales, shows significant improvements in edge detection accuracy. The experimental results highlight the multiscale method's superiority over single-scale techniques, demonstrating its effectiveness in reducing false positives and preserving the true edges' integrity.

Lopez-Molina et al. (2013) conducted an experiment to assess the effectiveness of edge detection using multiscale extensions, the impact of incremental Δr [2] in Gaussian Scale Space, and the tracking strategy's efficiency. This experiment uncovered an inverse relationship between precision (PREC) and recall (REC) in edge detection methods. With lower values of r, representing the standard deviation of Gaussian smoothing, a high recall was observed due to the detection of numerous edges, including false positives, leading to reduced precision. Conversely, an increase in r resulted in lower recall but higher precision, as fewer yet more significant edges were detected. The multiscale methods enhanced overall recall by accurately locating real edges, despite a slight decrease in precision due to the tracking process, which might capture more false positives. Nevertheless, these methods showed improved performance in the $F_{0.5}$ measure (MARTIN; FOWLKES; MALIK, 2004; LOPEZ-MOLINA; De Baets; BUSTINCE, 2013), indicating an efficient balance between accurate detection of real edges and the minimization of spurious responses.

In a subsequent work, Lopez-Molina et al. (2018) extend their investigation into image processing techniques, presenting an innovative approach to multiscale gradient fusion. This method is inspired by the human ability to selectively focus on different areas of a scene, aiming to replicate this selective process through the fusion of image gradients across multiple scales. The authors introduce two classes of weighted operators that automatically adapt for multiscale gradient fusion, proposing a method for image segmentation and edge detection that has been quantitatively tested on a popular dataset.

The proposed multiscale technique achieves a balanced interplay between precision (Prec) and recall (Rec), similar to their earlier work, while effectively mitigating the effects of Gaussian blurring and preserving its benefits. Despite the increase in scale leading to higher precision and lower recall, these effects are less pronounced than in monoscale methods, and the technique corrects edge displacement, which is crucial for certain applications. This research highlights the multiscale algorithm's ability to maintain stability with respect to scale settings, facilitating the configuration of the algorithms and demonstrating an improved performance and stability in multiscale image processing.

[2] r is the step of incremental in smoothing parameter

8.3 Chapter Conclusion

This work focused into the influence of image smoothing techniques on the efficacy of classic edge detection algorithms through a systematic literature review across major academic databases, employing stringent exclusion and inclusion criteria. The initial Scopus database search yielded 34 documents, primarily in computer science, narrowing down to 20 relevant articles and conference papers after language and domain filtering, with just three articles ultimately reviewed due to availability and relevance.

Similarly, an exploration in the ACM database uncovered 416 articles, encompassing a broad spectrum of topics from image processing to machine learning applications in various sectors. An extensive search in IEEE Xplore produced 192,176 results, refined to 81,975 entries, with a focused analysis on precision and recall leading to 25 pivotal papers in image processing and deep learning.

None of the studies sourced from the aforementioned databases provided an analysis of the impact of image smoothing on edge detection performance. However, the review of these articles stimulated further investigation of multiscale edge detection research. Within these studies, sections were discovered that evaluated the performance of their experiments with varying edge detection scales, yielding valuable information.

Then, the body of work reviewed here consistently demonstrates a nuanced relationship between precision (Prec) and recall (Rec), particularly in the context of multiscale edge detection. These studies underline the trade-offs inherent in optimizing these metrics, with lower scales favoring recall due to the detection of a broader range of edges, including false positives, thereby compromising precision.

As scale increases, precision improves at the expense of recall, highlighting the method's enhanced ability to discern more meaningful edges while omitting less significant ones. The development and refinement of multiscale techniques, especially evident in the transition from monoscale to multiscale methods and the introduction of self-adapting weighted operators, show a less pronounced trade-off between Prec and Rec, indicating a more balanced approach to edge detection.

This balance facilitates more accurate edge localization and minimizes the impact of spurious responses. The progression from initial edge detection strategies to sophisticated multiscale and adaptive methods reflects a significant advancement in image processing, emphasising improved accuracy and stability in detecting genuine edges while effectively reducing false positives.

After an extensive search and rigorous application of exclusion criteria, no works were identified that specifically evaluated the effects of blurring on the performance of edge detection in images. The only works retrieved by the employed methodology did not dedicate themselves to exploring this relationship directly. This gap motivated the investigations presented in the next chapter.

8.3.1 Publication

This chapter was published as a conference paper in the volume *Highlights in Practical Applications of Agents, Multi-Agent Systems, and Digital Twins: The PAAMS Collection*, corresponding to PAAMS 2024 (SILVA et al., 2025b).

9 EXPERIMENTAL INVESTIGATION OF THE IMPACT OF SMOOTHING ON THE PERFORMANCE OF EDGE DETECTION

As seen in Chapter 9, within the preprocessing phase for edge detection, image smoothing is one of the most crucial processes. This technique is essential for reducing noise and standardizing intensity variations between pixels, often implemented through filters such as Gaussian, mean, or median. The primary purpose of smoothing is to produce an image representation less susceptible to random disturbances, significantly facilitating subsequent analysis.

In the context of edge detection, smoothing is crucial for minimizing the occurrence of false positives, which can arise when minor intensity variations are mistakenly interpreted as edges. By applying smoothing techniques, the impact of these minor variations is reduced, allowing edge detection algorithms, like Sobel, Prewitt, or Canny, to operate with greater precision and efficiency.

However, image smoothing can have adverse effects, such as the loss of fine details and subtle edges, essential for analysis. The resulting “blurring"may eliminate critical information, especially in images with faint edges or subtle features.

Moreover, excessive smoothing can lead to over-homogenization, rendering distinct regions of the image indistinguishable and diminishing the effectiveness of edge detection algorithms. This is particularly problematic in applications requiring high edge precision, such as in pattern recognition or medical applications. Therefore, it is crucial to balance the application of smoothing techniques to ensure that noise reduction does not compromise the integrity of vital information in the images.

9.1 Related works

Through a comprehensive literature review and an extensive search across major academic databases, it was observed that only a subset of the studied articles directly related to the topic of edge detection. Focusing on the relationship between precision and recall, notable works include those by Lopez-Molina *et al.* (LOPEZ-MOLINA et al., 2011),

who developed the Modified Sobel (M-Sobel) method. This method integrates Gaussian smoothing at different scales, aiming to enhance edge detection accuracy. The research highlighted the trade-off between precision and recall, where lower Gaussian parameter σ values led to higher recall but lower precision due to increased false positives, while higher σ values improved precision but at the cost of recall.

Further exploration in subsequent studies by the same authors (LOPEZ-MOLINA et al., 2013) developed a multiscale approach that combined Gaussian smoothing with coarse-to-fine edge tracking. This method aimed to improve the detection of true edges and reduce false positives, again emphasizing the precision-recall balance. The multiscale strategy demonstrated that while increasing the scale σ led to better precision by reducing false positives, it could also decrease recall by missing some true edges.

In their continued research, Lopez-Molina *et al.* (LOPEZ-MOLINA et al., 2018) introduced multiscale gradient fusion, a technique inspired by human visual focus mechanisms. This approach attempted to balance precision and recall across multiple scales, reducing the impact of blurring while maintaining edge detection accuracy. The studies consistently highlighted the interplay between precision and recall, suggesting that multiscale methods can achieve a more balanced performance compared to single-scale techniques.

Despite these insights, as exposed on Chapter 8, the reviewed literature lacked specific studies on the impact of blurring on the precision and recall of edge detection methods.

9.2 Objectives

In this regard, the present study aims to bridge the gap in the state of the art in the field of image processing by conducting a comprehensive investigation into the effects of blurring, specifically Gaussian blur, on the efficiency of various edge detection methods, with a particular emphasis on the Canny operator. In addition to Canny, other edge detection techniques will be examined to determine how blurring influences the precision, recall, and F-measure of these methods.

The primary objective of this research is to quantitatively determine the positive and negative effects of blurring on the task of edge detection. Furthermore, we seek to ascertain whether there is a standard or optimal level of blurring that maximizes the efficacy of edge detection for a given detection threshold, considering the variable conditions of blurring in images.

This chapter is organized as follows: Section 5.1.2 presents discussions covering various pertinent techniques, followed by an exploration of smoothing filters (Section 5.1.2) and their role in reducing image noise. Additionally, the application of derivation filters for edge detection will be examined in Section 5.1.3. The Materials and Methods Section (Section 9.3) details the dataset and the methodology used for result quantifi-

cation (Section 9.3.1). The Results and Discussion Section (Section 9.4) presents and critically analyzes the findings. Finally, in the Conclusion Section (Section 9.5), the main results, contributions, and their implications are summarized, highlighting the study's significance. Consider the foundations and concepts subsection (Subsection 5.1) as the necessary background to understand this chapter, what includes a review of essential concepts, starting with an analysis of filtering methods in digital images (Subsection 5.1.1.

9.3 Materials and Methods

To achieve the goals of this research, initially, the smoothing filters Gaussian, mean shift, and Gravitational were considered. The first two are commonly used in the literature, while the latter represents a recent and highly robust filter. The Canny detector was initially chosen due to its widespread use and recognition in the literature. The parameters of each smoothing filter were exhaustively varied, followed by edge detection using the previously selected filter.

After each detection, the previously mentioned metrics were obtained through manual labeling, as will be explained later. The results were then tabulated for analysis. Regarding the parameter ranges used for each method, to ensure comparable results, they were: from 0 to 5 for the standard deviation in the case of the Gaussian filter, up to 50 iterations for the Gravitational filter, and from 0 to 5 for the spatial support number in the case of mshift.

The data underwent a series of analyses. It was divided into quantiles to examine the general performance behavior across the parameter variations. The study also aimed to establish correlations between the metrics and between each metric and its respective varied parameter.

In a subsequent phase of the research, the Gaussian filter was implemented in conjunction with the Canny edge detector. The smoothing parameters of the filter were varied in discrete intervals from 0 to 5, while the parameters of the Canny detector were adjusted from 1.25 to 5.25, with increments of 1. This procedure resulted in comprehensive data collection. Subsequently, this dataset was analyzed to investigate the presence of trends or systematic relationships between the parameters. The aim was to discern if it was feasible to directly establish the optimal parameter capable of maximizing either precision or recall, based on a given edge detection parameter, or vice versa.

Continuing with the analysis, special attention was given to the F-measure, representing the harmonic mean between precision and recall. This metric provides a balanced evaluation of the system's performance by weighing both characteristics. Considering the F-measure, the study sought to identify parameters that optimize both precision and recall simultaneously, thus offering an ideal balance point between the two metrics. Identifying such parameters could indicate configurations that maximize outcomes, reflecting supe-

rior performance in the edge detection process. Therefore, the investigation focused on determining whether there are specific values of the Gaussian filter and Canny detector parameters that result in the best weighted performances, as expressed by the F-measure.

9.3.1 Dataset and quantification of the results

As seen in Section 5.3, the experimental evaluation in this chapter follows the established protocol using the BSDS500 dataset. We adhere to the same quantitative framework previously detailed, utilizing Precision (20), Recall (21), and the $F_{0.5}$ measure (22) to ensure consistency and comparability with the benchmark results.

9.4 Results and discussion

In the current study, all validation images were utilized. For each image, smoothing techniques of varied intensities were applied using three distinct methods: Gaussian, Gravitational, and mshift. Subsequently, on each smoothed image, edge extraction was conducted using the Canny method with a fixed parameter value of ($\sigma = 2.25$). From the resulting edge images, metrics of precision (Prec), recall (Rec), and the F-measure were extracted, considering different intensity levels for each method applied to each image. These metrics were calculated according to the formulas presented in the methodology section of this work. The obtained values were meticulously tabulated and subjected to a detailed statistical analysis, allowing for a quantitative assessment of the applied smoothing methods.

To investigate the relationship between precision and recall as a function of the variation in the smoothing intensities of the filters, a correlation analysis was conducted. This analysis took into account the aforementioned metrics in relation to changes in the specific parameters of each smoothing method. Specifically, the standard deviation (σ) for the Gaussian method, the spatial support for the mshift, and the number of iterations for the Gravitational method were evaluated. The results of this correlation analysis are detailed in Table 12. Generally, an inverse correlation between precision and recall was observed. That is, as smoothing intensified, there was a significant decrease in the number of false positives, whereas the number of false negatives increased proportionally. In the specific case of the Gaussian filter, this correlation was less intense for the precision metric but showed an almost perfect correlation regarding recall. These findings suggest important nuances in the choice of smoothing methods for image analysis, depending on the specific objectives of each application.

To assess the performance of the image smoothing methods under study, a comprehensive descriptive analysis of the previously tabulated results was conducted. In this phase of the analysis, it was observed that the data distribution did not follow a standard pattern. Given this observation, the median was chosen as the statistical reference parameter for

Table 12: Correlations between Sigma, Precision (Prec), and Recall (Rec) for different types of blurring

Filter	**r: Sigma and Prec**	**r: Sigma and Rec**	**r: Prec and Rec**
Gaussian Blur	0.634	-0.983	-0.563
Gravitational Blur	0.863	-0.978	-0.876
mshift	0.990	-0.973	-0.996

comparing the methods, due to its robustness in non-normal distributions.

The findings indicated that the Gravitational method excelled in terms of precision, demonstrating a superior ability to effectively identify true positives. Conversely, the mshift method stood out in terms of recall, showing greater efficiency in minimizing false negatives. Additionally, mshift also exhibited better performance in the F-measure, which is the harmonic mean between precision and recall, suggesting a more suitable balance between these two metrics.

These observations are crucial for understanding the characteristics and potential applications of each smoothing method. The detailed data and comparative analyses can be found in Table 13, where the measurements and statistical calculations that support these conclusions are presented.

Table 13: Statistics for Gravitational, mshift, and Gaussian methods

Method	**Statistic**	**Precision**	**Recall**	**F**
Gravitational	Median	**0.793**	**0.747**	0.739
	Mean	0.755	0.718	0.717
	Standard Deviation	0.170	0.149	0.133
	Minimum	0.242	0.128	0.226
	Maximum	1.000	0.982	0.957
mshift	Median	**0.789**	**0.775**	0.752
	Mean	0.748	0.742	0.728
	Standard Deviation	0.172	0.138	0.131
	Minimum	0.234	0.208	0.314
	Maximum	1.000	0.964	0.954
Gaussian	Median	**0.785**	**0.759**	0.748
	Mean	0.745	0.739	0.725
	Standard Deviation	0.169	0.133	0.125
	Minimum	0.245	0.263	0.332
	Maximum	1.000	0.98	0.954

To enhance understanding of the evaluation metrics behavior in response to variations in smoothing parameters, and acknowledging the potential for distinct behaviors in specific subsets of images, especially those with unique characteristics, a segmented analysis approach was adopted. This involved dividing the data into groups based on performance percentiles. This strategy enabled a more detailed and specific assessment of the results, considering potential variations within the dataset.

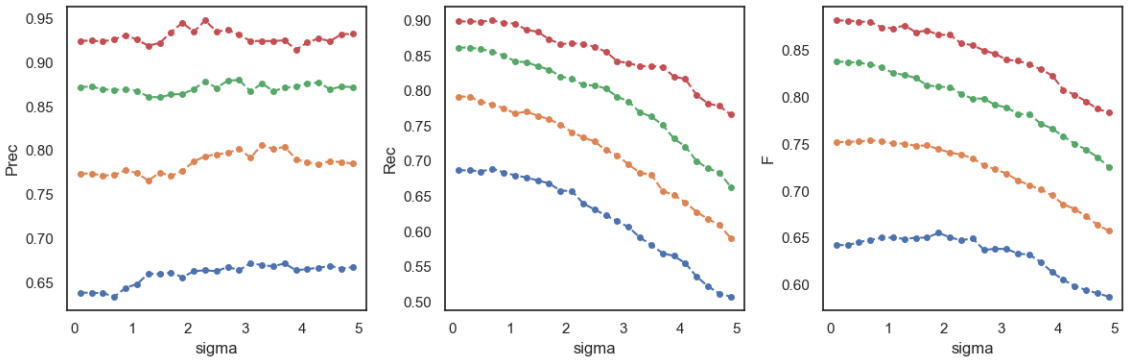


Figure 23: Percentiles for canny 2.25 with Gaussian sigma interval = **[0.1-5.0]**

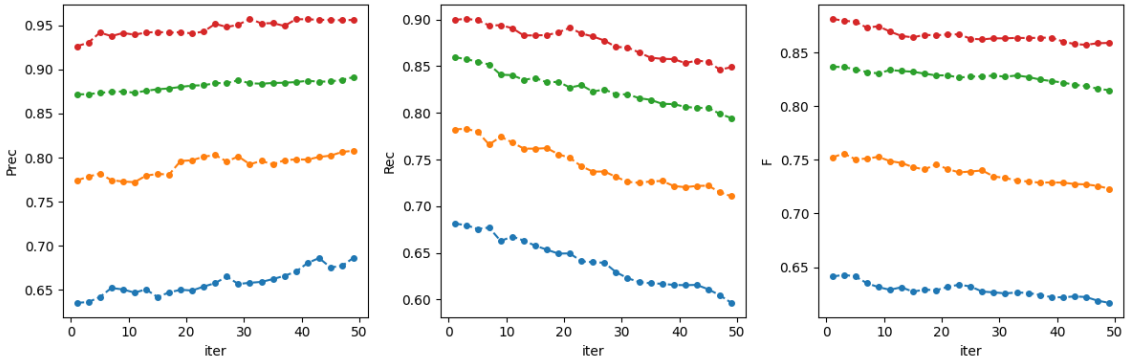


Figure 24: Percentiles for canny 2.25 with mshift iterations interval = **[1-50]**

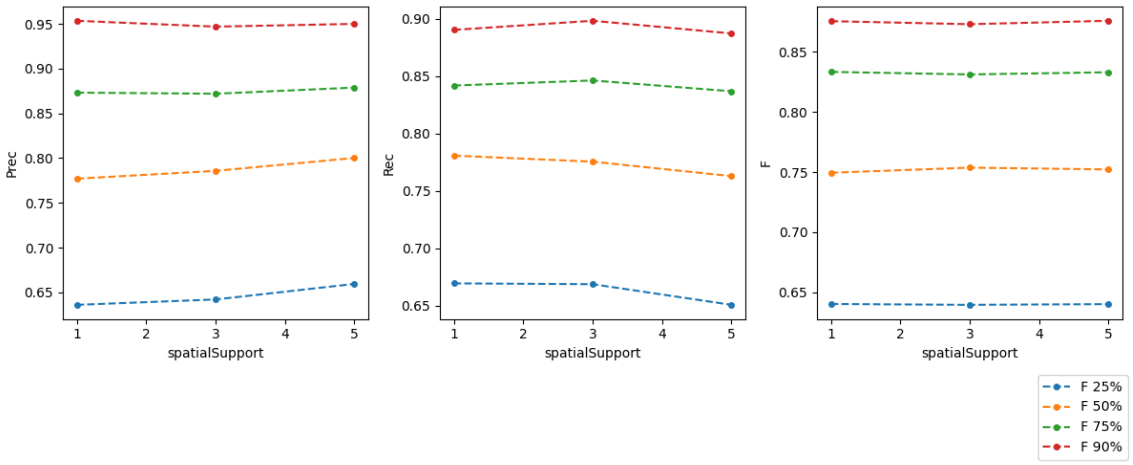


Figure 25: Percentiles for canny 2.25 with gravitational iterations interval = **[1-50]**

The outcomes of this segmented analysis are depicted in Figure 25. Graphical analysis reveals that, for the majority of the percentiles examined, there is a trend of slight increase in precision as the smoothing parameter values rise, while recall values tend to decrease. This trend varies between linear and quadratic, depending on the data subset in question. It is emphasized that, in an ideal scenario of smoothing for edge extraction, the recall graph would exhibit the smallest possible slope relative to the increase in precision values. This characteristic would indicate an optimal balance between minimizing false negatives (high recall) and effectively identifying true positives (high precision).

To gain deeper insight into the matter, a preliminary study was conducted to identify the optimal parameter values for each metric - precision, recall, and F-measure - within the dataset. This phase of the analysis involved a careful evaluation of each image individually to determine the specific parameter value that maximized each of these metrics. Following this thorough investigation, the average and median of these optimal values for each smoothing method were calculated.

The Gaussian method exhibited a moderate balance between precision and recall, with close average and median parameter values for precision (3.025 and 3.1, respectively) but a larger discrepancy for recall (1.162 and 0.7). This suggests consistency in identifying true positives but a tendency to miss some false negatives. The F-measure, with parameter values of 1.64 and 1.3, indicates a reasonable balance between the two metrics, though not exceptional. Conversely, the mshift method demonstrated a superior ability to minimize false negatives, as evidenced by the higher parameter values for recall (2.43 and 3.0). Moreover, this method exhibited a more balanced performance in the F-measure (2.95 and 3.0), suggesting a more effective compromise between precision and recall.

Table 14: Optimal values of metrics for each method with Canny fixed at 2.25

Method	**Precision**	**Recall**	**F-measure**
	Mean/Median	Mean/Median	Mean/Median
Gaussian	3.025 / 3.1	1.162 / 0.7	1.64 / 1.3
mshift	3.51 / 5.0	2.43 / 3.0	2.95 / 3.0
Gravitational	33.91 / 41.0	6.33 / 1.0	15.94 / 7.0

In contrast to the other two methods, the Gravitational method stood out for its exceptionally high precision, with surprisingly high parameter values (33.91 and 41.0), yet its recall performance was variable, as indicated by the significant difference between the average and median of the parameter (6.33 and 1.0). This implies that while the method is highly effective in identifying true positives, it may not be as consistent in minimizing false negatives. The F-measure for this method, with parameter values of 15.94 and 7.0, reflects an imbalance between precision and recall. These observations underscore the importance of selecting the most appropriate smoothing method, considering the application's specific requirements and the relative importance of precision versus recall in the context of image analysis. The results are detailed in Table 14.

Furthermore, a comprehensive assessment was conducted to analyze the relationship between the parameters of the Gaussian smoothing and Canny edge detection filters. The parameter σ_1 for the Gaussian filter was varied from 0 to 5, while the parameter σ_2 for the Canny filter was varied from 1.25 to 5.25, with increments of 0.1 and 1.0, respectively. For a clearer analysis of the results, for each σ_1 value, the combination of σ_2 that maximized precision, recall, and F-score for each image was identified. This resulted in the creation of a heatmap that highlighted the most effective combinations for achieving

Table 15: Median and Standard Deviation of blur parameter for Different Percentiles of the Metrics Prec, Rec, and F

Metric	Percentile	Median	Sd
Prec	25	3.3	1.578
	50	3.3	1.697
	75	3.4	1.758
	90	3.5	1.745
Rec	25	0.9	1.133
	50	0.7	1.112
	75	0.7	1.051
	90	0.7	1.103
F	25	1.7	1.349
	50	0.9	1.283
	75	0.7	1.176
	90	0.7	1.285

higher precision, recall, and F-score, respectively.

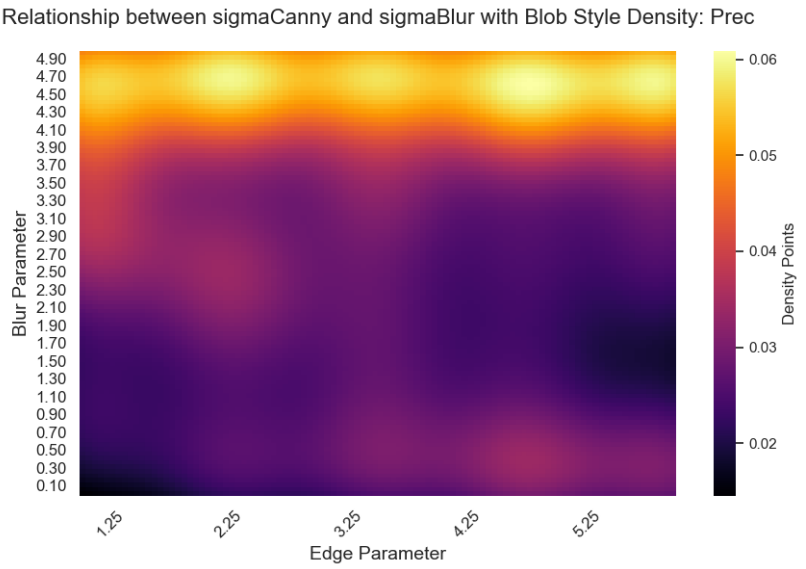


Figure 26: Relationship between edge parameter and blur parameter with Blob Style Density: **Precision**

Through the results of the heatmap, it is possible to observe that the best results for precision occur with higher values of Gaussian smoothing, while lower values of smoothing are more effective for recall, which is consistent with related studies. However, there is also a significant variation in these optimal combination values, indicating that the problem is not trivial and cannot be solved directly, such as by finding a linear function to determine the desired parameters.

The results also indicate that optimizing the F-score metric is associated with higher values of the Canny filter parameter, within a narrower range than 2 for Gaussian blur. The quantitative analyses of this experiment can be referenced in the table 16.

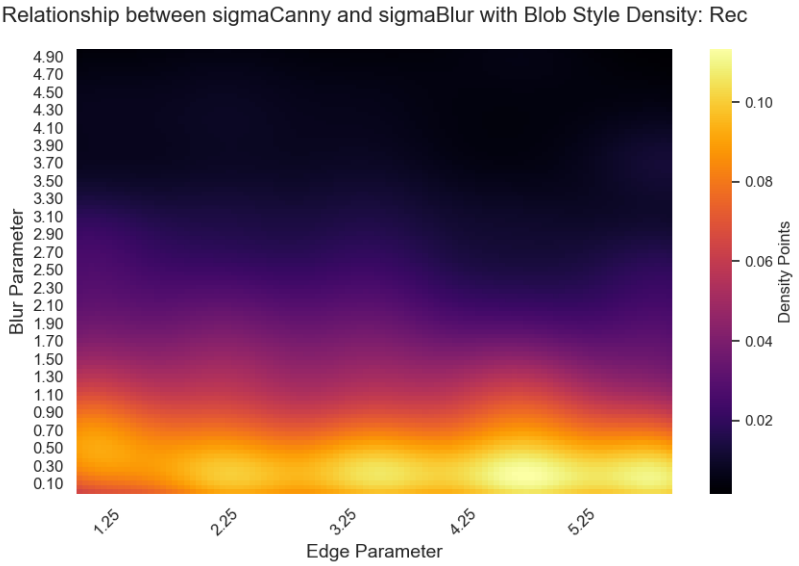


Figure 27: Relationship between edge parameter and blur parameter with Blob Style Density: **Recall**

Table 16: Quantitative analysis results

Metric	Perc.	inf.	sup.	Median	Sd
PREC	25	1.25	5.25	3.3	1.58
	50	1.25	5.25	3.3	1.70
	75	1.25	5.25	3.4	1.76
	90	1.25	5.25	3.5	1.74
REC	25	1.25	5.25	0.9	1.13
	50	1.25	5.25	0.7	1.11
	75	1.25	5.25	0.7	1.05
	90	1.25	5.25	0.7	1.10
F	25	1.25	5.25	1.7	1.35
	50	1.25	5.25	0.9	1.28
	75	1.25	5.25	0.7	1.17
	90	1.25	5.25	0.7	1.28

9.5 Chapter Conclusion

Edge detection is a crucial component in the field of image processing and computer vision, essential for discerning discontinuities within images. This technique is pivotal in delineating distinct boundaries between contrasting regions, which is critical for applications such as object detection and pattern recognition. The current study sought to investigate the impact of various smoothing methods on the effectiveness of edge detec-

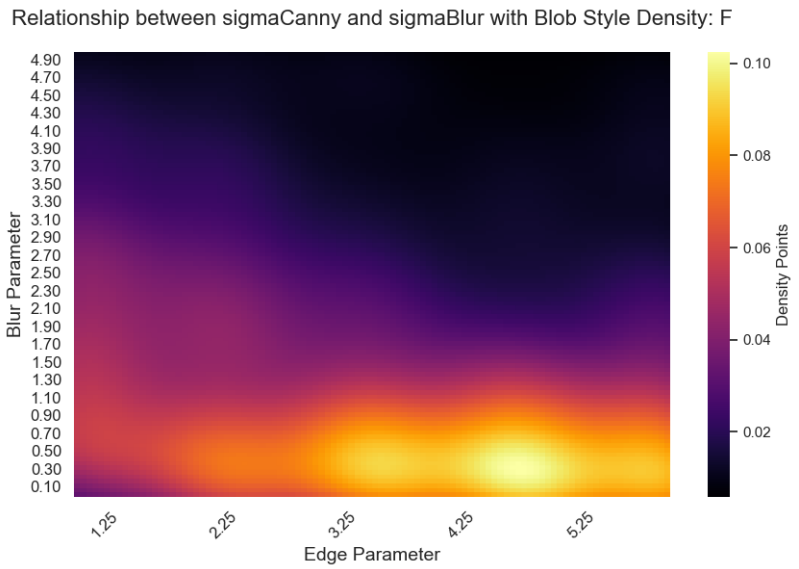


Figure 28: Relationship between edge parameter and blur parameter with Blob Style Density: **F**

tion algorithms, specifically focusing on the Canny operator and the interplay between precision and recall.

Edge detection's relevance extends across numerous practical domains, including autonomous driving and medical imaging, where precise detection can substantially enhance system functionality and reliability. The preprocessing stage, which typically involves image smoothing, is critical in this regard. Although necessary for noise reduction, smoothing can also obscure essential details and edges, thus influencing the effectiveness of subsequent edge detection processes.

Our review of the literature indicated a notable gap: studies seldom evaluate the performance characteristics of smoothing methods in the context of edge detection. Existing research predominantly concentrates on enhancing accuracy without sufficiently addressing the compromises between precision and recall. This research aims to fill this void by offering a detailed evaluation of Gaussian, mean shift, and Gravitational smoothing techniques and their impacts on edge detection metrics.

The findings reveal that while certain methods, such as Gravitational smoothing, excel in achieving high precision, they may not consistently reduce false negatives. This underscores a critical balance between noise reduction and the preservation of crucial image details. Our segmented analysis of the effects of different smoothing intensities further illustrates the nuanced impact of these methods on the precision and recall metrics, advocating for a finely balanced approach to optimize edge detection.

The prevalent arbitrary application of parameters in smoothing techniques, particularly Gaussian filters, in existing literature, often leads to suboptimal outcomes in edge detection. This study underscores the necessity for a more scientifically grounded approach to the selection of these parameters. The adoption of mathematical models to

determine optimal smoothing parameters could markedly propel the field forward, minimizing arbitrary parameter choices and enhancing the precision and efficacy of edge detection in computer vision applications.

Moreover, multiscale methods emerge not only as promising but as essential for handling the effects of preprocessing on digital images, especially in medical imaging where certain filters may eliminate critical fine details necessary for the intended analysis. These methods offer the potential to adaptively preserve or enhance features at different scales, thereby accommodating the diverse needs of various application areas.

Methods of this kind will be addressed in Chapters 12 and 13. Before that, in the next chapter, we will present a method based on sliding windows with an adaptive fuzzy measure. The main idea of this approach is to employ the Choquet integral together with an adaptive fuzzy measure in an edge detection method that takes into account the contextual information of each pixel.

9.5.1 Publication

Some of the results from this chapter was published in the *IPMU 2024 Lisboa Short Paper Proceedings*[1], corresponding to the 20th International Conference on Information Processing and Management of Uncertainty in Knowledge-Based Systems (IPMU 2024), held in Lisbon, Portugal (SILVA et al., 2025a).

[1] https://ipmu2024.inesc-id.pt

10 SLIDING-WINDOW-BASED ADAPTIVE FUZZY MEASURE FOR EDGE DETECTION

As edge detectors got more complex (see Chapters 5, 6, 7), there was a need to make sense of the process in a clear way and to have a normalised approach, so that a comparison of different methods could be appropriately done. This led to breaking down the process into steps that can be configured, improved and interpreted.

One of the most significant proposals for edge detection process normalisation, as mentioned in the introduction of this thesis (See Chapter 1, is the one by Bezdek, Chandrasekhar e Attikouzel (1998a). The method outlined in that paper breaks down the process of detecting edges into four distinct steps, each represented by a specific function: *conditioning* (c), which prepares the image by removing details and improving its overall clarity; *feature extraction* (f), where the system calculates differences in information between pixel neighbours; *blending* (b), the phase in which these differences are combined to highlight edge locations; and *scaling* (s), which refines these edges to produce a clear, binary outline of the image. From this perspective, applying edge detection (e) to an image I is achieved through the sequential application of these functions: $e(I) = s(b(f(c(I))))$. This sequence is subject to certain restrictions based on each function's input and output requirements.

Focusing on the blending step, the fusion process of the differences in information between pixel neighbours can be modelled on the light of fuzzy set/logic theory, which can easily deal with uncertain/incomplete/imperfect information (ZADEH, 2008). In this context, different aggregation-based approaches can be used(GRABISCH et al., 2009; BELIAKOV; Bustince Sola; CALVO, 2016). One important and novel methodology, proposed in different basis by Marco-Detchart *et al.* (MARCO-DETCHART et al., 2023a; MARCO-DETCHART et al., 2023b; MARCO-DETCHART et al., 2021), is to apply fuzzy integrals derived by the discrete Choquet integral(CHOQUET, 1953–1954), which is defined in terms of a fuzzy-set functions named fuzzy measures (CHOQUET, 1953–1954) presenting the desired property of considering the interrelation among the inputs to be aggregated.

However, in the literature, there is a discussion on the drawbacks of using predefined

definitions of the fuzzy measures, which remains fixed for any different subset of the data. In this manner, the fuzzy measure does not take into account the information provided by the input elements, but just the relation/cohesion among them. Some methods for learning fuzzy measures from the data can be found in the literature(BELIAKOV; WU, 2019; SALEH et al., 2018; BELIAKOV; WU; DING, 2024; WU et al., 2024), but none of them were proposed for the edge detection problem, being either oriented to specif applications (e.g., classification(SALEH et al., 2018) and decision making(BELIAKOV; WU; DING, 2024; WU et al., 2024)) or with high computational complexity(BELIAKOV; WU; DING, 2024).

Then, the objective of this Chapter is to propose an adaptative framework for detecting the appropriate fuzzy measures according to the information carried by pixels using sliding windows along the image, capturing the relationship between neighbouring pixels effectively. For that, different aggregation(GRABISCH et al., 2009; BELIAKOV; Bustince Sola; CALVO, 2016) and pre-aggregation(LUCCA et al., 2016; DIMURO et al., 2016a) functions (such as t-norms and t-conorms(KREINOVICH; MUKAIDONO, 2000), copulas(ALSINA; FRANK; SCHWEIZER, 2006) and overlap functions(BUSTINCE et al., 2010; BEDREGAL et al., 2013)) are applied to extract and aggregate information from the pixels in each sliding window. This process generates different fuzzy measure definitions, each one adapted to a specif window. Those fuzzy measures are then used in different C_t-integrals(LUCCA et al., 2016) and C_F-integrals(LUCCA et al., 2018a), some of the state-of-the-art generalisations(DIMURO et al., 2020) of the Choquet integral(CHOQUET, 1953–1954), which have been largely applied in classification(LUCCA et al., 2016; LUCCA et al., 2018a), brain computer interface(Ko et al., 2019) and also in our previous works on the edge detection problem(MARCO-DETCHART et al., 2023a; MARCO-DETCHART et al., 2023b; MARCO-DETCHART et al., 2021).

The rest of this Chapter is organised as follows: we start with the framework of the proposed method (Section 10.1) and the experimental setup (Section 10.2), then the results are presented (Section 10.3). Lastly, we wrap up what we have learned from all the experiments (Section 10.4). Further details on the related work and the state of the art can be found in the extended version of this chapter, published in a journal (MARCO-DETCHART et al., 2025).

10.1 Sliding-window based adaptative fuzzy measure framework

Typically, edge detection involves applying a kernel to the image through convolution to identify cues that signify the existence of edges. In this work, we use a convolution-like approach to check each pixel in the image with a small window of 3×3 pixels (Figure 29). By looking at the pixel in the middle of this window and comparing it with its eight neighbours, we can guess whether there is an edge at that pixel. After we get this

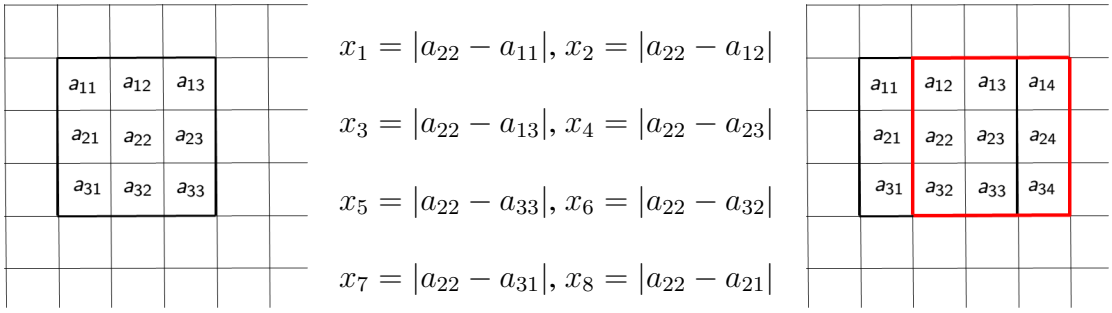


Figure 29: Feature extraction process with the central pixel a_{22} and its 8-neighbourhood, along with the intensity variation computation and the representation of the rolling window used.

information for each pixel, we have to combine all of these raw data to create the final image that shows where all the edges are. Since we end up with many different values for each pixel, we have to simplify this down to just one value per pixel.

To achieve this, we first merge the extracted features using the Choquet integral and its generalisations, which have been proven to be quite effective in differentiating and classifying data in complex scenarios (Table 3). This technique requires a way to measure how each feature influences the final outcome, which is where the concept of a fuzzy measure comes in, specifically through the use of the power measure (Eq. 2). This mathematical tool allows us to assess the contribution of each feature (in our case, the intensity variations) in a flexible manner.

The innovation in our approach lies in the adaptability of the q value within the power measure, which we adjust for each pixel based on its surrounding area. This adaptability ensures that our method is sensitive to the local characteristics of the image, providing a more nuanced and accurate detection of edges. In order to determine the optimal q value, we follow two approaches:

1. On the one hand, the q value is selected by using maximum (T_M), the minimum (S_M) and the mean (AVG) values of intensity differences of each pixel neighbourhood. This is the approach used in our previous work(MARCO-DETCHART et al., 2023a).

2. On the other hand, we use a variety of strategies (the (pre)-aggregation functions of Table 2) that take into account the intensity values of the pixel and its neighbours and then apply the average value of them, aiming to find a balance that best represents the presence of an edge.

Our experimentation is not limited to a single set of parameters; instead, we explore the performance of our edge detection framework under different conditions by adjusting the σ value of the Gaussian filter used in the conditioning phase. Specifically, we examine how the choice of $\sigma = 1$ (S_1) versus $\sigma = 2$ (S_2) affects the outcome. This step is crucial

as it allows us to understand the robustness and flexibility of our approach across varying degrees of image smoothing, which is what the Gaussian filter accomplishes.

In our experiments, we stick to the BBS (BEZDEK; CHANDRASEKHAR; ATTIKOUZEL, 1998a) framework, adding a final step for the evaluation, which renders into the following five phases:

- *Conditioning (c)*- Apply a smoothing filter, specifically a Gaussian filter ($\sigma = 2$). Although content-aware smoothing (e.g. Anisotropic Diffusion or Bilateral Filtering) is commonly acknowledged to produce better results for boundary detection, we are not focusing on evaluating smoothing techniques ;
- *Feature Extraction (f)*- Extract local variation features in each of the directions considered (Figure 29) and order them in an increasing way;
- *Blending (b)*- Fuse the local information with the proposed method, according to the two approaches mentioned above;
- *Scaling (s)*- Obtain a thin boundary image using non-maxima suppression (CANNY, 1986) and binarize the thinned image by applying the hysteresis method (MEDINA-CARNICER et al., 2011).
- *Quantification*- We use the approach presented in (MARTIN; FOWLKES; MALIK, 2004) in order to obtain a confusion matrix and compute performance measures.

In Figure 30 we show the different steps of the framework used with a visual example of each phase.

10.2 Experimental setup

As seen in Section 5.3 (Chapter 5), the experimental evaluation in this chapter follows the established protocol using the BSDS500 dataset. We adhere to the same quantitative framework previously detailed, utilizing Precision (20), Recall (21), and the $F_{0.5}$ measure (22) to ensure consistency and comparability with the benchmark results, based on the following representation:

Images, within the context of this study, are conceptualised as mappings ($D : R \times C \mapsto L$) from a discrete domain, defined by the Cartesian product of the set of rows $R = \{1, ..., r\}$ and the set of columns $C = \{1, ..., c\}$, to a set of luminance values L. In the case of binary images, L is constituted by the binary values $\{0, 1\}$, representing the two possible luminance levels. Conversely, for grayscale images, L spans the range $\{0, \ldots, 255\}$, offering a more nuanced representation of luminance through 256 distinct levels. Colour images extend this representation through the Cartesian product of three such sets, one for each primary colour channel, resulting in $L = \{0, ..., 255\}$ for RGB images. The current study is done using the analysis of colour images.

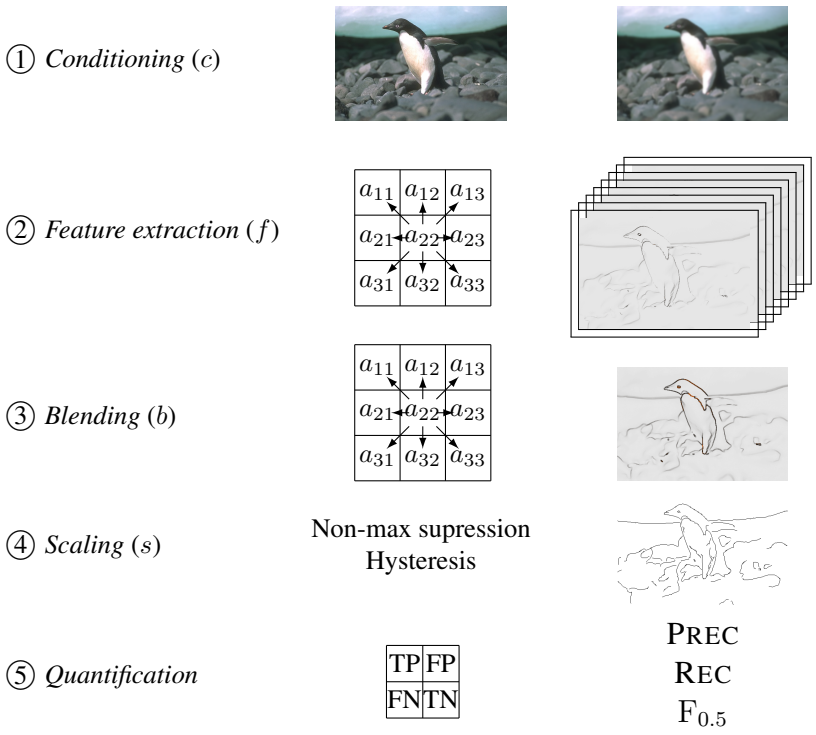


Figure 30: Diagram illustrating the BBS approach used in this study and the process for evaluating performance. In the depiction of the sliding window, a_{22} is identified as the central pixel.

10.3 Results

In this section, we analyse the outcomes obtained with the two methodologies proposed for calculating the q value, which is crucial for aggregating features related to each pixel in the image.

In the initial experiment reported in the original work (MARCO-DETCHART et al., 2023a), conducted on grayscale images and deriving q from pixel intensity variations, it is evident from Table 17 that under S_1 smoothing, which applies minimal blurring, the Choquet generalization combined with F_{BPC} and the adaptive fuzzy measure, where q is determined by the maximum value within each window, emerges as the superior performer in terms of $\mathrm{F}_{0.5}$, surpassing the Canny edge detector.

Upon examining the other methodologies, it is observed that most yield results comparable to those of the Canny method, with the exception of two (C_{T_M} and $\mathfrak{C}_{T_M}^{C_F}$) that achieve identical outcomes. Both employ the adaptive method for calculating q based on the maximum value, underscoring the efficacy of the adaptive approach in enhancing edge detection performance.

It is noteworthy that the sole generalization not benefiting from the adaptive fuzzy measure application is the Hamacher generalization, which attains optimal results with a constant $q = 1$ across the entire image.

Further analysis into the scenarios with increased blurring due to S_2 smoothing reveals

Table 17: Comparison of various setups for the power measure using the Choquet integral and its generalisations, alongside the Canny method, in terms of PREC, REC, and $\mathrm{F}_{0.5}$. The tests were conducted after applying Gaussian smoothing with sigma (σ) values of 1 (S_1) and 2 (S_2) and using adaptive q from intensity variations.

	Smoothing S_1			Smoothing S_2		
Method	PREC	REC	$\mathrm{F}_{0.5}$	PREC	REC	$\mathrm{F}_{0.5}$
C_1	.704	.756	.709	.730	.744	.719
C_{S_M}	.671	.818	.719	.745	.699	.705
C_{T_M}	.707	.738	.702	.760	.646	.681
C_{AVG}	.693	.777	.714	.751	.669	.691
$\mathfrak{C}_{p^{0.8}}^{C_F}$	.704	.754	.708	.734	.739	.718
$\mathfrak{C}_{S_M}^{C_F}$	.673	.815	.719	.744	.698	.704
$\mathfrak{C}_{T_M}^{C_F}$	.707	.739	.702	.759	.647	.681
$\mathfrak{C}_{AVG}^{C_F}$	.694	.774	.714	.750	.669	.691
$\mathfrak{C}_{p^1}^{O_B}$	.704	.760	.711	.738	.728	.714
$\mathfrak{C}_{S_M}^{O_B}$	.690	.783	.716	.751	.671	.692
$\mathfrak{C}_{T_M}^{O_B}$	.708	.735	.701	.759	.646	.681
$\mathfrak{C}_{AVG}^{O_B}$	.702	.756	.708	.756	.655	.685
$\mathfrak{C}_{p^{0.4}}^{F_{BPC}}$	.703	.757	.709	.731	.742	.718
$\mathfrak{C}_{S_M}^{F_{BPC}}$	.655	.850	**.722**	.730	.744	**.721**
$\mathfrak{C}_{T_M}^{F_{BPC}}$	.706	.740	.702	.759	.651	.683
$\mathfrak{C}_{AVG}^{F_{BPC}}$	.672	.817	.720	.743	.694	.702
$\mathfrak{C}_{p^1}^{\text{Hamacher}}$	.693	.776	.714	.750	.682	.698
$\mathfrak{C}_{S_M}^{\text{Hamacher}}$	.704	.748	.706	.760	.646	.681
$\mathfrak{C}_{T_M}^{\text{Hamacher}}$	.709	.734	.700	.762	.642	.680
$\mathfrak{C}_{AVG}^{\text{Hamacher}}$	.707	.740	.703	.761	.644	.680
$Canny$	.742	.730	.719	.747	.704	.707

that the adaptive method generally under-performs compared to the fixed q fuzzy measure approach, with the exception of the Choquet generalization with F_{BPC}. This trend suggests that the adaptive fuzzy measure's effectiveness diminishes with greater blurring, suggesting its potential strength in situations that do not rely heavily on smoothing before edge detection.

In terms of visual outcomes, it is apparent that the majority of the methods produce features and edges that are quite alike. The method that closely matches the outcome from the Canny edge detector is when employing $\mathfrak{C}_{T_M}^{F_{BPC}}$, which uniquely identifies the edge between the sky and the ground. Moreover, a significant number of Choquet-based

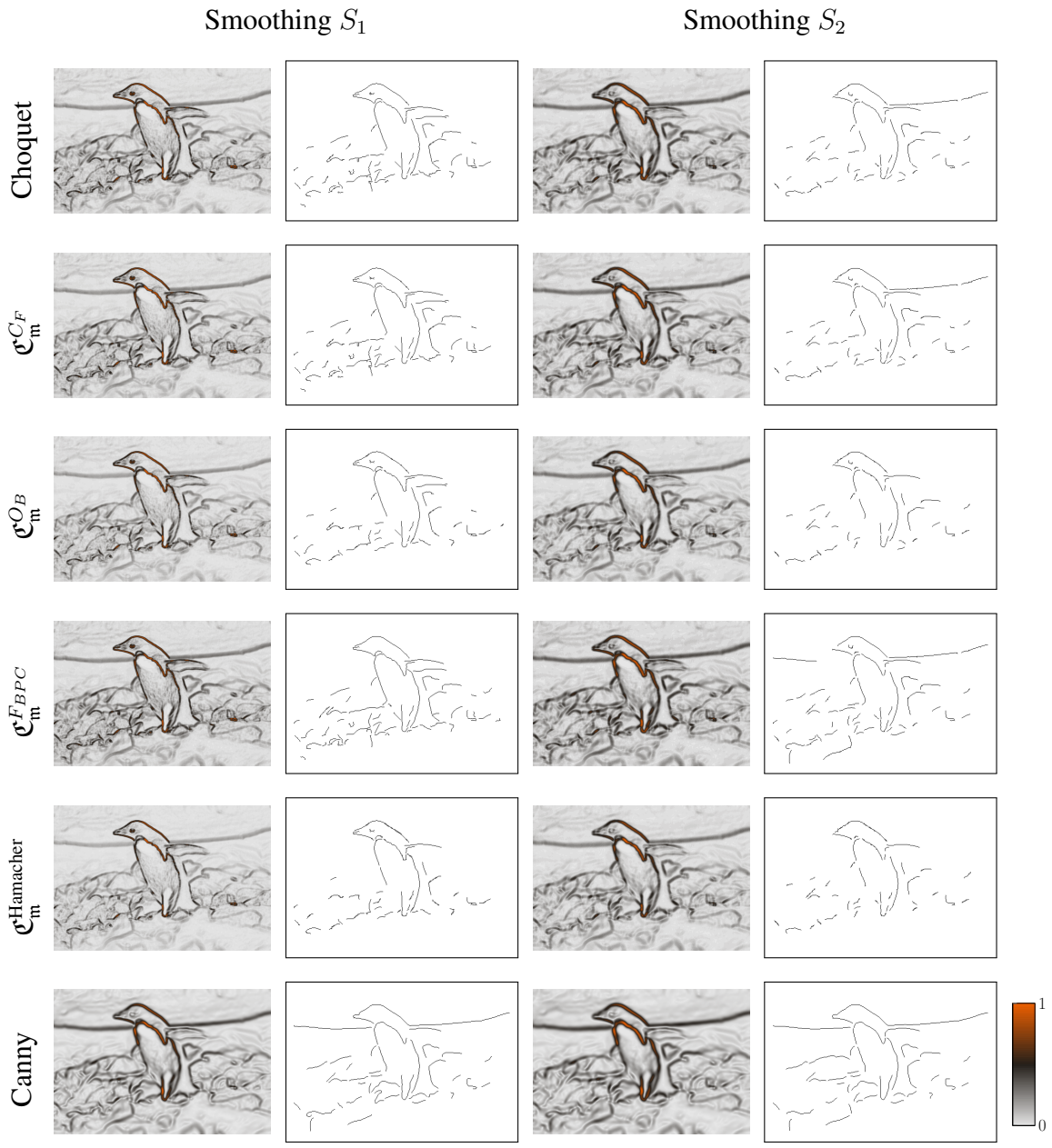


Figure 31: Visual comparison of features and edges extracted from the original image 106005 in the BSDS test set using the most effective methods in comparison to the conventional Canny edge detector.

strategies are able to detect the penguin's eye, whereas the top smoothing technique, S_1 , fails to outline it, thereby enhancing its resemblance to the ground-truth images.

When analysing the results from the extended experiment over colour images and computing the q from the average of the aggregated intensity values from each pixel neighbourhood, we show that the overall results with this second method have great performance.

The experimental outcomes, as summarised in Table 18, reveal nuanced differences in performance across the different configurations and smoothing levels. When focusing on the Choquet integral (C) and its generalisations ($\mathfrak{C}^{C_F}$, $\mathfrak{C}^{O_B}$, $\mathfrak{C}^{F_{BPC}}$, $\mathfrak{C}^{T_{HP}}$), it is evident that the adjustments in the methods lead to variations in PREC, REC, and $\mathrm{F}_{0.5}$.

For instance, under the T_M and S configurations with the first level of smoothing (S_1), the C integral and its variants exhibited a closely matched performance, with $\mathrm{F}_{0.5}$ scores hovering around 0.75. Notably, the $\mathfrak{C}^{F_{BPC}}$ configuration demonstrated a slightly higher recall in most cases, potentially indicating its adeptness at identifying relevant edges at the expense of Precision.

Upon increasing the smoothing level to S_2, a slight performance improvement was observable for several configurations, suggesting that additional smoothing might aid in reducing noise, thereby enhancing the edge detection capability. Specifically, the $\mathfrak{C}^{F_{BPC}}$ variant often showed improvements in $\mathrm{F}_{0.5}$, indicating a better balance between Precision and Recall with increased smoothing.

The results underscore the complexity of edge detection and the influence of various factors, including the choice of integration method and the level of smoothing applied. While the differences among the configurations might appear marginal in some instances, these nuances can significantly impact the application-specific requirements.

The $\mathfrak{C}^{F_{BPC}}$ variant frequently emerged as a strong performer, particularly with higher levels of smoothing, suggesting its robustness in handling noise. This observation might guide our research towards prioritising configurations that optimise Recall without severely compromising Precision, especially in scenarios where capturing as many relevant edges as possible is critical.

Moreover, the marginal differences between the smoothing levels highlight the delicate balance between noise reduction and edge preservation. Excessive smoothing might lead to the loss of critical edge information, while insufficient smoothing might not adequately suppress noise. Therefore, the choice of smoothing level should be carefully considered in relation to the specific characteristics of the images being processed and the overall objectives of the edge detection task.

Table 18: Comparison of various setups for the power measure using the Choquet integral and its generalisations, alongside the Canny method, in terms of PREC, REC, and $F_{0.5}$. The tests were conducted after applying Gaussian smoothing with sigma (σ) values of 1 (S_1) and 2 (S_2) and using adaptive q from pixel intensity values.

		Smoothing S_1			Smoothing S_2					Smoothing S_1			Smoothing S_2		
q	Method	PREC	REC	$F_{0.5}$	PREC	REC	$F_{0.5}$	q	Method	PREC	REC	$F_{0.5}$	PREC	REC	$F_{0.5}$
T_M	C	.714	.800	.755	.734	.800	.765	S	C	.696	.824	.755	.723	.820	.768
	$\mathfrak{C}^{C_F}$	.716	.795	.753	.734	.798	.765		$\mathfrak{C}^{C_F}$	.698	.820	.754	.723	.818	.768
	$\mathfrak{C}^{O_B}$	.715	.789	.750	.746	.767	.756		$\mathfrak{C}^{O_B}$	.702	.815	.754	.732	.797	.763
	$\mathfrak{C}^{F_{BPC}}$	.709	.809	.756	.726	.826	.773		$\mathfrak{C}^{F_{BPC}}$	.698	.817	.753	.719	.826	.769
	$\mathfrak{C}^{T_{HP}}$	.705	.792	.746	.755	.722	.738		$\mathfrak{C}^{T_{HP}}$	.691	.819	.749	.750	.739	.744
T_P	C	.716	.790	.752	.744	.772	.758	C_F	C	.715	.793	.752	.743	.776	.759
	$\mathfrak{C}^{C_F}$	.718	.786	.751	.746	.770	.757		$\mathfrak{C}^{C_F}$	.718	.789	.752	.743	.774	.758
	$\mathfrak{C}^{O_B}$	.714	.785	.748	.752	.745	.749		$\mathfrak{C}^{O_B}$	.714	.786	.749	.750	.749	.750
	$\mathfrak{C}^{F_{BPC}}$	.715	.796	.753	.740	.793	.766		$\mathfrak{C}^{F_{BPC}}$	.714	.799	.754	.739	.799	.768
	$\mathfrak{C}^{T_{HP}}$	.710	.782	.744	.757	.717	.736		$\mathfrak{C}^{T_{HP}}$	.709	.783	.744	.757	.717	.737
$T_Ł$	C	.716	.774	.744	.759	.729	.744	C_L	C	.702	.821	.757	.733	.807	.768
	$\mathfrak{C}^{C_F}$	.716	.774	.744	.760	.729	.744		$\mathfrak{C}^{C_F}$	.705	.815	.756	.734	.805	.768
	$\mathfrak{C}^{O_B}$	.715	.775	.744	.760	.723	.741		$\mathfrak{C}^{O_B}$	.708	.802	.752	.745	.772	.758
	$\mathfrak{C}^{F_{BPC}}$	.715	.774	.743	.757	.729	.743		$\mathfrak{C}^{F_{BPC}}$	.690	.839	.757	.724	.833	.775
	$\mathfrak{C}^{T_{HP}}$	.712	.777	.743	.756	.714	.734		$\mathfrak{C}^{T_{HP}}$	.703	.799	.748	.755	.723	.739
T_{HP}	C	.713	.797	.752	.741	.784	.762	AVG	C	.703	.819	.756	.733	.807	.768
	$\mathfrak{C}^{C_F}$	.714	.796	.753	.742	.781	.761		$\mathfrak{C}^{C_F}$	.707	.813	.756	.734	.805	.768
	$\mathfrak{C}^{O_B}$	.714	.789	.750	.750	.754	.752		$\mathfrak{C}^{O_B}$	.709	.800	.752	.742	.775	.758
	$\mathfrak{C}^{F_{BPC}}$	.708	.813	.757	.730	.816	.771		$\mathfrak{C}^{F_{BPC}}$	.690	.840	.757	.725	.832	.774
	$\mathfrak{C}^{T_{HP}}$	.707	.788	.745	.756	.718	.737		$\mathfrak{C}^{T_{HP}}$	.703	.798	.748	.755	.723	.739
O_B	C	.715	.793	.752	.740	.783	.761	O_{RS}	C	.714	.799	.754	.739	.787	.762
	$\mathfrak{C}^{C_F}$	.717	.789	.751	.741	.781	.761		$\mathfrak{C}^{C_F}$	.716	.792	.752	.740	.785	.762
	$\mathfrak{C}^{O_B}$	.715	.788	.750	.748	.756	.752		$\mathfrak{C}^{O_B}$	.715	.789	.750	.748	.758	.753
	$\mathfrak{C}^{F_{BPC}}$	.712	.802	.755	.734	.811	.771		$\mathfrak{C}^{F_{BPC}}$	.709	.808	.755	.731	.816	.771
	$\mathfrak{C}^{T_{HP}}$	.708	.787	.746	.756	.718	.737		$\mathfrak{C}^{T_{HP}}$	.707	.788	.745	.756	.718	.737
O_{mM}	C	.715	.787	.749	.753	.749	.751	F_{GL}	C	.697	.827	.757	.730	.814	.769
	$\mathfrak{C}^{C_F}$	.715	.784	.748	.753	.748	.750		$\mathfrak{C}^{C_F}$	.700	.823	.757	.729	.815	.769
	$\mathfrak{C}^{O_B}$	.713	.783	.746	.755	.733	.744		$\mathfrak{C}^{O_B}$	.706	.806	.753	.741	.777	.759
	$\mathfrak{C}^{F_{BPC}}$	.715	.787	.749	.747	.769	.758		$\mathfrak{C}^{F_{BPC}}$	.691	.835	.756	.721	.833	.773
	$\mathfrak{C}^{T_{HP}}$	.712	.779	.744	.756	.714	.735		$\mathfrak{C}^{T_{HP}}$	.699	.805	.748	.754	.728	.741
O_{Div}	C	.715	.795	.753	.740	.785	.762	F_{BPC}	C	.717	.779	.747	.754	.746	.750
	$\mathfrak{C}^{C_F}$	.718	.788	.751	.741	.783	.761		$\mathfrak{C}^{C_F}$	.718	.777	.747	.754	.744	.749
	$\mathfrak{C}^{O_B}$	.716	.788	.750	.749	.757	.753		$\mathfrak{C}^{O_B}$	.716	.777	.745	.755	.731	.743
	$\mathfrak{C}^{F_{BPC}}$	.711	.805	.755	.731	.816	.771		$\mathfrak{C}^{F_{BPC}}$	.719	.778	.747	.749	.763	.756
	$\mathfrak{C}^{T_{HP}}$	.707	.789	.745	.756	.718	.737		$\mathfrak{C}^{T_{HP}}$	.712	.777	.743	.757	.714	.735
GM	C	.705	.815	.756	.733	.807	.768	F_{NA}	C	.711	.806	.755	.738	.788	.762
	$\mathfrak{C}^{C_F}$	.709	.809	.756	.735	.804	.768		$\mathfrak{C}^{C_F}$	.713	.800	.754	.739	.786	.761
	$\mathfrak{C}^{O_B}$	.711	.798	.752	.742	.775	.758		$\mathfrak{C}^{O_B}$	.712	.793	.750	.747	.757	.752
	$\mathfrak{C}^{F_{BPC}}$	.693	.834	.757	.725	.832	.775		$\mathfrak{C}^{F_{BPC}}$	.702	.821	**.757**	.728	.820	.771
	$\mathfrak{C}^{T_{HP}}$	.703	.797	.747	.755	.723	.739		$\mathfrak{C}^{T_{HP}}$	.706	.790	.746	.756	.719	.737
HM	C	.707	.811	.756	.734	.806	.768	F_{NA2}	C	.706	.813	.756	.735	.794	.763
	$\mathfrak{C}^{C_F}$	.710	.807	.755	.735	.803	.768		$\mathfrak{C}^{C_F}$	.710	.807	.755	.736	.791	.762
	$\mathfrak{C}^{O_B}$	.711	.798	.752	.743	.775	.758		$\mathfrak{C}^{O_B}$	.711	.796	.751	.747	.759	.753
	$\mathfrak{C}^{F_{BPC}}$	.697	.828	.757	.724	.832	.774		$\mathfrak{C}^{F_{BPC}}$	.696	.831	.757	.726	.825	.772
	$\mathfrak{C}^{T_{HP}}$	.703	.796	.747	.755	.723	.739		$\mathfrak{C}^{T_{HP}}$	.705	.792	.746	.755	.719	.737
S_M	C	.693	.835	.757	.728	.816	.769								
	$\mathfrak{C}^{C_F}$	.696	.830	.757	.730	.813	.769								
	$\mathfrak{C}^{O_B}$	.703	.812	.754	.743	.775	.759								
	$\mathfrak{C}^{F_{BPC}}$	.680	.860	**.759**	.720	.843	**.776**								
	$\mathfrak{C}^{T_{HP}}$	.699	.803	.748	.755	.725	.739								

10.4 Chapter Conclusion

In this Chapter, we focused our attention on exploring the role played by fuzzy measures, particularly within the framework of the Choquet integral and its generalizations, focusing on the application to edge detection tasks. Our research was centred around applying the fuzzy power measure, considering both a scenario with a constant q value and two sliding window based adaptive approaches wherein the q value dynamically adjusts in response to the local characteristics of each pixel's neighbourhood.

In order to see the robustness of the different functions applied to the framework presented, our experimental setup included the application of Gaussian smoothing at two distinct levels of intensity. This aspect of our research aimed to shed light on how varying degrees of image smoothing might influence the performance of the adaptive q strategy in edge detection tasks.

The overall results show that the different functions perform well, but in a general way, the function that best adapts to all the situations is $\mathfrak{C}^{F_{BPC}}$.

In the next chapter, we will adopt Choquet integrals with RDFs. Since RDFs replace the subtraction operation in our integral, the idea is that these functions allow the method to respond in different ways to variations in contrast and illumination, depending on the choice of the different δ's (dissimilarity functions). A sliding-window strategy will also be employed, now associated with RDF-based functions for aggregating neighborhood values.

Throughout this chapter, we will investigate which integral achieved the best performance. Next, the results will be compared with one another in order to verify whether the best-performing methods differ significantly across the approaches considered. Finally, we will compare our results with the harmonic means obtained by other methods in the literature, highlighting, in terms of the balance between precision and recall, how the proposed method is positioned.

10.4.1 Publication

This chapter was published in the journal *Expert Systems* (MARCO-DETCHART et al., 2025).

11 EDGE DETECTION APPROACH BASED ON GENERALIZATIONS OF CHOQUET-LIKE INTEGRALS BY RESTRICTED DISSIMILARITY FUNCTIONS

In this chapter, we present a edge detection framework, which is based on the aggregation of local visual cues and employs different operators derived from variants of the Choquet integral with restricted dissimilarity functions (RDFs). We also describe our experimental framework. We then remark the dataset used in our evaluations, followed by the pre-processing pipeline and the proposed method for extracting local features. Next, we apply the operators defined in the Mathematical Foundations Chapter (see 4) to a sliding 3×3 window and provide an illustrative numerical example to demonstrate the per-pixel computation that yields the feature map. Finally, we briefly discuss how this map is converted into a binary edge image. A more detailed version of this chapter was published in (AMORIM et al., 2025).

11.1 Edge Detection Framework Proposed

In our experiments, we use images in the RGB space (see Section 5.3), normalized to $[0, 1]$, and smoothed using two alternative filters, the results of which are both reported in this study. The smoothing alternatives we use are Gaussian smoothing with a standard

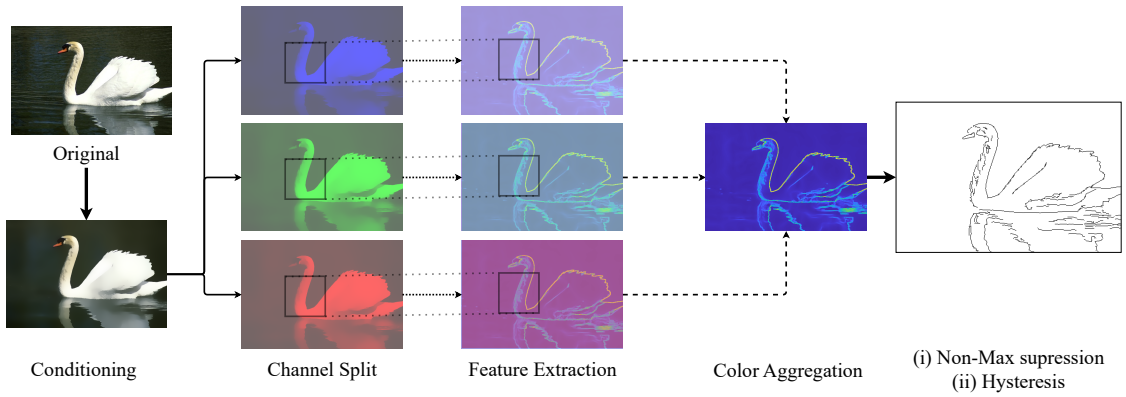


Figure 32: Methodology pipeline proposed for our work

deviation $\sigma = 2$ and Gravitational Smoothing (MARCO-DETCHART et al., 2018b), configured with 50 iterations, a gravitational constant $g = 0.05$, an interaction radius equal to 0.02 of the image diagonal, and Euclidean metrics in both color and position. The Gaussian filter provides a classical isotropic baseline, whereas the gravitational filter attenuates noise while better preserving high-contrast discontinuities. In accordance with our implementation, conversion to a single intensity map (grayscale-equivalent) occurs after per-channel feature extraction by fusing the channel-wise feature maps (e.g., via squared-sum, maximum, or mean). All subsequent stages (feature extraction, aggregation, and evaluation) are executed for both smoothing choices, enabling direct comparison of their impact on edge detection performance.

Classical edge features arise from viewing an image I as a function and computing local derivatives of I, typically via discrete masks that approximate the gradient ∇I (Prewitt, Sobel) (PREWITT, 1970; SOBEL; FELDMAN, 1973). Scale-aware schemes later dominated, most notably Gaussian/scale-space methods and the Canny edge detector (CANNY, 1986), together with ISEF smoothing (SHEN; CASTAN, 1992). In parallel, dissimilarity filters were proposed to measure local heterogeneity without explicit derivatives, from SUSAN (SMITH; BRADY, 1997) to the Compass operator of Ruzon and Tomasi, and its efficient reformulations used in BSDS-style pipelines (ARBELAEZ et al., 2011). Other influential operators, such as the Laplacian-of-Gaussian (LoG, "Mexican hat") (JR et al., 1988), rely on second–order differences and were motivated partly by early-vision evidence, while remaining difference-based in their mathematical form.

Rather than fixing a specific differential kernel (which implicitly aggregates neighborhood information through preset weights), we extract multi-directional, pairwise local cues by comparing each pixel to its neighbors and then fusing them with nonadditive, input-dependent weights. Concretely, we compute restricted dissimilarities on the ordered neighborhood samples and aggregate them with Choquet-family operators driven by a fuzzy measure. This design exposes the blending stage, which is central to our study while remaining robust to monotonic intensity transforms and avoiding sign ambiguities typical of finite differences.

On each conditioned image, along each pixel, we slide a window $W \in \mathbb{R}^{3\times 3}$ (stride 1). From every window, we build the ordered vector of intensities $\boldsymbol{x}_{(1)} \leq \cdots \leq \boldsymbol{x}_{(8)}$ (the center pixel is removed). The fuzzy weights $m_{(i)}$ follow the power measure. For an 8-connected neighborhood, we use:

$$m_{(1)} = 1, \qquad m_{(i)} = \left(\frac{9-i}{8}\right)^{q}, \;\; i = 2, \ldots, 8,$$

with $q = 0.1$. Between successive pairs $(x_{(i)}, x_{(i-1)})$, we compute the restricted dissimilarities δ_k, reported in Table 4. These dissimilarities feed into the aggregation step described next.

We adopt the power measure (Eq. 2) to parameterize the nonadditive weights because it offers a simple, monotonic, and tunable way to encode the increasing relevance of larger ordered contrasts while keeping the operator within $[0, 1]$. Prior studies that generalize Choquet-type integrals via restricted dissimilarities, such as the dC_F-integrals (WIECZYNSKI et al., 2023) and, more recently, the dCC-integrals (LUCCA et al., 2025), have reported competitive results in classification settings when coupling RDFs with the power measure. This pairing indicates that it provides a good balance between flexibility (through the exponent q) and stability in practice. We adopted a small q (here, $q = 0.1$) to gently downweight the tail of the ordered neighborhood while preserving sensitivity to the strongest local contrasts that are most informative for the boundary feature map.

With the vector of measures computed, we apply it to each pair (F, δ) that instantiates one of the three Choquet-type families introduced in the *Preliminaries*, whose combinations are listed in Tables 2 and 4, respectively. In notation, for example, the combination (F_{BPC}, δ_0) is written as $\mathfrak{C}^{F_{BPC}}_{\mathfrak{m},\,\delta_0}$. Applied to the 3×3 window, letting $A_{(i)}$ denote the index set associated with $x_{(i)}$ (so that $\mathfrak{m}_{(i)} = \mathfrak{m}(A_{(i)})$), and $\boldsymbol{x} \in [0, 1]^n$, the operators are given by the following equations.

d-CC (copula-based, expanded form). For a copula $C : [0, 1]^2 \to [0, 1]$ of Table 2,

$$\mathfrak{C}^{C}_{\delta,\mathfrak{m}}(\boldsymbol{x}) \;=\; x_{(1)} \;+\; \sum_{i=2}^{8} \delta\Big(C\big(x_{(i)}, \mathfrak{m}_{(i)}\big),\, C\big(x_{(i-1)}, \mathfrak{m}_{(i)}\big)\Big). \tag{23}$$

d-XC (expanded form with product).

$$\mathrm{X}\mathfrak{C}_{\delta,\mathfrak{m}}(\boldsymbol{x}) \;=\; x_{(1)} \;+\; \sum_{i=2}^{8} \delta\Big(x_{(i)}\,\mathfrak{m}_{(i)},\; x_{(i-1)}\,\mathfrak{m}_{(i)}\Big). \tag{24}$$

d-CF (CF-integral generalized by RDFs). For a bivariate function $F : [0, 1]^2 \to [0, 1]$ of Table 2,

$$\mathfrak{C}^{F}_{\mathfrak{m},\delta}(\boldsymbol{x}) \;=\; x_{(1)} \;+\; \sum_{i=2}^{8} F\Big(\delta\big(x_{(i)}, x_{(i-1)}\big),\; \mathfrak{m}_{(i)}\Big). \tag{25}$$

Figure 33 provides an illustrative single-window computation using $\mathfrak{C}^{F_{BPC}}_{\mathfrak{m},\,\delta_0}$. In our study, we evaluate several bivariate fusion operators and restricted dissimilarities; Here, we instantiate the pipeline with the bi-power copula $F_{BPC}(u, v) = u\,v^2$ solely to make the mechanics of the computation concrete. The eight neighbours of the central pixel are collected, sorted, and successive restricted dissimilarities $\delta_0(x_{(i)}, x_{(i-1)}) = |x_{(i)} - x_{(i-1)}|$ are paired with fuzzy weights from the power measure ($q = 0.1$). Each pair is combined via F_{BPC} and aggregated to yield a feature value; large contrast transitions amplified by the squared weights stand out as edges. Example 13 presents the computation for this 3×3 window using $\mathfrak{C}^{F_{BPC}}_{\mathfrak{m},\,\delta_0}$ to clarify how it operates.

0.10	0.85	0.90
0.12	(x, y)	0.88
0.11	0.14	0.13

$X = [0.10, 0.85, 0.90, 0.12, 0.88, 0.11, 0.14, 0.13]^\top$

$x_{(1:4)} = 0.10, 0.11, 0.12, 0.13$
$x_{(5:8)} = 0.14, 0.85, 0.88, 0.90$

Largest jump: $|x_{(6)} - x_{(5)}| = 0.71$

Figure 33: Illustrative single-window computation on a 3×3 neighbourhood and the computation example for this window.

Example 13 (Illustrative computation with $\mathfrak{C}_{\mathfrak{m},\,\delta_0}^{F_{BPC}}$)**.** *Consider the neighbourhood from* (x, y) *in Figure 33.*
The ordered vector be like.

$$(x_{(i)})_{i=1}^{8} = [\,0.10,\ 0.11,\ 0.12,\ 0.13,\ 0.14,\ 0.85,\ 0.88,\ 0.90\,].$$

Successive restricted dissimilarities ($\Delta_i = \delta_0(x_{(i)}, x_{(i-1)})$*).*

$$\Delta_i = [\,0.01,\ 0.01,\ 0.01,\ 0.01,\ 0.71,\ 0.03,\ 0.02\,], \quad i = 2, \ldots, 8.$$

Fuzzy weights from the power measure (q=0.1*) for the tail sets* $A_{(i)}$*.*

$$m_{(i)} = \left(\tfrac{9-i}{8}\right)^{0.1} \approx [\,0.987,\ 0.972,\ 0.954,\ 0.933,\ 0.907,\ 0.871,\ 0.812\,].$$

Squared weights used by the bi-power copula $F_{BPC}(u, v) = u\,v^2$*.*

$$m_{(i)}^2 \approx [\,0.974,\ 0.945,\ 0.909,\ 0.871,\ 0.823,\ 0.759,\ 0.659\,].$$

Recording the form of the Choquet Integral instantiated with F_{BPC}*:*

$$\mathfrak{C}_{\mathfrak{m},\,\delta_0}^{F_{BPC}}(\mathbf{x}) = \sum_{i=2}^{8} \delta_0(x_{(i)}, x_{(i-1)})\,[m_{(i)}]^2,$$

So the term-by-term contributions are:

i	2	3	4	5	6	7	8
Δ_i	0.01	0.01	0.01	0.01	0.71	0.03	0.02
$m_{(i)}^2$	0.974	0.945	0.909	0.871	0.823	0.759	0.659
$\Delta_i\, m_{(i)}^2$	0.00974	0.00945	0.00909	0.00871	**0.584**	0.0228	0.0132

Final feature map for that point $F_{BPC}(\Delta_i, m_{(i)}) = \Delta_i\, m_{(i)}^2$.:

$$\mathfrak{C}_{\mathfrak{m},\,\delta_0}^{F_{BPC}}(\mathbf{x}) \approx 0.657.$$

The feature map is dominated by the large transition $\Delta_6 = 0.71$ *between the low-intensity group* $[0.10–0.14]$ *and the high-intensity group* $[0.85–0.90]$*, amplified by the squared fuzzy weight.*

As previously mentioned, after the fusion of the neighborhood, which produces a feature map for each channel of the image, each pixel p is combined according to the functions listed in Table 19. In other words, given feature maps $F_1, \ldots, F_C : [0,1]^{H \times W} \to [0,1]$, we obtain a single fused map by applying the chosen function to the channelwise values at p.

Table 19: Channel-fusion formulas organized for reference.

Name	**Formula**
Squared–sum (Euclidean magnitude)	$F_{\mathrm{SqSum}}(p) = \sqrt{\sum_{c=1}^{C} \big(F_c(p)\big)^2}.$
Maximum	$F_{\max}(p) = \max_{1 \le c \le C} F_c(p).$
Mean (arithmetic average)	$F_{\mathrm{mean}}(p) = \frac{1}{C} \sum_{c=1}^{C} F_c(p).$

Given the feature map $S \in [0,1]$, we apply a power-law enhancement S^p with $p = 0.35$ to emphasize strong responses. Local orientations are then computed (channel-wise feature-orientation estimation), and non-maximum suppression is performed in the corresponding normal direction (CANNY, 1986). The resulting sparse map is binarized using the adaptive unimodal Rosin threshold; light median filtering, followed by the removal of short segments, produces the final binary edge map B.

11.2 Quantitative Evaluation

In this section, we present the quantitative evaluation procedure for our experiments. We begin by introducing the metrics adopted to validate the proposed model. Next, we detail the paired statistical analysis methodology used to identify the best operator across the combinations of parameters. Finally, we outline the descriptive evaluation protocol, comparing, within the limitations of our experiments, our results with those reported for the same edge detection task on the same dataset using distinct methods, including both trained and training-free approaches, some of which employ aggregation and pre-aggregation functions in their frameworks. We report the results in terms of the F-measure.

11.2.1 Quantitative evaluation

Each detected edge map B is evaluated on the BSDS protocol by matching it against all human annotations using the displacement-tolerant correspondence of Estrada and Jep-

son (ESTRADA; JEPSON, 2009), with spatial tolerance set to the 2.5% of the image diagonal. From the resulting correspondence, we compute Precision and Recall and summarize performance with the weighted F-measure F_α (as in (LOPEZ-MOLINA; De Baets; BUSTINCE, 2013)): Following common BSDS practice, we adopt $\alpha = 0.5$ ($F_{0.5}$). For each image, we retain the triplet $(\mathrm{Prec}, \mathrm{Rec}, F_{0.5})$ from the ground-truth map that yields the highest $F_{0.5}$; we then aggregate results over the 200-image test split (e.g., mean $\overline{F}$ and median $\mathrm{med}(F)$).

To identify the best operator across parameter combinations, we adopt the following paired-design analysis. For each image i and each function j, we observe $F_{i,j}$ and assemble the matrix $\mathbf{F} \in \mathbb{R}^{200\times K}$. Images act as *blocks* (controlling intrinsic variability) and functions as *treatments*. The global goal is to assess whether the functions differ in the distribution of F (conditional on blocks). The null hypothesis, H_0 (omnibus), states that all functions share the same distribution of F (DEMŠAR, 2006). The alternative hypothesis, H_1, asserts that at least one function differs.

To formally evaluate these hypotheses, we apply the Friedman test to $\mathbf{F}$ (treatments = functions; blocks = images) This rank-based test is a non-parametric equivalent of the repeated-measures ANOVA (DEMŠAR, 2006). and is suitable for this design as it does not assume normality of distributions (DEMŠAR, 2006). The reference is the function with the highest median of F; ties are broken by the highest mean.

While the Friedman test can identify the presence of significant differences, it does not specify which pairs of functions differ. For this, post-hoc tests are required. Following the omnibus test, we compare the reference against every competitor using the paired Wilcoxon (signed-rank) test, one-sided (DEMŠAR, 2006):

$$H_0 : \tilde{F}_{\mathrm{ref}} = \tilde{F}_{\mathrm{comp}}, \qquad H_1 : \tilde{F}_{\mathrm{ref}} > \tilde{F}_{\mathrm{comp}}.$$

Our choice to use the Wilcoxon test for pairwise comparisons, instead of post-hoc tests based on mean ranks (e.g., Nemenyi test), is deliberate. As pointed out by Jia, Liu e Zhang (2025), rank-based post-hoc tests can lead to counter-intuitive conclusions, as their results depend on the entire set of competing algorithms and not just on the pair being compared. The Wilcoxon test avoids this issue, providing a more direct and robust comparison between two functions (JIA; LIU; ZHANG, 2025). Family-wise error is controlled via Holm–Bonferroni at $\alpha = 0.05$, a procedure recommended for its power over the standard Bonferroni correction (DEMŠAR, 2006). As an effect-size summary, we report paired Cohen's d on differences $\Delta_i = F_{\mathrm{ref},i} - F_{\mathrm{comp},i}$, i.e., $d = \overline{\Delta}/s_\Delta$.

This pipeline is applied without modification under both smoothing conditions and images (blocks) are assumed independent. The Friedman–Wilcoxon path avoids normality assumptions and is stable under skewness and outliers (DEMŠAR, 2006). In order to prevent an overinterpretation of small differences in the F values that are not statis-

tically robust, two complementary perspectives are useful. The first perspective consists in considering the absolute ranking of the functions according to their F values, summarized both by mean and by median. The second perspective relies on statistical tests to determine whether a function can be regarded as significantly inferior to the reference (Holm-adjusted $p < 0.05$) or whether it remains statistically indistinguishable. This reduce the risk of attributing importance to differences in F that may arise merely from random variation.

11.2.2 External comparative evaluation

This subsection summarises how external, literature-based comparisons were documented; All inferential statistics in this Chapter are restricted to within-family comparisons among our variants, that is, external numbers are descriptive only. Our target metric is the F-score, as pointed before, rather than analysing precision and recall separately

- **Datasets and splits.** We restricted comparisons to the official test set and adhered to the dataset's standard evaluation partitioning.

- **Evaluation protocol and operating points.** We followed the boundary matching by Estrada-Jepson with a 2.5% diagonal tolerance and summarised performance with the F-measure. In line with common practice on BSDS500, external baselines that reported best-F from PR curves (obtained by threshold sweeping, often across multiple scales) were recorded as such. By contrast, our method was evaluated primarily in a training-free, single-scale configuration with a fixed hysteresis threshold. When informative, we additionally reported our own best-F under a controlled threshold sweep as an exploratory operating point (clearly labelled), distinct from the fixed setting and not used for statistical testing. No performance figures are disclosed here.

- **Smoothing and pre/post-processing alignment.** When prior work provided multiple smoothing or pre-processing options, we selected the configuration most comparable to ours. For instance, when a study included Gaussian columns (e.g., S_2, $\sigma = 2$), we aligned to that configuration for our Gaussian setting. Results under our Gravitational smoothing are reported for context but are not used to claim superiority over baselines restricted to Gaussian-only settings unless explicitly aligned.

- **Scope of comparison (aggregation-first).** On each dataset we prioritised papers that employed aggregation functions under the same dataset and protocol (e.g., the Sliding-Window Adaptive Fuzzy Measure framework (MARCO-DETCHART et al., 2025)), and complemented them with widely cited baselines and learning-based methods when available, such as RCF (LIU et al., 2019), DDS (LIU et al., 2021), COB (MANINIS et al., 2017), HED (XIE; TU, 2017), HFL (BERTASIUS; SHI;

TORRESANI, 2015b), DeepContour (SHEN et al., 2015), DeepEdge (BERTASIUS; SHI; TORRESANI, 2015a), OEF (HALLMAN; FOWLKES, 2015), MCG (PONT-TUSET et al., 2016), SE (DOLLÁR; ZITNICK, 2013), gPb-UCM (ARBELAEZ et al., 2011), ISCRA (REN; SHAKHNAROVICH, 2013), DEL (LIU et al., 2018), Pb (MARTIN; FOWLKES; MALIK, 2004), BEL (DOLLAR; TU; BELONGIE, 2006), HFS (CHENG et al., 2016), NCut (SHI; MALIK, 2000), EGB (FELZENSZWALB; HUTTENLOCHER, 2004), Canny (CANNY, 1986), MShift (COMANICIU; MEER, 2002), Sobel (SOBEL, 1972), and Roberts (ROBERTS, 1963). Only methods evaluated on the same dataset and compatible protocol were included in the comparison tables. These external numbers serve descriptive positioning only; no hypothesis testing is performed against them.

- **Extraction of external figures.** When prior work provided PR curves but no tabulated numbers, we read the best-F directly from official plots or benchmark materials. If a paper reported a single F value without specification, we treated it as best-F (threshold-swept) unless stated otherwise. All sources and the precise settings/columns used were cited.

- **Interpretation and caveats.** We documented boundary thinning, non-maximum suppression, and other minor post-processing choices whenever they could affect cross-paper comparability. To mitigate discrepancies, we aligned smoothing and matching as described above, recorded the exact settings for each baseline, and emphasised effect sizes over marginal decimal differences. Importantly, because many competing methods were trained and selected their operating points via multi-scale threshold sweeping, their best-F values represent an optimistic envelope; our primary single-scale figures were interpreted conservatively in the Results section, and no inferential claims are made against external methods.

11.3 Results And Discussion

We evaluate K fusion operators on the BSDS500 test split ($n = 200$ images). Each operator is specified by a pair $\langle F, \delta \rangle$ (a bivariate kernel F and a restricted dissimilarity δ), used together with the fuzzy measure $\mathfrak{m}$ (in our experiments, the power measure $\mathfrak{m}_{PM}$ with the stated value of q). For every image, the automatically detected boundary map is matched against all human annotations using the EjBCM procedure, and we keep the largest $F_{0.5}$ ("best match") per image. Table 20 reports, for each smoothing scenario, the best-performing operators according to two complementary criteria. Firstly, the highest median of $F_{0.5}$ across the 200 images (robust summary), and secondly, the highest mean of $F_{0.5}$ (absolute performance).

We observe a consistent gain with gravitational smoothing: the best medians and me-

Table 20: Best operators per scenario and criterion (mean/median of F over $n = 200$ images), using the notation adopted in the chapters for functions, measures, and dissimilarities.

Smoothing	Criterion	Function	Color Aggregation	$\overline{F}$	$\mathrm{med}(F)$
Gaussian	Best-by-median	$\mathfrak{C}^{T_M}_{\delta_4,\mathfrak{m}}$	F_{mean}	0.663	0.673
Gaussian	Best-by-mean	$\mathfrak{C}^{T_M}_{\delta_5,\mathfrak{m}}$	F_{mean}	0.672	0.668
Gravitational	Best-by-median	$\mathfrak{C}^{C_F}_{\delta_0,\mathfrak{m}}$	F_{SqSum}	0.740	0.774
Gravitational	Best-by-mean	$\mathfrak{C}^{F_{BPC}}_{\delta_0,\mathfrak{m}}$	F_{SqSum}	0.741	0.768

ans of $F_{0.5}$ exceed those obtained with Gaussian smoothing. In both settings, the power measure $\mathfrak{m}_{PM}(q = 0.1)$ repeatedly appears among the top configurations. Under Gaussian smoothing, the t-norm T_M (minimum) combined with dissimilarities based on quadratic or square–rooted differences—namely $\delta_4 = |x^2 - y^2|$ and $\delta_5 = (\sqrt{x} - \sqrt{y})^2$—is particularly competitive. Under gravitational smoothing, the kernels C_F and F_{BPC} paired with $\delta_0 = |x - y|$ yield the best results. Figure 34 illustrates the visual difference between the best Gaussian and Gravitational results.

11.3.1 Significance testing (paired design)

With image–wise paired measurements, we perform a nonparametric omnibus test followed by directed post hoc comparisons. Specifically, let $\mathbf{F} \in \mathbb{R}^{200\times K}$ collect, for each image (blocks) and each operator (treatments), the observed $F_{0.5}$. We first apply the Friedman test to assess the null hypothesis that all operators have the same distribution of $F_{0.5}$ conditional on the image. When the omnibus test is significant, we conduct one–sided Wilcoxon signed–rank comparisons between the reference operator (the one with the highest median $F_{0.5}$) and each competitor, testing. Family–wise error is controlled using the Holm adjustment at $\alpha = 0.05$. We report, for transparency, which operators are significantly inferior to the reference and which are statistically indistinguishable (ties), together with summary statistics (median/mean $F_{0.5}$) per operator.

- **Gaussian.** Friedman test with $p \approx 0$, indicating global differences across operators. Taking as reference the best-by-median configuration—T_M with the power measure $\mathfrak{m}_{PM}(q = 0.1)$ and $\delta_4 = |x^2 - y^2|$—out of 53 Holm-adjusted post hoc comparisons, 36 were significantly worse ($p_{\mathrm{Holm}} < 0.05$) and 17 were statistically indistinguishable (ties).

- **Gravitational.** Friedman test even more pronounced ($p \approx 0$). Using as reference the best-by-median configuration—C_F with the power measure $\mathfrak{m}_{PM}(q = 0.1)$ and $\delta_0 = |x - y|$—out of 117 comparisons, 112 were significantly worse ($p_{\mathrm{Holm}} < 0.05$) and 5 were ties.

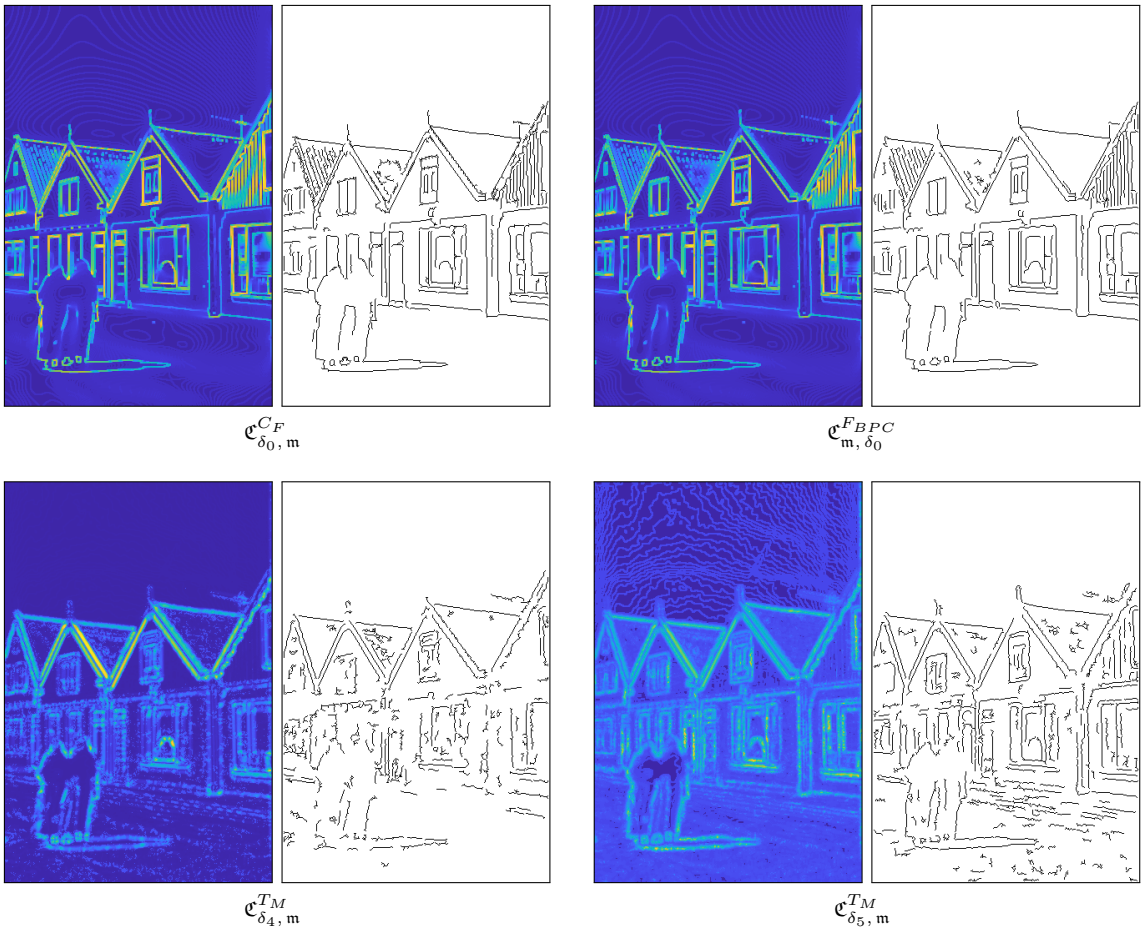


Figure 34: Four operator pairs on the house image. Each block shows feature (left) and edge (right). Top row: gravitational smoothing with C_F and F_{BPC} using $\delta_0 = |x - y|$. Bottom row: Gaussian smoothing with T_M using $\delta_4 = |x^2 - y^2|$ (left) and $\delta_5 = (\sqrt{x} - \sqrt{y})^2$ (right). All cases use the power measure $\mathfrak{m}_{PM}(q = 0.1)$.

These outcomes indicate that (i) there exists a top-tier core of statistically equivalent operators at the summit, and (ii) gravitational smoothing concentrates more mass at the top (fewer ties, more operators clearly inferior), suggesting a sharper separation between well- and poorly designed configurations. Notably, the agreement between the Top-10 ranked by mean and by median $F_{0.5}$ was moderate: under Gaussian smoothing the intersection comprised 5 operators, whereas under Gravitational smoothing it comprised 7 operators. The slight divergence is consistent with skewness/heavy tails in $F_{0.5}$ (the median is more robust), which supports using both summaries in tandem for interpretation.

11.3.2 External context

Although our method is training-free and evaluated under a single-scale configuration (fixed hysteresis threshold), it attains a median F-measure of 0.774 and a mean F-measure of 0.741. These benchmarks are provided solely to contextualize magnitude and should not be interpreted as inferential claims against learned baselines. Reported literature values for classical supervised methods (e.g., DeepContour (SHEN et al., 2015),

DeepEdge (BERTASIUS; SHI; TORRESANI, 2015a), HFL (BERTASIUS; SHI; TORRESANI, 2015b), ISCRA (REN; SHAKHNAROVICH, 2013)) and unsupervised baselines (e.g., gPb-UCM (ARBELAEZ et al., 2011), MCG (PONT-TUSET et al., 2016)) often reflect best-F obtained by threshold sweeping and, in many cases, multiscale settings. Likewise, recent deep approaches (e.g., RCF (LIU et al., 2019) and DDS (LIU et al., 2021)) report best-F values (around $F \approx 0.81$) under such protocols. In contrast, our evaluation uses a single fixed threshold (single-scale). Therefore, the numbers below are not directly comparable and are shown only as external context. All statistical testing in this paper is restricted to within-family comparisons among our variants.

Table 21 reflects best-F values reported for BSDS500, as read from PR curves and tables in (LIU et al., 2019; LIU et al., 2021; LIU et al., 2018; CHENG et al., 2016). These are descriptive references so no hypothesis testing is performed against them.

We provide external aggregation-based context by summarising two approaches from the literature that operate under the same BSDS500 protocol but do not rely on RDFs. Specifically, we consider the method of (MARCO-DETCHART et al., 2025), which fuses eight local intensity-difference cues via the Choquet integral and several of its generalisations, while adapting the power-measure parameter q per pixel from local intensity statistics and (MARCO-DETCHART et al., 2021), which aggregates multi-channel (colour/gradient) cues through alternative Choquet-based operators under the same Gaussian smoothing settings. Both works are aggregation-first and, therefore, methodologically close to our fusion perspective. The following summary is descriptive only so no hypothesis testing is performed against these external methods.

Table 22 provides this focused context on the S_2 smoothing column, reporting $F_{0.5}$. In the referenced works the S_2 column corresponds to results obtained with Gaussian smoothing using σ=2. We chose to compare against this subset because it aligns more closely with our pre-processing conditions. The left block lists representative top entries from Marco-Detchart et al. (2025) (predominantly variants of $\mathfrak{C}_m^{F_{BPC}}$); the middle block shows representative top entries extracted from Marco-Detchart et al. (2021) (including the classical baselines reported therein); and the right block presents our best single-scale, training-free configurations (fixed $q = 0.1$), separated by smoothing method (Gaussian vs. Gravitational) and by dissimilarity (e.g., $|x-y|$, $|x^2-y^2|$). This organisation makes three aspects explicit:

- We align like-for-like, that is the same dataset, the same S_2 smoothing column, and the same $F_{0.5}$ summary;
- We place aggregation-based methods side-by-side to highlight differences in the fusion operator rather than in training data or auxiliary cues;
- we retain a methodological caveat: literature entries typically report best-F obtained by threshold sweeping (often multiscale), whereas our primary figures are

Table 21: External context. Reported best-F values on BSDS500 from prior work (LIU et al., 2019; LIU et al., 2021; LIU et al., 2018; CHENG et al., 2016). Numbers are not directly comparable to our single-scale, fixed-threshold evaluation; no inferential claims are made against these methods.

Method	F	Reference
Human performance	0.803	–
RCF-ResNet101	0.819	Liu et al. (2019)
DDS	0.815	Liu et al. (2021)
RCF-ResNet50	0.814	Liu et al. (2019)
RCF-VGG16	0.811	Liu et al. (2019)
COB	0.793	Maninis et al. (2017)
HED	0.788	Xie e Tu (2017)
$\mathfrak{C}^{C}_{\delta_0,\,\mathfrak{m}}$ (ours, best median)	0.774	–
HFL	0.767	Bertasius, Shi e Torresani (2015b)
DeepContour	0.757	Shen et al. (2015)
DeepEdge	0.753	Bertasius, Shi e Torresani (2015a)
OEF	0.746	Hallman e Fowlkes (2015)
MCG	0.744	Pont-Tuset et al. (2016)
SE	0.743	Dollár e Zitnick (2013)
$\mathfrak{C}^{F_{BPC}}_{\mathfrak{m},\,\delta_0}$ (ours, best mean)	0.741	–
gPb-UCM	0.729	Arbelaez et al. (2011)
ISCRA	0.721	Ren e Shakhnarovich (2013)
DEL	0.703	Liu et al. (2018)
Pb	0.672	Martin, Fowlkes e Malik (2004)
BEL	0.651	Dollar, Tu e Belongie (2006)
HFS	0.650	Cheng et al. (2016)
NCut	0.634	Shi e Malik (2000)
EGB	0.614	Felzenszwalb e Huttenlocher (2004)
Canny	0.611	Canny (1986)
MShift	0.598	Comaniciu e Meer (2002)
Sobel	0.593	Sobel (1972)
Roberts	0.483	Roberts (1963)

computed at a fixed operating point (single-scale hysteresis threshold). Consequently, the table is intended solely as descriptive positioning; all inferential statistics in this Chapter are restricted to within-family comparisons among our variants.

11.3.3 Testing in the Unified Dataset for Edge Detection

To address generalization beyond BSDS500, we extended our evaluation to the Unified Dataset for Edge Detection (UDED) introduced with TEED (SORIA et al., 2023). UDED aggregates images from diverse sources, enabling cross-dataset testing under heterogeneous scenes, textures, and acquisition conditions.

UDED was created to streamline evaluation by selecting images from datasets focused

Table 22: External aggregation-based context on BSDS500 (S_2, reporting $F_{0.5}$ only). Left: representative top entries from Marco-Detchart et al. (2025); centre: representative top entries from Marco-Detchart et al. (2021); right: ours (fixed q=0.1, single–scale, fixed threshold). Descriptive only: values reproduced from prior work; not directly comparable to our single–scale evaluation; no hypothesis testing is performed against these methods.

Sliding-Window (MARCO-DETCHART et al., 2025)		
Method	**Description**	$\mathbf{F_{0.5}}$
$\mathfrak{C}_m^{F_{BPC}}$	block S_M (S_2)	.776
$\mathfrak{C}_m^{F_{BPC}}$	block GM (S_2)	.775
$\mathfrak{C}_m^{F_{BPC}}$	block AVG/HM (S_2)	.774
Neuro-Inspired (MARCO-DETCHART et al., 2021)		
Method	**Description**	$\mathbf{F_{0.5}}$
G_{S_M}	best classical (Table S_2)	.651
G_{S_P}	second best (S_2)	.642
Canny (σ=2)	reference (S_2)	.631
Ours (fixed $q = 0.1$)		
Method	**Description**	$\mathbf{F_{0.5}}$
$\mathfrak{C}_{\delta_0,\,m}^{C_F}$	Gravitational, $\lvert x-y\rvert$	0.774
$\mathfrak{C}_{m,\,\delta_0}^{F_{BPC}}$	Gravitational, $\lvert x-y\rvert$	0.741
$\mathfrak{C}_{\delta_4,\,m}^{C_{T_M}}$	Gaussian, $\lvert x^2-y^2\rvert$	0.674

on low- and mid-level tasks and carefully annotating perceptual edges. The proposed set contains 30 images drawn from the sources listed above, plus the classic cameraman image. The selection process computed the interquartile range (IQR) of intensity values for all candidate images; images larger than 720×720 were excluded. Images were then sorted by IQR, and 30 were uniformly chosen from the list, with roughly two per dataset, yielding statistical representativeness, by distribution, relative to the most commonly used edge-detection datasets.

Crucially, this dataset allows us to test our model across diverse real-world scenarios, extending the experiments to account for generalization to real-world conditions.

Table 23 shows the results of our investigation. We kept our single-scale, training-free protocol, reporting F-Measure for the best combination. As one can see, the FPBC variant with the gravitational dissimilarity ($|x-y|$) attains the highest mean $F_{0.5}$ on UDED (0.904), narrowly surpassing the CF variant with the same gravitational measure (0.903) and the FPBC variant with a Gaussian formulation (0.902).

In the benchmark reported by (SORIA et al., 2023), the best ODS (Best F-measure at a global scale) is achieved by TEEDup (0.834), followed by TEED (0.828), with other baselines ranging from 0.803 to 0.824 and Canny at 0.742. Importantly, the paper does

Table 23: Mean $F_{0.5}$ of the three best results for methods in UDED database and Optimal Dataset Scale (ODS) of the benchmark reported in (SORIA et al., 2023).

Method	**Description**	$F_{0.5}$
$\mathfrak{C}^{\mathrm{CF}}_{\delta_0,m}$	Gravitational, $\|x-y\|$ (Ours)	0.915
$\mathfrak{C}^{\mathrm{FPBC}}_{\delta_0,m}$	Gravitational, $\|x-y\|$(Ours)	0.904
$\mathfrak{C}^{\mathrm{FPBC}}_{\delta_0,m}$	Gaussian, $\|x-y\|(Ours)$	0.902
UDED database Benchmark (SORIA et al., 2023)		
Canny	—	0.742
DexiNed	—	0.815
PiDiNet	—	0.824
LDC	—	0.817
BDCN-B2	—	0.821
TIN	—	0.803
PiDiNet-small	—	0.821
PiDiNet-tiny-L	—	0.821
TEED	—	0.828
TEEDup	—	0.834

not state the diagonal-based tolerance used in the matching step to compute ODS; thus, exact one-to-one comparability is uncertain and we decided to compare our metrics with ODS, since our thresholding method also seeks an optimal threshold at a single scale. Adopting the BSDS convention and evaluating our outputs in parallel, we observe the same internal ranking of our variants and values that fall within the reported ODS range, while our best single-scale, training-free setting still attains the highest mean $F_{0.5}$ on UDED (0.904). Therefore, our findings remain competitive under a standardized protocol, though direct contrast with (SORIA et al., 2023) should be read with caution until the matching tolerance is explicitly fixed.

It can be observed that the UDED results are consistent with those obtained on BSDS500. UDED is proposed as a validation benchmark for general-purpose edge-detection methods. Accordingly, we can state that our methods may generalize across diverse real-world conditions and scenarios.

11.4 Chapter Conclusion

In this Chapter, we have analysed the problem of robust edge detection as a feature-fusion challenge: how to combine heterogeneous neighborhood-level cues (e.g., intensity and color contrasts) so that salient boundaries are preserved across illumination changes and local noise, without sacrificing the structural interactions among cues. Motivated by the limitations of using plain differences within classical aggregations, we applied Choquet-like integrals composed of RDFs. In this setting, the nonadditive measure captures inter-cue dependence, while the choice of dissimilarity controls contrast response; together, they provide a flexible operator to map multi-channel evidence into boundary

saliency.

Methodologically, we designed a single-scale, training-free pipeline. Each image was first smoothed (either Gaussian or Gravitational), local neighborhoods were ordered, and successive contrasts were aggregated by members of the d-Choquet family under a power-type fuzzy measure. The resulting feature maps were post-processed with non-maximum suppression and thresholding. We adhered to BSDS-style evaluation and targeted the harmonic mean of precision and recall (the F-score, with emphasis on $F_{0.5}$).

The empirical analysis indicates that the paired statistical tests support a clear performance gain when Gravitational smoothing is used as the preprocessing step, suggesting it was a decisive factor within our framework. In addition, external results reported in the literature provide numerical context for aggregation-first and learning-based approaches under the same dataset protocol; however, those values are not directly comparable to our single-scale, fixed-threshold setting and were not used for hypothesis testing. Taken together, the evidence indicates that composing Choquet-type operators with restricted dissimilarities is a promising direction for edge fusion and merits further analysis of component interactions and design choices.

To position our method relative to the state of the art, we compared our results with various trained and untrained models using the same dataset (BSDS500) and its standard evaluation protocol. Two of our best variants outperformed the classical methods, and one achieved performance comparable to some older supervised methods in the literature. We also compared our results with prior works that use functions or integrals from the Choquet family for edge detection, showing that our method attains a higher F-measure than standard baselines and remains competitive with approaches that employ adaptive measures, while our configuration uses a fixed parameter (q = 0.1).

To assess the generalization capacity of our models, we extended the experiments to UDED (SORIA et al., 2023), a dataset composed of a representative sample drawn from several well-established benchmarks in the edge-detection literature.

In the next chapter, we present the first pointwise edge detection method of this thesis. Unlike what has been discussed so far, we will not use neighborhood information. Instead, the information will be obtained across scale. This means that, for each image to be processed, a stack of feature maps subjected to different levels of conditioning will be produced. Each smoothing stage will generate a map capable of highlighting edges at different scales, which will ultimately be aggregated by means of our generalizations of the Choquet integral.

11.4.1 Publication

An extended and more detailed version of this chapter was published in (AMORIM et al., 2025).

12 MULTISCALE CHANNEL-MIXED EDGE DETECTION APPROACH BASED ON GENERALIZATIONS OF THE CHOQUET INTEGRAL

As seen in the introduction of this thesis (Chapter 1), recent advancements in feature fusion and edge detection have built upon a solid foundation laid in the early 21st century. Drawing inspiration from these advancements, this chapter proposes a multiscale channel-mixed edge detector based on modified and expanded Choquet pre-aggregation and aggregation functions. This method consists of multiple edge detections across different scales using a classic detector, such as Canny, and, unlike the methods previously presented in Chapters 10 and 11, is followed by a point-to-point aggregation of extracted features or visual cues. This multiscale approach mirrors the processing of visual information in the human retina and visual cortex, where neurons across different layers respond to stimuli of varying sizes and complexities (KANDEL; SCHWARTZ; JESSELL, 2000; BEAR; CONNORS; PARADISO, 2016).

Employing this pointwise method, analogous to the independent processing by cones in the retina, may allow for a more precise and detailed analysis of visual information that increases the robustness and adaptability of the system to different scenarios, significantly improving edge detection in complex images compared to methods that utilize a single level of analysis or a less discriminative approach (HUBEL; WIESEL, 1962a).

In addition to this introduction, the Chapter is organized as follows: the Methodology (Section 12.1) will present the entire model pipeline, as well as the evaluation steps and the results obtained. Subsequently, the Results (Section 12.2) will discuss the intermediate findings. Finally, the conclusions are presented in the Conclusion (Section 12.3).

12.1 Methodology

Our investigation utilizes the dataset presented in Chapter 5. Initially, each image in the RGB color space has its channels separated. Subsequently, each channel undergoes an initial conditioning through the application of Gaussian filtering with $\sigma_b = 2$, based on findings from Chapter 9. This chapter demonstrated that for the Canny detector, optimal

values predominantly fell below $\sigma_b = 2$, particularly for higher values of σ_c (the Canny parameter).

In the feature extraction stage, the aim was to capture simple indications of edges at each pixel, thereby emulating the receptive fields found in the retina. As previously noted, the Canny method was employed for edge detection (see Section 5.2). This method generates a feature map for the x and y directions, which ultimately form a feature map t for each channel. These are then stacked to compose a complete feature set.

This procedure is repeated over a range of σ_c values from 0 to 5 in the Canny parameter settings. The "Power measure"was varied from 0 to 1 in increments of 0.1. All these fused features create a stack of visual cues of edges at various scales, which are then aggregated point-by-point without considering a contextual window, as discussed in Chapter 10. Different aggregation functions are used for this purpose, including those from the standard Choquet families: CT-integrals, CF-integrals, and the extended: CC-integrals and CF_1F_2-integrals for $F1 = F2$ case. (refer to Section 4.1). Figure 35 illustrates the flow of the entire process.

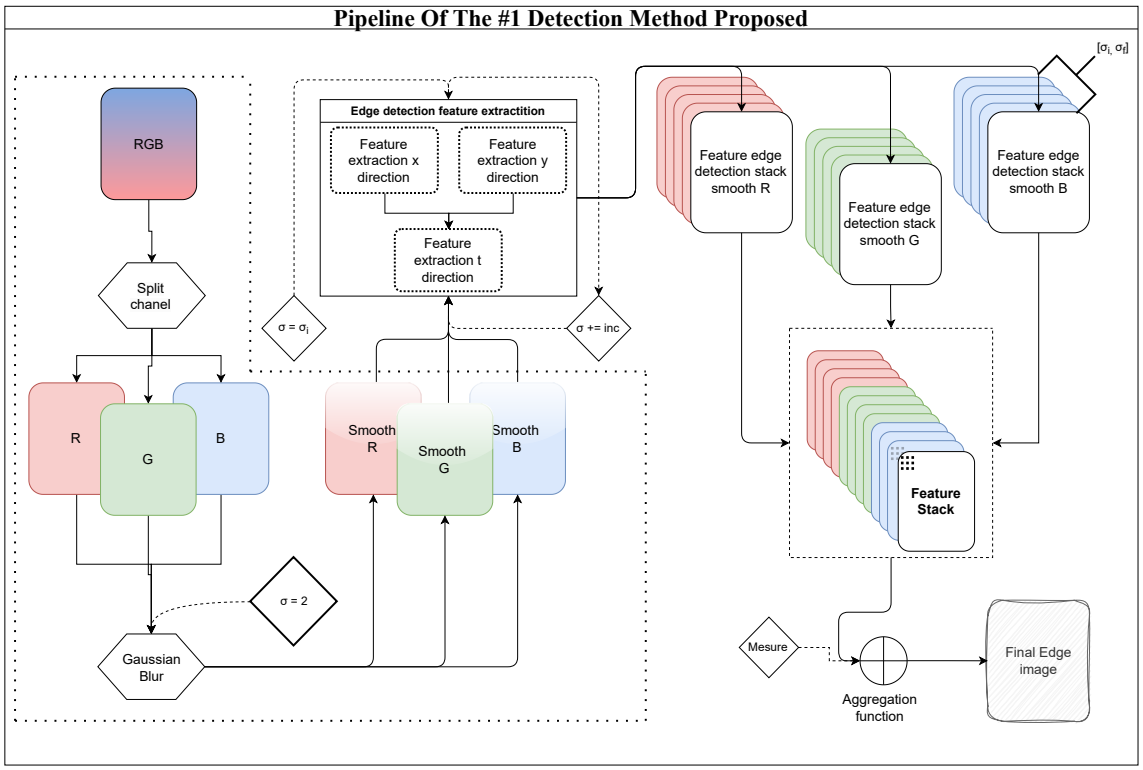


Figure 35: Multiscale channel mixed edge detection approach based on generalizations of choquet integral

After quantifying metrics such as precision, recall, and F-score derived from data processed using different parametric settings of the proposed edge detection method and comparing them with the classical Canny method, meticulous statistical analysis was conducted. The assessment involved checking for statistically significant differences between the last three parameters tested for each method. Initially, this function verifies the nor-

mality of the distributions of the metric values mentioned by employing the Shapiro-Wilk test for each of the last three parameters from both datasets. Depending on the results of the normality tests, the choice is made between the Student's t-test for normally distributed data or the Mann-Whitney U test for data exhibiting non-normal distributions.

Moreover, an analysis of the shapes of the data distributions is performed to investigate whether significant differences, in cases of non-normal distributions, might suggest not necessarily a rejection of the null hypothesis but a difference in the distribution's shape itself. This consideration is crucial, as the Mann-Whitney U test, unlike the t-test, does not assume a specific distribution and focuses on the difference between the samples' medians. Thus, a significant variation identified by this test may indicate not only shifts in central values but also variations in data dispersion or skewness. Therefore, it is imperative that, when interpreting the results, it is acknowledged that a rejection of the null hypothesis based on the Mann-Whitney U test may require further analysis concerning the shape of the distributions to ensure that conclusions regarding the performance of the methods are robust and not distorted by atypical data characteristics.

Consequently, the results provided establish a solid statistical foundation for determining which method demonstrates superiority under various conditions. If the differences between groups are statistically significant, this suggests that one method may consistently be more effective than the other in terms of edge detection accuracy, as measured by precision, recall, and F-score. This phase is crucial for validating the effectiveness of the proposed edge detection method relative to the traditional method and ensuring the reliability of the results obtained in the study.

The aggregations used in this experiment were Choquet in its various forms, as known from Section 4.1. The T-norms, copulas, and aggregation, pre-aggregation, and overlap functions employed in each Choquet integral are detailed in Table 2 (see Chapter 4)

The experimental evaluation in this chapter follows the consolidated methodology introduced in Section 5.3 and successfully applied in Chapters 9, 10, and 11. We maintain the treatment of edge detection as a binary classification task, adhering to the evaluation protocol proposed by Estrada and Jepson (ESTRADA; JEPSON, 2009).

As previously detailed, this protocol employs a pixel-by-pixel comparison between the generated edge maps and the ground truth. To ensure a balanced assessment that accounts for inherent localization challenges, we continue to utilize a spatial tolerance threshold of 2.5% of the image diagonal length to define True Positives (TP).Following the framework of Martin *et al.* (MARTIN; FOWLKES; MALIK, 2004) already established in our prior experiments (e.g., Chapter 10), the performance is quantified through the confusion matrix categories.

The efficacy of the proposed operators is assessed using the same fundamental metrics: Precision (20), Recall (21), and the $F_{0.5}$ measure (22). Consistent with the comparative standard of this thesis and the literature (MARTIN; FOWLKES; MALIK, 2004;

LOPEZ-MOLINA; De Baets; BUSTINCE, 2013), the $\mathrm{F}_{0.5}$ descriptor remains our primary metric for reporting and comparing the results.

12.2 Results

The metrics of Precision (P), Recall (R), and F-measure $(F_{0.5})$ were tabulated by grouping according to aggregation type and distinguished by the corresponding statistical measures, mean and median. The results from the CT-integral and CF-integral did not exhibit significant differences with respect to mean or median when compared to the methodology described in Chapter 10. Moreover, these methods did not demonstrate significantly superior performance compared to the classical Canny method (refer to Table 24). This observation suggests that while the advanced aggregation techniques incorporated in the CT-integral and CF-integral are capable of processing edge detection data effectively, they do not necessarily yield improvements over traditional methods under the conditions tested.

Table 24: Standard extensions results with individual Canny channel results

Function	$\bar{P}$	P_median	$\bar{R}$	R_median	$\bar{F}$	F_median	Channel
AVG	0.744	0.772	0.729	0.749	0.720	0.736	F
C_F	0.750	0.778	0.645	0.662	0.671	0.687	F
C_L	0.735	0.763	0.736	0.755	0.717	0.736	F
F_{BPC}	0.750	0.778	0.625	0.640	0.660	0.677	F
FIM	0.753	0.782	0.614	0.626	0.653	0.674	F
FIP	0.749	0.777	0.643	0.661	0.670	0.686	F
F_{NA}	0.738	0.765	0.715	0.734	0.706	0.725	F
F_{NA2}	0.744	0.774	0.671	0.685	0.683	0.698	F
F_{GL}	0.590	0.593	0.943	0.959	0.714	0.728	F
GM	0.678	0.690	0.823	0.850	0.724	0.744	F
HM	0.725	0.751	0.749	0.772	0.718	0.740	F
O_B	0.748	0.774	0.664	0.679	0.682	0.698	F
O_{Div}	0.746	0.773	0.681	0.698	0.691	0.708	F
O_{mM}	0.751	0.778	0.626	0.643	0.660	0.678	F
O_{RS}	0.710	0.729	0.743	0.760	0.704	0.723	F
T_{HP}	0.741	0.767	0.697	0.713	0.698	0.715	F
$T_{\text{Ł}}$	0.753	0.782	0.614	0.626	0.653	0.674	F
T_M	0.737	0.765	0.719	0.737	0.708	0.728	F
T_P	0.749	0.777	0.643	0.661	0.670	0.686	F
S	0.464	0.451	0.991	0.993	0.620	0.620	F
Canny R	0.742	0.776	0.716	0.731	0.711	0.733	R
Canny G	0.740	0.762	0.719	0.737	0.712	0.731	G
Canny B	0.747	0.787	0.695	0.704	0.701	0.724	B

In the course of our study on edge detection methods, we have generated visual repre-

sentations to elucidate the effectiveness of various edge detection algorithms as compared to a predefined ground truth. These visualizations are instrumental in providing a clear and intuitive understanding of how each algorithm performs in terms of detecting true edges, and distinguishing these from background noise or other non-edge elements.

The visual outputs, which can be visualized in Figure 36, were constructed using the following color-coded scheme to represent different outcomes in the detection process:

- True Positives are depicted in Green, indicating pixels that both the algorithm and the ground truth agree are edge locations.
- False Positives are shown in Red, representing pixels that the algorithm incorrectly identifies as edges, whereas the ground truth does not denote these as edge locations.
- False Negatives are colored in Yellow, highlighting edge locations according to the ground truth that the algorithm failed to detect.
- True Negatives are presented in White, marking the areas where both the algorithm and the ground truth concur on the absence of an edge.

By employing the Choquet Extensions over a σ range of [1.5, 2.5], we observed, at the 5% significance level, statistically significant differences in F-measure for both the AVG and GL functions when compared with the reference method (Canny). Since the normality assumption was rejected for all groups, the comparisons were performed using the Mann–Whitney U test, indicating that the central tendency of the distributions differs between the reference and these operators.

The inferential results indicate that the F_{GL} operator differed significantly from the reference method in all three aggregated metrics, namely $\bar{P}$ (precision), $\bar{R}$ (recall), and $\bar{F}$ (F-measure), although with distinct magnitudes.

For $\bar{P}$, the difference was statistically significant but negligible in practical terms ($r_{rb} = 0.027$), with F_{GL} showing a slightly lower median than the reference. For $\bar{R}$, the effect was markedly stronger ($r_{rb} = -0.351$), with F_{GL} presenting a higher median than the reference. For $\bar{F}$, the difference was also statistically significant ($p < 0.001$), with a small-to-moderate effect size ($r_{rb} = -0.189$) and a higher median for F_{GL}.

In contrast, it AVG did not differ significantly from the reference in $\bar{P}$ ($p = 0.832$), but it did show statistically significant differences in $\bar{R}$ and $\bar{F}$, although both with very small effect sizes ($r_{rb} = -0.060$ and $r_{rb} = -0.044$, respectively). Overall, these results suggest that F_{GL} yields the clearest gains relative to the reference, especially in recall and F-measure, whereas AVG produces more modest changes.

The descriptive results for $\bar{F}$ reinforce this interpretation. The F_{GL} operator achieved the highest central values among the compared groups, with mean $= 0.747$ and median



Figure 36: Comparative Visualization of Edge Detection Algorithms: This figure presents the evaluation results of various edge detection algorithms against a predefined ground truth. The images are color-coded to reflect the detection accuracy: Green for True Positives (correct edge detection), Red for False Positives (incorrectly identified edges), Yellow for False Negatives (missed true edges), and White for True Negatives (correct non-edge identification).

$= 0.771$, whereas AVG yielded intermediate values (mean $= 0.720$, median $= 0.736$) and the reference method presented the lowest ones (mean $= 0.711$, median $= 0.733$). All three groups exhibited negative skewness, with medians exceeding means, which is consistent with left-skewed distributions. In addition, F_{GL} showed slightly greater dispersion than the reference in terms of IQR, while AVG remained close to the reference. The number of outliers detected by the IQR criterion was substantially smaller for F_{GL} and AVG than for the reference, which suggests more concentrated empirical behavior in the tested samples. Taken together, these findings indicate that the improvement observed for F_{GL} in $\bar{F}$ is not merely associated with a shift in central tendency, but is also accompanied by a distributional profile consistent with stable performance. Tables 25 and 26 summarize these results.

Table 25: Descriptive summary of $\bar{F}$ (F-measure) for the reference method and the F_{GL} and AVG operators.

Group	n	Mean	Median	SD	IQR	Skewness	Kurtosis
Reference	200	0.711	0.733	0.125	0.167	-0.748	0.346
F_{GL}	200	0.747	0.771	0.126	0.172	-0.890	0.331
AVG	200	0.720	0.736	0.122	0.175	-0.753	0.154

Table 26: Inferential summary of the comparison between the reference method and the F_{GL} and AVG operators.

Operator	Variable	U	p-value	r_{rb}	Reference median	Operator median	Decision
F_{GL}	$\bar{P}$ (Precision)	24651410	0.043	0.027	0.776	0.761	Significant difference
F_{GL}	$\bar{R}$ (Recall)	15566365	< 0.001	-0.351	0.731	0.822	Significant difference
F_{GL}	$\bar{F}$ (F-measure)	19475220	< 0.001	-0.189	0.733	0.771	Significant difference
AVG	$\bar{P}$ (Precision)	23931750	0.832	-0.003	0.776	0.772	No significant difference
AVG	$\bar{R}$ (Recall)	22548400	< 0.001	-0.060	0.731	0.749	Significant difference
AVG	$\bar{F}$ (F-measure)	22953500	0.001	-0.044	0.733	0.736	Significant difference

The results for the CF-integrals, particularly for the GL case, demonstrate a substantial improvement over the sliding window method (see Table 27). They also indicate superiority to the classical method. Although the distributions are non-normal, the skewness and kurtosis values are relatively similar across groups, suggesting that the significant Mann-Whitney results are unlikely to be driven solely by substantial differences in tail behavior or distributional shape.

12.3 Chapter Conclusion

The proposed methodology, evaluated on the Berkeley Segmentation Dataset, showed a significant improvement over the best single-scale result, especially in the case of the CF-integrals. The best performance was achieved by F_{GL}, using a σ-variation range of $[1.5, 2.5]$. During the experiments, it was observed that excessively wide σ-variation

Table 27: Expanded extensions results

Function	$\bar{P}$	P_median	$\bar{R}$	R_median	$\bar{F}$	F_median	Channel
AVG	0.744	0.772	0.729	0.749	0.720	0.736	F
C_F	0.749	0.777	0.651	0.668	0.675	0.692	F
C_L	0.743	0.766	0.672	0.691	0.684	0.706	F
F_{BPC}	0.750	0.778	0.625	0.640	0.660	0.677	F
FIM	0.756	0.781	0.603	0.615	0.648	0.665	F
FIP	0.749	0.777	0.643	0.661	0.670	0.686	F
F_{NA}	0.740	0.765	0.666	0.683	0.678	0.694	F
F_{NA2}	0.746	0.772	0.643	0.664	0.668	0.684	F
F_{GL}	**0.735**	**0.761**	**0.793**	**0.822**	**0.747**	**0.771**	F
GM	0.747	0.774	0.673	0.689	0.687	0.703	F
HM	0.746	0.774	0.665	0.681	0.680	0.697	F
O_B	0.748	0.772	0.652	0.668	0.674	0.691	F
O_{Div}	0.749	0.774	0.648	0.666	0.672	0.690	F
O_{mM}	0.754	0.782	0.626	0.642	0.662	0.678	F
O_{RS}	0.749	0.777	0.642	0.659	0.669	0.684	F
T_{HP}	0.749	0.773	0.646	0.664	0.671	0.688	F
$T_{\text{Ł}}$	0.756	0.781	0.603	0.615	0.648	0.665	F
T_M	0.745	0.769	0.647	0.666	0.670	0.686	F
T_P	0.749	0.777	0.643	0.661	0.670	0.686	F
S	0.732	0.761	0.737	0.762	0.714	0.734	F

intervals tend to deteriorate the final metrics, since, although they incorporate a greater diversity of multiscale information, they also increase the amount of noise in the detection process.

Previous works, such as those by Lucca et al. (2018b) and Lucca et al. (2015), have shown that smaller values of the parameter q, used as the exponent in the *power measure*, tend to yield better results in classification problems, especially in contexts where the fuzzy measure values are learned, as proposed in (MARCO-DETCHART et al., 2025) (Chapter 10). In this sense, varying the exponent of the measure may constitute a promising strategy. On the other hand, certain choices of q may also increase sensitivity to noise and impair performance. Thus, in the context of edge detection, the use of smaller values for a fixed q, as well as the adoption of adaptive approaches, appears to be a more suitable path toward achieving better results.

In the next chapter, based on the experimental setup developed here and on the evidence obtained, an edge detection method is proposed that considers the chromatic information of the channels separately and uses a narrower range of σ values, since our preliminary experiments showed better results in this configuration, and expands the set of parameters and functions under analysis to obtain integrals such as $\mathfrak{C}_{\mathfrak{m}}^{F_1,F_2}$ (with $F1 \neq F2$), among others. In addition, the parameter q is fixed at a small value, in accordance with the evidence observed throughout this experimental stage.

13 MULTISCALE CHOQUET-BASED AGGREGATION APPROACH FOR EDGE DETECTION

As a continuation of the investigations initiated in Chapter 12, this chapter proposes a set of edge detections based on modified and expanded Choquet fusion, pre-aggregation, and aggregation functions. This method consists of multiple edge detections at different scales using gaussian filtering with sobel operators, followed by a pointwise aggregation of the extracted features or visual cues. This multiscale approach mirrors the processing of visual information in the human retina and visual cortex, where neurons in different layers respond to stimuli of varying sizes and complexities (KANDEL; SCHWARTZ; JESSELL, 2000; BEAR; CONNORS; PARADISO, 2016).

The fusion method using the modified Choquet integral emulates the human visual system's ability to effectively integrate information from multiple sources. This optimization may enhances the perception of contours and fine details under different lighting conditions and visual contexts (SCHWARTZ, 2010; KOLB; FERNANDEZ; NELSON, 2021). Following this introduction, the chapter is structured as follows: Section 13.1 introduces the New Choquet Multiscale - Edge detection Méthod, followed by Section 13.3, that presents and discusses the experimental results. Finally, Section 13.4 summarizes the main findings of this study. As pointed out in Chapter 5, we primally used the Berkeley Segmentation Dataset

13.1 Introducing the New Choquet Multiscale – Edge Detection (GMC-ED)

This section introduces our edge detection model based on multiscale aggregation, which utilizes a fuzzy measure and generalizations of the Choquet integral. We first provide a brief overview of the dataset used in the experiments, followed by a detailed description of the model's pipeline and the experimental framework.

13.1.1 Processing Step

Figure 37 presents a visual summary of our experimental workflow. The pipeline begins with input RGB images, which are first smoothed using Gaussian filters at multiple σ scales (sweeping a range of σ values $S \in [1.0, 2.25]$ with a step of 0.25) to generate gradient feature maps through Sobel operators (LOPEZ-MOLINA et al., 2011).

These maps are subsequently fused channel-wise and across scales using the proposed generalized Choquet-based aggregation operators, producing a single enhanced feature map that encodes multiscale edge evidence.

A power-law enhancement (For each pixel r in feature map $\mathcal{I} \in [0, 1]$, $S = r^p$ with $p = 0.35$) is then applied to emphasize strong edge responses, followed by non-maximum suppression along the local gradient orientation (CANNY, 1986). Finally, the binarized edge map is obtained through Rosin's Unimodal Thresholding (ROSIN, 2001).

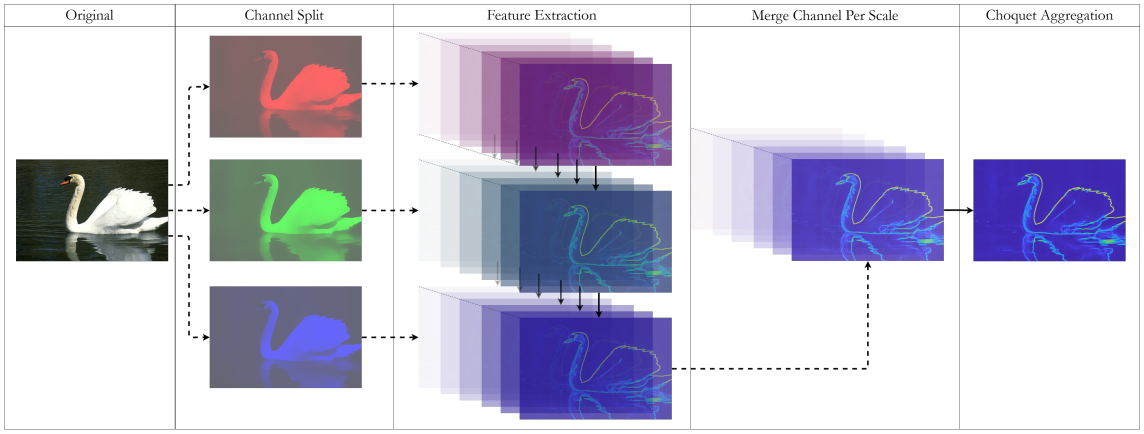


Figure 37: Overview of the full experimental pipeline, from Gaussian–Sobel gradient extraction to multiscale Choquet-based fusion

The channel-wise feature maps are fused within each scale to obtain a single gray-level map per scale, using three strategies, whose formulas are summarized in Table 19 (see chapter 11). Let S be the set of scales and let $F_c^{(s)}(p) \in [0, 1]$ denote the feature-map value at pixel p for channel $c \in \{R, G, B\}$ and scale $s \in S$.

$$\begin{aligned} G^{(s)}(p) &= \Phi\big(\{F_c^{(s)}(p)\}_{c\in\{R,G,B\}}\big), \\ \Phi &\in \{F_{\mathrm{SqSum}},\ F_{\max},\ F_{\mathrm{mean}}\}. \end{aligned} \tag{26}$$

Stacking $\{G^{(s)}\}_{s\in S}$ yields a multiscale volume which is then aggregated pointwise across scales. To this end, we evaluate the Cartesian product of nine integral families, with a catalog of 21 bivariate fusion functions (listed in Table 2). Denoting by $\mathcal{I}(p)$ the chosen integral parameterized by a bivariate function G from this catalog.

Let $\mathcal{A}$ be any aggregation operator such that

$$\mathcal{A} \in \left\{\mathfrak{C}_{\mathfrak{m}}, \mathfrak{C}_{\mathfrak{m}}^{F}, \mathfrak{C}_{\mathfrak{m}}^{C}, \mathfrak{C}_{\mathfrak{m}}^{F_1,F_2}\right\}, \tag{27}$$

and the final edge evidence at each pixel p is given by

$$\mathcal{I}(p) = \mathcal{A}\big(\{G^{(s)}(p)\}_{s\in S}\big).$$

which implements the local, pointwise aggregation of multiscale evidence regarding the presence of an edge at p.

As pointed by Lopez-Molina et al. (2011), when an image is progressively smoothed with increasing Gaussian standard deviation σ, the sharpness of tonal transitions diminishes, reducing gradient magnitudes and making inter-scale gradients not directly comparable. To address this, they introduce a compensation factor $Q(\sigma_1, \sigma_2)$ derived from the analysis of the step edge response under variable Gaussian smoothing, ensuring that gradients across scales become comparable. This observation supports our pixelwise multiscale aggregation strategy, since performing local fusion of gradients (or feature maps) at each pixel allows us to naturally integrate information from both coarse and fine scales while preserving relative relevance. The relevance of the inter-scale factor is visualized in Figure 38 .

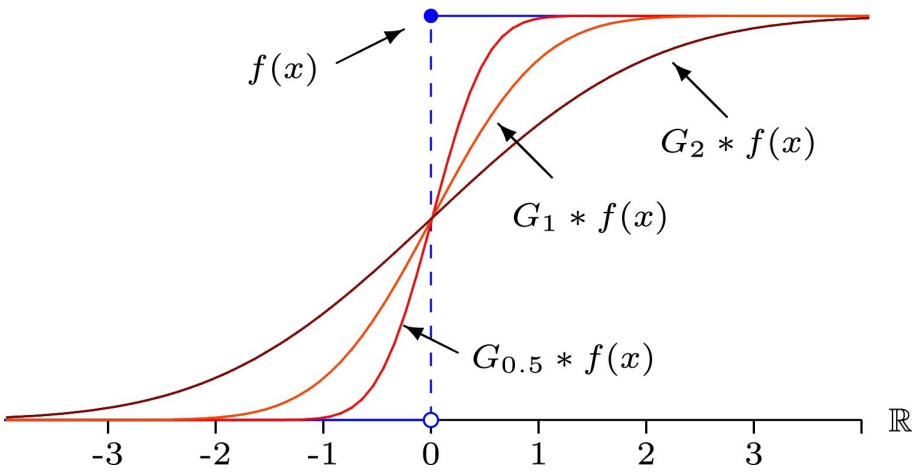


Figure 38: Step signal $f(x)$ with a discontinuity at x=0 and its responses after Gaussian smoothing, $G_\sigma * f(x)$ for $\sigma \in \{0.5, 1, 2\}$. Increasing σ progressively blurs the step, reducing gradient sharpness and making gradients across scales not directly comparable. As discussed by (LOPEZ-MOLINA et al., 2011), this motivates the use of a scale-compensation factor so that multiscale gradients can be fairly fused/compared—an idea aligned with our pixelwise multiscale aggregation strategy. (Figure adapted from (LOPEZ-MOLINA et al., 2011).)

At small scales (low σ), edges are crisp and well localized, which tends to increase true positives (TP) but also makes the detector more sensitive to noise, raising false positives (FP). As σ increases, Gaussian smoothing suppresses noise and reduces FP, but it also blurs/expands transitions, degrading localization and potentially missing fine details (lower TP). Our pixelwise multiscale aggregation reconciles these trade-offs by fusing fine-scale evidence (high TP) with coarse-scale robustness (low FP), thereby balancing

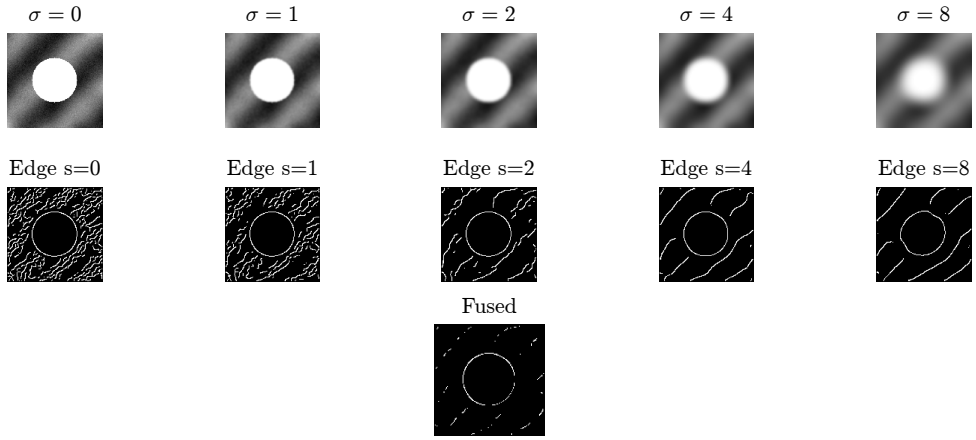


Figure 39: Multiscale edge behavior and fusion. *Top row:* Gaussian smoothing at $\sigma \in \{0, 1, 2, 4, 8\}$ progressively blurs tonal transitions. *Middle row:* per-scale edge maps (e.g., Canny/Sobel-based) show that small σ preserves sharp details but is noise-prone (higher FP), while large σ suppresses noise (lower FP) yet broadens contours and may miss fine structures (lower TP). *Bottom:* pixelwise multiscale fusion (example: $D\text{-}XCE$ with F_{NA} and F_{SqSum} color aggregation) combines both regimes, improving the precision–recall balance. See (LOPEZ-MOLINA et al., 2011) for the rationale behind inter-scale compensation.

precision and recall and yielding edge maps that remain stable across thresholds, fully aligned with the motivation in (LOPEZ-MOLINA et al., 2011). This is illustrated in Figure 39.

The unimodal thresholding method proposed by Rosin (ROSIN, 2001) addresses cases in which the image histogram lacks the usual bimodal structure required by classical thresholding techniques such as Otsu (OTSU, 1979). Instead of seeking two distinct peaks, the algorithm assumes a single dominant mode corresponding to the background (low–intensity class) and detects the transition toward a smaller, higher–intensity population. Let H_i denote the histogram bin at intensity i. The method draws a straight line between the histogram's main peak (x_s, y_s) and the end of the tail (x_f, y_f), defined as

$$\begin{aligned}(x_s, y_s) &= \left(\arg\max_i H_i,\ \max_i H_i\right), \\ (x_f, y_f) &= \left(\max\{i \mid H_i = 0 \wedge H_{i-1} \neq 0\},\ 0\right).\end{aligned} \tag{28}$$

The optimal threshold t^* is then the index that maximizes the perpendicular distance between each histogram point (i, H_i) and that line:

$$t^* = \arg\max_i \frac{|(y_f - y_s)i - (x_f - x_s)H_i + x_f y_s - y_f x_s|}{\sqrt{(y_f - y_s)^2 + (x_f - x_s)^2}} \tag{29}$$

Intuitively, this identifies the corner at the base of the main peak, which separates the dominant (background) class from the minority (foreground) class. Rosin demonstrated that this geometrical criterion is robust to noise and effective in edge detection, motion differencing, and segmentation tasks, particularly when histograms are strongly skewed

or nearly unimodal.

13.2 Experimental Framework

In accordance with the BSDS protocol, each detected edge image B is evaluated against all human annotations using the displacement-tolerant correspondence of Estrada and Jepson (ESTRADA; JEPSON, 2009), with the spatial tolerance set to 2.5% of the image diagonal.

From this correspondence, we obtain TP, FP, and FN and compute the evaluation metrics *precision*, *recall*, and the F*-measure*.

Following common BSDS practice, we adopt $\alpha = 0.5$ (i.e., $F_{0.5}$). For each image, we select the triplet $\big(\mathrm{Prec}, \mathrm{Rec}, F_{0.5}\big)$ associated with the ground-truth map that yields the largest $F_{0.5}$; results are then aggregated over the 200-image test set, reporting the mean $\overline{F}$ and the median $\mathrm{med}(F)$.

The edge extracted from the aggregated feature map using the aforementioned strategy represents an attempt to approximate the optimal result. This method is aligned with previous works involving applications of Choquet integrals in edge detection problems, enabling a direct comparison with the results reported by those authors.

In order to compare with other methods in the literature, either trained or not, that propose an edge detector using the same BSDS500 evaluation dataset, the final aggregated feature maps are used to extract edge maps at various thresholds, and performance is computed according to the benchmark protocol.

From this, we obtain values of P, R, and F for each threshold, for each image, and subsequently compute the quantitative summaries: ODS (Optimal Dataset Scale), OIS (Optimal Image Scale), and AP (Average Precision).

In practical terms, ODS corresponds to the highest F-score obtained over the entire dataset when using a single global threshold; OIS is the average of the best F_i values selected independently for each image (each with its own optimal threshold); and AP refers to the area under the precision–recall curve across the full recall range, providing a summary of performance that is independent of threshold selection.

These metrics allow us to represent the Precision vs. Recall (PR) curve and to perform a direct comparison with state-of-the-art methods under the same evaluation protocol.

The experiments were conducted over parameter combinations involving functions and extensions of the Choquet integral. For each of the 21 bivariate fusion functions (used as substitutes for the product in the integral's terms), we considered 4 integral variants and 3 strategies for fusing color channels.

In the future, alternative filters such as mean-shift or the gravitational filter (computationally more expensive) may be assessed within the same experimental framework (see Section 13.1). In total, 50.400 executions were produced for the 200 images in the

BSDS500 *test* set (ARBELAEZ et al., 2011), corresponding to 252 unique combinations per image ($21 \times 4 \times 3$).

At the end of the execution, we obtained precision, recall, and F-measure for each of the 252 methods, using a spatial tolerance of 2.5% of the image diagonal under the displacement-tolerant correspondence of Estrada and Jepson (ESTRADA; JEPSON, 2009) (Section 13.1).

13.3 Results and Discussion

In this section we present the results obtained in this Chapter; we discuss them and compare against benchmarks available in the literature, as well as against prior works that apply Choquet integrals to edge-detection problems (MARCO-DETCHART et al., 2023a; MARCO-DETCHART et al., 2023b; MARCO-DETCHART et al., 2021; MARCO-DETCHART et al., 2025).

As explained earlier, we propose two ways of extracting edges for comparison against the ground truth and for computing the evaluation metrics: one follows the methodology of previous Choquet-based works on edge detection, and the other adheres to the standard protocol used by BSDS500 benchmarks. In the first method, before binarization, we apply a power-law enhancement $\mathcal{I}^{p}$ with $p = 0.35$, followed by local orientation estimation in each channel, non-maximum suppression in the corresponding normal direction (CANNY, 1986), and adaptive binarization via Rosin's unimodal thresholding (ROSIN, 2001). A light median filtering and the removal of short segments then yield the final binary edge map B (see Section 13.1 for details).

From these per-threshold, per-image results, we compute, for each method, the performance statistics aggregated over the *test* set and sort them from highest to lowest F-measure. We report the top methods in Table 13.3 (see the formal definitions in Section 4 and Section 13.1).

According to Table 13.3, the two best results were obtained by $\mathfrak{C}_{\mathfrak{m}}^{F_{NA},F_{NA}}$ with color aggregation F_{SqSum} and by $\mathfrak{C}_{\mathfrak{m}}^{O_{RS},O_{RS}}$ with color aggregation $(F_{\max})$ The best-performing method shows a slight, simultaneous advantage in both precision and recall, which yields the highest $(\bar{F})$. To situate our results within the literature, we compare against studies that employ Choquet-type functions for edge-detection problems.

In (MARCO-DETCHART et al., 2021), the authors model the fusion of low-level edge cues (early-vision primitives) via generalizations of the Choquet integral, using different families of bivariate functions F (t-norms, overlaps, and copulas) to replace the product in the incremental terms.Their three best reported performances occur with gravitational smoothing (S3/S4), with $F_{0.5}$ around 0.658. As it can see in Table 29:

Table 28: Top 10 results of our method with different aggregation and color fusion strategies.

Method	**Color Aggregation**	$\bar{P}$	$\bar{R}$	$\bar{F}$
$\mathfrak{C}_{\mathfrak{m}}^{F_{NA},F_{NA}}$	F_{SqSum}	0.957	0.921	0.939
$\mathfrak{C}_{\mathfrak{m}}^{O_{RS},O_{RS}}$	$F_{\max}$	0.948	0.921	0.934
$\mathfrak{C}_{\mathfrak{m}}^{F_{GL},AVG}$	$F_{\max}$	0.983	0.879	0.928
$\mathfrak{C}_{\mathfrak{m}}^{F_{GL},AVG}$	F_{SqSum}	0.921	0.913	0.916
$\mathfrak{C}_{\mathfrak{m}}^{C_F}$	F_{mean}	0.883	0.946	0.913
$\mathfrak{C}_{\mathfrak{m}}^{C_L}$	$F_{\max}$	0.929	0.895	0.912
$\mathfrak{C}_{\mathfrak{m}}^{T_M}$	F_{SqSum}	0.858	0.972	0.911
$\mathfrak{C}_{\mathfrak{m}}^{AVG,AVG}$	F_{SqSum}	0.890	0.929	0.909
$\mathfrak{C}_{\mathfrak{m}}^{O_{mM},O_{mM}}$	F_{SqSum}	0.966	0.847	0.902
$\mathfrak{C}_{\mathfrak{m}}^{O_{mM},O_{mM}}$	F_{mean}	0.847	0.949	0.895

Table 29: Top configurations and their performance metrics

Configuration	**Prec**	**Rec**	$\boldsymbol{F_{0.5}}$
$\mathfrak{C}_{p=0.8}^{C_F}$	0.623	0.744	0.658
$\mathfrak{C}_{p=0.4}^{F_{BPC}}$	0.618	0.747	0.658
$\mathfrak{C}_{p=1}^{O_B}$	0.615	0.745	0.657

In (MARCO-DETCHART et al., 2025), the proposal differs by *locally* learning the fuzzy measure with a 3×3 sliding window: for each neighborhood, (pre)-aggregators (e.g., F_{GL}, AVG, SM, etc.) synthesize intensity differences to estimate the exponent q of the *power measure*, which then parametrizes generalized Choquet-type integrals (e.g., $\mathfrak{C}_{\mathfrak{m}}^{F}$, $\mathfrak{C}_{\mathfrak{m}}^{T}$). In this adaptive setting, the three best BSDS500 results reach $F_{0.5} \approx 0.72$. See Table 30.

Table 30: Top configurations and their performance metrics

Configuration	**Prec**	**Rec**	$\boldsymbol{F_{0.5}}$
$\mathfrak{C}_{F_{NA}}^{F_{BPC}}$	0.702	0.821	0.757
$\mathfrak{C}_{S_M}^{T_{HP}}$	0.680	0.860	0.759
$\mathfrak{C}_{S_M}^{T_{HP}}$	0.720	0.843	0.776

Using a multiscale fusion paradigm, Lopez-Molina et al. (2011) propose self-adapting ordered–weighted gradient fusion operators that combine gradient maps across Gaussian scales to form a single multiscale edge map. The method analyzes gradient behavior in Gaussian scale–space and fuses per–scale gradients with data–dependent weight vectors

$(h_1, \ldots, h_6)$ that emphasize strongest responses or balance precision–recall trade–offs. Their multiscale fusion attains a peak $F_{0.5}$ comparable to the best monoscale setting, but, crucially, sustains near–peak performance over a much broader range of scales; the best configurations are those privileging the largest gradients (h_1/h_2) and the more balanced vectors (h_3/h_4).

Moreover, when evaluation uses the displacement–sensitive Symmetric Distance (SD_k), the multiscale fusion clearly surpasses the monoscale baseline by correcting edge shifts induced at larger (σ). These findings jointly indicate that the two strongest setups in (LOPEZ-MOLINA et al., 2011) are the multiscale (h_1/h_2), highest recall at similar precision, and the balanced (h_3/h_4), best compromise, which deliver the top $(F_{0.5})$-level performance while improving geometric fidelity under (SD_k).

A visual inspection of Fig. 8 in Lopez-Molina et al. (2011), reveals that the peak $(F_{0.5})$ per weight vector lies approximately in the following bands at the canonical (2.5%) diagonal tolerance with the best performance typically around (h_3/h_4), as it can see in Table 31:

Table 31: Approximate $(F_{0.5})$ ranges of h_i

$(F_{0.5})$ **Range**
$h_1 \approx 0.66$–0.69
$h_2 \approx 0.67$–0.70
$h_3 \approx 0.70$–0.73
$h_4 \approx 0.69$–0.72
$h_5 \approx 0.63$–0.66
$h_6 \approx 0.62$–0.65

Our best configurations surpass the above $(F_{0.5})$ bands by a clear margin (cf. our top results reported in Table 13.3), reinforcing that the proposed Choquet-based multiscale fusion achieves stronger precision–recall trade–offs than the self-adapting **OWA** scheme of Lopez-Molina et al. (2011).

Figure 40 visually compares edge–continuity in our two best methods and shows that the variant $\mathfrak{C}_{\mathfrak{m}}^{F_{NA},F_{NA}}$ yields longer, more cohesive contours with fewer breaks and "holes," especially along fine structures (e.g., antlers and the animal's back within the red ROI). While $\mathfrak{C}_{\mathfrak{m}}^{O_{RS},O_{RS}}$ tends to emphasize strong local gradients, it fragments segments under high–frequency background textures (producing interruptions and short stray strokes). In contrast, the F_{NA}–based operator smooths inter–scale and inter–channel discrepancies, penalizes isolated responses, and reinforces continuity along consistent gradient directions. As a result, the F_{NA} method adheres more faithfully to the annotated contour topology (fewer micro–gaps and halos), preserving the principal strokes with higher connectivity and fewer spurious fragments.

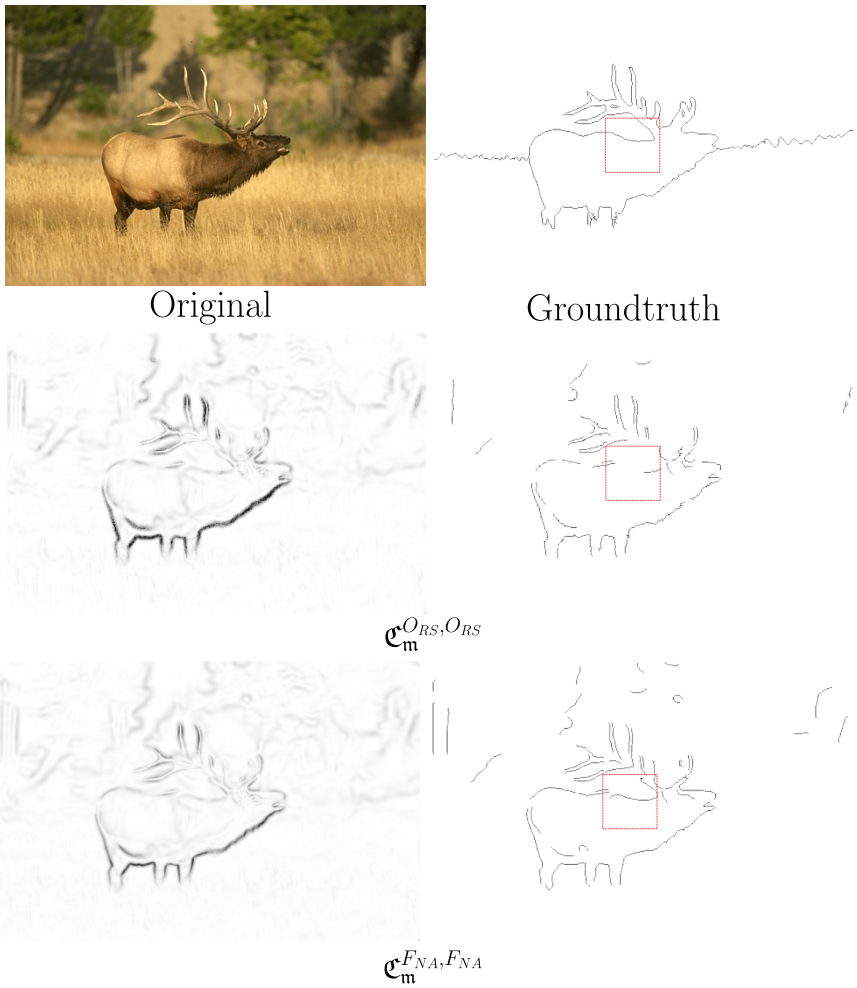


Figure 40: Visual comparison of edge continuity between our two best methods. Top: original image and one ground–truth map. Middle: response of $\mathfrak{C}_{\mathfrak{m}}^{O_{RS},O_{RS}}$. Bottom: response of $\mathfrak{C}_{\mathfrak{m}}^{F_{NA},F_{NA}}$. The red ROI highlights regions where $\mathfrak{C}_{\mathfrak{m}}^{F_{NA},F_{NA}}$ exhibits longer, more connected contours with fewer breaks.

The second evaluation protocol proposed in our methodology was designed to enable a fairer comparison with other edge–detection models that use the standard BSDS500 metrics: ODS, OIS, and AP. This procedure consists of extracting binary edge maps from the aggregated feature maps at multiple thresholds for all test images, restricted to the best-performing methods previously ranked, and computing the corresponding *Precision–Recall* curves. From these, we obtain the quantitative indicators ODS, OIS, and AP, which are used for direct comparison with classic benchmarks. Figure 41 illustrates the comparison of our best-performing using this evaluation method, $\mathfrak{C}_{\mathfrak{m}}^{O_{RS},O_{RS}}$, against traditional detectors using the aforementioned metrics.

Notice that our best-performing method under the alternative evaluation protocol was $\mathfrak{C}_{\mathfrak{m}}^{F_{NA},F_{NA}}$. However, when evaluated using the ODS, OIS, and AP metrics, $\mathfrak{C}_{\mathfrak{m}}^{O_{RS},O_{RS}}$ ranks first, while $\mathfrak{C}_{\mathfrak{m}}^{F_{NA},F_{NA}}$ takes second place.

As shown in Figure 41 and resumed in Table 32, our best method (*GMC-ED#1*) subs-

tantially surpasses the classical edge detectors in both precision and recall across the full threshold range.While the Roberts and Sobel operators exhibit limited consistency due to their sensitivity to noise and lack of multiscale adaptability, the Canny detector achieves a stronger balance.

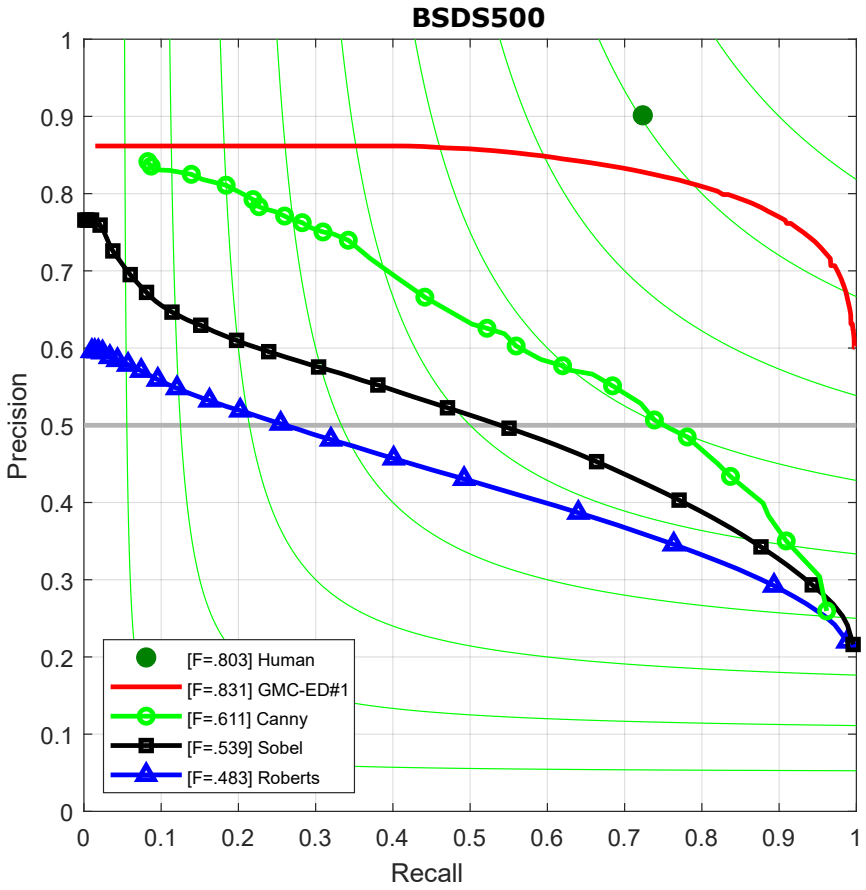


Figure 41: PR curve for the $\mathfrak{C}_{\mathfrak{m}}^{O_{RS},O_{RS}}$

To situate our untrained multiscale Choquet–based fusion within the recent edge-detection literature, we also contrast it with trained deep models evaluated on BSDS500 under the standard ODS/OIS protocol. Using our best configuration $\mathfrak{C}_{\mathfrak{m}}^{O_{RS},O_{RS}}$ with F_{SqSum}, we obtain ODS=0.831, OIS=0.866, and AP=0.827. By comparison, (BAO et al., 2023) (a lightweight CNN with pixel-difference convolutions and multiscale-aware fusion) reports ODS=0.818; (LIU et al., 2025) (CPD-Net, a U-shaped network with cycle pixel-difference convolutions) achieves ODS(S)=0.775 under S-Eval; and (GAO, 2025) (ML-EdgeNet, built on BDCN with a centralized feature pyramid and multi-dilated channel refiner) reports ODS=0.837 and OIS=0.851. Thus, our untrained fusion surpasses PDUF and CPD-Net on ODS, is within 0.006 of ML-EdgeNet on ODS, and *exceeds* ML-EdgeNet on OIS (0.866 vs. 0.851), while also delivering a strong AP (0.827). These results indicate that a principled, parameter-free multiscale fusion via generalized Choquet operators can approach, and in certain aspects, surpass trained CNN baselines on the

Table 32: ODS/OIS/AP on BSDS500 for a range of trained and untrained methods reported in prior work, compared to our two best configurations.

Method	**ODS**	**OIS**	**AP**	**Reference**	**year**
Roberts	0.483	0.513	0.261	(ROBERTS, 1963)	1963
Sobel	0.539	0.575	0.539	(SOBEL, 1972)	1972
MShift	0.598	0.645	0.725	(COMANICIU; MEER, 2002)	2002
Canny	0.611	0.676	0.751	(CANNY, 1986)	1986
EGB	0.614	0.658	0.771	(FELZENSZWALB; HUTTENLOCHER, 2004)	2004
NCut	0.634	0.664	0.797	(SHI; MALIK, 2000)	2000
HFS	0.650	0.688	0.822	(CHENG et al., 2016)	2016
BEL	0.651	0.674	0.817	(DOLLAR; TU; BELONGIE, 2006)	2006
Pb	0.672	0.695	0.824	(MARTIN; FOWLKES; MALIK, 2004)	2004
DEL	0.703	0.735	0.874	(LIU et al., 2018)	2018
ISCRA	0.717	0.752	0.882	(REN; SHAKHNAROVICH, 2013)	2013
gPb-UCM	0.729	0.755	0.892	(ARBELAEZ et al., 2011)	2011
SE	0.743	0.764	0.925	(DOLLÁR; ZITNICK, 2013)	2013
MCG	0.744	0.777	0.911	(PONT-TUSET et al., 2016)	2016
OEF	0.746	0.770	0.918	(HALLMAN; FOWLKES, 2015)	2015
DeepEdge	0.753	0.772	0.915	(BERTASIUS; SHI; TORRESANI, 2015a)	2015
DeepContour	0.757	0.776	0.916	(SHEN et al., 2015)	2015
HFL	0.767	0.788	0.892	(BERTASIUS; SHI; TORRESANI, 2015b)	2015
HED	0.788	0.808	0.923	(XIE; TU, 2017)	2017
COB	0.793	0.819	0.927	(MANINIS et al., 2017)	2017
RCF-VGG16	0.811	0.830	0.913	(LIU et al., 2019)	2019
RCF-ResNet50	0.814	0.833	0.910	(LIU et al., 2019)	2019
DDS	0.815	0.834	0.888	(LIU et al., 2021)	2021
RCF-ResNet101	0.819	0.836	0.909	(LIU et al., 2019)	2019
PDUF	0.818	0.836	0.862	(BAO et al., 2023)	2023
CPDNet	0.775	0.625	0.291	(LIU et al., 2025)	2025
ML-EdgeNet	0.837	0.851	*not reported*	(GAO, 2025)	2025
GMC-ED#1	**0.831**	**0.866**	**0.827**	Our	2025
GMC-ED#2	**0.819**	**0.861**	**0.977**	Our	2025

classical BSDS500 benchmark.

To provide broader context, we juxtapose our results with a spectrum of *untrained* classical detectors and *trained* learning-based methods. Classical baselines such as Roberts (ROBERTS, 1963), Sobel (SOBEL, 1972), Mean-Shift (COMANICIU; MEER, 2002), Canny (CANNY, 1986), EGB (FELZENSZWALB; HUTTENLOCHER, 2004), NCut (SHI; MALIK, 2000), HFS (CHENG et al., 2016), BEL (DOLLAR; TU; BELONGIE, 2006), Pb/gPb-UCM (MARTIN; FOWLKES; MALIK, 2004; ARBELAEZ et al., 2011), SE (DOLLÁR; ZITNICK, 2013), MCG (PONT-TUSET et al., 2016), OEF (HALLMAN; FOWLKES, 2015), DeepEdge (BERTASIUS; SHI; TORRESANI, 2015a), DeepContour (SHEN et al., 2015), HFL (BERTASIUS; SHI; TORRESANI, 2015b), HED (XIE; TU, 2017), COB (MANINIS et al., 2017), and the RCF family (LIU et al., 2019) (plus DDS (LIU et al., 2021) and DEL (LIU et al., 2018)) cover decades of progress from gradient heuristics to deep supervision.

Using the exact ODS/OIS/AP figures reported in those works (see Table 32), we find that our best untrained fusion ($GMC - ED\#1$) surpass all classical non–deep baselines

and matching or exceeding several trained detectors on at least one summary. Our second configuration ($GMC-ED\#2$) further delivers a remarkably high AP$=0.977$ with ODS$=0.819$ and OIS$=0.861$, illustrating that generalized Choquet-based multiscale fusion could rival modern trained systems under the standard BSDS500 protocol.

The main difference between our two best methods lies in the AP metric. it summarizes performance across operating points and is independent of any single threshold choice. Thus, while both methods achieve comparable ODS and OIS, $\mathfrak{C}_{\mathfrak{m}}^{O_{RS},O_{RS}}$ attains a higher AP, indicating more consistently favorable precision–recall trade–offs across thresholds.

This explains why the method with the highest AP rises to the top under the multi-threshold protocol. Although $\mathfrak{C}_{\mathfrak{m}}^{F_{NA},F_{NA}}$ delivered the best single-threshold ($F_{0.5}$) when we selected an optimal cutoff via unimodal thresholding, $\mathfrak{C}_{\mathfrak{m}}^{O_{RS},O_{RS}}$ preserves strong precision–recall trade-offs over a broad sweep of thresholds, yielding a larger area under the PR curve. In other words, the former peaks higher at one operating point, while the latter is more stable across operating points, hence its superior standing when performance is summarized by AP alongside ODS/OIS.

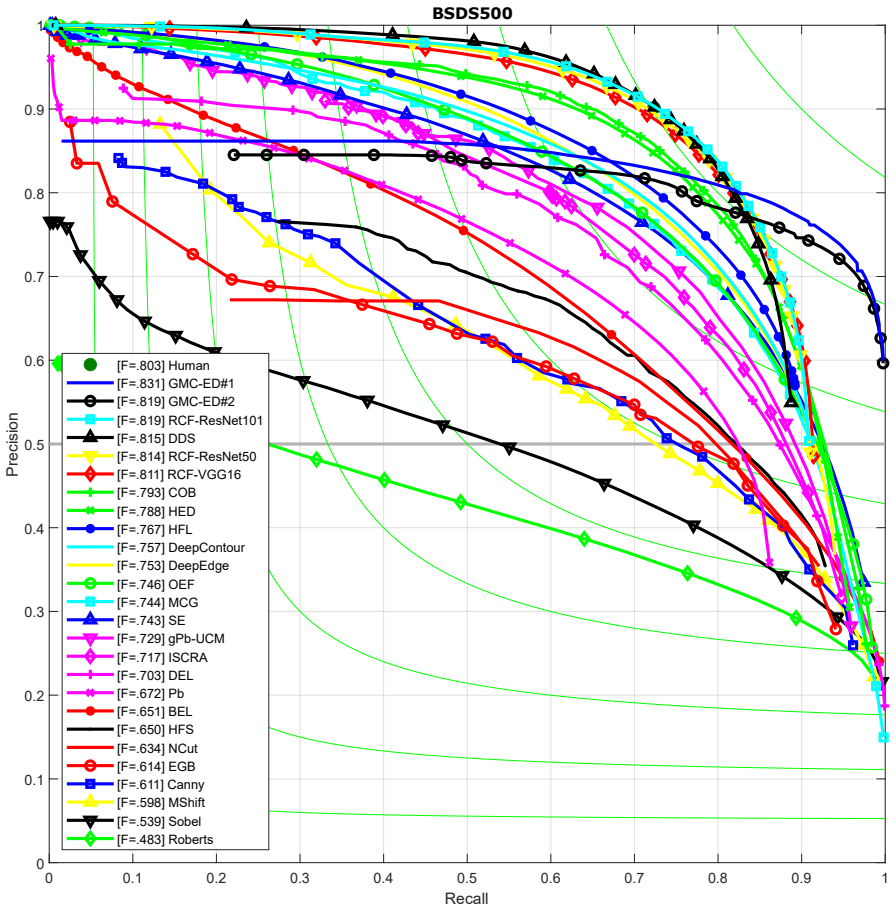


Figure 42: Comparison of our best method with other methods from the literature.

13.3.1 Evaluation on the Unified Dataset for Edge Detection

To investigate the generalization capability beyond the BSDS500 benchmark, we further conducted experiments on the Unified Dataset for Edge Detection (UDED), introduced alongside TEED (SORIA et al., 2023). UDED consolidates images from multiple heterogeneous sources, thereby supporting cross-dataset evaluation under a wide range of scenes, textures, and acquisition settings.

The dataset was designed to standardize evaluation by curating images from collections dedicated to low- and mid-level vision tasks, with careful annotation of perceptually relevant edges. The final dataset comprises 30 images selected from the aforementioned sources, in addition to the classical *cameraman* image. The selection procedure involved computing the interquartile range (IQR) of intensity values for each candidate image, excluding those with spatial resolutions exceeding 720×720. Subsequently, the images were ordered according to their IQR values, and 30 samples were uniformly selected, approximately two per source dataset, ensuring statistical representativeness in terms of distribution with respect to widely adopted edge-detection benchmarks.

The use of UDED enables the assessment of the proposed method across diverse real-world conditions, thereby extending the experimental analysis toward evaluating its generalization performance in practical scenarios.

Initially, we evaluated the same top ten methods obtained on the BSDS500 dataset using the UDED benchmark. The corresponding results are reported in Table 33. It can be observed that, although precision generally remains high and the F-measure stays above the 70% range, there is a noticeable drop in recall. This behavior is consistent with the purpose of the second dataset, which is smaller but more generalist than the former. Differences in color, texture, illumination, and other visual characteristics between the datasets may affect performance, such that models achieving strong results on a dataset with more homogeneous characteristics do not necessarily generalize equally well to datasets with greater diversity, as is the case with UDED.

For this reason, all methods were evaluated on the UDED dataset with the aim of identifying and analyzing those that perform best on a more generalist benchmark. Table 34 summarizes the 18 best results obtained for this dataset. It can be observed that all color aggregation combinations associated with the function $\mathfrak{C}_{\mathfrak{m}}^{O_{RS}}$ appear among the top ten methods. A similar behavior is observed for $\mathrm{X}\mathfrak{C}_{\delta,\mathfrak{m}}^{F_{IP}}$, which also consistently ranks within the top-10 regardless of the chromatic aggregation strategy adopted. In addition, variants based on $\mathfrak{C}_{\mathfrak{m}}^{F_{GL}}$ and $\mathfrak{C}_{\mathfrak{m}}^{O_{GM}}$ likewise remain among the best-performing methods for all three color aggregation schemes considered. These results indicate that such operators exhibit a high degree of robustness with respect to the color fusion stage, suggesting that their ability to capture relevant edge structures is predominantly determined by the underlying fuzzy aggregation mechanism rather than by the specific choice of color channel combination. In contrast, other operators achieve competitive performance only under

Table 33: Top 10 results of our method for UDED database using the functions applied to the BSDS500 dataset

Method	**Color Aggregation**	$\bar{P}$	$\bar{R}$	$\bar{F}$
$\mathfrak{C}_{\mathfrak{m}}^{F_{NA},F_{NA}}$	F_{SqSum}	0.995	0.568	0.705
$\mathfrak{C}_{\mathfrak{m}}^{O_{RS},O_{RS}}$	$F_{\max}$	0.989	0.662	0.779
$\mathfrak{C}_{\mathfrak{m}}^{F_{GL},AVG}$	$F_{\max}$	0.653	0.903	0.739
$\mathfrak{C}_{\mathfrak{m}}^{F_{GL},AVG}$	F_{SqSum}	0.659	0.913	0.747
$\mathfrak{C}_{\mathfrak{m}}^{C_F}$	F_{mean}	0.990	0.632	0.757
$\mathfrak{C}_{\mathfrak{m}}^{C_L}$	$F_{\max}$	0.986	0.695	0.803
$\mathfrak{C}_{\mathfrak{m}}^{T_M}$	F_{SqSum}	0.989	0.672	0.787
$\mathfrak{C}_{\mathfrak{m}}^{AVG,AVG}$	F_{SqSum}	0.991	0.619	0.748
$\mathfrak{C}_{\mathfrak{m}}^{O_{mM},O_{mM}}$	F_{SqSum}	0.992	0.615	0.744
$\mathfrak{C}_{\mathfrak{m}}^{O_{mM},O_{mM}}$	F_{mean}	0.993	0.597	0.730

specific color aggregation configurations, revealing a higher sensitivity to this stage of the pipeline and, consequently, reduced stability in scenarios with more pronounced chromatic variations.

A comparison of the results obtained on the BSDS500 and UDED datasets shows that, despite the significant differences between the datasets, the operators achieving the best performance mostly belong to the same mathematical families. In both scenarios, overlap functions, smooth fusion functions, and operators based on balanced aggregation schemes stand out, such as O_{RS}, O_{GM}, F_{GL} and F_{NA}. The recurrence of these functions among the top-performing results suggests that their superior performance may stem from their intrinsic structural properties.

13.4 Chapter Conclusion

The nature of Edge detection problem remains intrinsically diffuse: the conceptual ambiguity of an *edge* directly affects the production of ground truths and, consequently, their evaluation. When the task is to detect edges without a restricted semantic scope, it is necessary to admit multiple annotator opinions and treat them statistically (ARBELAEZ et al., 2014). Moreover, the inherent limitations of the acquisition process and the spatial shifts introduced by algorithms require displacement-tolerant evaluation protocols (ESTRADA; JEPSON, 2009). These aspects render the problem naturally amenable to modeling through the lens of fuzzy set theory (ZADEH, 2008).

From an algorithmic standpoint, modern detectors are frequently multiscale: neural networks and classical methods explore different σ values and perform information fusion. In CNNs, for example, this fusion occurs across convolutional layers and multi-level

Table 34: Top 18 results of our method for UDED database with all combinations.

Method	**Color Aggregation**	$\bar{P}$	$\bar{R}$	$\bar{F}$
$\mathfrak{C}_{\mathfrak{m}}^{F_{NA},C_F}$	F_{max}	0.941	0.911	0.922
$\mathfrak{C}_{\mathfrak{m}}^{F_{NA},T_P}$	F_{max}	0.939	0.910	0.921
$\mathfrak{C}_{\mathfrak{m}}^{T_L,T_M}$	F_{max}	0.933	0.916	0.920
$\mathfrak{C}_{\mathfrak{m}}^{T_M,T_L}$	F_{max}	0.923	0.923	0.920
$\mathfrak{C}_{\mathfrak{m}}^{O_{mM},T_L}$	F_{max}	0.916	0.932	0.919
$\mathfrak{C}_{\mathfrak{m}}^{F_{GL}}$	F_{max}	0.909	0.899	0.900
$\mathfrak{C}_{\mathfrak{m}}^{O_{RS}}$	F_{max}	0.928	0.875	0.897
$\mathfrak{C}_{\mathfrak{m}}^{O_{GM}}$	F_{max}	0.914	0.887	0.896
$\mathfrak{C}_{\mathfrak{m}}^{F_{GL}}$	F_{SqSum}	0.911	0.888	0.895
$\mathfrak{C}_{\mathfrak{m}}^{O_{GM}}$	F_{SqSum}	0.918	0.879	0.894
$\mathfrak{C}_{\mathfrak{m}}^{F_{GL}}$	F_{mean}	0.912	0.885	0.894
$\mathfrak{C}_{\mathfrak{m}}^{O_{GM}}$	F_{mean}	0.919	0.877	0.893
$\mathfrak{C}_{\mathfrak{m}}^{O_{RS}}$	F_{SqSum}	0.930	0.863	0.891
$\mathfrak{C}_{\mathfrak{m}}^{O_{RS}}$	F_{mean}	0.931	0.861	0.890
$\text{X}\mathfrak{C}_{\mathfrak{m},\delta_0}^{F_{IP}}$	F_{max}	0.979	0.739	0.831
$\text{X}\mathfrak{C}_{\mathfrak{m},\delta_0}^{F_{IP}}$	F_{SqSum}	0.979	0.728	0.823
$\text{X}\mathfrak{C}_{\mathfrak{m},\delta_0}^{F_{IP}}$	F_{mean}	0.978	0.724	0.820
$\mathfrak{C}_{\mathfrak{m}}^{F_{NA}}$	F_{max}	0.985	0.708	0.812

aggregations (KRIZHEVSKY; SUTSKEVER; HINTON, 2017; LOPEZ-MOLINA et al., 2011). Recent literature has emphasized precisely this fusion stage, where integrals and functions from the Choquet family have shown promising results by enabling the adaptive and aggregation of local and multiscale evidence (GRABISCH et al., 2009; CHOQUET, 1953–1954; MARCO-DETCHART et al., 2023a; MARCO-DETCHART et al., 2023b; MARCO-DETCHART et al., 2021; SILVA et al., 2023).

In this work, we investigated a family of generalized Choquet-inspired aggregators for the multiscale fusion of edge evidence, emphasizing pointwise aggregation of feature maps across different σ values. We adopted the BSDS500 benchmark with its official split and the displacement-tolerant correspondence of Estrada–Jepson (tolerance of 2.5% of the image diagonal). Our pipeline (Fig. 37) applies multiscale Gaussian smoothing, gradient extraction, intra-channel fusion, and then pointwise multiscale aggregation via generalized integrals $\mathfrak{C}$ parameterized by 21 bivariate functions F and nine integral families. Post-processing includes power-law enhancement, local orientation estimation, non-maximum suppression (NMS), and Rosin's unimodal thresholding, producing binary maps aligned with the BSDS protocol.

The experiments (Section 13.3) covered 252 combinations per image. Under our $F_{0.5}$ protocol with per-image optimal thresholding, the best method was $\mathfrak{C}_{\mathfrak{m}}^{\mathbf{F_{NA}},\mathbf{F_{NA}}}$ with color fusion F_{SqSum}, achieving $\bar{P} = 0.9570$, $\bar{R} = 0.9214$, and $\bar{F} = 0.9388$ (Table 13.3). Under the standard ODS/OIS/AP protocol, the top result was $\mathfrak{C}_{\mathfrak{m}}^{\mathbf{O_{RS}},\mathbf{O_{RS}}}$ with F_{SqSum} (Fig. 41), yielding ODS $= 0.831$, OIS $= 0.866$, and AP $= 0.827$. Qualitatively and quantitatively, these variants surpass classical detectors and match or exceed several trained models in specific metrics (e.g., OIS), showing that a training-free, parameter-agnostic multiscale fusion can be highly competitive when properly grounded.

To assess generalization, we further considered the Unified Dataset for Edge Detection (UDED), a heterogeneous benchmark that stresses robustness under broader variations of scene content and acquisition conditions. When transferring the BSDS500 top-10 configurations to UDED (Table 33), we observed that precision remains high while recall decreases, consistent with UDED's diversity. However, the full exploration of the operator space on UDED (Table 34) revealed that the most competitive families are largely consistent with those found for BSDS500, notably overlap-based operators and smooth fusion schemes. Crucially, UDED identifies operators that are structurally robust to the color-fusion stage, such as $\mathfrak{C}_{\mathfrak{m}}^{O_{RS}}$, $\mathfrak{C}_{\mathfrak{m}}^{F_{GL}}$ and those with F_{NA}, which perform consistently across the chromatic aggregation strategies.

Overall, the results indicate that local multiscale aggregation via generalized Choquet integrals improves the stability of the precision–recall balance. The cross-dataset analysis suggests that robust generalization is associated with structural properties such as smoothness, near-symmetry, and moderated penalization, which mitigate abrupt saturation and reduce the undue dominance of extreme responses.
The main contributions of this Chapter are:

1 A training-free multiscale edge-fusion pipeline grounded on generalized Choquet-type integrals for pointwise aggregation across σ;

2 A systematic study of a large operator space under a displacement-tolerant protocol; and

3 A cross-dataset analysis on UDED identifying operator families with structural robustness to chromatic fusion.

As limitations, we note that:

1 The pipeline relies on a specific post-processing stack;

2 Fuzzy measures were not learned but fixed within a design space; and

3 The broad combinatorial evaluation is computationally demanding.

14 CONCLUSION

Edge detection is one of the most common approaches for identifying *discontinuities* in digital images and remains a foundational component of computer vision and image processing, supporting applications that range from autonomous driving and augmented reality to medical image analysis (SURESH; SRINIVASA, 2019; MUTHALAGU; BOLIMERA; KALAICHELVI, 2020; ORHEI; VERT; VASIU, 2020; ORUJOV et al., 2020). Historically, the development of edge detectors sought to operationalize the notion of an edge as the boundary between regions with distinct properties, progressing from classical gradient-based operators and the Canny paradigm to multiscale and learning-based approaches (ROBERTS, 1980; SOBEL; FELDMAN, 1973; PREWITT, 1970; CANNY, 1986).

Motivated by the uncertainty and imprecision intrinsic to digital image formation and annotation, this thesis examined advances that move beyond purely crisp formulations, emphasizing the integration of fuzzy theory and aggregation/pre-aggregation functions, particularly Choquet-type models and their generalizations, as principled, mechanisms for incorporating contextual information and improving robustness in edge detection (GRABISCH et al., 2009; CHOQUET, 1953–1954; MARCO-DETCHART et al., 2023a; MARCO-DETCHART et al., 2021; SILVA et al., 2023).

To establish a coherent basis for the proposed models, the thesis first develops the theoretical foundations required to understand what is meant by an edge beyond purely operational definitions. In this direction, a formal and non-reductionist characterization is articulated in the first section of Chapter 3, grounding the subsequent methodological choices in a clear semantic perspective. After a review of the history of philosophy and computing, a non-reductionist definition for the concept of an edge was reached.

Firstly, it was observed that, based on our pre-theoretical experience, there were two categories of edges that ultimately represented the same entity: bona fide and fiduciary edges. In computational literature, these categories encompass what is commonly represented by the terms edge (properly speaking), contours, and boundaries.

Through the Clouser-Dooyeweerdian ontology, it was possible to define a modal concept of an edge that accounts for its fuzzy and uncertain nature, given the significance of

its fiduciary (pistic) aspect, founded on its physical aspect and logically guided. Based on the definition achieved, it follows that an edge, in a computational context, must be well-defined regarding its semantic properties, including issues of scale and contextual composition.

With this conceptual basis in place, the thesis then examines how the literature has attempted to operationalize such diffuse and uncertain boundaries, starting with approaches explicitly grounded in fuzzy logic. Accordingly, Chapter 6 reports a systematic review of fuzzy edge detection methods and clarifies their historical evolution and practical motivations. This chapter highlighted the transition from traditional methods to fuzzy logic-based approaches, which are better suited to handle the uncertainty and imprecision of digital images. It also identified a gap in the literature for dedicated review papers focusing on fuzzy methods in edge detection, emphasizing the need for continued research and evaluation in this area.

The findings from this chapter confirmed the effectiveness of integrating fuzzy logic, significantly enhancing the performance of edge detection systems and making them more adaptable to varying image conditions. This chapter responds to the first specific objective by evaluating the state of the art of edge detection methods using fuzzy logic, considering the inherently diffuse nature of edges through fuzzy theory.

Beyond fuzzy membership modeling, another key axis for handling uncertainty and contextual dependence lies in the fusion mechanism itself. Thus, Chapter 7 shifts the focus to aggregation and pre-aggregation functions, surveying how these operators have been used to encode contextual interactions and refine edge detection decisions.

This systematic review revealed a sparse but growing body of literature that exploits these mathematical functions to refine edge detection techniques. The chapter categorized existing methods into three groups based on their approach to integrating these functions, highlighting the potential for improved robustness and precision in edge detection.

The findings underscored the importance of developing new edge detection models that incorporate these functions to better capture and utilize contextual information from images. This chapter achieved the second specific objective by assessing the state of the art of edge detection methods that utilize aggregation and pre-aggregation functions.

However, the performance of edge detection pipelines is not determined solely by fusion operators: it is also strongly influenced by the *conditioning* stage. For this reason, Chapters 8 and 9 investigate smoothing techniques and clarify how noise suppression and detail preservation must be balanced to avoid degrading meaningful discontinuities.

These chapters provided an in-depth examination of how various smoothing methods impact the performance of an edge detection algorithm. The reviews demonstrated that while smoothing is essential for reducing noise, it can also obscure important features in images. The chapters advocated for a balanced approach to applying smoothing techniques, ensuring that the reduction of noise does not compromise the detection of significant

edges.

This nuanced understanding of smoothing's impact is critical for developing more sophisticated edge detection algorithms that can effectively differentiate between noise and important textual features in images. These chapters collectively addressed the third specific objective by understanding the effects of smoothing on edge detection.

The need for balance, highlighted by the conditioning analyses, motivates adaptive mechanisms that respond to local image characteristics rather than relying on fixed parameters. In this context, Chapter 10 introduces a novel edge detection approach based on adaptive fuzzy measures within the Choquet integral framework, targeting robustness across heterogeneous regions and noise conditions.

This research introduced an adaptive model that adjusts the parameters of the fuzzy measures based on the local characteristics of image regions. This adaptability allows the model to maintain high performance across different noise levels and image details. The chapter's findings highlighted the potential of fuzzy measures to enhance the adaptability and accuracy of edge detection systems, suggesting directions for future research in refining these models.

While adaptive fuzzy measures address local variability through parameter adjustment, contextual modeling can also be enriched by how disparities among inputs are quantified and weighted. Therefore, Chapter 11 extends the investigation to Choquet-type integrals generalized by RDFs, enabling flexible weighting of local contrasts within sliding windows and supporting rigorous statistical evaluation.

Within the scope of this study, distinct color channel fusion strategies were applied, in addition to a statistical protocol to evaluate the harmonic mean between precision and recall (F-measure). The results obtained using the BSDS500 (primary) and UDED (generalist) datasets were compared with state-of-the-art models, restricted to those that were methodologically comparable. A promising performance was observed, outperforming classical methods and performing on par with training-based models.

Having established the promise of generalized integral-based fusion under comparable protocols, the thesis then advances from fixed-scale designs to multiscale formulations. Accordingly, Chapter 12 presents a multiscale mixed-channel method based on modified and expanded Choquet pre-aggregation and aggregation functions, inspired by point-to-point processing patterns observed in early vision. Key findings highlight the effectiveness of integrating complex fuzzy methods and multiscale strategies, validated through a statistical analysis and empirical testing using the Berkeley Segmentation Dataset.

To consolidate these multiscale insights into a broader and systematically explored operator space, the method is further refined in Chapter 13. This final stage incorporates controlled chromatic fusion and Choquet integrals generalized by bivariate functions (F), enabling an expanded family of operators to be evaluated under displacement-tolerant protocols. The investigation encompassed nine integral families and 21 pre-aggregation func-

tions described in Chapter 4. Under evaluation protocols with displacement tolerance (the Estrada–Jepson criterion), models based on overlap operators and smooth fusion schemes, such as the $\mathfrak{C}_{\mathfrak{m}}^{O_{RS},O_{RS}}$ variant, achieved goods results on the BSDS500 dataset, reaching an ODS of 0.831 and an OIS of 0.866.

These metrics may indicate that the methods are competitive to state-of-the-art trained models. The robustness of the approach was tested with the generalization analysis on the UDED dataset, where the identified families maintained consistent performance under diverse acquisition conditions. These results support the central hypothesis of this thesis: it is possible to design unsupervised mathematical-computational models that, by exploring multiscale aggregation via fuzzy logic, challenge current expectations in the literature regarding the hegemony of purely supervised models.

As for future investigation, an especially promising direction is to unite, within a single framework, the "best of both worlds":

i the contextual sliding-window approach, which explores local dependencies and neighborhood-driven adaptations, and

ii the multiscale approach, which allows for the validation of fine-scale responses through coarse-scale evidence, increasing robustness and controlling false positives.

iii To make operators sensitive to local contrasts between ordered components, *restricted dissimilarity functions* (RDFs) on $[0, 1]$ can be applied, acting as calibrated substitutes for absolute differences (BUSTINCE et al., 2021).

A natural strategy is to introduce an intermediate aggregation stage (per channel or per feature group) before the final pointwise aggregation, creating a pipeline in which context at the same scale is consolidated first and only then coupled to the multiscale stack.

Furthermore, it is plausible to advance toward adaptive models capable of analyzing local and global features to select, driven by explicit criteria, the operator families that tend to perform better for a given content profile. Alternatively, a flexible model could be developed based on the best-performing operators, utilizing an adaptive mechanism, for instance, through a fuzzy measure, as demonstrated in Chapter 10. In this thesis, the practical use of fuzzy measures was heavily anchored in the power measure (and its variations/adaptations), suggesting expanding the study to other classes of measures and comparing sensitivity regimes and their impacts on contextual fusion.

Finally, regarding the family of integrals generalized by RDFs, although the results support the relevance of the "Choquet + restricted dissimilarities"composition, the space of possible combinations among operator choices (e.g., functions), dissimilarities, and associated parameters (such as exponents/hyperparameters) has not yet been exhausted.

A particularly relevant direction for future work is the formulation of a new RDF-based generalization, here denoted as d-$C_{F_1F_2}$, conceived as an extension of the $C_{F_1F_2}$

integral itself. Such a model would make it possible to incorporate restricted dissimilarity functions directly into the two-stage fusion mechanism, thereby increasing sensitivity to local contrast relations between ordered components while preserving the flexibility of the original F_1–F_2 construction.

A promising avenue is to employ this new extension within the multiscale method proposed in Chapter 13. More specifically, the idea is to replace or expand the generalized integrals currently adopted in that framework by introducing the d-$C_{F_1F_2}$ model, allowing restricted dissimilarity functions to operate within the multiscale and multichannel fusion process itself. This would make it possible to assess whether incorporating RDFs into the $C_{F_1F_2}$ structure can further improve the combination of responses across different scales and color channels, potentially enhancing sensitivity to relevant local contrasts while preserving the robustness already observed in the final multiscale architecture.

14.1 Scientific Contributions Developed During the Thesis Period

The following scientific contributions were produced during the development of this thesis. Together, they reflect the theoretical, review-based, and experimental advances achieved throughout the research. Whenever applicable, each contribution is explicitly related to the corresponding thesis chapter.

1. **Fuzzy Logic Based Edge Detection Methods: A Systematic Literature Review**

   This publication is directly related to Chapter 6, in which the state of the art of fuzzy-logic-based edge detection methods is systematically reviewed.

   Publication details:

   - Silva, M. A. S.; Dimuro, G.; Borges, E.; Lucca, G.; Marco-Detchart, C. *Fuzzy Logic Based Edge Detection Methods: A Systematic Literature Review*. In: Proceedings of the 25th International Conference on Enterprise Information Systems (ICEIS 2023), Volume 1, pp. 385–394.
   - Status: Published conference paper.
   - Related thesis chapter: Chapter 6.
   - Venue note: conference proceedings paper; journal impact factor not applicable.

2. **Systematic Review of Aggregation Functions Applied to Image Edge Detection**

   This article is associated with Chapter 7, which presents the systematic review of aggregation and pre-aggregation functions applied to edge detection.

   Publication details:

- Amorim, M.; Dimuro, G.; Borges, E.; Dalmazo, B. L.; Marco-Detchart, C.; Lucca, G.; Bustince, H. *Systematic Review of Aggregation Functions Applied to Image Edge Detection*. *Axioms*, 2023, 12, 330.
- Status: Published journal article.
- Journal: *Axioms*.
- Impact Factor (2024): 1.6.
- Journal Rank: JCR - Q2 (Mathematics, Applied)
- Related thesis chapter: Chapter 7.

3. **Impact of Blurring on Edge Detection Performance: A Survey**

   This contribution is related to Chapter 8, which presents the systematic review on the influence of smoothing filters on edge detection performance.

   Publication details:

   - Santos Silva, M. A.; Lucca, G.; Marco-Detchart, C.; Acosta, R.; Dimuro, G. P. *Impact of Blurring on Edge Detection Performance: A Survey*. Conference paper, pp. 179–186.
   - Status: Published conference paper.
   - Related thesis chapter: Chapter 8.
   - Venue note: conference/book chapter publication; journal impact factor not applicable.

4. **Experimental Investigation of the Impact of Smoothing on the Performance of Edge Detection**

   This contribution corresponds to the experimental developments presented in Chapter 9, where the practical influence of smoothing strategies on edge detection performance is investigated empirically. Part of the results obtained in this chapter was published in the *IPMU 2024 Lisboa Short Paper Proceedings*, corresponding to the 20th International Conference on Information Processing and Management of Uncertainty in Knowledge-Based Systems (IPMU 2024), held in Lisbon, Portugal (SILVA et al., 2025a).

   Publication details:

   - Partial results published in the *IPMU 2024 Lisboa Short Paper Proceedings* (SILVA et al., 2025a).
   - Status: partially published conference contribution.
   - Related thesis chapter: Chapter 9.

5. **Sliding Window Based Adaptative Fuzzy Measure for Edge Detection**

   This article is directly related to Chapter 10, in which an adaptive edge detection framework based on sliding windows and fuzzy measures is proposed.

   Publication details:

   - Marco-Detchart, C.; Lucca, G.; Santos Silva, M. A.; Rincon, J. A.; Julian, V.; Dimuro, G. *Sliding Window Based Adaptative Fuzzy Measure for Edge Detection*. *Expert Systems*, 2025, 42, e13730.
   - Status: Published journal article.
   - Journal: *Expert Systems*.
   - Journal Impact Factor: 2.3.
   - CiteScore: 9.1.
   - Related thesis chapter: Chapter 10.

6. **Generalizations of Choquet-like Integrals by Restricted Dissimilarity Functions Applied to Multi-Channel Edge Detection Problems**

   This article is related to Chapter 11, in which the study of Choquet-like integral generalizations based on restricted dissimilarity functions is developed for edge detection.

   Publication details:

   - Amorim, M.; Lucca, G.; Dalmazo, B. L.; Marco-Detchart, C.; Dimuro, G. P. *Generalizations of Choquet-like Integrals by Restricted Dissimilarity Functions Applied to Multi-Channel Edge Detection Problems*. *Applied Sciences*, 2025, 15, 13273.
   - Status: Published journal article.
   - Journal: *Applied Sciences*.
   - 5-Year Impact Factor: 2.7 (2024)
   - JCR Quartiles: Q2 (Engineering, Multidisciplinary)/ CiteScore - Q1 (General Engineering).
   - Related thesis chapter: Chapter 11.

7. **Analysis of Fuzzy Techniques in Edge Detection**

   Related contribution:

- SILVA, M. A. S.; DIMURO, G. P.; BORGES, E. N.; LUCCA, G.; MARCO-DETCHART, C. *Analysis of Fuzzy Techniques in Edge Detection*. In: FILIPE, J.; ŚMIAŁEK, M.; BRODSKY, A.; HAMMOUDI, S. (Eds.). *Lecture Notes in Business Information Processing*. Cham: Springer Nature Switzerland, 2024, v. 518, p. 161–180.

- Status: Published conference paper / book chapter
- Area: Fuzzy Logic / Edge Detection

8. **Registered Software: Sliding Window Based Adaptative Fuzzy Measure for Edge Detection**

   Technological contribution:

   - LUCCA, G.; DIMURO, G. P.; MARCO-DETCHART, C.; SANTOS SILVA, M. A.; RINCON, J. A.; INGLADA, V. J. *Sliding window based adaptative fuzzy measure for edge detection*. Computer software registration, INPI – Instituto Nacional da Propriedade Industrial, registration number BR512024003860-4, registration date: 28/05/2024.

   - Status: Registered software / technological product
   - Institution: INPI
   - Area: Edge Detection / Software Registration

REFERENCES

ABE, S. *Neural Networks and Fuzzy Systems*. [S.l.]: Springer US, 1997. ISBN 9781461562535.

ADELSON, E. et al. Pyramid methods in image processing. *RCA Eng.*, v. 29, 11 1983.

AGGARWAL, P. et al. Review of segmentation techniques on multi-dimensional images. In: *2018 International Conference on Power Energy, Environment and Intelligent Control, PEEIC 2018*. [S.l.]: Institute of Electrical and Electronics Engineers Inc., 2019. p. 268–273.

AGRAWAL, A.; BHOGAL, R. K. A review—edge detection techniques in dental images. In: PANDIAN, D. et al. (Ed.). *International Conference on ISMAC in Computational Vision and Bio-Engineering 2018 (ISMAC-CVB)*. Cham: Springer International Publishing, 2019. p. 1359–1378.

ALSINA, C.; FRANK, M. J.; SCHWEIZER, B. *Associative Functions: Triangular Norms and Copulas*. Singapore: World Scientific Publishing Company, 2006.

AMORIM, M. et al. Systematic review of aggregation functions applied to image edge detection. *Axioms*, v. 12, n. 4, 2023. ISSN 2075-1680.

AMORIM, M. et al. Generalizations of choquet-like integrals by restricted dissimilarity functions applied to multi-channel edge detection problems. *Applied Sciences*, v. 15, n. 24, 2025. ISSN 2076-3417.

AQUINO, T. d. *Summa Theologica*. New York: Benziger Bros., 1947.

ARBELAEZ, P. et al. Contour detection and hierarchical image segmentation. *IEEE Transactions on Pattern Analysis and Machine Intelligence*, IEEE, v. 33, n. 5, p. 898–916, 2011.

ARBELAEZ, P. et al. Multiscale combinatorial grouping. In: *2014 IEEE Conference on Computer Vision and Pattern Recognition*. Columbus, OH, USA: IEEE, 2014. p. 328–335.

ARIA, M.; CUCCURULLO, C. bibliometrix : An r-tool for comprehensive science mapping analysis. *Journal of Informetrics*, v. 11, n. 4, p. 959–975, 2017.

ARISTOTLE. Metaphysics. In: BARNES, J. (Ed.). *The Complete Works of Aristotle. The Revised Oxford Translation, Volume 2*. Princeton, NJ: Princeton University Press, 1984. p. 1552–1728.

BACHELARD, G. *La formation de l'esprit scientifique: contribution à une psychanalyse de la connaissance*. [S.l.]: J. Vrin, 1993. (Bibliothèque des textes philosophiques). ISBN 9782711611508.

BAGHBANI, R.; JAMASB, S.; KHODABAKHSHI, M. B. A method for image edge detection based on interval-valued fuzzy sets. *JOURNAL OF INTELIGENT & FUZZY SYSTEMS*, v. 37, n. 2, p. 2275–2288, 2019.

BALABANTARAY, B. K. et al. A quantitative performance analysis of edge detectors with hybrid edge detector. *JOURNAL OF COMPUTERS*, v. 12, n. 2, p. 165–173, 2017.

BAO, S.-S. et al. Pixel difference unmixing feature networks for edge detection. *IEEE Access*, v. 11, p. 52370 – 52380, 2023. Cited by: 1.

BARRENECHEA, E. et al. Using the Choquet integral in the fuzzy reasoning method of fuzzy rule-based classification systems. *Axioms*, v. 2, n. 2, p. 208–223, 2013.

BEAR, M. F.; CONNORS, B. W.; PARADISO, M. A. *Neuroscience: Exploring the Brain*. 4. ed. [S.l.]: Wolters Kluwer, 2016. ISBN 978-1-4511-0954-9.

BEDREGAL, B. et al. Generalized interval-valued owa operators with interval weights derived from interval-valued overlap functions. *International Journal of Approximate Reasoning*, v. 90, p. 1 – 16, 2017. ISSN 0888-613X.

BEDREGAL, B. C. et al. New results on overlap and grouping functions. *Information Sciences*, v. 249, p. 148–170, 2013.

BELIAKOV, G.; Bustince Sola, H.; CALVO, T. *A Practical Guide to Averaging Functions*. [S.l.]: Springer International Publishing, 2016. v. 329. (Studies in Fuzziness and Soft Computing, v. 329). ISBN 978-3-319-24751-9.

BELIAKOV, G.; PRADERA, A.; CALVO, T. *Aggregation Functions: A Guide for Practitioners*. Berlin: Springer, 2007.

BELIAKOV, G.; WU, J.-Z. Learning fuzzy measures from data: Simplifications and optimisation strategies. *Information Sciences*, v. 494, p. 100–113, 2019. ISSN 0020-0255.

BELIAKOV, G.; WU, J.-Z.; DING, W. Representation, optimization and generation of fuzzy measures. *Information Fusion*, v. 106, p. 102295, 2024. ISSN 1566-2535.

BENTKOWSKA, U. et al. New fuzzy local contrast measures: Definitions, evaluation and comparison. In: *IEEE International Conference on Fuzzy Systems*. [S.l.]: IEEE, 2020. p. 1–8.

BERTASIUS, G.; SHI, J.; TORRESANI, L. DeepEdge: A multi-scale bifurcated deep network for top-down contour detection. In: *IEEE Conference on Computer Vision and Pattern Recognition*. [S.l.: s.n.], 2015. p. 4380–4389.

BERTASIUS, G.; SHI, J.; TORRESANI, L. High-for-low and low-for-high: Efficient boundary detection from deep object features and its applications to high-level vision. In: *IEEE International Conference on Computer Vision*. [S.l.: s.n.], 2015. p. 504–512.

BETTELHEIM, C. *Les théories contemporaines de l'emploi*. [S.l.]: Centre de documentation universitaire, 1951. (Économie politique et problèmes du travail).

BEZDEK, J.; CHANDRASEKHAR, R.; ATTIKOUZEL, Y. A geometric approach to edge detection. *IEEE Trans. Fuzzy Syst.*, v. 6, n. 1, p. 52–75, 1998. ISSN 10636706.

BEZDEK, J.; CHANDRASEKHAR, R.; ATTIKOUZEL, Y. A geometric approach to edge detection. *IEEE Transactions on Fuzzy Systems*, v. 6, n. 1, p. 52–75, 1998.

BRODAL, A. Neurological anatomy. *Relation to Clinical Anatomy.*, Oxford University Press, 1981.

BUDZYN, G.; RZEPKA, J. Review of edge detection algorithms for application in miniature dimension measurement modules. *Journal of Machine Engineering*, v. 20, n. 4, p. 74–85, 2020.

BUENO, R. et al. Two-phase flow bubble detection method applied to natural circulation system using fuzzy image processing. *Nuclear Engineering and Design*, v. 335, p. 255–264, 2018.

BUSTINCE, H. et al. Ordered directionally monotone functions. justification and application. *IEEE Transactions on Fuzzy Systems*, v. 26, n. 4, p. 2237–2250, 2017.

BUSTINCE, H. et al. Directional monotonicity of fusion functions. *European Journal of Operational Research*, v. 244, n. 1, p. 300–308, 2015.

BUSTINCE, H. et al. Overlap functions. *Nonlinear Analysis: Theory, Methods & Applications*, v. 72, n. 3-4, p. 1488–1499, 2010.

BUSTINCE, H. et al. d-choquet integrals: Choquet integrals based on dissimilarities. *Fuzzy Sets and Systems*, v. 414, p. 1–27, 2021. ISSN 0165-0114. Aggregation Functions.

BUSTINCE, H. et al. On some classes of directionally monotone functions. *Fuzzy Sets and Systems*, v. 386, p. 161–178, 2020.

CANNY, J. A computational approach to edge detection. *IEEE Transactions on Pattern Analysis and Machine Intelligence*, PAMI-8, n. 6, p. 679–698, 1986.

CASTILLO, O. et al. Review of recent type-2 fuzzy image processing applications. *INFORMATION*, v. 8, n. 3, 2017.

CHAKRAPANI, S. et al. A survey of sobel edge detection vlsi architectures. In: *Journal of Physics: Conference Series*. [S.l.]: IOP Publishing Ltd, 2021. v. 1804.

CHEN, W.-S. et al. Kernel machine-based one-parameter regularized fisher discriminant method for face recognition. *IEEE Transactions on Systems, Man and Cybernetics, Part B (Cybernetics)*, v. 35, n. 4, p. 659–669, 2005.

CHENG, M.-M. et al. HFS: Hierarchical feature selection for efficient image segmentation. In: SPRINGER. *European Conference on Computer Vision*. [S.l.], 2016. p. 867–882.

CHI, Z. et al. Dual deep network for visual tracking. *IEEE Transactions on Image Processing*, v. 26, n. 4, p. 2005–2015, 2017.

CHOQUET, G. Theory of capacities. *Annales de l'Institut Fourier*, v. 5, p. 131–295, 1953–1954.

CLOUSER, R. *The Myth of Religious Neutrality*. Brasília: Monergism, 2022.

COMANICIU, D.; MEER, P. Mean shift: A robust approach toward feature space analysis. *IEEE Transactions on Pattern Analysis and Machine Intelligence*, IEEE, v. 24, n. 5, p. 603–619, 2002.

COSTA, C. *Filosofia da mente*. [S.l.]: Zahar, 2005.

COSTA, I. P. d. Uma introdução à ontologia de herman dooyeweerd. *Alamedas*, v. 11, n. 2, p. 89–100, 2023.

DAOU, R. A. Z. et al. Fractional derivatives for edge detection: Application to road obstacles. In: *Smart Cities Performability, Cognition, & Security*. Cham: Springer International Publishing, 2020. p. 115–137.

DAVIES, E. R. *Machine Vision. Theory, Algorithms, Practicalities*. 4. ed. Amsterdam: Elsevier, 2012.

DELIć, M.; NEDOVIć, L.; PAP, E. Extended power-based aggregation of distance functions and application in image segmentation. *Information Sciences*, v. 494, p. 155–173, 2019.

DEMŠAR, J. Statistical comparisons of classifiers over multiple data sets. *Journal of Machine Learning Research*, v. 7, n. Jan, p. 1–30, 2006.

DENG, R. et al. Learning to predict crisp boundaries. In: *Computer Vision – ECCV 2018*. [S.l.]: Springer International Publishing, 2018. p. 570–586.

DESCARTES, R. Meditações (coleção os pensadores). *São Paulo: Nova Cultural.(Originalmente publicado em 1641)*, 1999.

DHARGUPTA, S. et al. Fuzzy edge detection based steganography using modified gaussian distribution. *MULTIMEDIA TOOLS AND APPLICATIONS*, v. 78, n. 13, p. 17589–17606, 2019.

DHIVYA, R.; PRAKASH, R. Edge detection of satellite image using fuzzy logic. *Cluster Computing*, v. 22, p. 11891–11898, 2019.

DIAS, C. A. et al. Using the Choquet integral in the pooling layer in deep learning networks. In: BARRETO, G. A.; COELHO, R. (Ed.). *Fuzzy Information Processing*. Cham: Springer International Publishing, 2018. p. 144–154. (Best Paper Award, 2nd place).

DIMURO, G. et al. On the definition of the concept of pre-t-conorms. In: *IEEE International Conference on Fuzzy Systems*. [S.l.]: Institute of Electrical and Electronics Engineers Inc., 2017.

DIMURO, G. P.; BEDREGAL, B. Additive generators of overlap functions. In: BUSTINCE, H. et al. (Ed.). *Aggregation Functions in Theory and in Practice*. Berlin: Springer, 2013, (Advances in Intelligent Systems and Computing, v. 228). p. 167–178.

DIMURO, G. P.; BEDREGAL, B. Archimedean overlap functions: The ordinal sum and the cancellation, idempotency and limiting properties. *Fuzzy Sets and Systems*, v. 252, p. 39 – 54, 2014.

DIMURO, G. P.; BEDREGAL, B. On residual implications derived from overlap functions. *Information Sciences*, v. 312, p. 78 – 88, 2015. ISSN 0020-0255.

DIMURO, G. P. et al. New results on pre-aggregation functions. In: *Uncertainty Modelling in Knowledge Engineering and Decision Making, Proceedings of the 12th International FLINS Conference (FLINS 2016)*. Singapura: World Scientific, 2016, (World Scientific Proceedings Series on Computer Engineering and Information Science, v. 10). p. 213–219.

DIMURO, G. P. et al. On additive generators of overlap functions. *Fuzzy Sets and Systems*, v. 287, p. 76 – 96, 2016. ISSN 0165-0114. Theme: Aggregation Operations.

DIMURO, G. P. et al. QL-operations and QL-implication functions constructed from tuples (O, G, N) and the generation of fuzzy subsethood and entropy measures. *International Journal of Approximate Reasoning*, v. 82, p. 170 – 192, 2017.

DIMURO, G. P. et al. New results on pre-aggregation functions: Introducing (light) pre-t-norms. In: *2017 Joint 17th World Congress of International Fuzzy Systems Association and 9th International Conference on Soft Computing and Intelligent Systems (IFSA-SCIS)*. Los Alamitos: IEEE, 2017. p. 1–6.

DIMURO, G. P. et al. The state-of-art of the generalizations of the choquet integral: From aggregation and pre-aggregation to ordered directionally monotone functions. *Information Fusion*, v. 57, p. 27–43, 2020.

DIMURO, G. P. et al. Generalized CF1F2-integrals: From choquet-like aggregation to ordered directionally monotone functions. *Fuzzy Sets and Systems*, 2019. ISSN 0165-0114. (in Press, Corrected Proof).

DIMURO, G. P. et al. CMin-Integral: A Choquet-like aggregation function based on the minimum t-norm for applications to fuzzy rule-based classification systems. In: TORRA, V.; MESIAR, R.; BAETS, B. D. (Ed.). *Aggregation Functions in Theory and in Practice*. Cham: Springer International Publishing, 2018. p. 83–95. ISBN 978-3-319-59306-7.

DIMURO, G. P. et al. Penalty-based functions defined by pre-aggregation functions. In: MEDINA, J. et al. (Ed.). *Information Processing and Management of Uncertainty in Knowledge-Based Systems. Theory and Foundations*. Cham: Springer International Publishing, 2018. p. 403–415.

DING, H. et al. A feature aggregation network for contour detection inspired by complex cell properties. *Visual Computer*, 2024.

DOLLAR, P.; TU, Z.; BELONGIE, S. Supervised learning of edges and object boundaries. In: IEEE. *IEEE Conference on Computer Vision and Pattern Recognition*. [S.l.], 2006. p. 1964–1971.

DOLLÁR, P.; ZITNICK, C. L. Structured forests for fast edge detection. In: *IEEE International Conference on Computer Vision*. [S.l.: s.n.], 2013. p. 1841–1848.

DOOYEWEERD, H. *A New Critique of Theoretical Thought*. 3. ed. Ontario: Paideia Press, 1984. v. 3.

DOOYEWEERD, H. *A New Critique of Theoretical Thought*. 3. ed. Ontario: Paideia Press, 1984. v. 2.

DORRANI, Z.; FARSI, H.; MOHAMADZADEH, S. Image edge detection with fuzzy ant colony optimization algorithm. *INTERNATIONAL JOURNAL OF ENGINEERING*, v. 33, n. 12, p. 2464–2470, 2020.

DROLIA, U. et al. Cachier: Edge-caching for recognition applications. In: *2017 IEEE 37th International Conference on Distributed Computing Systems (ICDCS)*. Atlanta, GA, USA: IEEE, 2017. p. 276–286.

DURANTE, F.; FERNANDEZ-SANCHEZ, J.; QUESADA-MOLINA, J. J. On the α-migrativity of multivariate semi-copulas. *Information Sciences*, v. 187, p. 216 – 223, 2012.

ELDER, J. H. Shape from contour: computation and representation. *Annual Review of Vision Science*, v. 4, n. 1, p. 423–450, 2018.

ELKANO, M. et al. Enhancing multi-class classification in FARC-HD fuzzy classifier: On the synergy between n-dimensional overlap functions and decomposition strategies. *IEEE Transactions on Fuzzy Systems*, v. 23, n. 5, p. 1562–1580, 2015.

ESTRADA, F. J.; JEPSON, A. D. Benchmarking Image Segmentation Algorithms. *International Journal of Computer Vision*, v. 85, n. 2, p. 167–181, nov 2009. ISSN 0920-5691.

EUCLID. *The Elements*. 2. ed. Cambridge: Cambridge University Press, 1926.

FANG, A.; ZHAO, X.; ZHANG, Y. Cross-modal image fusion guided by subjective visual attention. *Neurocomputing*, v. 414, p. 333–345, 2020.

FELZENSZWALB, P. F.; HUTTENLOCHER, D. P. Efficient graph-based image segmentation. *International Journal of Computer Vision*, Springer, v. 59, n. 2, p. 167–181, 2004.

FLORES-VIDAL, P. et al. New aggregation approaches with hsv to color edge detection. *International Journal of Computational Intelligence Systems*, v. 15, n. 1, p. 78, 2022.

FLORES-VIDAL, P. A. et al. A new edge detection approach based on fuzzy segments clustering. In: *ADVANCES IN FUZZY LOGIC AND TECHNOLOGY 2017, VOL 2*. GEWERBESTRASSE 11, CHAM, CH-6330, SWITZERLAND: SPRINGER INTERNATIONAL PUBLISHING AG, 2018. (Advances in Intelligent Systems and Computing, v. 642), p. 58–67.

FLORES-VIDAL, P. A. et al. A new edge detection method based on global evaluation using fuzzy clustering. *SOFT COMPUTING*, v. 23, n. 6, SI, p. 1809–1821, 2019.

FUSTER, J. M. *Cortex and mind: Unifying cognition*. [S.l.]: Oxford university press, 2002.

GALLERY, N. *Georges Seurat: The Seine seen from La Grande Jatte*. 2024.

GAO, Z. Multiscale feature fusion and local detail enhancement-based edge detection. In: CHEN, L.; ZAIN, A. B. M. (Ed.). *Fourth International Conference on Electronic Information Engineering and Data Processing (EIEDP 2025)*. [S.l.]: SPIE, 2025. v. 13574, p. 135740A.

GARCIA-ALVAREZ, J. C.; RODRIGUEZ, J. E.; FüHR, H. Evaluation of detection methods in an image edge error measure. In: *Proceedings of the 6th International Conference on Computer Vision / Computer Graphics Collaboration Techniques and Applications*. New York, NY, USA: Association for Computing Machinery, 2013. (MIRAGE '13). ISBN 9781450320238.

GE, Y. et al. Wgi-net: A weighted group integration network for rgb-d salient object detection. *Computational Visual Media*, v. 7, n. 1, p. 115–125, 2021.

GELLIUS, A. *Auli Gellii Noctes Atticae*. Italy: apud Georgium de Caballis, 1565.

GHOSH, C. et al. Different edge detection techniques: A review. In: MALLICK, P. K. et al. (Ed.). *Electronic Systems and Intelligent Computing*. Singapore: Springer Singapore, 2020. p. 885–898.

GIRALT, N.; BLOOM, P. How special are objects? children's reasoning about objects, parts, and holes. *Psychological Science*, v. 11, p. 503–507, 2000.

GONZALEZ, C.; MELIN, P.; CASTILLO, O. Edge detection method based on general type-2 fuzzy logic applied to color images. *Information (Switzerland)*, v. 8, n. 3, 2017.

GONZALEZ, C. et al. Edge detection methods based on generalized type-2 fuzzy logic systems. *SpringerBriefs in Applied Sciences and Technology*, p. 21–35, 2017.

GONZALEZ, R. C.; WOODS, R. E. *Digital Image Processing*. [S.l.]: Prentice Hall, 2002.

GORDO, A. et al. Deep image retrieval: Learning global representations for image search. In: LEIBE, B. et al. (Ed.). *Computer Vision – ECCV 2016*. Cham: Springer International Publishing, 2016. p. 241–257.

GRABISCH, M. Capacities and games on lattices: A survey of results. In: TORRA, V.; NARUKAWA, Y.; MIYAMOTO, S. (Ed.). *Modeling Decisions for Artificial Intelligence*. Berlin, Heidelberg: Springer Berlin Heidelberg, 2005. p. 9–12.

GRABISCH, M. Fuzzy measures and integrals: Recent developments. In: TAMIR, D. E.; RISHE, N. D.; KANDEL, A. (Ed.). *Fifty Years of Fuzzy Logic and its Applications*. Cham: Springer International Publishing, 2015. p. 125–151.

GRABISCH, M. et al. *Aggregation Functions*. Cambridge: Cambridge University Press, 2009.

GU, Y. et al. An improved wavelet modulus algorithm based on fusion of light intensity and degree of polarization. *Applied Sciences*, v. 12, n. 7, p. 3558, 2022.

GUDIPALLI, A. et al. Hybrid colour infrared image edge detection using rgb-ycbcr image fusion. *International Journal of Advanced Science and Technology*, v. 28, n. 19, p. 101–108, 2019.

HAIT, S. et al. The bonferroni mean-type pre-aggregation operators construction and generalization: Application to edge detection. *Information Fusion*, v. 80, p. 226–240, 2022.

HALLMAN, S.; FOWLKES, C. C. Oriented edge forests for boundary detection. In: *IEEE Conference on Computer Vision and Pattern Recognition*. [S.l.: s.n.], 2015. p. 1732–1740.

HAUSDORFF, F. *Grundzüge der Mengenlehre*. Leipzig: Veit, 1914.

HE, J. et al. Bdcn: Bi-directional cascade network for perceptual edge detection. *IEEE Transactions on Pattern Analysis and Machine Intelligence*, Institute of Electrical and Electronics Engineers (IEEE), v. 44, n. 1, p. 100–113, 2022.

HESSEN, J. *Teoria do conhecimento*. [S.l.]: Martins Fontes, 1968.

HUANG, J. et al. Contrastive learning enhanced mobilemamba for real time industrial defect detection on edge devices. *Scientific Reports*, v. 16, n. 1, 2026. Cited by: 0; All Open Access, Gold Open Access, Green Open Access. Disponível em: <https://www.scopus.com/inward/record.uri?eid=2-s2.0-105029462993&doi=10.1038%2fs41598-026-35515-4&partnerID=40&md5=358c36d4cdabf5cad1f79c60ed9ab948>.

HUANG, Q.; HUANG, J. Comprehensive review of edge and contour detection: from traditional methods to recent advances. *Neural Computing and Applications*, v. 37, p. 2175–2209, 2025.

HUANG, Y.-C. et al. An adaptive edge detection based colorization algorithm and its applications. In: *13th annual ACM international conference on Multimedia - MULTIMEDIA '05*. Hilton, Singapore: ACM Press, 2005. p. 351.

HUBEL, D. H.; WIESEL, T. N. Integrative action in the cat's lateral geniculate body. *The Journal of Physiology*, v. 155, n. 2, p. 385–398, 1961.

HUBEL, D. H.; WIESEL, T. N. Mechanisms of feature extraction in the mammalian visual cortex. *Proceedings of the National Academy of Sciences of the United States of America*, National Academy of Sciences, v. 48, p. 1542–1557, 1962.

HUBEL, D. H.; WIESEL, T. N. Receptive fields, binocular interaction and functional architecture in the cat's visual cortex. *The Journal of Physiology*, v. 160, n. 1, p. 106–154, 1962.

HUME, D. *Investigação sobre o entendimento humano*. [S.l.]: Leya, 2013.

ISA, M. et al. Review of edge-based image segmentation on electrical tree classification in cross-linked polyethylene (xlpe) insulation. In: *Journal of Physics: Conference Series*. [S.l.]: IOP Publishing Ltd, 2021. v. 1878.

ISHIBUCHI, H.; NOJIMA, Y. Pattern classification with linguistic rules. In: BUSTINCE, H.; HERRERA, F.; MONTERO, J. (Ed.). *Fuzzy Sets and Their Extensions: Representation, Aggregation and Models*. Berlin: Springer, 2008, (Studies in Fuzziness and Soft Computing, v. 220). p. 377–395.

JACKENDOFF, R. *Consciousness and the Computational Mind*. Cambridge, MA: MIT Press, 1987.

JAIN, A. K. Fundamentals of digital image processing. *Prentice-Hall, Inc.*, 1989. Section on Gaussian Blur.

JAMAL, A. T.; ISHAK, A. B.; ABDEL-KHALEK, S. Tumor edge detection in mammography images using quantum and machine learning approaches. *Neural Computing and Applications*, v. 33, n. 13, p. 7773–7784, 2021.

JIA, B.-B.; LIU, J.-Y.; ZHANG, M.-L. Pairwise statistical comparisons of multiple algorithms. *Frontiers of Computer Science*, Higher Education Press, v. 19, n. 12, p. 1912372, 2025.

JING, J. et al. Recent advances on image edge detection: A comprehensive review. *Neurocomputing*, v. 503, p. 259–271, 2022.

JR, T. S. et al. Edge detection in images using Marr-Hildreth filtering techniques. *Journal of neuroscience methods*, v. 26, n. 1, p. 75–81, 1988.

KANDEL, E. R.; SCHWARTZ, J. H.; JESSELL, T. M. *Principles of Neural Science*. 4. ed. [S.l.]: McGraw-Hill, 2000. ISBN 978-0-8385-7701-1.

KANIZSA, G. Margini quasi-percettivi in campi con stimolazione omogenea. *Rivista di Psicologia*, v. 49, p. 7–30, 1955. English translation by W. Gerbino, 'Quasi-Perceptual Margins in Homogeneously Stimulated Fields', in S. Petry and G. E. Meyer (eds.), The Perception of Illusory Contours, New York: Springer, 1987, pp. 40–49.

KANT, I. *Crítica da razão pura*. [S.l.]: Edipro, 2020.

KAUR, B. R.; AAYUSHI, A. Image edge detection techniques using sobel, t1fls, and it2fls. In: *INFORMATION AND COMMUNICATION TECHNOLOGY FOR INTELLIGENT SYSTEMS, ICTIS 2018, VOL 2*. [S.l.]: SPRINGER INTERNATIONAL PUBLISHING AG, 2019. (Smart Innovation Systems and Technologies, v. 107), p. 303–317.

KAUR, G.; GARG, H. A new method for image processing using generalized linguistic neutrosophic cubic aggregation operator. *Complex and Intelligent Systems*, v. 8, p. 4911–4937, 2022.

KAUR, S.; KAUR, P. An edge detection technique with image segmentation using ant colony optimization: A review. In: *Proceedings of 2016 Online International Conference on Green Engineering and Technologies, IC-GET 2016*. [S.l.]: Institute of Electrical and Electronics Engineers Inc., 2017.

KELLER, J. M.; GRAY, M. R.; GIVENS, J. A. A fuzzy k-nearest neighbor algorithm. *IEEE Transactions on Systems, Man, and Cybernetics*, SMC-15, n. 4, p. 580–585, 1985.

KELSO, J. S. *Dynamic patterns: The self-organization of brain and behavior*. [S.l.]: MIT press, 1995.

KITCHENHAM, B.; CHARTERS, S. *Guidelines for performing Systematic Literature Reviews in Software Engineering*. [S.l.], 2007.

KLEMENT, E. P.; MESIAR, R.; PAP, E. *Triangular Norms*. Dordrecht: Kluwer Academic Publisher, 2000.

KLEMENT, E. P. et al. Universal integrals based on copulas. *Fuzzy Optimization and Decision Making*, v. 13, n. 3, p. 273–286, 2014.

Ko, L. et al. Multimodal fuzzy fusion for enhancing the motor-imagery-based brain computer interface. *IEEE Computational Intelligence Magazine*, v. 14, n. 1, p. 96–106, 2019.

KOFFKA, K. *Principles of Gestalt Psychology*. London: Kegan Paul, Trench, Trubner, 1935.

KOLB, H.; FERNANDEZ, E.; NELSON, R. *The Organization of the Retina and Visual System*. 2021.

KOSKO, B. *Fuzzy engineering*. [S.l.]: Prentice-Hall, Inc., 1996.

KREINOVICH, V.; MUKAIDONO, M. Interval (pairs of fuzzy values), triples, etc.: Can we thus get an arbitrary ordering? In: *Proceedings of 9th IEEE International Conference on Fuzzy Systems,S an Antonio, TX, USA, 2000*. Los Alamitos: IEEE, 2000. v. 1, p. 234–238.

KRIZHEVSKY, A.; SUTSKEVER, I.; HINTON, G. E. Imagenet classification with deep convolutional neural networks. *Commun. ACM*, Association for Computing Machinery, New York, NY, USA, v. 60, n. 6, p. 84–90, maio 2017. ISSN 0001-0782.

KUMAR, S.; SINGH, A.; KUMAR, M. Information hiding with adaptive steganography based on novel fuzzy edge identification. *DEFENCE TECHNOLOGY*, v. 15, n. 2, p. 162–169, 2019.

KUMAWAT, A.; PANDA, S. A robust edge detection algorithm based on feature-based image registration (fbir) using improved canny with fuzzy logic (icwfl). *VISUAL COMPUTER*, 2021.

KüHNE, G.; RICHTER, S.; BEIER, M. Motion-based segmentation and contour-based classification of video objects. In: *9th ACM international conference on Multimedia - MULTIMEDIA '01*. Ottawa, Canada: ACM Press, 2001. p. 41.

LEAL-TAIXé, L.; CANTON-FERRER, C.; SCHINDLER, K. Learning by tracking: Siamese cnn for robust target association. In: *2016 IEEE Conference on Computer Vision and Pattern Recognition Workshops (CVPRW)*. Los Alamitos: IEEE, 2016. p. 418–425.

LENT, R. Cem bilhões de neurônios: conceitos fundamentais de neurociência. In: *Cem bilhões de neurônios: conceitos fundamentais de neurociência*. [S.l.]: Editora Atheneu Ltda, 2004. p. 698–698.

LI, B.; ZHENG, C.-H.; HUANG, D.-S. Locally linear discriminant embedding: An efficient method for face recognition. *Pattern Recognition*, v. 41, n. 12, p. 3813–3821, 2008.

LI, F. et al. a biologically inspired contour detection model based on multiple visual channels and multi-hierarchical visual information. *IEEE Access*, v. 8, p. 15410–15422, 2020.

LI, M. et al. Photo-sketching: Inferring contour drawings from images. In: *2019 IEEE Winter Conference on Applications of Computer Vision (WACV)*. Los Alamitos: IEEE, 2019. p. 1403–1412.

LIN, C.; WANG, Q.; WAN, S. Dxyw: a depth-guided multi-channel edge detection model. *Signal, Image and Video Processing*, v. 17, p. 481–489, 2023.

LIN, C. et al. A lightweight biologically inspired contour detection network. *Complex & Intelligent Systems*, v. 10, n. 3, p. 4275–4291, 2024.

LIN, K. et al. Deep learning of binary hash codes for fast image retrieval. In: *2015 IEEE Conference on Computer Vision and Pattern Recognition Workshops (CVPRW)*. Boston, MA, USA: IEEE, 2015. p. 27–35.

LIU, C. et al. Cycle pixel difference network for crisp edge detection. *Neurocomputing*, v. 619, p. 129153, 2025. ISSN 0925-2312.

LIU, Y. et al. Semantic edge detection with diverse deep supervision. *International Journal of Computer Vision*, 2021.

LIU, Y. et al. Richer convolutional features for edge detection. *IEEE Transactions on Pattern Analysis and Machine Intelligence*, IEEE, v. 41, n. 8, p. 1939–1946, 2019.

LIU, Y. et al. DEL: Deep embedding learning for efficient image segmentation. In: *International Joint Conference on Artificial Intelligence*. [S.l.: s.n.], 2018. p. 864–870.

LJUBO, N.; MARIJA, D.; M., R. N. Owa aggregated distance functions and their application in image segmentation. In: *IEEE 16TH International Symposium on Intelligent Systems and Informatics (SISY 2018)*. [S.l.]: IEEE, 2018. p. 311–316.

LOCKE, J. *An Essay Concerning Human Understanding*. [S.l.]: T. Tegg, 1823. (An Essay Concerning Human Understanding, v. 1).

LOPEZ-MOLINA, C. et al. Multiscale edge detection based on the sobel method. In: *2011 11th International Conference on Intelligent Systems Design and Applications*. [S.l.: s.n.], 2011. p. 666–671.

LOPEZ-MOLINA, C.; De Baets, B.; BUSTINCE, H. Quantitative error measures for edge detection. *Pattern Recognition*, v. 46, n. 4, p. 1125–1139, 2013. ISSN 00313203.

LOPEZ-MOLINA, C. et al. Multiscale edge detection based on gaussian smoothing and edge tracking. *Knowledge-Based Systems*, v. 44, p. 101–111, 2013. ISSN 0950-7051.

LOPEZ-MOLINA, C. et al. Self-adapting weighted operators for multiscale gradient fusion. *Information Fusion*, v. 44, p. 136–146, 2018. ISSN 1566-2535.

LOWE, D. G. Distinctive image features from scale-invariant keypoints. *International Journal of Computer Vision*, Springer Science and Business Media LLC, v. 60, n. 2, p. 91–110, nov. 2004. ISSN 0920-5691.

LUCCA, G. et al. dcc-integrals: A generalization of cc-integrals by restricted dissimilarity functions with applications on two different contexts. *Applied Soft Computing*, v. 181, p. 113517, 2025. ISSN 1568-4946.

LUCCA, G. et al. Improving the performance of fuzzy rule-based classification systems based on a nonaveraging generalization of CC-integrals named $C_{F_1F_2}$-integrals. *IEEE Transactions on Fuzzy Systems*, v. 27, n. 1, p. 124–134, Jan 2019. ISSN 1063-6706.

LUCCA, G. et al. A family of Choquet-based non-associative aggregation functions for application in fuzzy rule-based classification systems. In: *2015 IEEE International Conference on Fuzzy Systems (FUZZ-IEEE)*. Los Alamitos: IEEE, 2015. p. 1–8.

LUCCA, G. et al. Analyzing the behavior of aggregation and pre-aggregation functions in fuzzy rule-based classification systems with data complexity measures. In: KACPRZYK, J. et al. (Ed.). *Advances in Fuzzy Logic and Technology 2017*. Cham: Springer International Publishing, 2018. p. 443–455. ISBN 978-3-319-66824-6.

LUCCA, G. et al. Applying aggregation and pre-aggregation functions in the classification of grape berries. In: *2018 IEEE International Conference on Fuzzy Systems (FUZZ-IEEE)*. Los Alamitos: IEEE, 2018. p. 1–6.

LUCCA, G. et al. Preaggregation functions: Construction and an application. *IEEE Transactions on Fuzzy Systems*, v. 24, n. 2, p. 260–272, apr 2016. ISSN 1063-6706.

LUCCA, G. et al. Cc-integrals: Choquet-like copula-based aggregation functions and its application in fuzzy rule-based classification systems. *Knowledge-Based Systems*, Elsevier, v. 119, p. 32–43, 2017.

LUCCA, G. et al. CF-integrals: A new family of pre-aggregation functions with application to fuzzy rule-based classification systems. *Information Sciences*, v. 435, p. 94 – 110, 2018.

LUCCA, G. et al. A proposal for tuning the α parameter in $c_\alpha c$-integrals for application in fuzzy rule-based classification systems. *Natural Computing*, Apr 2018.

LUIJPEN, W. *Introdução à fenomenologia existencial*. [S.l.]: Editora Pedagógica e Universitária, 1973.

LUO, Z. et al. Blednet: A lightweight bio-inspired neural network for edge detection. *Engineering Applications of Artificial Intelligence*, v. 124, p. 106530, 2023.

MAGNIER, B. Edge detection: a review of dissimilarity evaluations and a proposed normalized measure. *MULTIMEDIA TOOLS AND APPLICATIONS*, v. 77, n. 8, p. 9489–9533, 2018.

MAGNIER, B.; ABDULRAHMAN, H.; MONTESINOS, P. A review of supervised edge detection evaluation methods and an objective comparison of filtering gradient computations using hysteresis thresholds. *Journal of Imaging*, v. 6, n. 4, p. 74, 2018.

MAHADEV, N. et al. Intelligent real-time wildfire detection using image processing techniques with edge-ai integration. *Discover Computing*, v. 29, n. 1, 2026. Cited by: 0; All Open Access, Gold Open Access, Green Open Access.

MAHDJOUB, J. et al. A multi-agent approach for the edge detection in image processings. In: KEPLICZ, B. D.; OMICINI, A.; PADGET, J. (Ed.). *Proceedings of the 4th European Workshop on Multi-Agent Systems EUMAS'06*. [S.l.]: CEUR, 2006. (SEUR Workshop Proceedings, v. 223), p. n. 62.

MANDELBROT, B. *The Fractal Geometry of Nature*. New York: W. H. Freeman and Company, 1983. Este livro discute o conceito de dimensão fractal e aplica-o a vários fenômenos naturais, incluindo o mapeamento de costas.

MANINIS, K.-K. et al. Convolutional oriented boundaries: From image segmentation to high-level tasks. *IEEE Transactions on Pattern Analysis and Machine Intelligence*, IEEE, v. 40, n. 4, p. 819–833, 2017.

MARCO-DETCHART, C. et al. Ordered directional monotonicity in the construction of edge detectors. *Fuzzy Sets and Systems*, Elsevier, v. 421, p. 111–132, 2021.

MARCO-DETCHART, C. et al. Consensus image feature extraction with ordered directionally monotone functions. *Communications in Computer and Information Science*, v. 831, p. 155–166, 2018.

MARCO-DETCHART, C. et al. A gravitational approach to image smoothing. In: KACPRZYK, J. et al. (Ed.). *Advances in Fuzzy Logic and Technology 2017*. Cham: Springer International Publishing, 2018. p. 468–479. ISBN 978-3-319-66824-6.

MARCO-DETCHART, C. et al. Adaptative fuzzy measure for edge detection. In: QUARESMA, P. et al. (Ed.). *Intelligent Data Engineering and Automated Learning – IDEAL 2023*. Cham: Springer Nature Switzerland, 2023. p. 497–505. ISBN 978-3-031-48232-8.

MARCO-DETCHART, C. et al. Fuzzy integrals for edge detection. In: MASSANET, S. et al. (Ed.). *Fuzzy Logic and Technology, and Aggregation Operators*. Cham: Springer Nature Switzerland, 2023. p. 330–341. ISBN 978-3-031-39965-7.

MARCO-DETCHART, C. et al. Neuro-inspired edge feature fusion using choquet integrals. *Information Sciences*, v. 581, p. 740–754, 2021.

MARCO-DETCHART, C. et al. Sliding window based adaptative fuzzy measure for edge detection. *Expert Systems*, v. 42, n. 2, p. e13730, 2025.

MARÍAS, J.; BERLINER, C. *História da filosofía*. [S.l.]: Martins Martins Fontes, 2004.

MARR, D. Early processing of visual information. *Philosophical Trans. of the Royal Society of London. B, Biological Sciences*, v. 275, n. 942, p. 483–519, 1976.

MARR, D. *Vision*. [S.l.]: MIT Press, 1982.

MARR, D.; HILDRETH, E. Theory of edge detection. *Proceedings of the Royal Society of London. Series B. Biological Sciences*, v. 207, n. 1167, p. 187–217, 1980.

MARTIN, D. R.; FOWLKES, C. C.; MALIK, J. Learning to detect natural image boundaries using local brightness, color, and texture cues. *IEEE Transactions on Pattern Analysis and Machine Intelligence*, IEEE, v. 26, n. 5, p. 530–549, 2004.

MARTINEZ, G. E. et al. General type-2 fuzzy sugeno integral for edge detection. *Journal of Imaging*, v. 8, n. 5, p. 71, 2019.

MAYOR, G.; TRILLAS, E. On the representation of some aggregation functions. In: *Proceedings of IEEE International Symposium on Multiple-Valued Logic*. Los Alamitos: IEEE, 1986. p. 111–114.

MCGEE, T. *The Urbanization Process in the Third World: Explorations in Search of a Theory*. [S.l.]: Bell, 1971. (Third World books). ISBN 9780713516234.

MCILHAGGA, W. The canny edge detector revisited. *International Journal of Computer Vision*, Springer Science and Business Media LLC, v. 91, n. 3, p. 251–261, 2010.

MEDINA-CARNICER, R. et al. A novel method to look for the hysteresis thresholds for the canny edge detector. *Pattern Recognition*, v. 44, n. 6, p. 1201–1211, 2011. ISSN 0031-3203.

MEDLIN, B. The origin of motion. *Mind*, v. 72, p. 155–175, 1963.

MELIN, P. et al. Edge-detection method for image processing based on generalized type-2 fuzzy logic. *IEEE Transactions on Fuzzy Systems*, Institute of Electrical and Electronics Engineers (IEEE), v. 22, n. 6, p. 1515–1525, 2014.

MERLEAU-PONTY, M. *Phenomenology of Perception*. London: Routledge & Kegan Paul, 1962. Esta tradução em inglês é amplamente utilizada e respeitada, tornando os conceitos de Merleau-Ponty acessíveis a um público de língua inglesa.

MESIAR, R.; SEMPI, C. Ordinal sums and idempotents of copulas. *Aequationes Mathematicae*, v. 79, n. 1-2, p. 39–52, 2010.

MESIAR, R.; STUPŇANOVÁ, A. A note on CC-integral. *Fuzzy Sets and Systems*, v. 355, p. 106 – 109, 2019. ISSN 0165-0114. Theme: Generalized Integrals.

MNTTZRI, A. *Handsome Bearded Man Posing Outdoors*. Pexels, 2021. Acesso em: 30 mar. 2026. Disponível em: <https://www.pexels.com/photo/handsome-bearded-man-posing-outdoors-7904073/>.

MOHAN, K. et al. Facial expression recognition using local gravitational force descriptor-based deep convolution neural networks. *IEEE Transactions on Instrumentation and Measurement*, v. 70, p. 1–12, 2021.

MOYA-ALBOR, E.; PONCE, H.; BRIEVA, J. An edge detection method using a fuzzy ensemble approach. *ACTA POLYTECHNICA HUNGARICA*, v. 14, n. 3, SI, p. 149–168, 2017.

MUBASHAR, M. et al. Have we solved edge detection? a review of state-of-the-art datasets and dnn based techniques. *IEEE Access*, p. 1–1, 2022.

MUROFUSHI, T.; SUGENO, M.; MACHIDA, M. Non-monotonic fuzzy measures and the Choquet integral. *Fuzzy Sets and Systems*, v. 64, n. 1, p. 73 – 86, 1994.

MUTHALAGU, R.; BOLIMERA, A.; KALAICHELVI, V. Lane detection technique based on perspective transformation and histogram analysis for self-driving cars. *Computers & Electrical Engineering*, v. 85, p. 106653, 2020.

NAGARAJAN, D. et al. A type-2 fuzzy in image extraction for dicom image. *International Journal of Advanced Computer Science and Applications*, v. 9, n. 12, p. 351–362, 2018.

NAGARAJAN, D. et al. Edge detection on dicom image using triangular norms in type-2 fuzzy. *International Journal of Advanced Computer Science and Applications*, v. 9, n. 11, p. 462–475, 2018.

NEDOVIC, L.; RALEVIC, N. M.; PAVKOV, I. Aggregated distance functions and their application in image processing. *Soft Computing*, v. 22, n. 14, p. 4723–4739, 2018.

NELSEN, R. B. *An introduction to copulas*. New York: Springer, 1999. v. 139. (Lecture Notes in Statistics, v. 139).

NELSON, R.; PALMER, S. E. Of holes and wholes: The perception of surrounded regions. *Perception*, v. 30, p. 1213–1226, 2001.

OJHA, S.; SAKHARE, S. Image processing techniques for object tracking in video surveillance- a survey. In: *2015 International Conference on Pervasive Computing (ICPC)*. Pune, India: IEEE, 2015. p. 1–6.

OPPENHEIM, A. V.; SCHAFER, R. W. *Discrete-Time Signal Processing*. [S.l.]: Prentice Hall, 1999.

ORHEI, C.; VERT, S.; VASIU, R. A novel edge detection operator for identifying buildings in augmented reality applications. In: *Information and Software Technologies*. Cham: Springer International Publishing, 2020. v. 1283, p. 208–219.

ORUJOV, F. et al. Fuzzy based image edge detection algorithm for blood vessel detection in retinal images. *Applied Soft Computing*, v. 94, p. 106452, 2020.

OTSU, N. A threshold selection method from gray-level histograms. *IEEE Transactions on Systems, Man, and Cybernetics*, v. 9, n. 1, p. 62–66, 1979.

PANG, X. et al. Biologically inspired parallel xyw pathway network for edge detection. *Expert Systems with Applications*, v. 237, p. 121649, 2024.

PAP, E.; NEDOVIć, L.; RALEVIć, N. Image fuzzy segmentation using aggregated distance functions and pixel descriptors. *Studies in Computational Intelligence*, v. 973, p. 255–273, 2021.

PAVITHRA, L.; SHARMILA, T. S. An efficient framework for image retrieval using color, texture and edge features. *Computers & Electrical Engineering*, v. 70, p. 580–593, 2018.

PLATO. Parmenides. In: COOPER, J. M. (Ed.). *Plato. Complete Works*. Indianapolis, IN: Hackett, 1997. p. 359–397.

PONT-TUSET, J. et al. Multiscale combinatorial grouping for image segmentation and object proposal generation. *IEEE Transactions on Pattern Analysis and Machine Intelligence*, IEEE, v. 39, n. 1, p. 128–140, 2016.

PRATT, W. K. *Digital Image Processing: PIKS Scientific Inside*. [S.l.]: Wiley-Interscience, 2007.

PREWITT, J. Object enhancement and extraction. *Picture processing and Psychopictorics*, Academic Press New York, v. 10, n. 1, p. 15–19, 1970.

PU, M. et al. Edter: Edge detection with transformer. In: *2022 IEEE/CVF Conference on Computer Vision and Pattern Recognition (CVPR)*. [S.l.]: IEEE, 2022.

PURVES, D. et al. *Neurociencia*. [S.l.]: Panamericana, 2007.

QIAO, J.; HU, B. Q. On interval additive generators of interval overlap functions and interval grouping functions. *Fuzzy Sets and Systems*, v. 323, p. 19 – 55, 2017.

QIAO, J.; HU, B. Q. The distributive laws of fuzzy implications over overlap and grouping functions. *Information Sciences*, v. 438, p. 107 – 126, 2018. ISSN 0020-0255.

QIAO, J.; HU, B. Q. On generalized migrativity property for overlap functions. *Fuzzy Sets and Systems*, 2018. (in press, corrected proof online).

QIAO, J.; HU, B. Q. On multiplicative generators of overlap and grouping functions. *Fuzzy Sets and Systems*, v. 332, p. 1 – 24, 2018.

QIU, B. et al. Recurrent convolutional neural networks for 3d mandible segmentation in computed tomography. *Journal of Personalized Medicine*, v. 11, n. 6, p. 492, 2021.

QIU, H. et al. Learning from human uncertainty by choquet integral for optic disc segmentation. In: *ACM International Conference Proceeding Series*. [S.l.]: Association for Computing Machinery, 2021. p. 7–12.

RADENOVIC, F. et al. Revisiting oxford and paris: Large-scale image retrieval benchmarking. In: *2018 IEEE/CVF Conference on Computer Vision and Pattern Recognition*. Los Alamitos: IEEE, 2018. p. 5706–5715.

RAHEJA, S.; KUMAR, A. Edge detection based on type-1 fuzzy logic and guided smoothening. *Evolving Systems*, v. 12, n. 2, p. 447–462, 2021.

RALEVIĆ, N. et al. Color image segmentation using distance functions based on aggregation of pixels colors. In: KAHRAMAN, C. et al. (Ed.). *Intelligent and Fuzzy Techniques for Emerging Conditions and Digital Transformation*. Cham: Springer International Publishing, 2022. p. 717–724.

RALEVIć, N.; DELIć, M.; NEDOVIć, L. Aggregation of fuzzy metrics and its application in image segmentation. *Iranian Journal of Fuzzy Systems*, v. 19, n. 3, p. 19–37, 2022.

REN, Z.; SHAKHNAROVICH, G. Image segmentation by cascaded region agglomeration. In: *IEEE Conference on Computer Vision and Pattern Recognition*. [S.l.: s.n.], 2013. p. 2011–2018.

REVIEWS, C. for; DISSEMINATION. *CRD's guidance for undertaking reviews in healthcare*. 3. ed. ed. York: York Publ. Services, 2009. (Systematic reviews).

ROBERTS, J. *Machine Percept 3D Solids*. [S.l.]: Dissertations-G, 1980.

ROBERTS, L. G. *Machine perception of three-dimensional solids*. Tese (Doutorado) — Massachusetts Institute of Technology, 1963.

ROSIN, P. L. Unimodal thresholding. *Pattern Recognition*, v. 34, n. 11, p. 2083–2096, 2001.

RUBIN, E. *Synsoplevede figurer. Studier i psykologisk Analyse*. Copenhagen: Gyldendal, 1915. Abridged English translation by M. Wertheimer: 'Figure and ground', in D. C. Beardslee and M. Wertheimer (eds.), Readings in Perception, Princeton, NJ: Van Nostrand, 1958, pp. 194–203.

RUSSO, F. Edge detection in noisy images using fuzzy reasoning. *IEEE Transactions on Instrumentation and Measurement*, v. 47, n. 5, p. 1102–1105, 1998.

SAKIYAMA, T.; SASAKI, A.; GUNJI, Y.-P. Origin of kanizsa triangle illusion. In: RHEE, S.-Y.; PARK, J.; INOUE, A. (Ed.). *Soft Computing in Machine Learning*. Cham: Springer International Publishing, 2014. p. 95–103. ISBN 978-3-319-05533-6.

SALEH, E. et al. Learning fuzzy measures for aggregation in fuzzy rule-based models. In: TORRA, V. et al. (Ed.). *Modeling Decisions for Artificial Intelligence*. Cham: Springer International Publishing, 2018. p. 114–127. ISBN 978-3-030-00202-2.

SANTOS, M. *Pobreza urbana*. [S.l.]: edUsp-Editora da Universidade de São Paulo, 1978.

SCHULTZ, D.; SCHULTZ, S. *História da psicologia moderna*. [S.l.]: Cultrix, 1996. ISBN 9788531601972.

SCHUMANN, F. Beiträge zur analyse der gesichtswahrnehmungen. erste abhandlung. einige beobachtungen über die zusammenfassung von gesichtseindrücken zu einheiten. *Zeitschrift für Psychologie und Physiologie der Sinnesorgane*, v. 23, p. 1–32, 1900. English translation by A. Hogg, 'Contributions to the Analysis of Visual Perception, First Paper: Some Observations on the Combination of Visual Impressions into Units', in S. Petry and G. E. Meyer (eds.), The Perception of Illusory Contours, New York: Springer, 1987, pp 21–34.

SCHWARTZ, S. H. *Visual Perception: A Clinical Orientation*. 4. ed. [S.l.]: McGraw-Hill Medical, 2010. ISBN 978-0-07-160461-1.

SCHWEIZER, B.; SKLAR, A. *Probabilistic Metric Spaces*. New York: North-Holland, 1983.

SHAHADE, A. K.; DESHMUKH, P. V. Edge-enhanced dual branch cnn with adaptive attention for robust apple leaf disease detection. *BMC Plant Biology*, v. 26, n. 1, 2026. Cited by: 0; All Open Access, Gold Open Access, Green Open Access.

SHEN, J.; CASTAN, S. An optimal linear operator for step edge detection. *CVGIP: Graphical Models and Image Processing*, v. 54, n. 2, p. 112–133, 1992. ISSN 1049-9652.

SHEN, W. et al. DeepContour: A deep convolutional feature learned by positive-sharing loss for contour detection. In: *IEEE Conference on Computer Vision and Pattern Recognition*. [S.l.: s.n.], 2015. p. 3982–3991.

SHI, J.; MALIK, J. Normalized cuts and image segmentation. *IEEE Transactions on Pattern Analysis and Machine Intelligence*, IEEE, v. 22, n. 8, p. 888–905, 2000.

SHORTEN, C.; KHOSHGOFTAAR, T. M. A survey on image data augmentation for deep learning. *Journal of Big Data*, v. 6, n. 1, p. 1–48, 2019.

SHOTTON, J.; BLAKE, A.; CIPOLLA, R. Multiscale categorical object recognition using contour fragments. *IEEE Transactions on Pattern Analysis and Machine Intelligence*, v. 30, n. 7, p. 1270–1281, 2008.

SILVA, M. et al. Fuzzy logic based edge detection methods: A systematic literature review. In: *Proceedings of the 25th International Conference on Enterprise Information Systems*. [S.l.]: SCITEPRESS - Science and Technology Publications, 2023. (Proceedings of the 25th International Conference on Enterprise Information Systems).

SILVA, M. A. S. et al. Efects of image blurring on the eficiency of edge detection algorithms. In: *IPMU2024 Lisboa - Short Paper Proceedings*. Lisbon, Portugal: Zenodo, 2025.

SILVA, M. A. S. et al. Impact of blurring on edge detection performance a survey. In: GONZÁLEZ-BRIONES, A. et al. (Ed.). *Highlights in Practical Applications of Agents, Multi-Agent Systems, and Digital Twins: The PAAMS Collection*. Cham: Springer Nature Switzerland, 2025. p. 179–186. ISBN 978-3-031-73058-0.

SMITH, B. On drawing lines on a map. In: FRANK, A. U.; KUHN, W. (Ed.). *Spatial Information Theory. A Theoretical Basis for GIS*. Berlin: Springer, 1995. p. 475–484.

SMITH, S. M.; BRADY, J. M. SUSAN- a new approach to low level image processing. *International Journal of Computer Vision*, v. 23, p. 45–78, 1997. ISSN 0920-5691.

SOBEL, I. *Camera models and machine perception*. [S.l.], 1972.

SOBEL, I.; FELDMAN, G. A 3x3 isotropic gradient operator for image processing. In: DUDA, R.; HART, P. (Ed.). *Pattern Classification and Scene Analysis*. [S.l.]: John Wiley and Sons, 1973. p. 271–272. Presented at a talk at the Stanford Artificial Project (1968); unpublished but often cited, orig.

SONKA, M.; HLAVAC, V.; BOYLE, R. *Image Processing, Analysis, and Machine Vision*. [S.l.]: Cengage Learning, 2014.

SORIA, X. et al. Tiny and efficient model for the edge detection generalization. In: *2023 IEEE/CVF International Conference on Computer Vision Workshops (ICCVW)*. [S.l.: s.n.], 2023. p. 1356–1365.

SU, Z. et al. Pixel difference networks for efficient edge detection. In: *2021 IEEE/CVF International Conference on Computer Vision (ICCV)*. [S.l.]: IEEE, 2021.

SUAREZ, F. *Metaphysical Disputation II: On the Essential Concept Or Concept of Being*. United States: Catholic University of America Press, 2023.

SUGENO, M. *Theory of fuzzy integrals and its applications*. Tese (Doutorado) — Tokyo Institute of Technology, 1974.

SUN, T.-H. et al. Adversarial colorization of icons based on contour and color conditions. In: *27th ACM International Conference on Multimedia - MM '19*. New York, NY, USA: Association for Computing Machinery, 2019. p. 683–691.

SURESH, K.; SRINIVASA, P. Various image segmentation algorithms: A survey. In: *Smart Intelligent Computing and Applications*. Singapore: Springer, 2019, (Smart Innovation, Systems and Technologies, v. 105). p. 233–239.

TICALA, C.; PINTEA, C.-M.; MATEI, O. Sensitive ant algorithm for edge detection in medical images. *Applied Sciences*, v. 11, n. 23, 2021. ISSN 2076-3417.

TRIPATHI et al. Edge detection on medical images using intuitionistic fuzzy logic. *Communications in Computer and Information Science*, v. 1376 CCIS, p. 236–246, 2021.

VERSACI, M.; MORABITO, F. C. Image edge detection: A new approach based on fuzzy entropy and fuzzy divergence. *International Journal of Fuzzy Systems*, Springer Science and Business Media LLC, v. 23, n. 4, p. 918–936, 2021.

VINCI, L. da. *The Notebooks*. London: Reynal & Hitchock, 1938.

VU, N.-S.; CAPLIER, A. Enhanced patterns of oriented edge magnitudes for face recognition and image matching. *IEEE Transactions on Image Processing*, v. 21, n. 3, p. 1352–1365, 2012.

WANG, X.-F.; HUANG, D.-S.; XU, H. An efficient local chan–vese model for image segmentation. *Pattern Recognition*, v. 43, n. 3, p. 603–618, 2010.

WANG, Y. et al. Using local edge pattern descriptors for edge detection. *International Journal of Pattern Recognition and Artificial Intelligence*, v. 32, n. 3, p. 1850006, 2018.

WEI, Y. et al. Stc: A simple to complex framework for weakly-supervised semantic segmentation. *IEEE Transactions on Pattern Analysis and Machine Intelligence*, v. 39, n. 11, p. 2314–2320, 2017.

WERTHEIMER, M. Untersuchungen zur lehre von der gestalt. ii. *Psychologische Forschung*, v. 4, p. 301–350, 1923. English translation by M. Wertheimer and K. W. Watkins, 'Investigations on Gestalt Principles', in M. Wertheimer, On Perceived Motion and Figural Organization (ed. by L. Spillmann), Cambridge, MA: MIT Press, 2012, pp. 127–182.

WHARTON, E. J.; PANETTA, K.; AGAIAN, S. S. Logarithmic edge detection with applications. In: *2007 IEEE International Conference on Systems, Man and Cybernetics*. [S.l.: s.n.], 2007. p. 3346–3351.

WIBISONO, J. K.; HANG, H.-M. Fined: Fast inference network for edge detection. In: *2021 IEEE International Conference on Multimedia and Expo (ICME)*. [S.l.]: IEEE, 2021.

WIECZYNSKI, J. et al. d-xc integrals: on the generalization of the expanded form of the choquet integral by restricted dissimilarity functions and their applications. *IEEE Transactions on Fuzzy Systems*, IEEE, v. 30, n. 12, p. 5376–5389, 2022.

WIECZYNSKI, J. et al. dc_F-integrals: Generalizing c_F-integrals by means of restricted dissimilarity functions. *IEEE Transactions on Fuzzy Systems*, v. 31, n. 1, p. 160–173, 2023.

WIECZYNSKI, J. C. et al. Generalizing the gmc-rtopsis method using ct-integral pre-aggregation functions. In: *2020 IEEE International Conference on Fuzzy Systems (FUZZ-IEEE)*. [S.l.: s.n.], 2020. p. 1–8.

WILKIN, T.; BELIAKOV, G. Weakly monotonic averaging functions. *International Journal of Intelligent Systems*, v. 30, n. 2, p. 144–169, 2015.

WITTGENSTEIN, L. *Philosophical Investigations / Philosophische Untersuchungen*. Oxford: Blackwell, 1953.

WU, J.-Z.; BELIAKOV, G. Nonadditivity index and capacity identification method in the context of multicriteria decision making. *Information Sciences*, v. 467, p. 398 – 406, 2018. ISSN 0020-0255.

WU, J.-Z.; BELIAKOV, G. Nonmodularity index for capacity identifying with multiple criteria preference information. *Information Sciences*, v. 492, p. 164 – 180, 2019. ISSN 0020-0255.

WU, J.-Z. et al. Random generation of linearly constrained fuzzy measures and domain coverage performance evaluation. *Information Sciences*, v. 659, p. 120080, 2024. ISSN 0020-0255.

XIE, S.; TU, Z. Holistically-nested edge detection. *International Journal of Computer Vision*, Kluwer Academic Publishers Norwell, MA, USA, v. 125, n. 1-3, p. 3–18, 2017.

XU, Y.; BROWNJOHN, J.; KONG, D. A non-contact vision-based system for multipoint displacement monitoring in a cable-stayed footbridge. *Structural Control and Health Monitoring*, v. 25, n. 5, p. e2155, 2018.

YADAV, R.; PANDEY, M. Image segmentation techniques: A survey. *Lecture Notes on Data Engineering and Communications Technologies*, v. 90, p. 231–239, 2022.

YAGER, R. R. On ordered weighted averaging aggregation operators in multicriteria decision making. *Systems, Man and Cybernetics, IEEE Transactions on*, IEEE, v. 18, n. 1, p. 183–190, 1988.

YANG, J. et al. Object contour detection with a fully convolutional encoder-decoder network. In: *2016 IEEE Conference on Computer Vision and Pattern Recognition (CVPR)*. [S.l.]: IEEE, 2016.

YANG, K. et al. Efficient color boundary detection with color-opponent mechanisms. In: *2013 IEEE Conference on Computer Vision and Pattern Recognition*. [S.l.]: IEEE, 2013.

YANG, M.-H.; KRIEGMAN, D.; AHUJA, N. Detecting faces in images: a survey. *IEEE Transactions on Pattern Analysis and Machine Intelligence*, v. 24, n. 1, p. 34–58, 2002.

YANG, Y. et al. Multimodal medical image fusion based on fuzzy discrimination with structural patch decomposition. *IEEE Journal of Biomedical and Health Informatics*, v. 23, n. 4, p. 1647–1660, 2019.

YOGESH et al. A comparative review of various segmentation methods and its application. In: *2017 6th International Conference on Reliability, Infocom Technologies and Optimization: Trends and Future Directions, ICRITO 2017*. [S.l.]: Institute of Electrical and Electronics Engineers Inc., 2018. v. 2018-January, p. 645–650.

ZADEH, L. Fuzzy sets. *Information and Control*, v. 8, n. 3, p. 338–353, 1965.

ZADEH, L. A. Is there a need for fuzzy logic? *Information sciences*, Elsevier, v. 178, n. 13, p. 2751–2779, 2008.

ZENG, C. et al. Contour detection based on a non-classical receptive field model with butterfly-shaped inhibition subregions. *Neurocomputing*, v. 74, n. 10, p. 1527–1534, 2011.

ZHANG, K. et al. A level set approach to image segmentation with intensity inhomogeneity. *IEEE Transactions on Cybernetics*, v. 46, n. 2, p. 546–557, 2016.

ZHANG, L. et al. Efficient cnn architecture design guided by visualization. In: *2022 IEEE International Conference on Multimedia and Expo (ICME)*. [S.l.: s.n.], 2022. p. 1–6.

ZHANG, W. et al. Discrete curvature representations for noise robust image corner detection. *IEEE Transactions on Image Processing*, v. 28, n. 9, p. 4444–4459, 2019.

ZHANG, W. et al. Corner detection using gabor filters. *IET Image Processing*, v. 8, n. 11, p. 639–646, 2014.

ZHANG, W. et al. Noise robust image edge detection based upon the automatic anisotropic gaussian kernels. *Pattern Recognition*, Elsevier BV, v. 63, p. 193–205, 2017.

ZHANG, W.-C.; SHUI, P.-L. Contour-based corner detection via angle difference of principal directions of anisotropic gaussian directional derivatives. *Pattern Recognition*, v. 48, n. 9, p. 2785–2797, 2015.

ZHANG, Y. et al. A mixture model for image boundary detection fusion. *IEICE Transactions on Information and Systems*, E101D, n. 4, p. 1159–1166, 2018.

ZHAO, Z.-Q.; HUANG, D.-S.; SUN, B.-Y. Human face recognition based on multi-features using neural networks committee. *Pattern Recognition Letters*, v. 25, n. 12, p. 1351–1358, 2004.

ZHOU, C. et al. Multi-scale pseudo labeling for unsupervised deep edge detection. *Knowledge-Based Systems*, v. 280, p. 111057, 2023. ISSN 0950-7051.

ZHU, Y.; LI, P. Survey on the image segmentation algorithms. *Springer Series in Geomechanics and Geoengineering*, p. 475–488, 2019.